AFFDL-TR-67-179
PART I

ANALYSIS OF VTOL HANDLING QUALITIES REQUIREMENTS

PART I. LONGITUDINAL HOVER AND TRANSITION

SAMUEL J. CRAIG
ANTHONY CAMPBELL

Systems Technology, Inc.

FOREWORD

This report covers the first phase of an analytical effort to analyze and consolidate the available experimental data and to further an understanding of the manual piloting control problems associated with VTOL type aircraft.

The work was performed by Systems Technology, Inc., Hawthorne, California, under the sponsorship of the Air Force Flight Dynamics Laboratory, Directorate of Laboratories, Air Force Systems Command, Wright-Patterson Air Force Base, Ohio. The research was conducted from July 1966 to June 1968 under Subcontract S-67-1 to the Cornell Aeronautical Laboratory as Part III of the VTOL Integrated Flight Control Systems Program (VIFCS), Contract AF 33(615)-3736, Project 698DC and the report was submitted for approval as STI TR 171-1. The AFSC project engineer was Mr. Wilfred Klotzback and the CAL project engineer was Mr. Charles Chalk.

Many of the authors' colleagues at Systems Technology, Inc., contributed to this program. In particular, Mr. Robert F. Ringland performed many analytical computations presented in the study of transition control and assisted in the editing of the material in Section III; Mr. Irving Ashkenas assisted additionally with interpretation of the experimental results analyzed in Section II and the review and technical editing of the report; and finally, Mr. Jun Taira and the publications staff prepared this report.

This technical report has been reviewed and is approved.

C. B. Westbrook

C. B. WESTBROOK
Chief, Control Criteria Branch
Flight Control Division
AF Flight Dynamics Laboratory

ABSTRACT

Analyses of results from available handling qualities experiments were performed to determine dynamic and control requirements for VTOL aircraft. The basis for this treatment was an examination of the pilot/vehicle as a closed-loop servo system. The quasi-linear pilot describing function has been applied. The results of the studies suggest that the primary factors identifying satisfactory and unacceptable hover mode dynamic features are primarily related to the closed-loop pilot/vehicle system. Preliminary consideration is given to the longitudinal techniques and multiloop control structures suitable for manual control in transition.

CONTENTS

FIGURES

TABLES

SYMBOLS

b	Airplane wing span
c.g.	Center of gravity
dB	Decibel $\equiv 20 \log_{10} \left| \ \right| = \left| \ \right|_{dB}$
g	Acceleration due to gravity
G(s)	Open-loop transfer function; also specific transfer function if particularized by subscript(s)
$G(-\sigma)$ $G(j\omega)$	G(s) with s replaced by $-\sigma$ and $j\omega$, respectively; for $G(-\sigma) < 0$, values of $\left|G(-\sigma)\right| = 1$ identify real roots
h	Altitude perturbation
I	Moment of inertia
I_x, I_y, I_z	Moments of inertia about x, y, and z axes, respectively
I_{xz}	Product of inertia in XZ plane
j	$\sqrt{-1}$
$j\omega$	The imaginary portion of the complex variable $s = \sigma \pm j\omega$
k	Spring rate of manipulator
K	Bode gain of controlled element, particularized by subscript
K_M	Gain margin
K_{p_λ}	Pilot gain of λ degree of freedom
L	Integral scale of turbulence
m	Mass of aircraft
M	Pitching moment/I_y
M_q	$\partial M/\partial q$
M_u	$\partial M/\partial u$
M_w	$\partial M/\partial w$
$M_{\dot{w}}$	$\partial M/\partial \dot{w}$
M_δ	$\partial M/\partial \delta$
N(s)	Transfer function numerator

$N_{\delta_1\delta_2}^{\lambda_1\lambda_2}$	Coupling numerator relating output motion quantity to control deflection, particularized by subscripts
$N_{\delta}^{\lambda}(s)$	Numerator of transfer function relating output motion quantity to control deflection, particularized by subscripts
POR or PR	Pilot's rating
q	Dynamic pressure
q	Pitch rate, angular velocity about the Y axis, positive nose going up
RHP	Right half plane
rms	Root mean square
s	Laplace operator, $\sigma \pm j\omega$
S	Wing area
SAS	Stability Augmentation System
t	Time
1/T	Inverse time constant, particularized by subscript
T_E	Equalization time constant, attitude loop, $K_\theta/K_{\dot{\theta}}$
T_I	Human pilot lag time constant
T_L	Human pilot lead time constant
T_N	Human pilot neuromuscular time constant
T_u	Equalization time constant, position loop, K_{ax}/K_u
T_λ	Time constant of λ zero or pole
$T_{\lambda_i\lambda_j}$	Coupling numerator time constant for variables $\lambda_i\lambda_j$
u	Perturbation velocity along x-axis
u_g	Gust velocity along x-axis
U_o	Steady-state velocity along x-axis
w	Perturbation velocity along z-axis
W	Vehicle weight
x	Horizontal displacement in direction of x-axis
X	Force in x-direction divided by aircraft mass

X_q	$= \partial X/\partial q$
X_u	$= \partial X/\partial u$
X_δ	$= \partial X/\partial \delta$
Y_f	Transfer function of filter
$Y_{p(\lambda)}$	Human pilot transfer function, particularized with respect to general variable
z	Vertical displacement in direction of z-axis, positive downward
Z	Force in z-direction divided by aircraft mass
Z_q	$= \partial Z/\partial q$
Z_u	$= \partial Z/\partial u$
Z_w	$= \partial Z/\partial w$
Z_δ	$= \partial Z/\partial \delta$
α	Angle of attack, $\doteq \omega/U_o$
γ	Perturbed flight path angle, $\theta - \alpha$
δ	Control deflection (Positive: forward stick)
δ_e	Pitch control deflection
ΔR_i	Increment between the actual and control of ith single axis
ΔR_k	Increment between the actual and optimum pilot rating
$\Delta(s)$	Denominator of airframe transfer functions; characteristic equation when set equal to zero
$\Delta\lambda$	Perturbation angle of thrust vector
ζ	Damping ratio of linear second-order transfer function quantity, particularized by subscript
θ	Pitch angle
θ_1	Pitch angle response in 1 sec
λ	General variable (u, v, w, θ, φ, ψ, etc.)
λ_o	Thrust vector angle at trim condition
σ	Real part of s
σ_λ	Root-mean-squared value of λ
τ	Time delay

τ_e	Effective pilot time delay, τ,plus neuromuscular time constant
φ	Phase angle, degrees
φ_M	Phase margin
Φ_λ	λ power spectrum
ω	Imaginary part of s
ω_c or ω_{c_o}	Crossover frequency
ω_{c_λ}	Crossover frequency of general closed-loop variable
ω_λ	Undamped natural frequency of λ zero or pole

Special Subscripts:

c	Command; crossover; controlled element (vehicle), collective
CL	Closed loop
e	Error, or elevator's pitch control (longitudinal cyclic)
eff	Effective
g	Gust
h	Altitude numerator for control input
hi	High frequency
o	Basic (unperturbed) condition
OL	Open-loop
p	Phugoid
p	Pilot
r	Yaw control (tail rotor or differential lateral cyclic)
R	Roll subsidence
s	Spiral
sp	Short-period
ss	Steady state
T	Throttle; Thrust
u	Airspeed numerator for control input

Special Superscripts:

( )'	Primes denoting loop closure. Primes on a transfer function or time constant indicate that it has been modified by inner-loop closures, the number of primes corresponding to the number of closures.
( )"	
$(\dot{})$	Denotes derivative with respect to time, d/dt
$(\ddot{})$	Denotes second derivative with respect to time, d^2/dt^2

Mathematical Symbols:

<	Less than
>	Greater than
<<	Much less than
>>	Much greater than
/	Not (e.g., $\neq$, not equal to); divided by
$\doteq$	Approximately equal to
→	Fed to; approaches
∂	Partial differential
λ/δ	Generalized transfer function, $\lambda(s)/\delta(s)$
]	Outer loop with inner loop(s) closed
∠	Angle
| |	Modulus
e	2.7183
✕	Pole (root of denominator)
⊙	Zero (root of numerator)
▮	Closed-loop root
$(1/T_i)$	First-order factors of transfer function
$[\zeta_i, \omega_i]$	Second-order factors of transfer function

Notational Rules for Closed-Loop Quantities:

1. The number of primes present indicates the number of loops closed previously.

2. The notation for the closed-loop factor is the same as that for the open-loop factor (plus a prime) when the closed-loop and open-loop forms are the same. In this case the origin of the closed-loop factor is always at hand (e.g., $\omega_d \rightarrow \omega_d'$, $\omega_\varphi \rightarrow \omega_\varphi'$, $T_R \rightarrow T_R'$, $T_{\varphi_1} \rightarrow T_{\varphi_1}'$, $T_{d_1} \rightarrow T_{d_1}'$, etc.)

3. When the closed-loop factors differ in form from their open-loop origins, several possibilities exist.

    a. For closed-loop factors which have the same form as, and are approaching, open-loop zeros, the closed-loop factor notation is that of the open-loop zeros (plus a prime). For example, open-loop quantities $(s + 1/T_s)$ and $(s + 1/T_{d_2})$, which couple to form a quadratic approaching the open-loop zeros of $(s^2 + 2\zeta_r\omega_r s + \omega_r^2)$, would give rise to a closed-loop factor ordinarily denoted as $(s^2 + 2\zeta_r'\omega_r' s + \omega_r'^2)$.

    b. For closed-loop factors which differ in form from both the open-loop poles from which they depart and the open-loop zeros which they ultimately approach, a special notation is coined which ordinarily reflects the origin of the factor. For example, closed-loop factors which start from $s = 0$ and $s = -1/T_R$, couple to form a quadratic, and subsequently decouple to end finally at two real zeros, would be denoted $s^2 + 2\zeta_R'\omega_R' s + \omega_R'^2$ in the quadratic region.

    c. Closed-loop factors which have no readily identified origin or end point, such as one starting at $s = 0$ and approaching $s = \infty$ as gain increases, are given a specially coined notation, e.g., $1/T_c'$.

4. When the application of these rules by rote would result in great confusion in the local context, a new form is substituted for the closed-loop factor involved. Primes, however, are always retained.

SECTION I

INTRODUCTION

One of the problems most often cited as impeding both design and development of the VTOL aircraft during the past decade has been the lack of rational flying quality requirements. However, more fundamental even than this lack of requirements has been the absence of a basis for understanding and the means for consolidation of the enormous amount of handling quality information generated experimentally during this period.

The effort reported here has been directed specifically at these two tasks, (1) understanding and (2) consolidation of all documented experimental results. The treatment utilized throughout this study rests primarily on the servo analysis of the pertinent closed-loop piloting tasks for the longitudinal axes, and considers both hover and transition flight regimes.

The present study takes off from the rather complete literature survey and analysis of Ref. 1 in which the results and conclusions of the pertinent published material up to approximately 1965 are examined, listed, and, where suitable, analyzed. In addition, because the basic approach and treatment as utilized here draws on the experience and background gained in previous V/STOL handling qualities analyses, it is suggested that the reader may find it worthwhile to review the studies of Refs. 1, 2, and 3.

Section II considers the hover mode dynamic features which have been tested in various simulator programs. A broad range of dynamics features are assembled, identified in terms of open-loop properties, and finally classified as to their "effective" controlled element form. For each controlled element form, the characteristics are defined for both "satisfactory" and "unacceptable" handling quality levels. Selective closed-loop analyses are performed to complete the picture and as a means of understanding the pilot/vehicle control situation associated with each handling quality level.

In Section III the quasi-linear pilot's describing function and closed-loop control aspects are applied in an attempt to provide a basis for minimum control power and sensitivity requirements for the closed-loop regulatory control in a gust environment.

In Section IV of the report, alternate perturbation control techniques and various vehicle factors influencing (pilot's) closed-loop control of transition are explored in order to gain an appreciation for potential problem areas and pertinent specification parameters. Since there is very little experimental data available in this region, the XC-142 was used as a representative base model which is expanded generically to show the effect of other types of vehicle configurations on transition control.

Another important aspect of study was the effort taken to explain apparent differences among the individual references as to "satisfactory" or "unacceptable" characteristics. These considerations and correlations have weighed such factors as gust disturbance effects, stability, fixed- versus moving-base simulation, etc., and are presented in Appendix A. In extending and explaining these differences we reexamined "old" and sought out "new" data. Among the new sources of data, those supplied by United Aircraft Research Laboratories were

very important because of the well-documented compensatory tracking experiments that were performed on their simulator. Since UARL was part of the overall VTOL Integrated Flight Control Systems Program (VIFCS), their simulator results were made immediately available to us through progress reports and letters, as well as in published form (Refs. 4 and 5).

SECTION II

LONGITUDINAL HOVER DYNAMICS AND CONTROL

The handling qualities and augmentation requirements for VTOL aircraft in the hover mode have been the subject of much experimental activity in the past decade. The majority of such efforts have been devoted to establishing empirical correlations between vehicle open-loop parameters and a pilot rating or opinion scale (e.g., Cooper Rating Scale, Ref. 6). Unfortunately, the results have often appeared conflicting or inadequate when comparisons among experiments have been attempted on the basis of the suggested dynamic factors. However, these data provide a logical starting point for the present analysis as well as a basis for future criteria. Accordingly, the analyses and correlations to follow are based on a review and interpretation of the existing experimental data and results.

In scope, the present review has included the available ground-simulated and flight-tested hover dynamics from both governmental and industry-sponsored research. Most of the sources for the data utilized are given in the cited references; however, in specific cases some unpublished results have been used. Approximately 100 different dynamic configurations were studied in detail. Where possible, the "raw" pilot rating data were used to eliminate the effects of interpolation and fairing in the documented results.

With this abundance of data, the underlying objective of this effort was first to unify past results and secondly to provide the rationale for future handling quality criteria. To perform these two tasks, we have employed servo analysis techniques, utilized the latest crossover model concepts for the pilot describing function, and established closed-loop control structure logic consistent with observed piloting techniques.

All previous attempts to correlate the VTOL results on the basis of single or complex open-loop features have had only limited success. Therefore, in the present analyses the open-loop characteristics were examined in light of the related closed-loop handling quality merits. Table I identifies these pertinent merits and their significance to the present studies.

The assumed partitioning into the various related handling quality merits is the fundamental basis for this study of VTOL dynamics. The emphasis at the initial stage is placed on the single performance merit — stability. The most pertinent indicator of this merit is the effective vehicle control-input transfer function in the desired crossover frequency region. Such characteristics, obtained from the various data sources, were examined by constructing families of Bode plots and root loci for two pilot opinion regions — the satisfactory ($3 \leq PR \leq 4$) and the unacceptable ($5.5 \leq PR \leq 7.5$).*

*In the case of the unacceptable classification, the expanded range of opinion data classified as unacceptable was used to insure that a good overlapping of marginal dynamic features was included.

TABLE I

SIGNIFICANT HANDLING QUALITY MERITS

RELATED HANDLING QUALITY MERITS	SIGNIFICANCE TO THE HOVERING TASK PILOT OPINION
1. Performance a. Stability, K_m, φ_m	Basic factor: Control in a multiloop situation depends upon the stable inner loop to suppress subsidiary modes and to provide equalization for the outer loops. Gain and phase margins are indicative of allowable tolerances on the pilot's adaptation.
b. Performance, σ_e Gust factors Remnant	Tracking error index basically shows the relative rms error due to the pilot inherent remnant (noise) and his ability to maintain performance under various environmental conditions such as gusty air.
2. Pilot activity a. Compensation and gain T_L, T_I, and K_p	The degree of compensation required is a direct measure of the tolerance and the complexity of the dynamic situation. High or low pilot gain is indicative of sluggishness or oversensitivity.
b. Effort, σ_δ	The control effort σ_δ is a direct measure of the pilot output and increases can be expected as the difficulty of the control task increases or as the disturbance level increases.
3. Maneuver aspects a. Primary control response (attitude)	The control response features of the inner loop are based on θ response in 1 sec (Ref. 1). The crossover frequencies for this loop are greater than 2 rad/sec ($\omega_{c_\theta} \geq 2$ rad/sec).
b. Secondary response (position or velocity)	Response of the position loops are defined by bandpass near 1 rad/sec ($\omega_{c_X} \doteq 1$ rad/sec).

This restriction may be generally justified by our desire to delineate these boundary conditions for specification purposes.

To further restrict the potential factors influencing the pilot rating levels, only the best or optimum ratings were used for each dynamic configuration so that the effects of control power and sensitivity were minimized. Also the data were limited initially to low gust-response levels corresponding to a sensitivity factor, $M_u\sigma_{u_g} \leq 0.1$. As indicated in the sketch below, the change in pilot rating due to gusts is relatively small, below $M_u\sigma_{u_g} = 0.1$, regardless of the vehicle dynamics. However, this gust-response limitation appears unnecessarily restrictive in view of the final correlations, which show that it applies only to the marginal control situations (PR $\doteq$ 6.5).

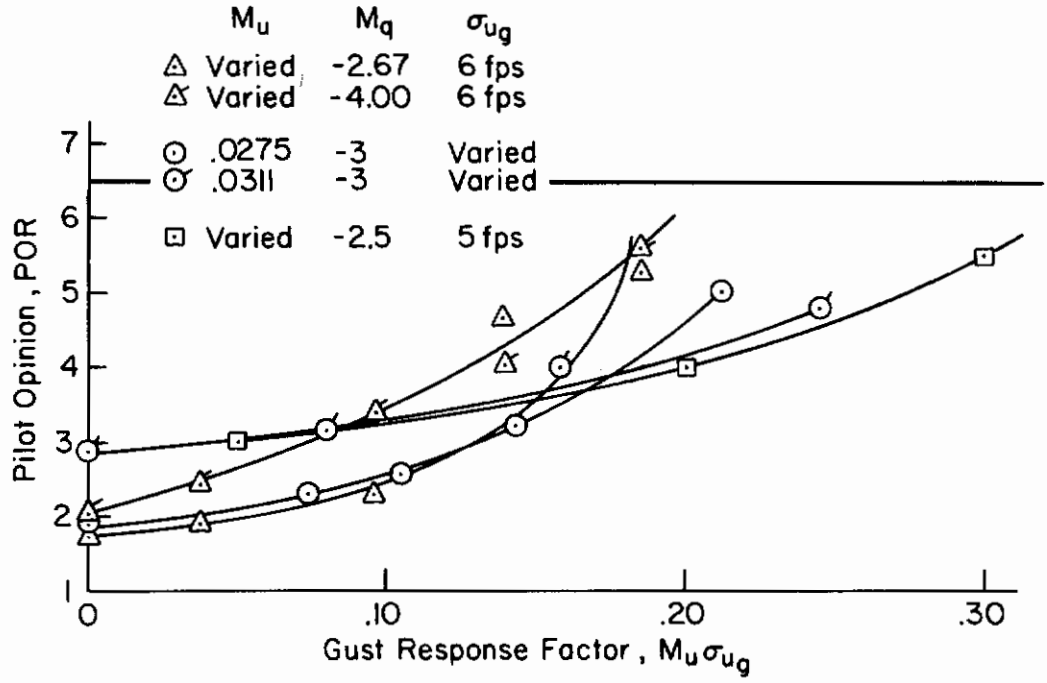

Sketch A. Sensitivity of Pilot Opinion to Vehicle Gust Response Factor, $M_u\sigma_{u_g}$

In addition to pilot opinion factors which stem directly from closed-loop control, detailed consideration has been given to the subjective factors affecting pilot ratings. For example, some of the variance in the opinion data among the data sources used may be explained by such factors as the instructions to the pilot, overall task, and the simulation facilities used. Considerable effort was expended to obtain some appreciation of the intersource pilot rating variances. Primarily this involved direct comparison among the various data sources of situations having essentially the same controlled element dynamics. The details of this effort, as well as a brief review of the various experiments, appears in Appendix A. The major conclusions reached are:

1. The pilot rating differences between fixed- and moving-base or flight test simulators for conditions where $M_q > 1.0$ rad/sec were less than ±1/2 rating point for the satisfactory level and approximately ±1.3 rating

points at the unacceptable level. However, major rating differences were observed at the low M_q and M_u levels for the satisfactory ratings, and at the extremely large M_u and X_u configurations (i.e., $M_u > 0.1$ and $-X_u > 1.0$) for the unacceptable level.

2. The effective change in rating due to gust conditions for small perturbations in M_u or σ_{u_g} is proportional to the sensitivity factor, $M_u\sigma_{u_g}$. This proportionality varies as a function of level of vehicle stability and M_u. Neither σ_{u_g} nor M_u may be interchanged except at constant dynamic situations.

3. The effects of changes in task and instruction to the pilot were significant only for the configurations studied by Bruel (Ref. 7).

A. "EFFECTIVE VEHICLE" CONTROL CHARACTERISTICS

The hover control task involves a multiloop control structure in which both attitude and horizontal position are controlled by the pilot with a single controller (i.e., longitudinal stick or cyclic control). Therefore, the characteristics of two effective controlled elements are pertinent in the present study. These elements are:

- The primary characteristics associated with attitude-loop control, θ/δ.
- The secondary characteristics related to translational or position control, x/δ.

For these two controlled elements the generally applicable transfer function forms are:

$$\text{Attitude:} \quad \frac{\theta}{\delta} = \frac{M_\delta(s + 1/T_{\theta_1})}{(s + 1/T_{sp_2})(s^2 + 2\zeta_p\omega_p s + \omega_p^2)}$$

$$\text{Position:} \quad \frac{x}{\delta} = \frac{-gM_\delta}{s(s + 1/T_{sp_2})(s^2 + 2\zeta_p\omega_p s + \omega_p^2)}$$

These forms are derived in Appendix C from the three-degree-of-freedom equations of motion. Also given there are the approximate literal relations expressing the factored pole/zero roots (i.e., $1/T_{sp}$, ω_p, $1/T_{\theta_1}$, and ζ_p) in terms of basic aerodynamic derivatives, M_u, X_u, M_q, and M_δ.

A variety of pole/zero combinations may be related to the above transfer function forms as a result of changes in either the pertinent derivatives or in the stability augmentation system. Accordingly, we subdivide the dynamic features to identify the effective controlled elements as one of the following:

- Conventional VTOL Systems (including the subsidiary form)
- Attitude Augmentation Systems
- Position or Translational-Loop Augmentation Systems
- Combined Attitude and Translation Systems

Where augmented features are involved a prime notation identifies the augmented "effective" characteristics; the unprimed quantities relate to the bare airframe.

1. Conventional VTOL Aircraft Dynamics

The conventional VTOL aircraft dynamics which have been reviewed in this study are grouped according to source and presented in Appendix B for reference. The "conventional VTOL dynamics" nomenclature is applied to indicate that these dynamics do not include complex stabilization features and the θ responses approach acceleration or rate response to control inputs. The subsidiary transfer function forms associated with this classification are defined in Table II. Fundamentally, these forms are specified by the vehicle's aerodynamic properties; accordingly, the features range from the simple non-aerodynamic inertial body form to the general form which involves both airspeed and angular damping parameters.

TABLE II

EFFECTIVE CONTROLLED ELEMENT FORMS FOR CONVENTIONAL VTOL SYSTEM

BASIC FEATURES AND SUBSIDIARY FORMS	PRIMARY CONTROL-ATTITUDE θ/δ	SECONDARY CONTROL POSITION x/δ
A. Inertial form (i.e., $X_u = M_u = M_q = 0$)	M_δ/s^2	$-gM_\delta/s^4$
B. Angular damping form ($M_q \neq 0$, $X_u = M_u = 0$)	$\dfrac{M_\delta}{s(s + 1/T_{sp_2})}$	$\dfrac{-gM_\delta}{s^3(s + 1/T_{sp_2})}$
C. Aerodynamic form (i.e., u and q terms unequal to zero)	$\dfrac{M_\delta(s + 1/T_{\theta_1})}{(s + 1/T_{sp_2})(s^2 + 2\zeta_p\omega_p s + \omega_p^2)}$	$\dfrac{-gM_\delta}{s(s + 1/T_{sp_2})(s^2 + 2\zeta_p\omega_p s + \omega_p^2)}$

An extensive range of aerodynamic properties and corresponding transfer functions has been reviewed in the present study. In terms of the three primary derivatives which define the transfer functions, aerodynamic properties are given by

$$0 < M_u < 0.16$$

$$-0.36 < X_u < 0$$

$$0 < -M_q < 6.7$$

In terms of the pole/zero roots of the transfer functions, the range of dynamics is equally substantial, as is shown below:

$$0 < 1/T_{sp_2} < 7.0$$

$$-0.05 < 1/T_{\theta_1} < 0.36$$

$$0 < \omega_p < 1.6$$

$$-0.48 < \zeta_p < 0.45$$

From the dynamic data of Appendix B, the Bode and root loci diagrams were calculated for both the satisfactory and unacceptable pilot ratings. A comparison of the two opinion regimes is made in the following subsection to show that the pole/zero combination making up these data is significantly different.

a. Satisfactory Regimes. The satisfactory θ-loop features require three basic forms of the Bode and root loci to represent the variety of pole/zero combinations covered by this rating. Generally the θ-loop can range from one with stable open-loop dynamics and a broad K/s asymptotic region centered about 2 rad/sec to one with unstable dynamics and a K/s^2 asymptote near 2 rad/sec. While such a broad range of attitude dynamics suggest that satisfactory conditions are somewhat ill defined, common dynamic features are evident. For example, the oscillatory mode frequency, ω_p, is always equal to or less than 0.5 rad/sec. Likewise, the majority of the configurations have a broad K/s-like region near 2 rad/sec (see Fig. 1a-b).

The exceptions to the latter aspect are the configurations with K/s^2 asymptotic features near 2 rad/sec described by the Bode diagram in Fig. 1c. Fortunately, such features are characteristic of vehicles with very low angular damping (i.e., $M_q \doteq 0$) and aerodynamic derivatives (e.g., $M_u = X_u = M_w \doteq 0$). In addition such inertial body-like configurations were considered satisfactory only when motion cues were available to the pilot (e.g., moving-base simulations or flight test experiments) and the external disturbances were small. When the above inertial-body configurations are excluded, the distinctive feature of the satisfactory position-loop dynamics is the K/s^3-like asymptotic form of the Bode diagram near 1 rad/sec.

b. Unacceptable Regimes. Two Bode and root loci forms are used in Fig. 2 to define the unacceptable θ-loop dynamics. Basically these dynamics are characterized by a moderately high frequency ($\omega_p \geq 1.0$) unstable mode with a large K/s^2 asymptotic region beyond 2 rad/sec.

The unacceptable position loop shown in Fig. 2 is characterized by the K/s^4 asymptotic form near the crucial 1 rad/sec frequency region.

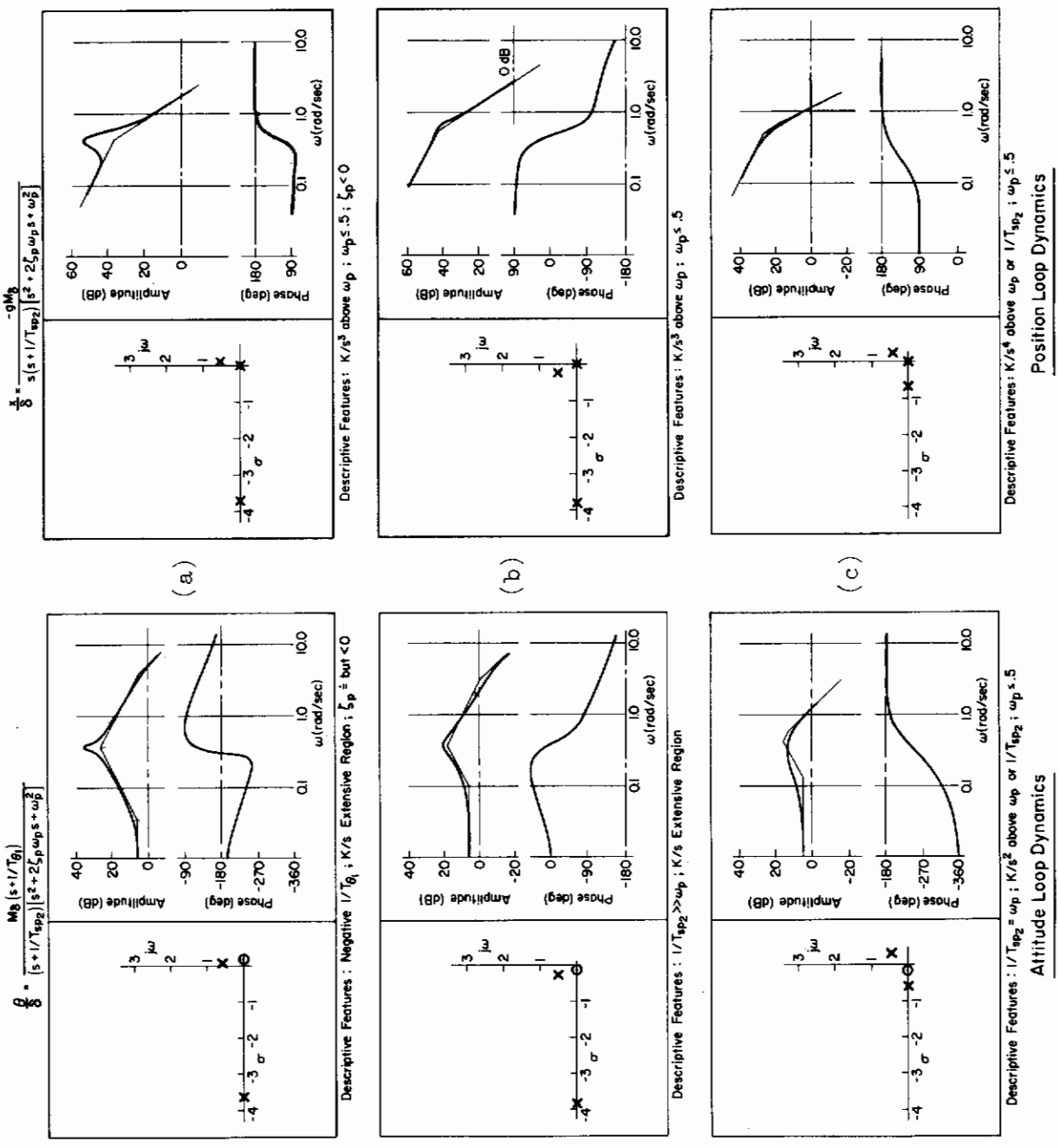

Figure 1. Satisfactory ($3 \leq PR \leq 4$) Conventional VTOL Attitude and Position Loop Dynamics

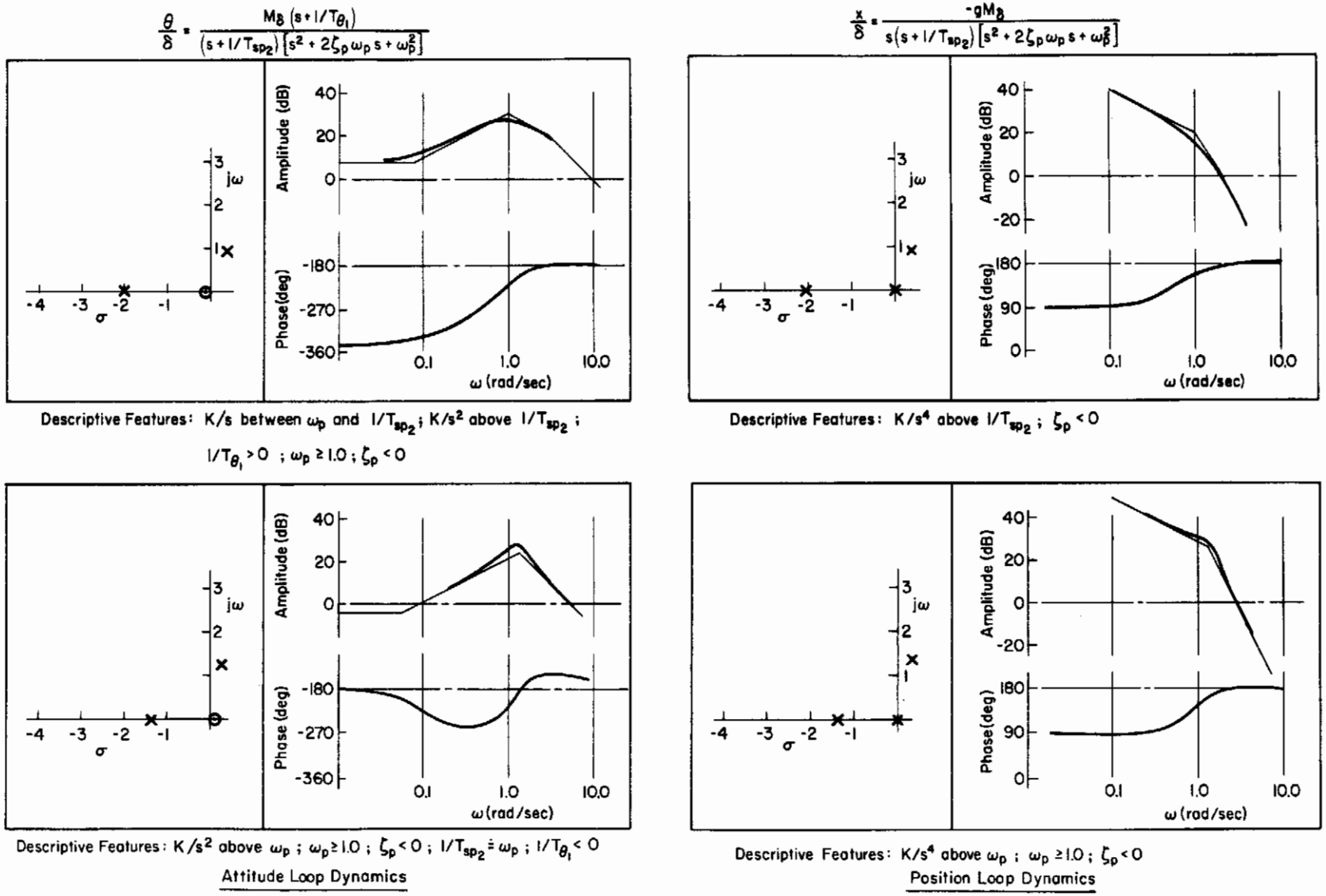

Figure 2. Unacceptable ($6 < PR < 7$) Conventional VTOL Attitude and Position Loop Dynamics

c. **Comparison of Satisfactory and Unacceptable Regimes.** The detailed features of the two handling quality levels, satisfactory and unacceptable, are given in Table III. The more specific features indicated here were defined from the detailed Bode diagrams calculated for each configuration during the Bode survey. These diagrams are not included in the text due to the total number (approximately 90) involved. The diagrams defined from this survey are available in Ref. 8.

The conditions imposed by the results of the Bode survey as given in Table III may be considered as describing necessary but not always sufficient conditions. In this light, these pole/zero combinations may be expressed in terms of the primary aerodynamic derivatives M_q and M_u, using the expressions in Appendix C. Figure 3 shows the resulting M_u versus M_q satisfactory boundaries ($3 < PR < 4$) inferred from the Bode survey. The correlation among various data sources is remarkably good considering the range of configurations and environmental conditions covered by the data. Particularly good correlation is noted between the boundaries and the recent data from UARL. Note that this relation is valid only for a constant X_u or $1/T_{\theta_1}$ level, although it is shown in Appendix A that the overall effect of X_u values near zero is small.

2. Augmented VTOL Dynamic Features

The augmented dynamic features are separated into two groups — attitude augmentation systems and position-loop augmentation systems. The resulting effective vehicle transfer characteristics in each group are considered as a function of feedback dynamics; and correlations with the extant data, based on these characteristics, are shown. Attitude systems are considered first; then position systems; and finally, combinations of both. Table IV provides the general transfer function expected of each of these systems.

Before discussing the satisfactory or unacceptable features of these augmentation groups it is worthwhile to review the consequences of the various forms of attitude and position feedbacks on the basic vehicle dynamics.

a. **Attitude Augmentation.** Attitude-loop feedback systems involve the basic block diagram structure below. The feedback term $1/T_E$ is needed to insure stability and is given by the ratio of attitude and attitude rate feedback. The effective airframe dynamics are then determined by the size

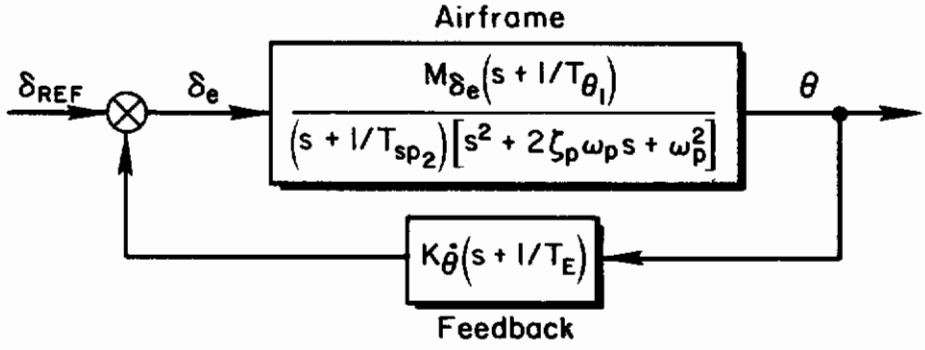

Attitude Feedback Diagram

TABLE III

SUMMARY OF CONVENTIONAL VTOL DYNAMIC FEATURES NECESSARY FOR SATISFACTORY AND UNACCEPTABLE HANDLING QUALITIES DEFINED FROM THE SURVEY

DYNAMIC PROPERTIES	SATISFACTORY $3 \leq PR \leq 4$	UNACCEPTABLE $6 \leq PR \leq 7$
Attitude Loop		
1. Oscillatory Mode		
a. Frequency, ω_p	$\omega_p \lesssim 0.5$ rad/sec	$\omega_p > 0.8$ rad/sec
b. Damping, ζ_p	$\zeta_p \gtrsim 0$ (stable) or $\zeta_p\omega_p > -0.25$*	$\zeta_p < -0.15$ (unstable)
2. Aperiodic Mode		
$1/T_{sp_2}$	$1/T_{sp_2} \gtrsim 1$	$1/T_{sp_2} \doteq \omega_p$
3. Numerator Term		
$1/T_{\theta_1}$	$0 \doteq 1/T_{\theta_1} < 1/2(\omega_p)$	
4. Dominant vehicle asymptotic dynamic form near 2 rad/sec ω_{c_θ}	K/s	K/s^2
5. Phase Margin near limiting ω_p	$\varphi_M > 0$**	$\varphi_M \lesssim -40^\circ$
6. Lowest frequency for stability, ω_{c_1}†	$\omega_{c_1} < 1.0$**	$\omega_{c_1} \gtrsim 1.0$
Position Loop		
1. Dominant vehicle asymptotic dynamic form near 1 rad/sec ω_{x_c}	K/s^3	K/s^4
Gust Sensitivity		
1. $M_u\sigma_{u_g}$	0.1**	0.1

*Requires moving-base of flight test simulation conditions.

**Conditions required only for $\zeta_p\omega_p > -0.25$.

†The lowest frequency for which the phase margin is zero (see Figs. 1, 3a).

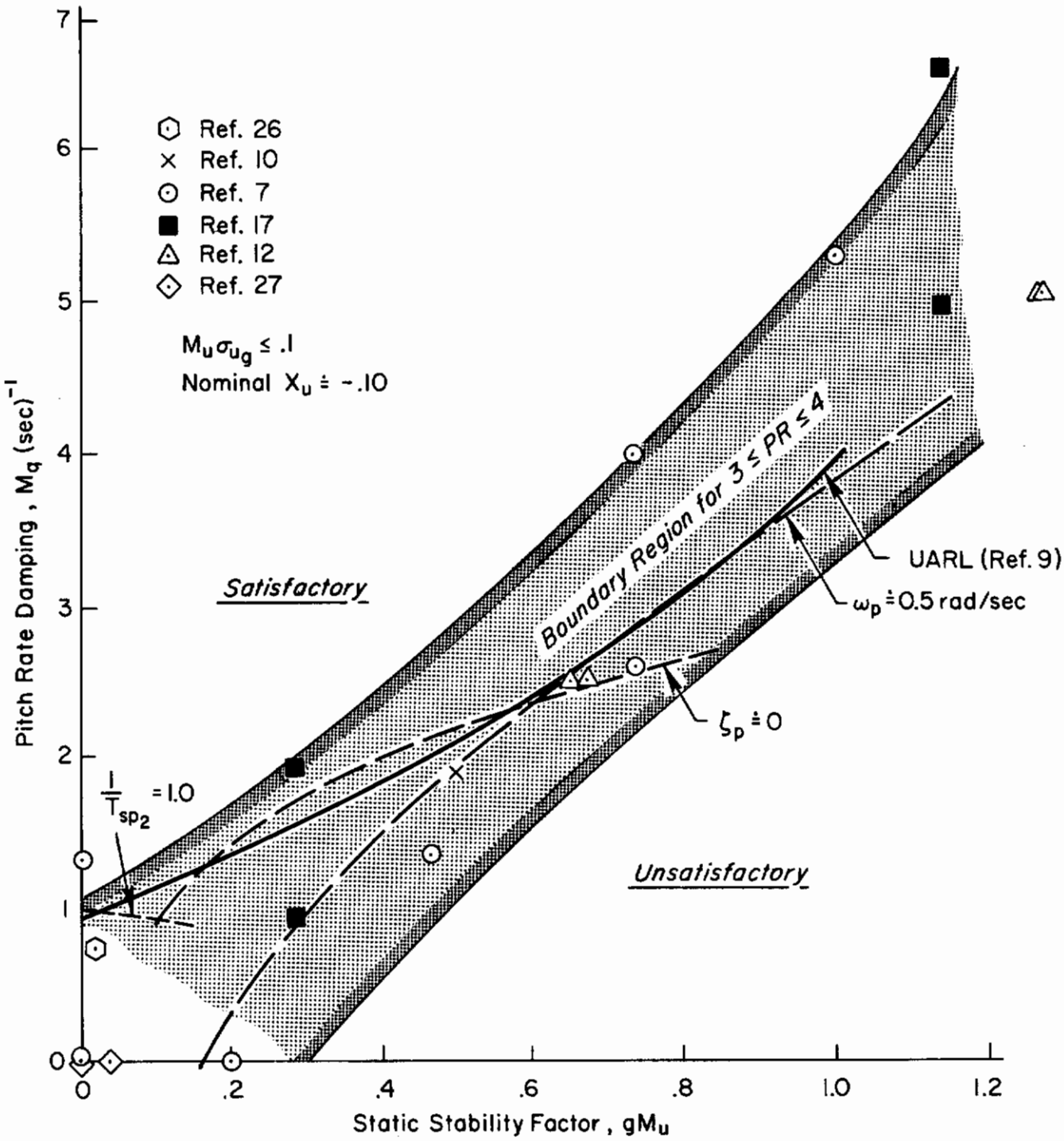

Figure 3. Pitch Rate Damping Requirement Implied from Open-Loop Dynamics for Satisfactory Handling Qualities

TABLE IV

EFFECTIVE CONTROLLED ELEMENT FORMS

BASIC FEATURES	PRIMARY CONTROL-ATTITUDE, θ/δ	SECONDARY CONTROL-POSITION, x/δ
Attitude Augmentation System $[\delta_e/\theta = K_{\dot\theta}'(T_E s + 1)]$		
Case 1. $1/T_E \le 1/T_{sp_2}$ $\omega_p' \le \omega_p$	$\dfrac{M_\delta(s + 1/T_{\theta_1})}{(s + 1/T'_{sp_2})(s^2 + 2\zeta_p'\omega_p' s + \omega_p'^2)}$	$\dfrac{-gM_\delta}{s(s + 1/T'_{sp_2})(s^2 + 2\zeta_p'\omega_p' s + \omega_p'^2)}$
Case 2. $1/T_E > 1/T_{sp_2}$ $(s + 1/T_{\theta_1})/(s + 1/T'_{sp_2}) \doteq 1$	$\dfrac{M_\delta}{s^2 + 2\zeta_p'\omega_p' s + \omega_p'^2}$	$\dfrac{-gM_\delta}{s^2(s^2 + 2\zeta_p'\omega_p' s + \omega_p'^2)}$
Position-Loop Augmentation $\delta_T/u = K_u(T_u s + 1)$		
Case 1. $1/T_{\theta_1} \doteq 1/T_{sp_2}$ $\omega_p > 1/T'_{sp_2}$	$\dfrac{M_\delta}{s^2 + 2\zeta_p'\omega_p' s + \omega_p'^2}$	$\dfrac{-gM_\delta}{s(s + 1/T'_{sp_2})(s^2 + 2\zeta_p'\omega_p' s + \omega_p'^2)}$
Case 2. $1/T_{\theta_1} \doteq \omega_p' < 1/T'_{sp_2}$	$\dfrac{M_\delta(s + 1/T_{\theta_1})}{(s + 1/T'_{sp_2})(s^2 + 2\zeta_p'\omega_p' s + \omega_p'^2)}$	$\dfrac{-gM_\delta}{s(s + 1/T'_{sp_2})(s^2 + 2\zeta_p'\omega_p' s + \omega_p'^2)}$
Combined Attitude and Translational Augmentation Systems $\delta_e/\theta = K_{\dot\theta}'(T_E s + 1)$, $\delta_T/u = K_u(T_u s + 1)$		
$1/T'_{\dot\theta} > 1.0$ rad/sec Case 1. $1/T'_{\theta_1} \doteq \omega_p'$ and $1/T'_{sp_2} > \omega_p'$	$\dfrac{M_\delta}{s^2 + 2\zeta_p'\omega_p' s + \omega_p'^2}$	$\dfrac{-gM_\delta}{s(s + \omega_p')}$
Case 2. $1/T'_{\theta_1} \doteq 1/T'_{sp_2}$ and $\omega_p' \gg 1/T'_{sp_2}$	$\dfrac{M_\delta}{s^2 + 2\zeta_p'\omega_p' s + \omega_p'^2}$	$\dfrac{-gM_\delta}{s(s + 1/T'_{sp_2})}$

of $1/T_E$ relative to the airframe parameter $1/T_{sp_2}$. For example, if $1/T_E$ is selected to be smaller than $1/T_{sp_2}$, we see from the root loci and Bode sketches below that the phugoid mode moves into the two zeros near the origin (i.e., $1/T_E$ and $1/T_{\theta_1}$) and the $1/T_{sp_2}$ mode moves out along the $-\sigma$ axis.

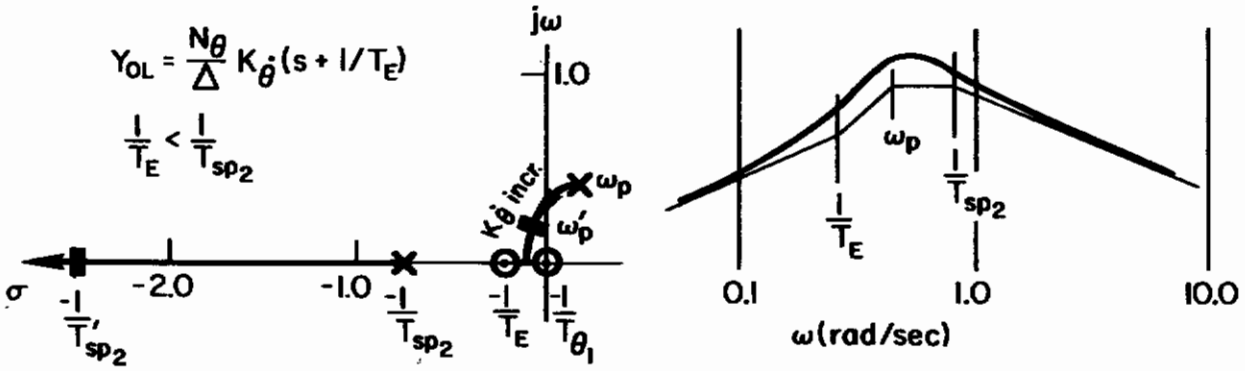

Attitude Rate Feedback Gain Loci

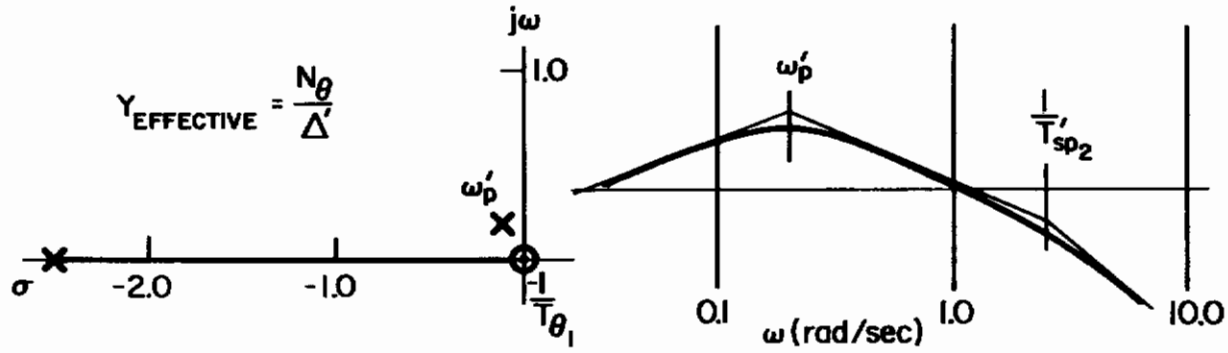

"Effective" Augmented Features

Selecting a moderately high gain and a corresponding moderately high crossover frequency results in a well-damped low-frequency phugoid and a reasonably high first-order mode, $1/T_{sp_2}'$. The "effective" augmented airframe now has a K/s characteristic over a wide frequency band (between ω_p' and $1/T_{sp_2}'$). Thus the dominant response is that of attitude rate proportional to control input. The airframe exhibits only a small attitude stability at the lower frequencies and, in general, exhibits "conventional" VTOL dynamics, but with large rate damping.

The limiting case for $|1/T_E| < |1/T_{sp}|$ is the use of pure rate feedback ($1/T_E = 0$). With two zeros at or near the origin (i.e., if $1/T_{\theta_1} \doteq 0$) the phugoid poles move directly into the zeros without passing into the stable left-half plane, as sketched on the next page.

The overall effective θ-loop feature of the vehicle is quite similar to the previous case except in that the phugoid mode is at about the same frequency; however, the phugoid will be less stable (i.e., $\zeta_p < 0$).

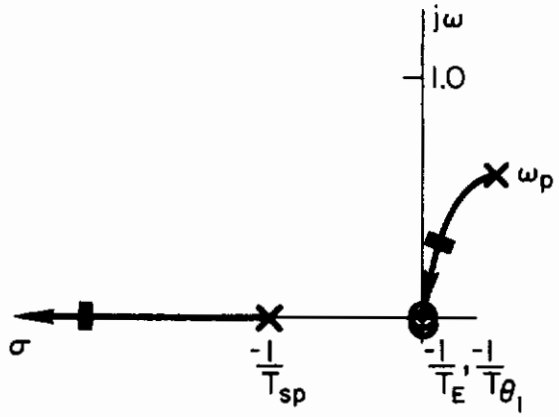

"Pure" ($1/T_E = 0$) Rate Feedback Gain Loci

The position or translational loop response also has conventional VTOL dynamics for this case and is described adequately by the dynamics in Fig. 1b. That is, the asymptotic feature is K/s^3 in frequency region near 1 rad/sec (i.e., between ω_p' and $1/T_{sp_2}'$).

In the case where $1/T_E > 1/T_{sp_2}$ the short-period inverse time constant, $1/T_{sp_2}$, is driven toward the $1/T_{\theta_1}$ root as the loop gain is increased (see adjacent sketch). For very high gains $1/T_{sp_2}'$ will effectively cancel the low-frequency basic airframe numerator term, $1/T_{\theta_1}$. The effective airframe pitch response to a command will be that of a second-order positional system in which pitch attitude, θ, is proportional to control deflection, δ, over the frequency band $\omega < \omega_p'$.

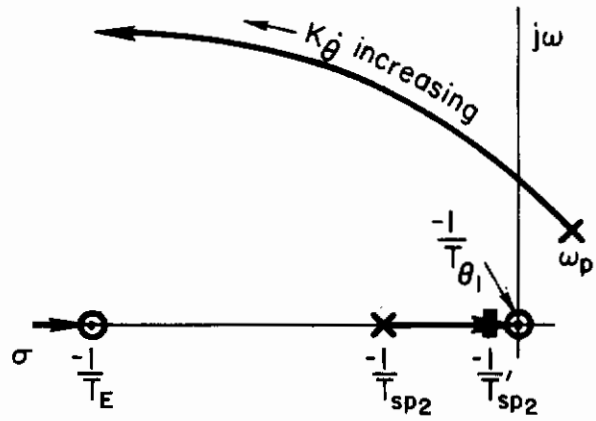

Attitude Rate Feedback Gain Loci

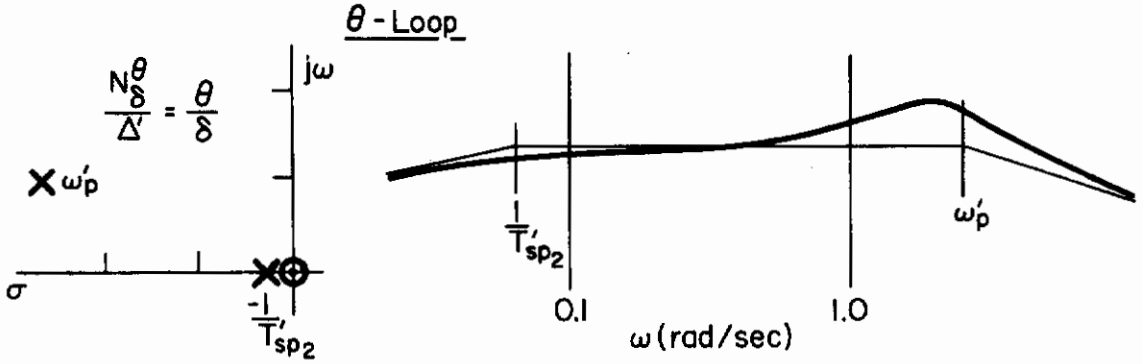

Controlled Element Features with Attitude-Loop Augmentation

The position response is also modified (see sketch below) since the $1/T'_{sp_2}$ root is now effectively at the origin (i.e., $1/T_{\theta_1} \doteq 1/T'_{sp_2} \doteq 0$). Thus the effective outer-loop asymptotic dynamics are K/s^2 over the frequency range $1/T'_{sp_2}$ to ω'_p.

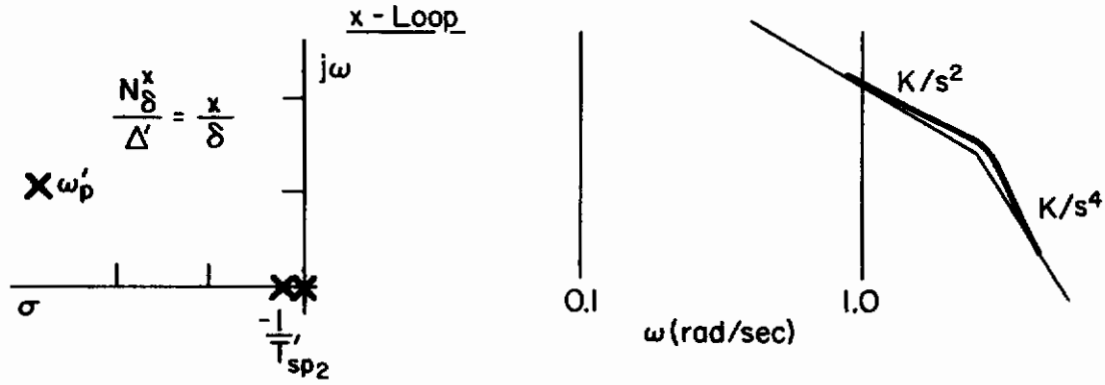

Controlled Element Features of Position Loop

In summary, with attitude-loop augmentation the effective θ-loop controlled-element dynamics can span all asymptotic features associated with conventional VTOL (i.e., $K/s^2 \rightarrow K/s$) plus, depending upon the level of stiffness, those in which attitude response is dominated by a high-frequency second-order mode or command-loop features (i.e., $\theta/\delta \doteq K$). We have also noted that the outer or translational control loop is modified by the attitude feedback. The features of this loop will vary between K/s^4 and K/s^2 in the critical 1 rad/sec region.

We are now better equipped to appraise the features associated with the satisfactory and unacceptable dynamics. First of all, at the lower stiffness levels ($1/T_E < 1/T_{sp_2}$), the dynamics are equivalent to conventional VTOL dynamics, and thus we may assume that the previously described boundaries of Table III are valid. A number of cases in Ref. 9 may be cited to support this conclusion; however, it is appropriate to supplement these experimental findings by considering the SAS features of operational VTOL's such as the XC-142 tilt-wing vehicle. Reference 10 indicates that the XC-142 attitude stabilization system was designed with $1/T_E \doteq 0.5 < 1/T_{sp_2}$.* The sketch below

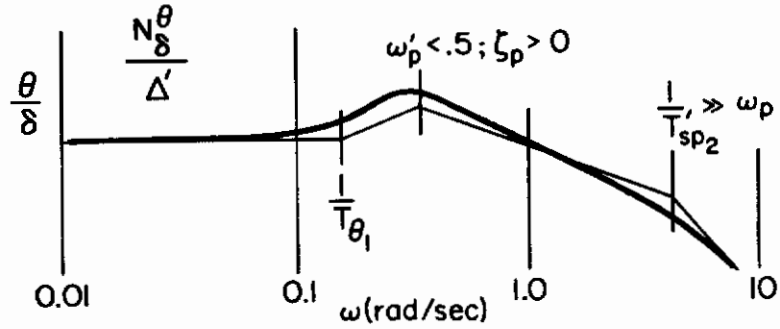

Attitude Loop Bode Features, XC-142

*The reader may easily verify this fact from the reference by remembering that in the attitude transfer function the numerator term $1/T_{\theta_2}$ is approximately equal to the denominator aperiodic root of $1/T_{sp_1}$, that is, $1/T_{\theta_2} \doteq 1/T_{sp_1} \doteq -Z_w$.

shows the resulting effective θ/δ controlled-element Bode for this augmentation. A comparison of these Bode features with the satisfactory boundary conditions of Table III verifies that the θ-loop features are satisfactory. In particular, the θ-loop has a broad K/s region near 2 rad/sec and the low-frequency ($\omega_p < 0.5$) phugoid mode is stable.

We conclude, therefore, that VTOL aircraft incorporating attitude feedback systems with $1/T_E < 1/T_{sp_2}$ should, for classification purposes, be considered as conventional. Turning therefore to the effective attitude systems, where $1/T_E > 1/T_{sp_2}$, we consider now the satisfactory and unacceptable dynamic features for the M_θ augmented vehicles, where $1/T_E > 1/T_{sp_2}$.

The Bode sketches in Fig. 4 illustrate the dynamic features which fall into the satisfactory and unacceptable situations. These features were derived from the data presented in Appendix B.

The satisfactory dynamics are described by a single Bode form for both the θ/δ and x/δ responses (see Fig. 4a). These detailed Bode features are given in Table V. (The primes indicate augmented basic factors.)

The unacceptable dynamic situations (see Fig. 4b) are dominated by the lightly damped second-order mode which appears in both the θ- and x-responses. The pole/zero features for this boundary are $\omega_p' > 0.8$; $\zeta_p' < 0$ and $1/T_{\theta_1} \doteq 1/T_{sp_2}'$.

TABLE V

SATISFACTORY CONDITIONS FOR ATTITUDE AUGMENTATION SYSTEMS

MOTION QUANTITY	DESCRIPTIVE FEATURES	
	ASYMPTOTES (FREQUENCY REGION)	CONDITIONS
Attitude (θ-loop)	K $(1/T_{sp_2}' < \omega < \omega_p')$	$1/T_{sp_2}' \doteq 1/T_{\theta_1}$ $2 < \omega_p' < 5$
Position (x-loop)	K/s^2 $(1/T_{sp_2} < \omega < \omega_p')$	$\zeta_p' > 0.25$

b. Translational or Position-Loop Augmentation. If we consider the conveniently-measured time derivatives of position as suitable feedbacks, the augmentation features for a position loop are akin to those for attitude stabilization. For example, the dynamics obtained by feeding back linear acceleration or attitude are essentially the same, i.e.,

$$\frac{x}{\theta} \doteq \frac{-g}{s(s + 1/T_{\theta_1})}$$

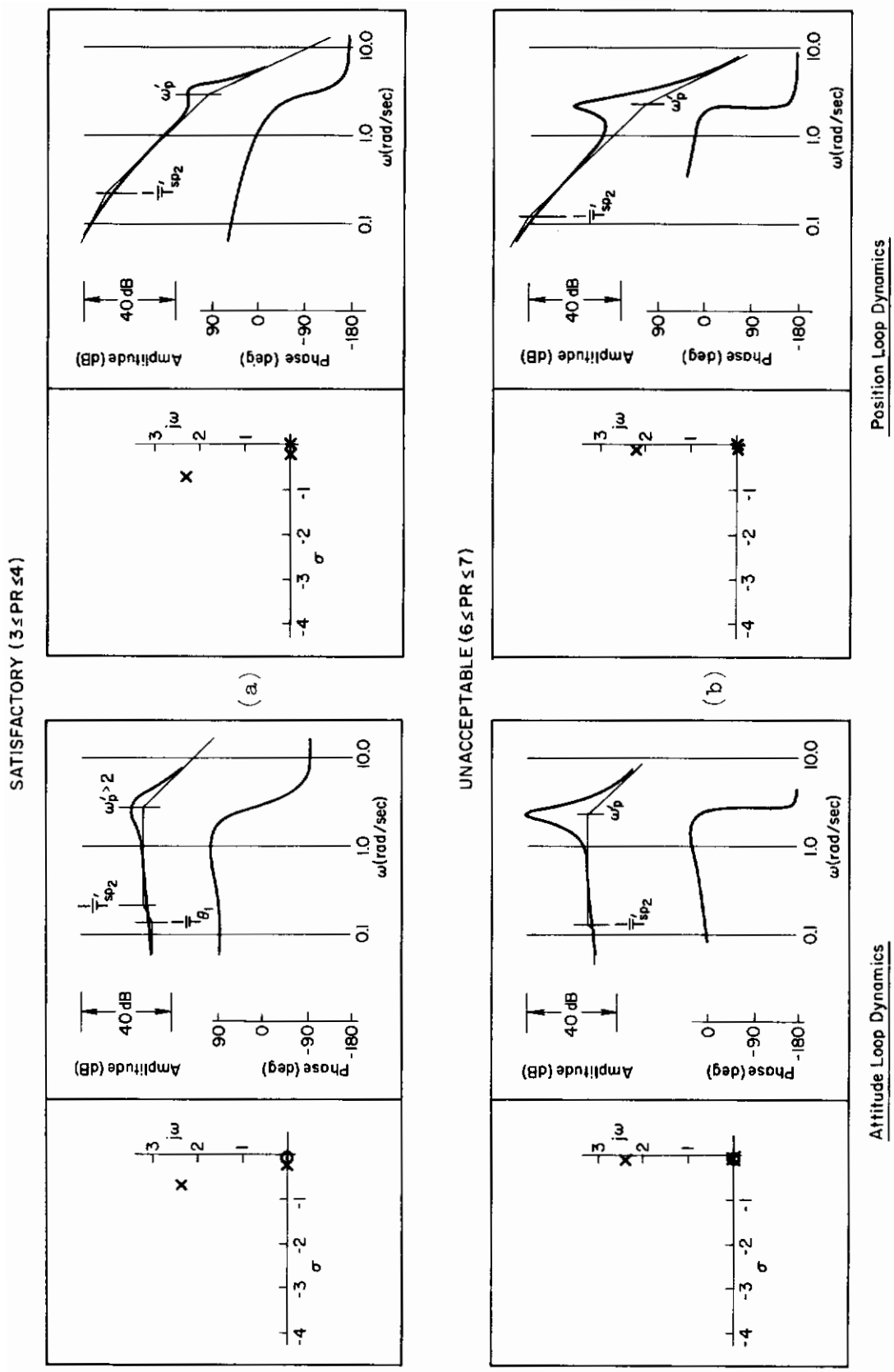

Figure 4. Effective Controlled Element for Attitude Augmentation ($1/T_E > 1/T_{sp_2}$)

and for $1/T_{\theta_1} \doteq 0$, $a_x/\theta \doteq -g$. This x/θ response ratio thus indicates that basically no new dynamic features will result from a linear acceleration feedback to the elevator. For instance, the ratio of an acceleration feedback gain to a θ feedback gain, $Ka_x/K\dot{\theta}$, is a lead equivalent to $K_\theta/K_{\dot{\theta}}$ or $1/T_E$ and the discussions and criteria covering the θ-loop dynamics would be expected to apply.

Similarly the use of translational velocity feedback to an axial-force or thrust control in effect changes the u derivatives, X_u, Z_u, and M_u; but such changes do not alter the general character of the loop dynamics, which remain the same as for the θ and $\dot{\theta}$ feedbacks. We may thus consider the outer loop or translational augmentation as an extension of the θ, inner-loop features. The tentative requirements would therefore have to be based upon an assumption that the inner-loop requirements are satisfied first. To satisfy the inner-loop damping requirement we may employ a combination of either M_q or X_u feedback because of the equivalent effect of these terms in the characteristic equation [i.e., $s(s-X_u)(s-M_q)+gM_u = 0$]. However, X_u augmentation has the additional advantage of changing the attitude numerator term, $1/T_{\theta_1}$, which will improve the pilot's closed-loop control of the outer loop. This closed-loop aspect is explored in subsection B.2.b.

At present only a limited amount of data is available to define the properties of the translational mode augmentation. In fact, aside from the very limited descriptive experiments conducted by Ellis and Carter in Ref. 11, the only pilot opinion information available is that obtained by A'Harrah and Kwiatkowski (Ref. 12). These latter results were obtained with an "effective" velocity feedback to a pure X-force thrust control. In this case the derivative, $X_u \doteq -1/T_{\theta_1}$, was varied to simulate changes in the velocity stability of the vehicle. The simulation assumed that airspeed (rather than inertial or ground speed) was sensed and, accordingly, the tested u-gust disturbance increased with X_u. We would expect the pilot opinion data to reflect some conservatism because of the higher gust sensitivity, which would not occur with inertial velocity feedback.

The dynamic characteristics derived from these data (i.e., Ref. 12) define the two Bode sketches in Fig. 5. Both of these cases are near the satisfactory boundary (i.e., $3 < PR < 4$). In general, the features of the two Bode sketches have similar attitude features; each Bode response has the appearance of a stable, low-frequency attitude system. This is because of the tendency of the augmented numerator term $1/T'_\theta$ to be equal to either the phugoid mode frequency, ω'_p (Fig. 5a), or the short-period aperiodic mode, $1/T'_{sp_2}$ (Fig. 5b).

In the x-loop the features have slightly different characteristics (i.e., K/s to K/s^2) in the neighborhood of 1 rad/sec. This difference is due primarily to the level of the oscillatory mode frequency, ω_p. In the first case, the frequency is approximately 1 rad/sec, while in the second case it is closer to 0.5 rad/sec. In each case the oscillatory mode is stable and the effective damping, $\zeta_p\omega_p > 0.2$.

Some unacceptable dynamic features are identified from the X_u augmented data, also. These attitude-loop features have properties similar to the unacceptable conventional VTOL dynamics described in Fig. 4b [i.e., $\omega'_p > 0.8$ rad/sec, $\zeta_p < -0.15$ (unstable), and K/s^2 asymptotic dynamics near 2 rad/sec^2]. Here a K/s^2 feature is produced because the numerator

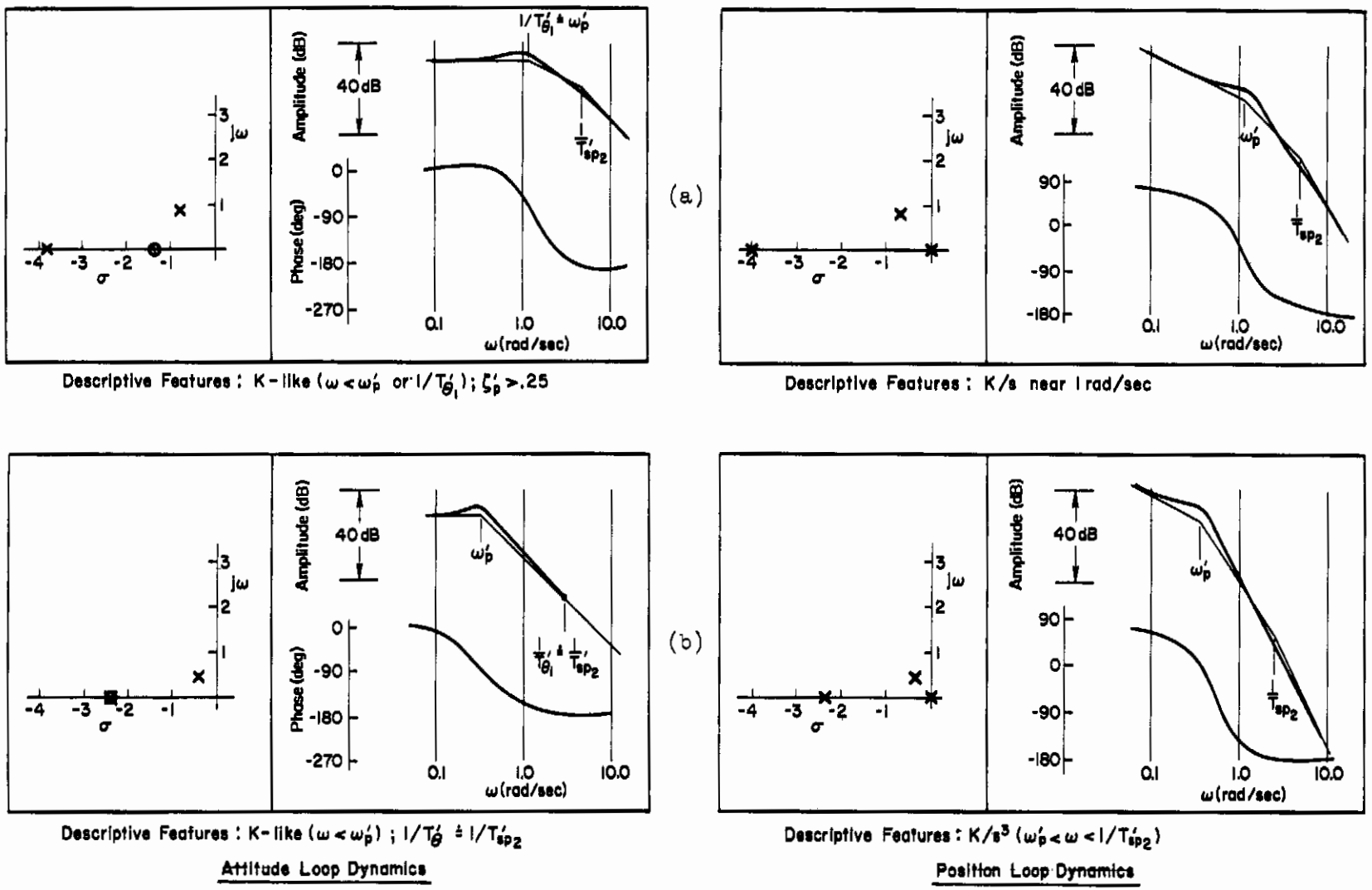

Figure 5. Effective Controlled Element Dynamics, Position or Translation Augmentation, Satisfactory ($3 \leq PR \leq 4$) Bode Features

term $1/T'_{\theta_1}$ nearly cancels the short-period mode, $1/T'_{sp_2}$. Thus the dominant feature of the attitude-loop ($\theta \rightarrow \delta_e$) is the second-order unstable phugoid mode (see Fig. 6).

Basically, the asymptotic dynamic forms for the position-loop features are K/s below $\omega_p \doteq 1$ rad/sec, but break rapidly to K/s^4 at the short-period root, $1/T_{sp_2}$. A comparison with the unacceptable features for conventional VTOL system shows that, except for the small region of K/s^3 in the present case between ω'_p and $1/T'_{sp_2}$ [i.e., $\omega'_p \doteq 1/2(1/T_{sp_2})$], both have similar asymptotic features.

We may assume on the basis of the limited results that the characteristics are generally representative of satisfactory and unacceptable conditions, respectively, but not necessarily of a boundary, because of the relatively poor coverage in pilot rating afforded by the available data. The range of detailed dynamics expressing these conditions is shown in Table VI.

TABLE VI

TENTATIVE CONDITIONS FOR TRANSLATIONAL AUGMENTATION SYSTEMS

OPINION LEVEL	MOTION QUANTITY	DESCRIPTIVE FEATURES	
		ASYMPTOTES (FREQUENCY REGION)	CONDITIONS
Satisfactory	Attitude (θ-loop)	K ($\omega < 1/T'_{sp_2}$ or ω'_p)	$1/T'_{\theta_1} \geq \omega_p$ $\zeta'_p > 0.25$
	Position (x-loop)	K/s (near 1 rad/sec ω_{c_x})	$1/T'_{sp_2} > 1/T'_{\theta_1}$ or ω'_p $1/T'_{sp_2} > 2.0$
Unacceptable	Attitude (θ-loop)	K/s^2 ($\omega > \omega_p$)	$\omega'_p > 1$ rad/sec $\zeta'_p < -0.2$
	Position (x-loop)	$K/s^3 \rightarrow K/s^4$ (above 1 rad/sec ω_{c_x})	$1/T'_{sp_2} \doteq 1/T'_{\theta_1}$

c. Combined Attitude and Translational Augmentation. The effective controlled-element features (see Table IV) for combined attitude and translational feedback has been studied briefly in Ref. 11. While no pilot opinion data were given, it is possible to judge rating levels from the descriptive comments made during simulated hovering flight. In addition, these data indicated clearly that the effective vehicle forms are unchanged by the θ and u combination of feedbacks.

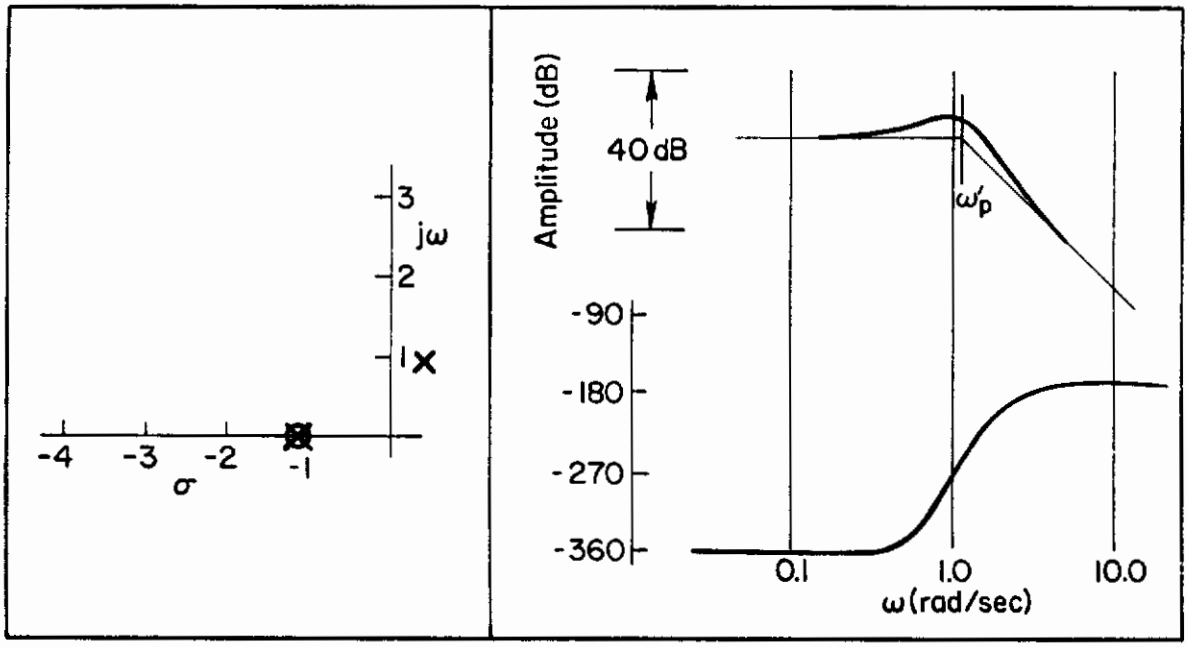

Attitude θ/δ $(1/T_{\theta_1} = 1/T'_{sp_2})$

Descriptive Features : $K/s^2 > \omega'_p$; $\omega'_p > 1$ rad/sec, $\zeta_p < -0.2$

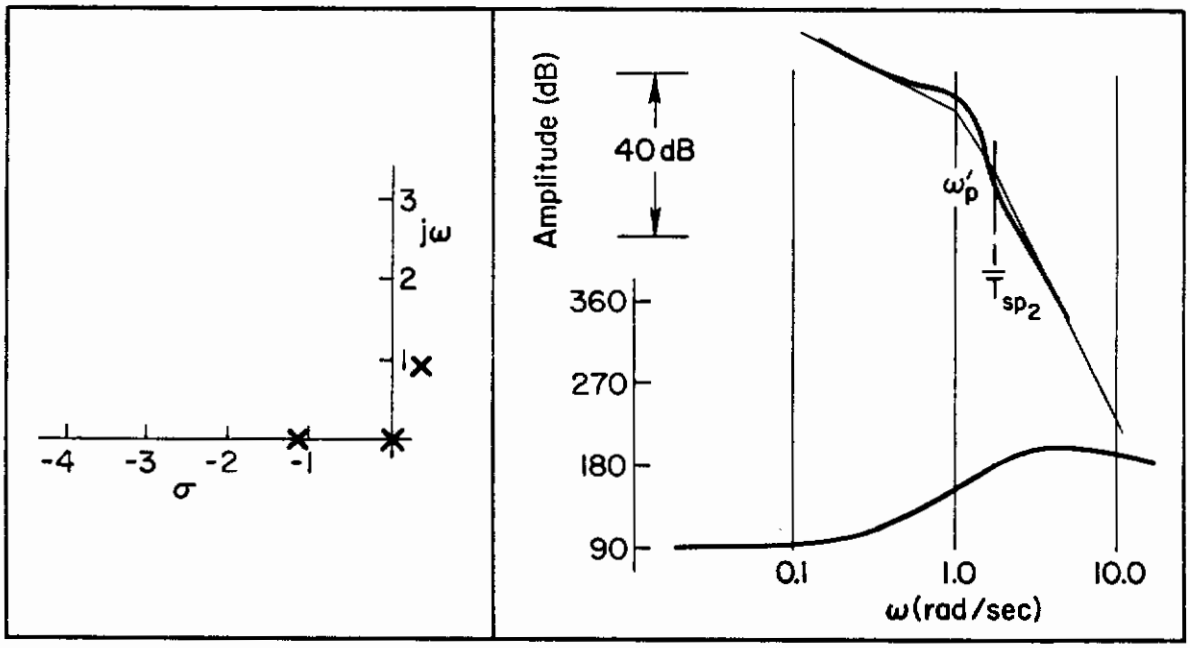

Position x/δ

Descriptive Features : $K/s^3 \rightarrow K/s^4$ above ω'_p or $1/T'_{sp_2}$

Figure 6. Effective Controlled Element Dynamics, Position or Translation Augmentation, Unacceptable $(6 \leq PR \leq 7)$ Bode Features

The three typical configurations which appear to indicate satisfactory handling qualities levels from the comments given in Ref. 11 are shown in Table VII.

In Configuration A the effective dynamics of the hovering vehicle are easily identified as

$$\omega_p' > 1.0 \quad ; \quad 1/T_{\theta_1}' \doteq \omega_p \quad ; \quad 1/T_{sp_2}' >> \omega_p' \quad ; \quad \zeta_p'\omega_p' \doteq 1$$

Except for the somewhat higher $\zeta_p\omega_p$, these features fit the conditions derived for the simple translational feedbacks. The comments of Table VII suggest a somewhat better than "satisfactory" hovering control situation, with or without gust inputs (see Fig. 7a).

In cases B and C, $1/T_{sp_2}' \doteq 1/T_{\theta_1}'$, $\omega_p' > 1/T_{sp_2}'$ or $1/T_{\theta_1}'$. The basic controlled-element features of this condition represent the converse of the above conditions; however, they fit the description for the satisfactory attitude ($1/T_E > 1/T_{sp_2}$) loop feedbacks. Here the θ/δ asymptotic feature is K-like below ω_p, and the x/δ feature is K/s near 1 rad/sec (see Fig. 7b).

These brief considerations suggest that the independent single-loop augmentation requirements must be maintained for the combined attitude and translational feedback systems. Also based upon these limited data, the condition described by

$$1/T_{\theta_1}' \doteq 1/T_{sp_2}'$$

$$\omega_p' > 2 \quad ; \quad \omega_p' > 1/T_{sp_2}'$$

$$\zeta_p' > 0.35$$

for combined M_θ and X_u augmentation is a satisfactory controlled element.

There are insufficient data to consider that the preceding augmentation dynamics define boundary conditions. However, as will be shown in the following subsection, since both the "effective" attitude loop and the position loop show desirable dynamics from the pilot's closed-loop viewpoint, we can anticipate that these features are representative of satisfactory handling quality levels.

B. PILOT/VEHICLE CLOSED-LOOP ASPECTS

The closed, multiple-loop aspects of the hovering task considered in this section are based on the effective vehicle dynamics defined as satisfactory and unacceptable in the previous section. The control structure considered is the basic series loop system shown in Fig. 8. Because of the numerous diverse dynamic situations in which closed-loop stability might be an important factor, the analysis efforts have been limited to detailed consideration of selective "conventional" VTOL dynamics, and a brief study of the simple attitude and translational augmentation systems.

TABLE VII

HOVERING FLIGHT

COMBINED FEEDBACKS θ and $\dot{\theta}$, u and $\dot{u}$

RUN NO.	CONFIG.	CONTROLLED ELEMENT DYNAMICS	GUST	COMMENT
30	A	$1/T'_{\theta_1}$ = 1.25 rad/sec; $1/T_{sp_2}$ = 3.2 rad/sec	No	Centered, held and moved easily.
31		ω'_p = 1.5 rad/sec; ζ'_p = 0.72	Yes	Can be held on or near center with small δ_s.
32	B	$1/T'_{\theta_1}$ = 1.5 rad/sec; $1/T_{sp_2}$ = 2.0 rad/sec	No	Small δ_s, slight oscillation.
33		ω'_p = 2.0 rad/sec; ζ'_p = 0.37	Yes	Can be held on or near center with small δ_s.
34	C	$1/T'_{\theta_1}$ = 1.5 rad/sec; $1/T_{sp_2}$ = 1.75 rad/sec	No	Very precise, moves quickly. Stops very precisely.
35		ω_p = 3.8 rad/sec; ζ_p = 0.7	Yes	Very precise, can cope with gusts easily.

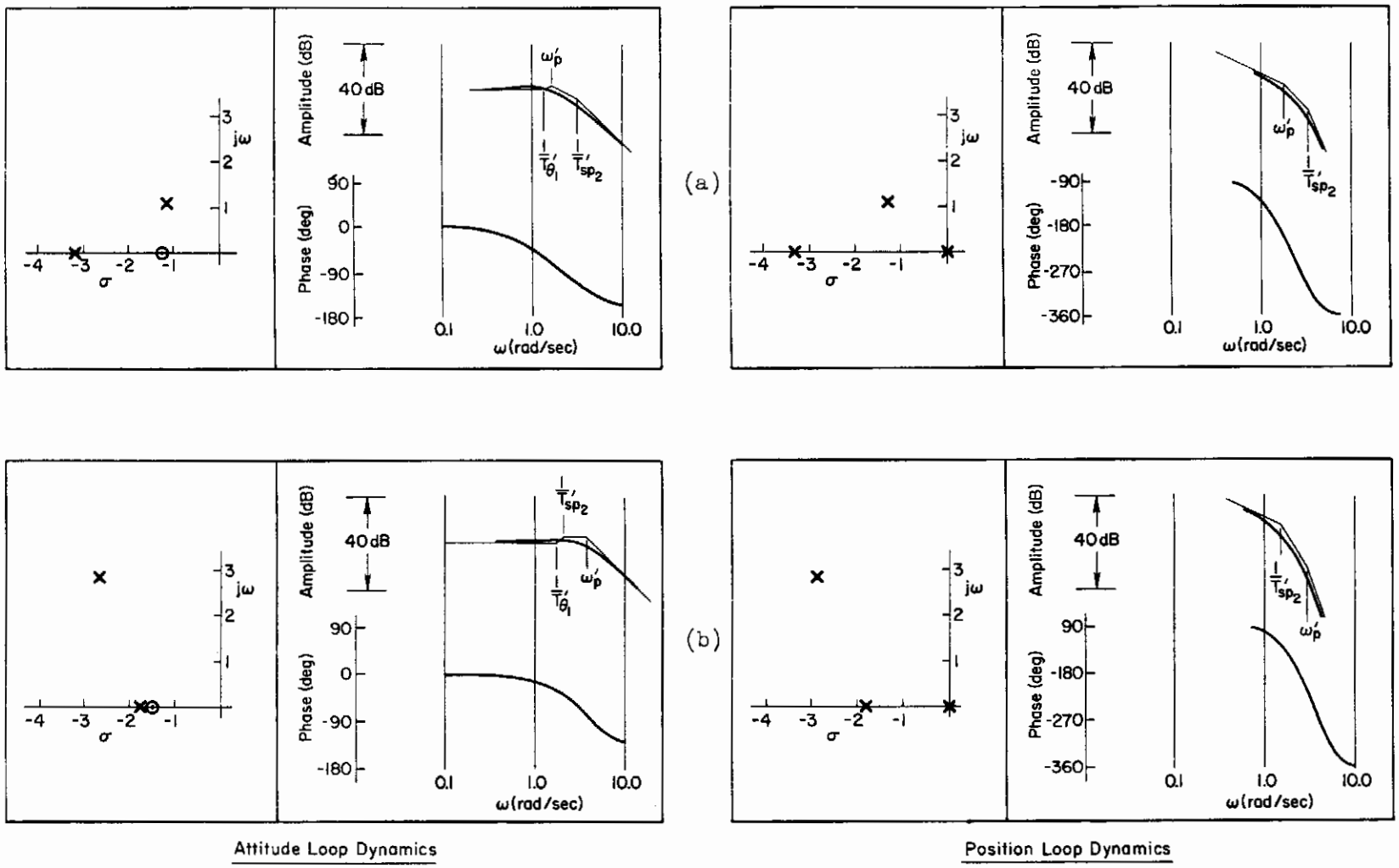

Figure 7. Effective Controlled Element Dynamics, Combined Attitude and Translational Augmentation, Satisfactory ($3 \leq PR \leq 4$) Bode Features

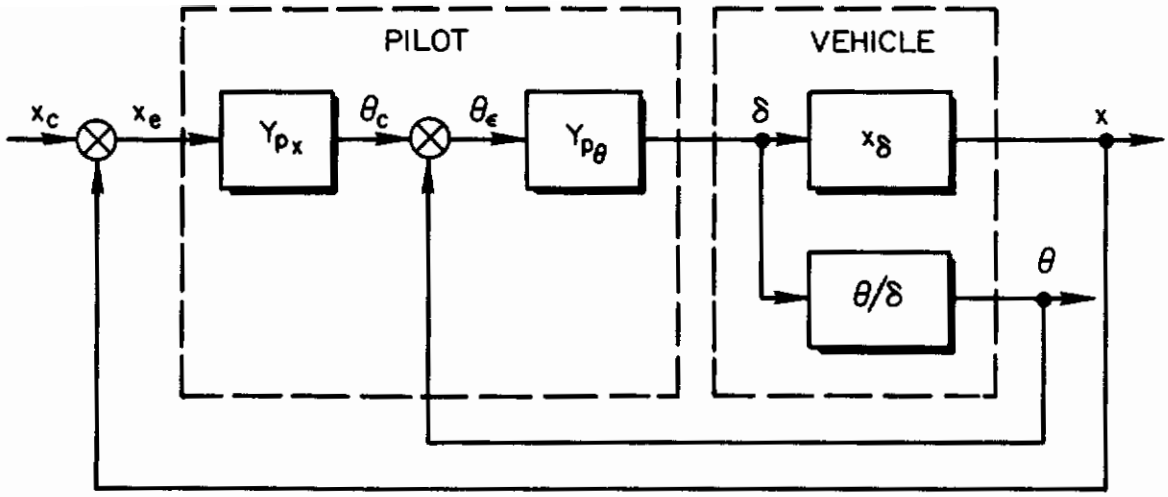

Figure 8. Series Closed-Loop Hover Control Structure

The pilot model features used in the closed-loop analyses are based on the controlled-element dynamics in the region of expected crossover. Recent measurements of the pilot describing function in a multiloop task involving a single controller (as in the present hover task) are reported in Ref. 13. These results support the use of the crossover model concept for these multiloop situations and indicate that the inner-loop (attitude) closures are quite similar to those of single-loop attitude tracking tasks. The representation of the pilot describing function is therefore based on the adjustment rules presented in Ref. 14 (for single loops).

The pilot models used in the present studies were (1) basic crossover model for stable controlled elements with K/s asymptotic features near ω_c, and (2) the extended crossover model for unstable controlled elements which approach the features of the critical attitude tracking task in the crossover region (see Refs. 15 and 16).

The detailed aspects of the selection and application of the pilot models used in this study of hover dynamics are presented in Appendix D for reference. However, in each of the control loop analyses the pilot's effective time delay, τ_e, is represented by a second-order lead/lag Padé approximation

$$e^{-\tau_e s} \doteq \frac{(s-4/\tau_e)^2}{(s+4/\tau_e)^2} \doteq \left(\frac{s-10}{s+10}\right)^2$$

where $\tau_e = 0.4$ sec.

1. Closed-Loop Considerations of Conventional VTOL Dynamics

Selected vehicle dynamic situations which cover the satisfactory and unacceptable controlled-element dynamics are considered in the following paragraphs. The exemplary closures shown here are representative and

define the pilot compensation requirements typified by the twenty situations studied in detail.

In addition, to simplify the discussion, the minimal compensation features are shown which provide a stable control situation. While these closures provide good inner-loop features and exhibit reasonable crossover properties throughout, the outer-loop (i.e., x-loop) often does not meet the specific crossover model closure rules suggested in Ref. 14. Typically, after the closure of the inner, θ-loop, the x-loop (outer-loop) dynamics are K/s^2-like (i.e., on the asymptotes). Strict adherence to the adjustment rules would require a low-frequency lead compensation for this loop to achieve a good K/s crossover region. This additional compensation is not considered in the present surveys, although a brief indication of the potential improvement in crossover frequencies is indicated.

a. **Closure Aspects of Satisfactory Dynamics.** Five representative, conventional vehicles having satisfactory handling qualities were analyzed. These are listed in Table VIII. Table IX identifies the data sources where each configuration was tested. Typical closure features for the attitude and the position loops are summarized in Tables X and XI. Basically the pilot compensation requirements indicated in these tables are not excessive and crossover frequencies are adequate for either the attitude or the position loops. Thus one can readily conclude that manual control by the pilot of these hover configurations is no particular problem.

The more subtle features of the pilot control requirements for these controlled-element dynamics are obtained from the system surveys in Figs. 9 through 14. The three controlled elements analyzed in these surveys are Configurations 1, 3, and 5 of Table IX. The attitude dynamics of these configurations range from a relatively unstable situation, Configuration 1, with a K/s^2 asymptote in the region of 2 rad/sec (Fig. 9) to the stable features of Configuration 5 (Fig. 14) which shows an extended region of K/s. The position loop, x/δ, looks like either K/s^4 or K/s^3 for the respective configurations. Attitude control is the basic requirement for each configuration and will be considered first.

In Fig. 9, control of the unstable situation and the pilot's normal desire for a net K/s-like crossover both require that he introduces a moderately high lead ($T_L \doteq 1.3$). This amount of lead effectively cancels the basic vehicle short-period root, $1/T_{sp_2}$. The minimum stable gain range then approaches 16 dB, which provides for a 2 rad/sec crossover having 6 dB gain and 20 deg phase margins, as shown. However, because of the degrading effects of lead on the pilot rating, this configuration is marginal [and cannot achieve the better pilot rating (i.e., PR < 4.0)].

The significant feature of this closure situation is the relation between the open-loop requirements in Table III and the predicted pilot compensation. In particular, it is obvious from Fig. 9 that limiting the unstable phugoid frequency to below 0.5 rad/sec in combination with the very-low-frequency lead term ($1/T_{\theta_1} \doteq 0$) sets the stage for the moderate pilot compensation needs of the above closure. Note that the stable gain range is bracketed by $1/T_{\theta_1}$ at the low-frequency end, and the $1/T_L$ lead required at the high-frequency end. The lead required is determined by the (negative) phase margin existing in the region of desired crossover (2 rad/sec) due to the ω_p and short-period root, $1/T_{sp_2}$, contribution. The minimal compensation

TABLE VIII

DYNAMIC CHARACTERISTICS FOR SATISFACTORY BOUNDARY DATA

CONFIGURATION NUMBER	APPROXIMATE AERODYNAMIC DERIVATIVES			VEHICLE TRANSFER FUNCTIONS
	X_u	gM_u	M_q	
1	−0.1	0.2	0	$\Delta = (s+0.62)[s^2-(0.458)(0.568)s+(0.568)^2]$ $N_\delta^\theta = M_\delta(s+0.1)$ $N_\delta^x = -gM_\delta/s$
2	−0.1	0.467	−1.33	$\Delta = (s+1.54)[s^2-(0.1)(0.551)s+(0.551)^2]$ $N_\delta^\theta = M_\delta(s+0.1)$ $N_\delta^x = -gM_\delta/s$
3	−0.1	0.733	−2.67	$\Delta = (s+2.77)[s^2+(0.0008)(0.515)s+(0.515)^2]$ $N_\delta^\theta = M_\delta(s+0.1)$ $N_\delta^x = -gM_\delta/s$
4	−0.1	0.733	−4.00	$\Delta = (s+4.06)[s^2+(0.064)(0.426)s+(0.426)^2]$ $N_\delta^\theta = M_\delta(s+0.1)$ $N_\delta^x = -gM_\delta/s$
5	−0.1	1.0	−5.33	$\Delta = (s+5.3654)[s^2+(0.0748)(0.4317)s+(0.4317)^2]$ $N_\delta^\theta = 1(s+0.1)$ $N_\delta^x = -gM_\delta/s$

TABLE IX

CONVENTIONAL VTOL DYNAMICS
SATISFACTORY BOUNDARY DATA SOURCES

CONFIGURATION NUMBER	DYNAMIC CHARACTERISTICS†			REFERENCE SOURCES					
	$1/T_{sp_2}$	ζ_p	ω_p	Bruel	A'Harrah	Princeton	Tapscott	Bell	UARL
0	0.0	0.0	0.0	x‡					
1	0.62	−0.458	0.568	x			x	x	
*						x	x		x
2	1.54	−0.10	0.551	x					
*							x		
3	2.77	0.0008	0.515	x	x				
*					x				x
4	4.06	0.064	0.426	x	x				
*					x	x		x	
5	5.36	0.075	0.432	x	x				x
*						x			

*The "x's" in these rows indicate intermediate dynamic characteristics.

† Numerator zero, $1/T_{\theta_1} \doteq 0.10$ sec^{-1} for all configurations.

‡Configuration 0 achieved satisfactory (PR = 3.2) rating in this moving-base simulation.

TABLE X

SATISFACTORY ATTITUDE INNER-LOOP CLOSURE FEATURES

CONFIGURATION NUMBER	PHASE MARGIN φ_m		GAIN MARGIN AT CLOSURE, K_m (dB)		CROSSOVER FREQUENCY, ω_c (rad/sec)		PILOT COMP.
	Nominal Closure ω_c	Peak	Nominal	Peak	Nominal	Maximum	$1/T_L$
1	15°	50°	4	10	2.3	3.5	1.0
2	25°	56°	5	25	2.9	3.0	1.54
3	25°	244°	7.8	42	3.0	5	2.77
4	25°	232°	3	34.5	3.0	4.2	4.059
5	25°	225°	3.5	34.5	3.0	4.3	5.3654

TABLE XI

POSITION OUTER-LOOP CLOSURE FEATURES FOR SATISFACTORY BOUNDARY

CONFIGURATION NUMBER	CROSSOVER FREQUENCY, ω_c (rad/sec)	
	$T_L = 0$	$T_L = 0.5$
1	0.4	1.5
2	0.65	1.45
3	0.7	1.4
4	0.63	1.25
5	0.60	1.4

needed is that required to cancel the adverse effects of the low-frequency short-period root.

At this point one significant feature of this controlled element can be indicated which apparently contributes to both the marginally satisfactory handling quality rating (i.e., PR $\doteq$ 4) given for low-gust condition ($M_u\sigma_{u_g} < 0.1$) and the deterioration of rating with an increase in the gust level. If we envision that the pilot attempts to tighten his control (e.g., to regulate

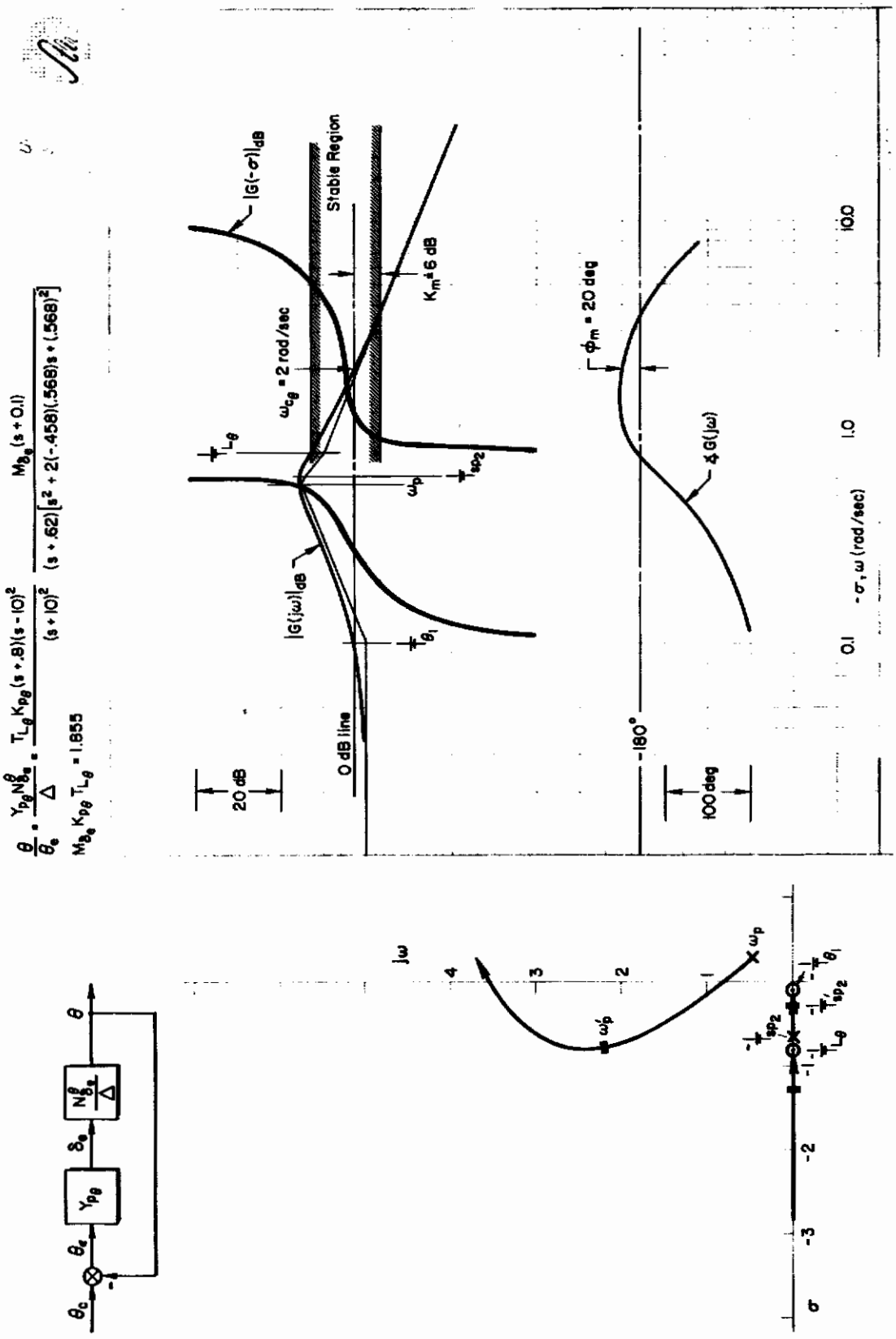

Figure 9. Attitude Loop Closures ($\theta \rightarrow \delta_e$) Satisfactory Condition, Configuration 1

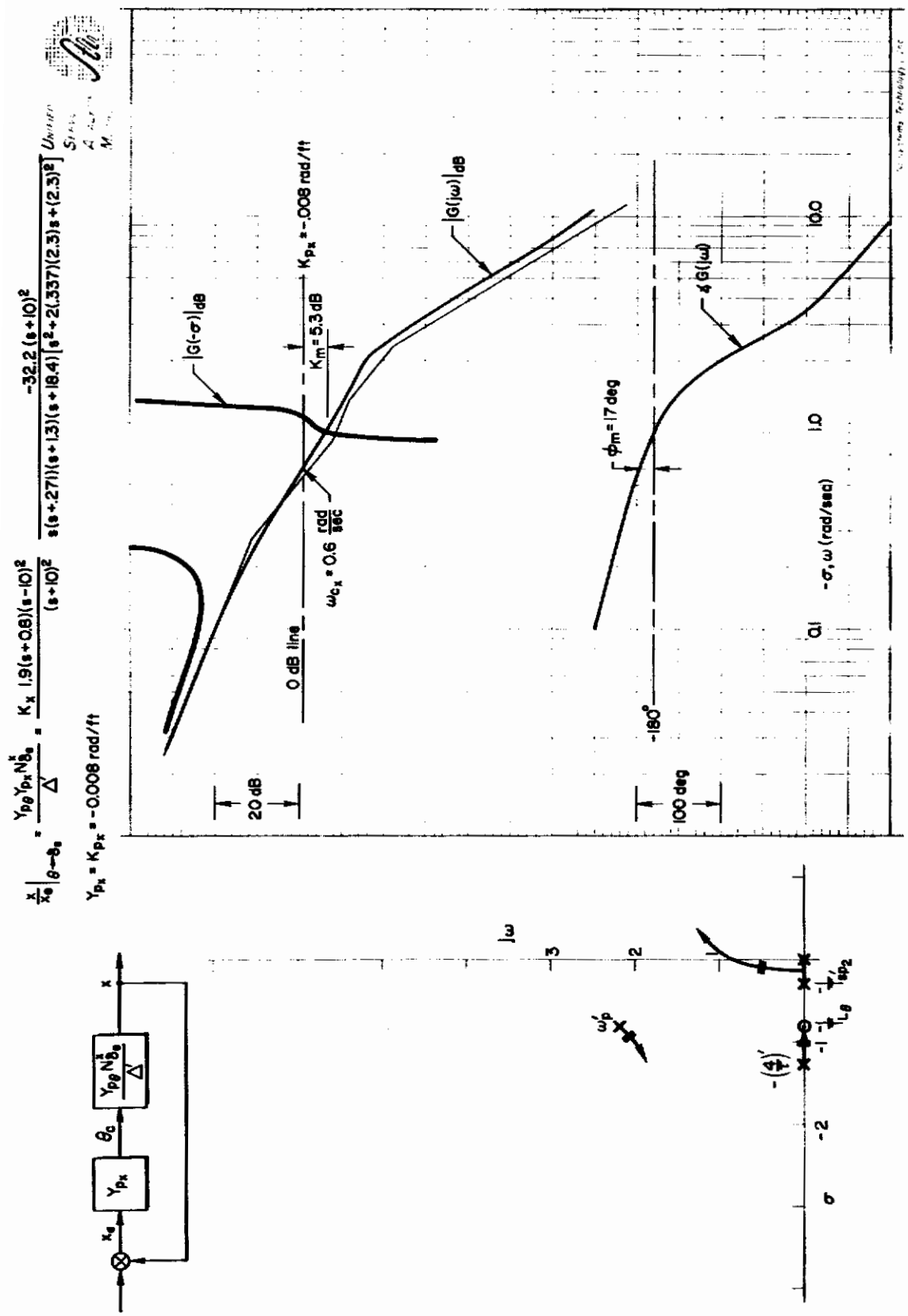

Figure 10. Position Loop Closure (x, θ → δe) Satisfactory Condition, Configuration 1

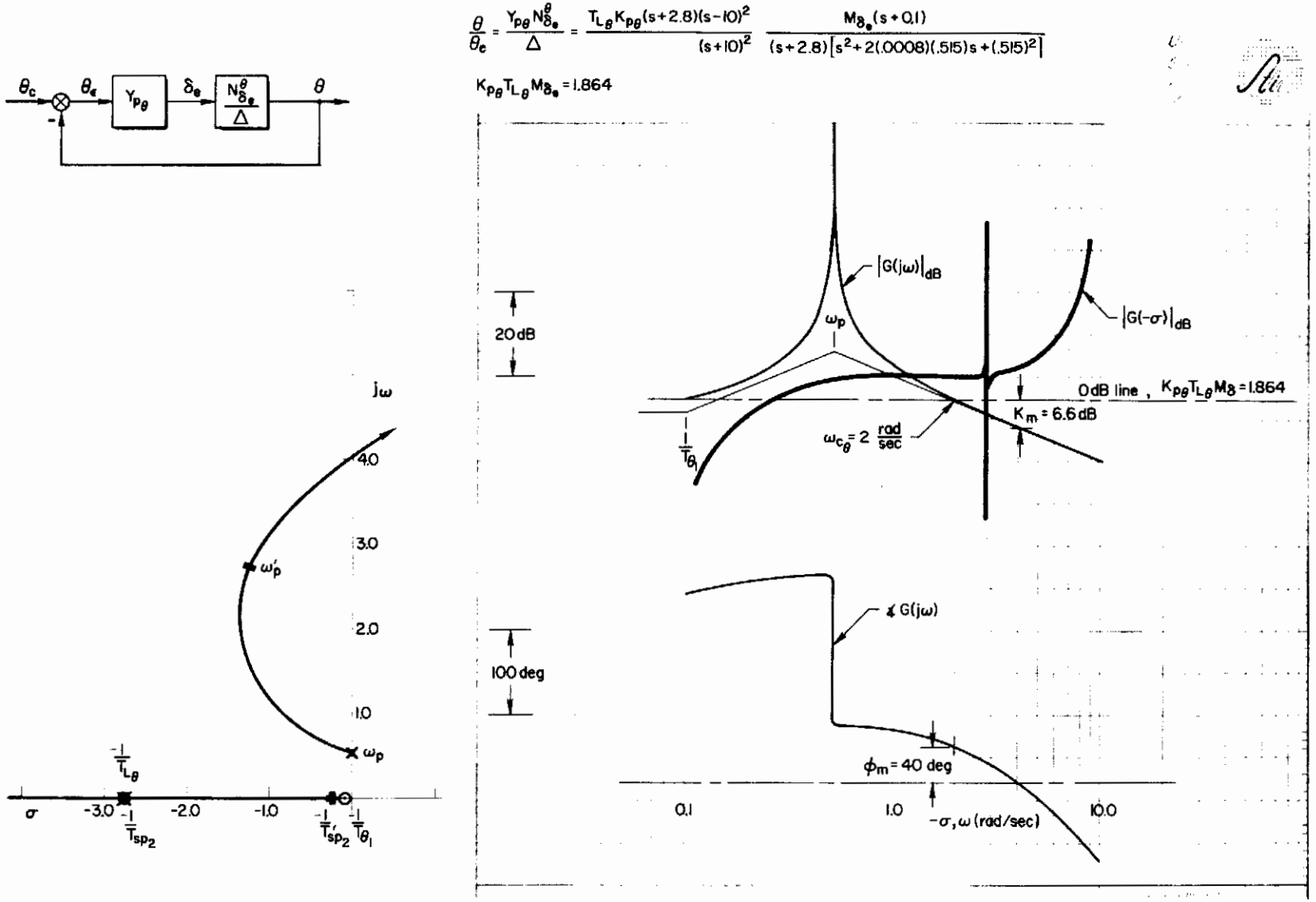

Figure 11. Attitude Loop Closure ($\theta \rightarrow \delta_e$) Satisfactory Condition, Configuration 3

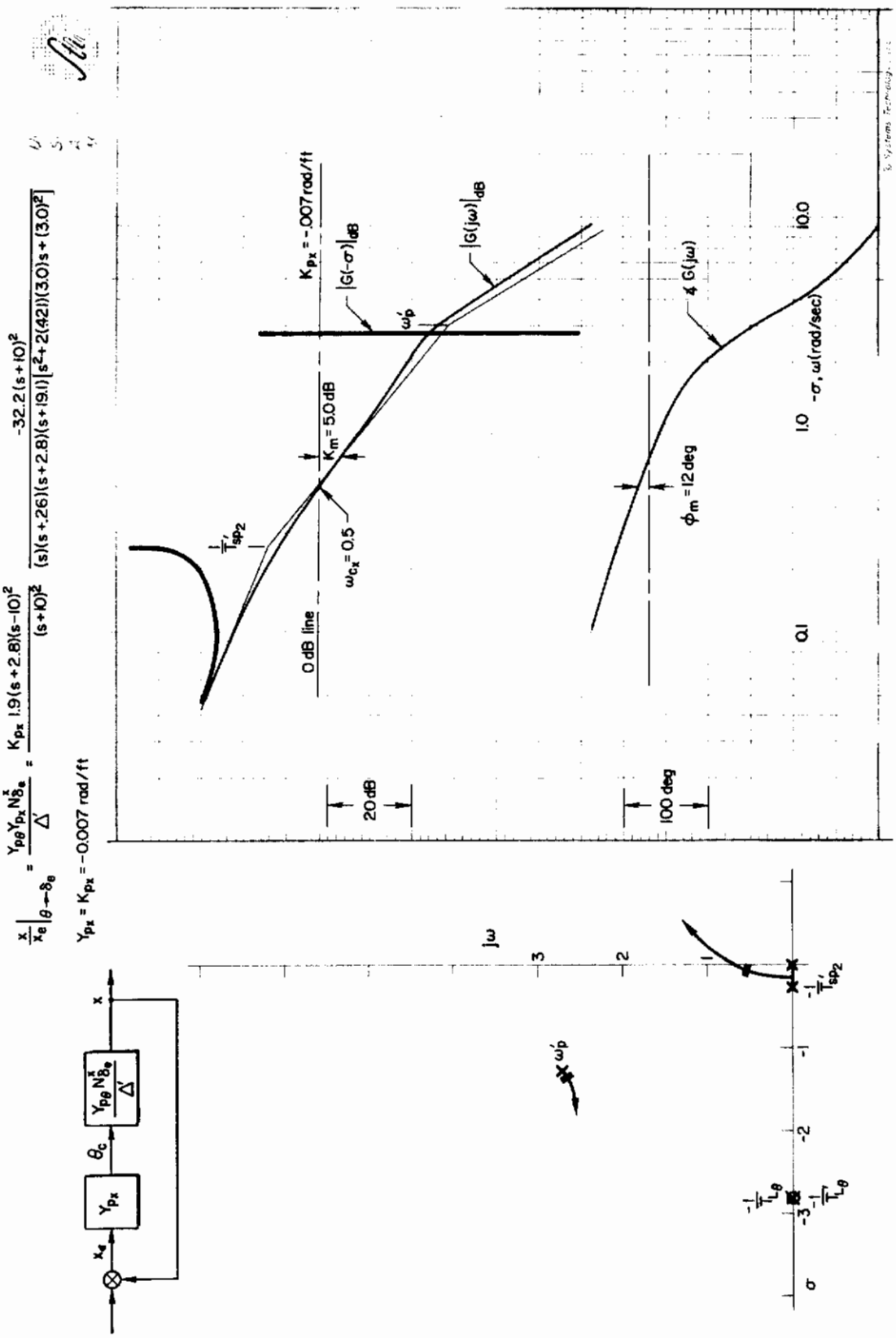

Figure 12. Position Loop Closure (x, $\theta \rightarrow \delta_e$) Satisfactory Condition, Configuration 3

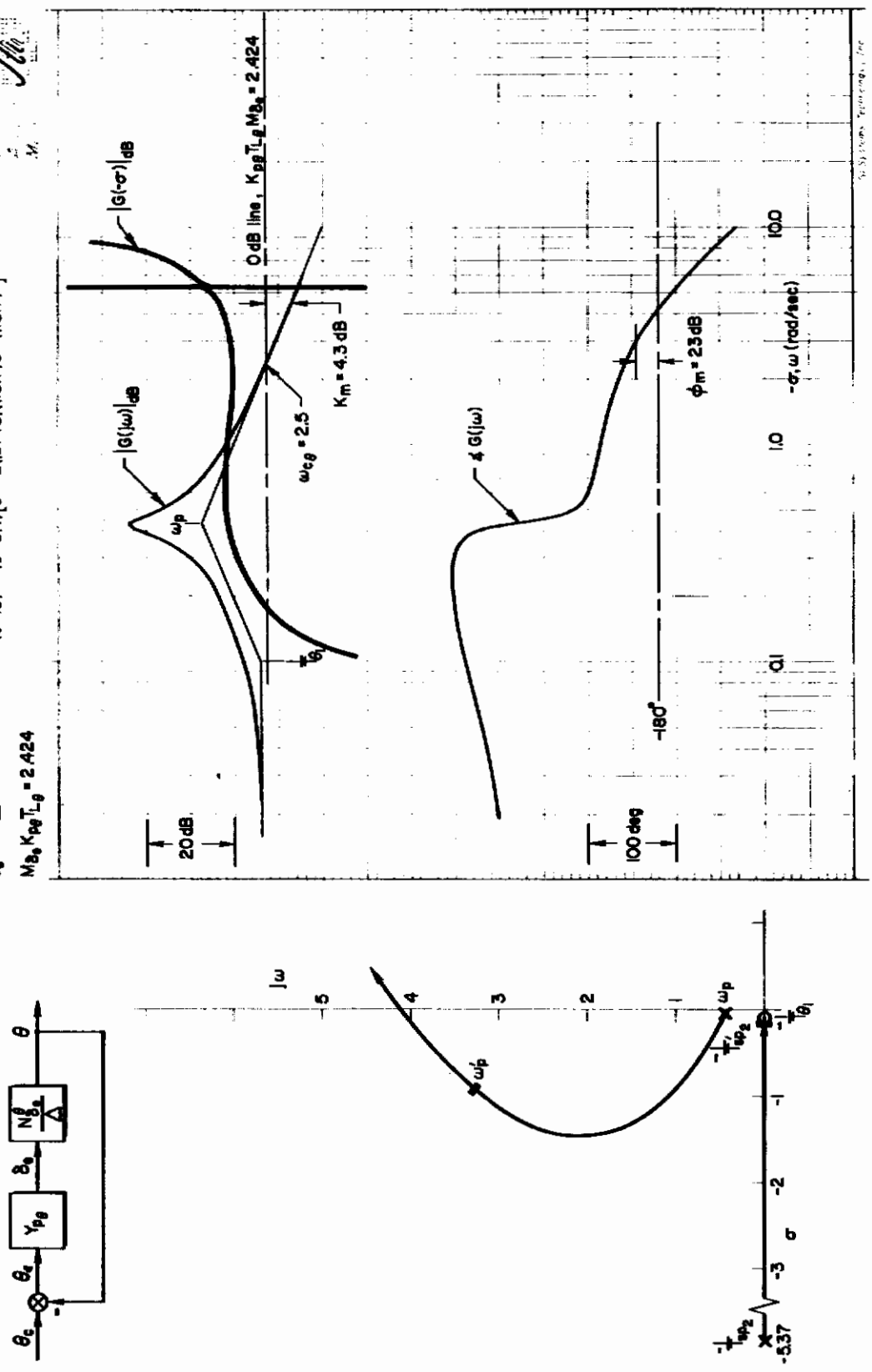

Figure 13. Attitude Loop Closure ($\theta \rightarrow \delta_e$) Satisfactory Condition, Configuration 5

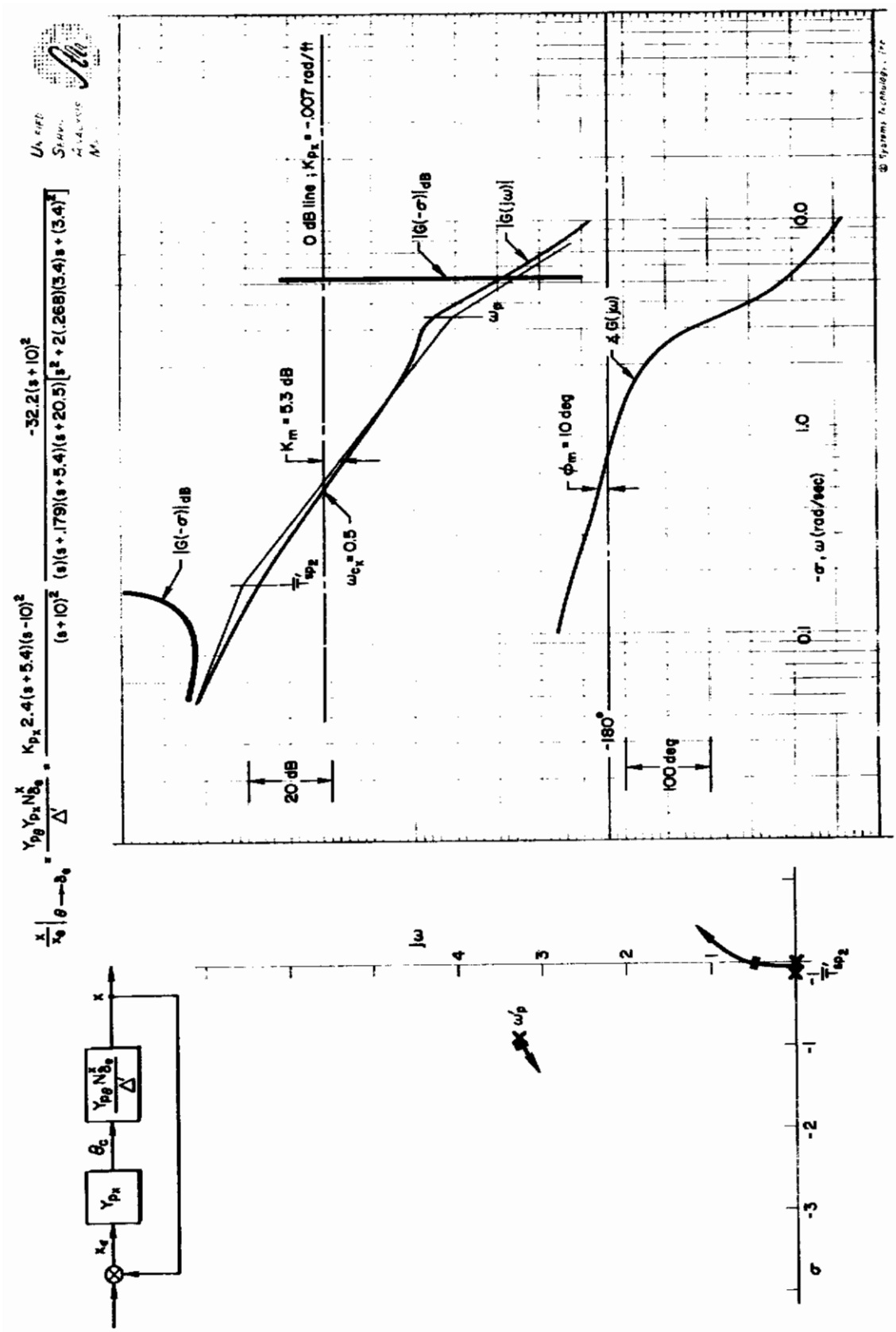

Figure 14. Position Loop Closure (x, θ → δe) Satisfactory Condition, Configuration 5

against a gust) by increasing his lead, the Bode sketch (Fig. 15) shows that, although the crossover frequency may be slightly increased, both the stable gain region and the low-frequency gain are reduced. In effect his net regulatory capability is decreased and the overall pitch attitude errors will increase. As will be discussed later in this section, situations where increased lead does not improve control have an unfavorable effect on the level of pilot opinion.

In summary, the restrictions deduced from the survey of satisfactory effective attitude controlled elements (i.e., ω_p, $1/T_{\theta_1}$, and $1/T_{sp_2}$) are clearly related in this case to closed-loop stability levels which may be achieved with minimal pilot compensation.

The closure features for the attitude loops of Configurations 3 and 5 are shown in Figs. 11 and 13. For these stable configurations the closed-loop properties are less dramatic. Minimal pilot compensation ($1/T_L > 2.5$) is required to cancel the short-period mode, $1/T_{sp_2}$, and eliminate its adverse effects on the phase margin. This minimal compensation does not adversely affect pilot rating and is adequate to achieve the desired 2 rad/sec crossover.

The position-loop closures are given in Figs. 10, 12, and 14 for each of the attitude-loop closures. As a result of closing attitude, the open-loop Bode features of the three configurations are equivalent, and all have K/s^2-like features near 1 rad/sec. The maximum crossovers with reasonable gain and phase margins are slightly greater than 0.5 rad/sec. With a pure-gain closure, the closed-loop situations are essentially equal. Note that the slightly improved crossover frequency ($\omega_{c_x} = 0.6$ versus 0.5 rad/sec) for Configuration 1 is due to the low-frequency lead introduced in the attitude loop. In the series closures used here, the inner-loop compensation carries over into the outer-loop. This follows from the characteristic equation given below:

$$\Delta'' = \Delta + Y_{p_\theta} N_\delta^\theta + Y_{p_x} Y_{p_\theta} N_\delta^x = \Delta' + Y_{p_x} Y_{p_\theta} N_\delta^x \qquad (1)$$

The closed-loop features for the three configurations are summarized in Table XII. These features can be judged representative of satisfactory handling qualities based upon the level of pilot compensation required to maintain a stable multiloop situation. The loop closures are not critical and appear tolerant of changes in pilot compensation.

b. **Closure Aspects of the Unacceptable Dynamics.** The effective controlled-element dynamics for five cases were used to study the closed-loop aspects of unacceptable ($6 < PR < 7$) handling qualities. However, in the following discussion only two cases are considered because of the basic similarity of the unacceptable data. The specific configurations discussed in this study are listed in Table XIII. Configuration 2 was obtained from Ref. 7, but similar features were tested in Refs. 12 and 17. The pilot ratings given for these controlled-element dynamics ranged from 5.3 (Ref. 7) to 6.5 (Ref. 12). This variance in rating is attributed to the differences in simulation techniques, i.e., fixed- versus moving-base. (The intersource rating differences are discussed in Appendix A.)

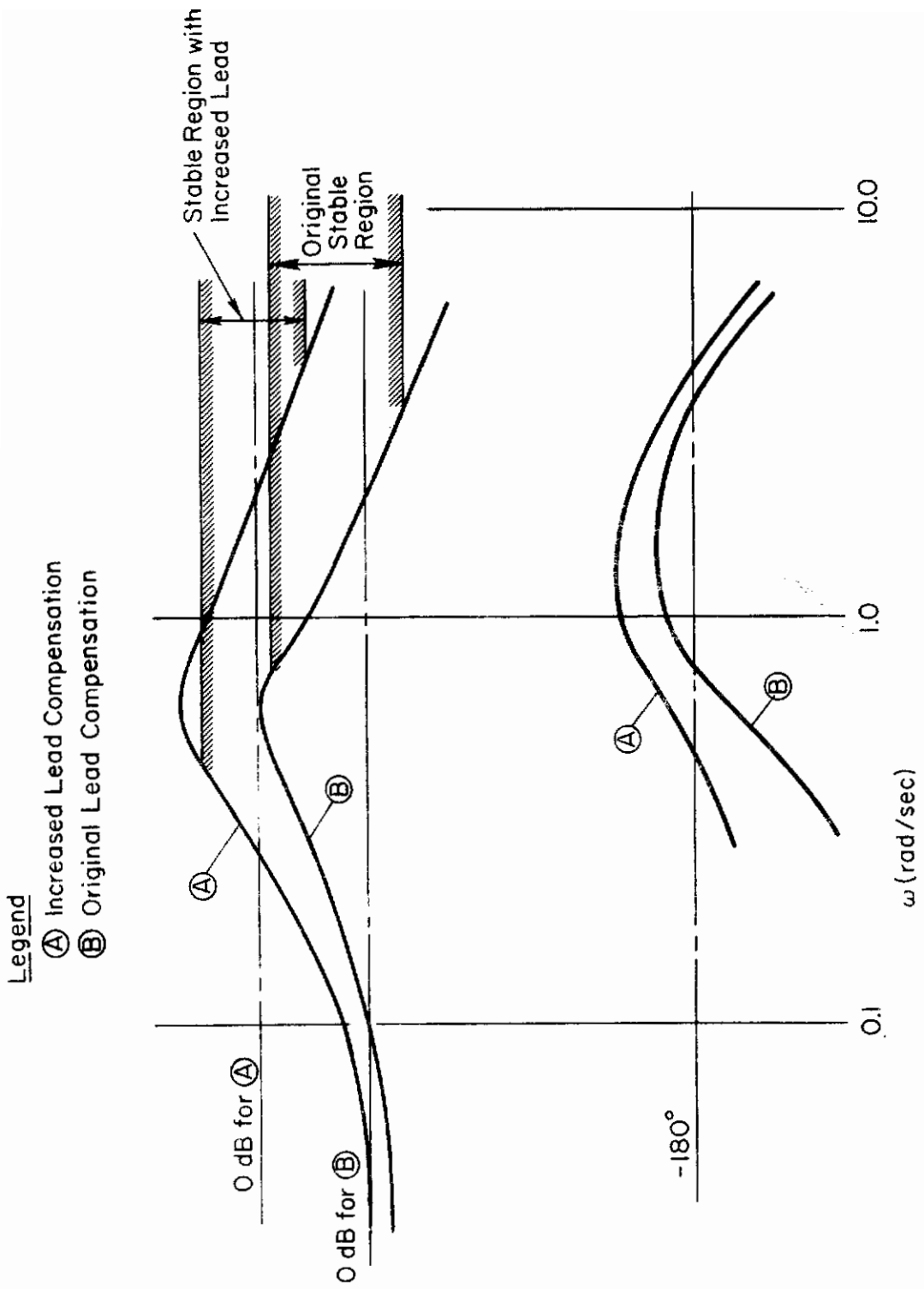

Figure 15. Effect of Lead Compensation on Attitude Loop

TABLE XII

SUMMARY OF SATISFACTORY CLOSED-LOOP FEATURES

	CONFIGURATION		
	1	3	5
$K_\theta T_{L_\theta}$	1.86	1.864	2.424
K_{θ_p}	1.5	5.16	13.00
$1/T_{L_\theta}$ rad/sec	0.8	2.77	5.37
ω_{c_θ} rad/sec	2	2	2.5
K_{m_θ} dB	6	6.6	4.3
Φ_{m_θ} deg	20	40	33
K_x rad/ft	−0.008	−0.007	−0.007
ω_{c_x} rad/sec	0.6	0.5	0.5
K_{m_x} dB	5.3	5.0	5.3
Φ_{m_x} deg	17	12	10

TABLE XIII

UNACCEPTABLE CONTROLLED ELEMENTS

CONFIG. NO.	AERODYNAMIC DERIVATIVES			DYNAMIC FACTORS				PR
	X_u	gM_u	M_q	$1/T_{\theta_1}$	$1/T_{sp_2}$	ζ_p	ω_p	
1	−0.15	3.38	−0.99	−0.044	1.9	−0.3	1.28	6.5
2	−0.10	0.467	0	0.1	0.81	−0.47	0.76	5.3

Since the dynamics of Configuration 1 were flight tested in Ref. 17 and were always rated 6.5 or greater in the other references, this configuration is considered more representative of overall unacceptable handling qualities.

The attitude response Bode features for Configuration 1 are shown in Fig. 16. The moderately high frequency ($\omega_p > 1$ rad/sec) and instability of the phugoid mode represent a control situation where use of the simple crossover model appears inadequate. In fact, except for the low dc gain, the Bode feature is quite similar to the second-order "critical task" (Ref. 16) sketched in Fig. 17. Note further that the pilot's control situations are equivalent in the crucial crossover frequency region.

The selection of the appropriate pilot model for this controlled element is considered in Appendix D. From these studies we can conclude that the extended, rather than the simple, crossover model of Ref. 14 is more appropriate for analysis of this divergent control situation. This refinement is desirable because the stable gain region is a function of the lowest stable crossover frequency. The low-frequency α-effects appearing in the extended crossover model,

$$Y_p \doteq K_p\left(T_L(j\omega) + 1\right) e^{-j(\omega\tau_e + \alpha/\omega)}$$

will influence this crossover point. The pilot reaction time delay, τ_e, and α are inversely related; that is, an increase in the low-frequency phase lag accompanies a decrease in the effective delay, τ_e. This conflict between the low- and high-frequency phase lags appears to be a significant factor in the pilot's ability to control diverging controlled elements such as the present Configuration 2. Typically, for unstable second-order or K/s^2 controlled elements, α's of approximately 0.33 rad/sec for τ_e's of about 0.35 have been observed (Ref. 14). For purposes of clarity, however, we will use the simple crossover model in the comparisons about to be made. This amounts to considering that additional low-frequency phase lags contributed by the α-effect will be uniformly degrading so that the actual situation is somewhat worse than that pictured (see Appendix D for details).

The closure features are described in the system survey of Fig. 16 for Configuration 1 and a nominal $\tau_e = 0.4$. Two closures are illustrated in the figure: (1) a nominal pilot lead ($1/T_L \doteq 1.3$ rad/sec) required for stability (i.e., $1/T_L \doteq 1/T_{sp_2}$) and (2) an extreme lead ($1/T_L = 0.2$ rad/sec) condition for maximum bandpass. It is obvious from the figure that increasing the lead beyond that required for stability (i.e., decreasing $1/T_L$) decreases the stable gain range and the damping and frequency of the closed-loop phugoid mode (ω_p'), thereby potentially degrading the outer-loop closure and crossover frequency (see Fig. 16).

In the above control situation the pilot gain and lead equalization are constrained within narrow limits but otherwise are not necessarily demanding. In fact, the nominal lead value ($1/T_L = 1.3$) is less than that for several of the satisfactory conditions (Table X). However, the fact that increased lead does not improve the situation and that, as shown in Appendix D, only reductions in τ_e (with accompanying α-effects) are helpful, combine to make the configuration marginal. Furthermore, the expected error performance in regulating against gust disturbances will be poor because of the low closed-loop dc gain. Attempts to improve the latter by adopting low-frequency lag won't work because the lag will also appear in the outer x-loop (Eq. 1) where it is intolerable. Also the introduction of low-frequency lag would require pilot generation of a double lead at higher frequency in the inner loop to obtain the net lead required for stable crossover. Such activities are inimical to good ratings.

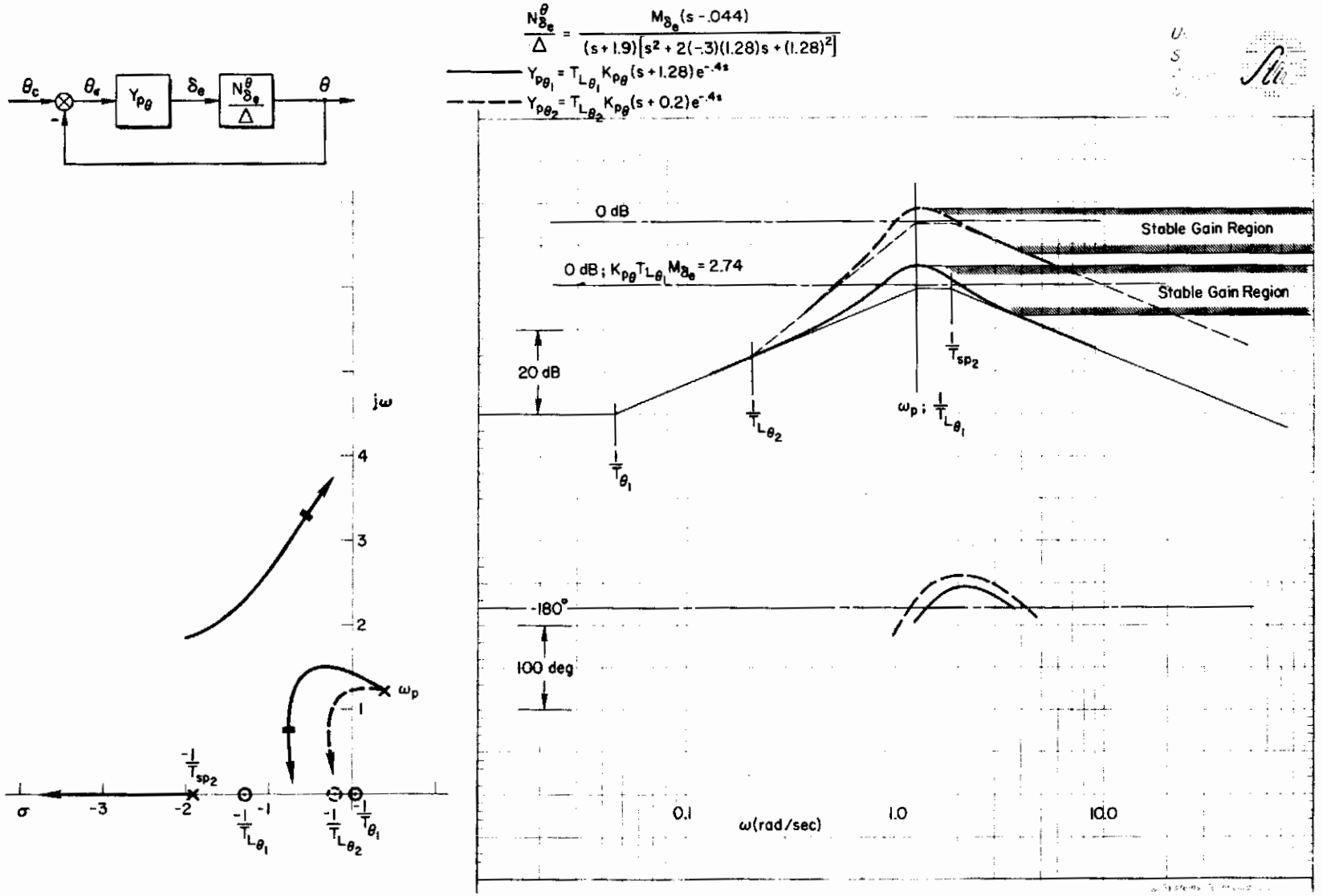

Figure 16. Attitude Loop Closure ($\theta \rightarrow \delta_e$) Unacceptable Dynamics, Configuration 1

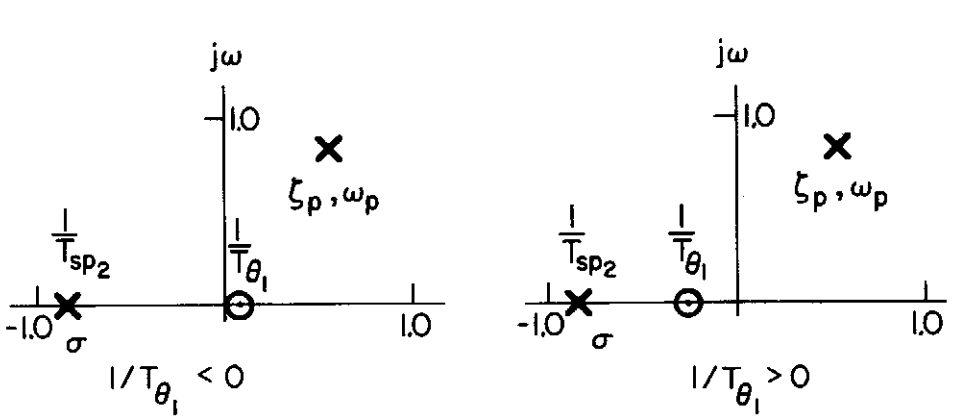

Vehicle Dynamics , Typical Data for PR ≐ 6.5

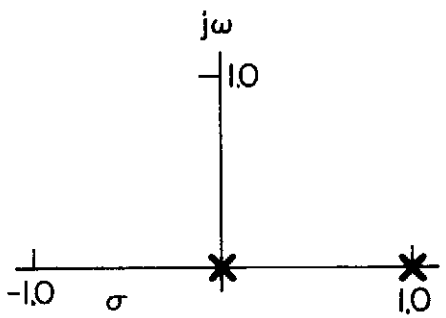

Second Order "Critical Task" Dynamics

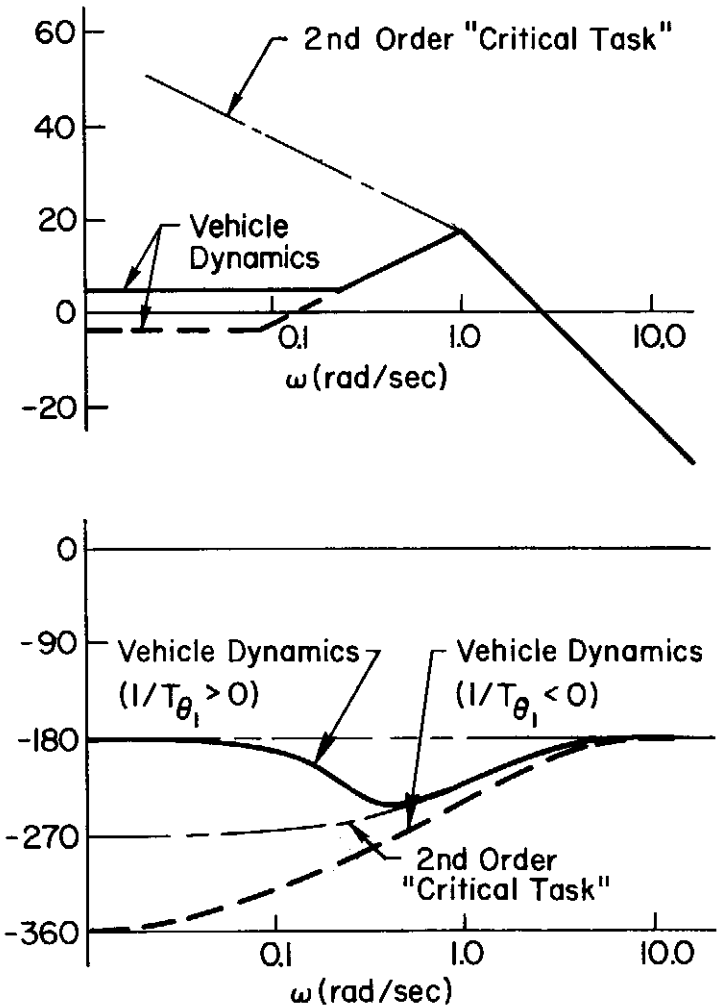

Figure 17. Comparison of Unacceptable (PR ≐ 6.5) Vehicle Dynamics with Second-Order "Critical Task" Dynamics

The closure of the x-loop for the nominal lead condition is shown in Fig. 18. Basically the higher closed-loop phugoid mode, ω_p', is beneficial in the x-loop and affords a K/s-like feature near 1 rad/sec. A simple gain closure can be used by the pilot without conflicting with the adjustment rules of Ref. 14.

The larger ω_p' and resulting x-loop improvement may be traced directly to the basic vehicle static stability term M_u as was noted in Ref. 2; however, it is apparent that the attitude-loop stability and regulation demands imposed on the pilot by this larger M_u will far outweigh any gain.

The closures for Configuration 1 of Table XIII are shown in Figs. 19 and 20 for the θ- and x-loops. It is obvious that the intermediate levels of ω_p and phugoid mode instability infer an intermediate rating level (relative to the previous 6.5 case). The pilot's task in the θ-closure is to provide a low-frequency lead to cancel the adverse phase effects of the vehicle's short-period mode (i.e., $1/T_L \doteq 1/T_{sp_2}$). With this equalization, a near-optimum stable gain region is obtained. A lead equalization below the phugoid mode (i.e., $1/T_L < \omega_p$) will tend to reduce the allowable gain region. This will effectively deteriorate the stability characteristics of the attitude loop because of the pilot's normal tendency to vary his gain. The pilot must depend upon his ability to reduce the effective time delay, τ_e, to improve the overall stability of the θ-loop (e.g., improve K_m and φ_m). However, the overall situation for this intermediate case is not much different from that shown for the marginally satisfactory case in Fig. 9. In fact, the major change appears to be the somewhat higher frequency at which pilot lead compensation is ineffective and the lower dc gain available. Both of these features are expected to degrade attitude regulation in gusty air.

The x-loop characteristics are generally unchanged from the previous satisfactory conditions and exhibit K/s^2 features above 1 rad/sec. As noted in the previous unacceptable case (Fig. 18), there is some improvement in the overall x-loop due to the larger ω_p, but the poor features of the θ-loop apparently dominate.

In summary, for conventional VTOL dynamics the unacceptable ratings ($6 < PR < 7$) are apparently due to deterioration of the attitude-loop stability and regulation, and the excessive equalization required of the pilot to improve the gain and phase margin significantly. The underlying aspect of the pilot equalization problem for these unstable elements is the relative ineffectiveness of normal lead generation; and the conflict between his desire to increase phase margin by decreasing τ_e and the accompanying low-frequency phase lag (i.e., α-effects). This tie between τ_e and α involves the neuromuscular system and hence represents a physical limit to the pilot's abilities.

c. Performance Trends for Conventional Dynamics. Performance considerations for conventional VTOL dynamics have been studied for the selected pilot rating conditions in Table IX. The closed-loop error characteristics for attitude, θ, and position, x, due to a random gust, were calculated using the closures obtained for minimal pilot compensation. The gust power spectra representations given in Ref. 2 were utilized and the rms errors were normalized on the basis of a horizontal gust, σ_{u_g}, of 1 ft/sec. The closed-loop gust response transfer functions are given in Appendix C for the multiloop hover task assuming a series control structure.

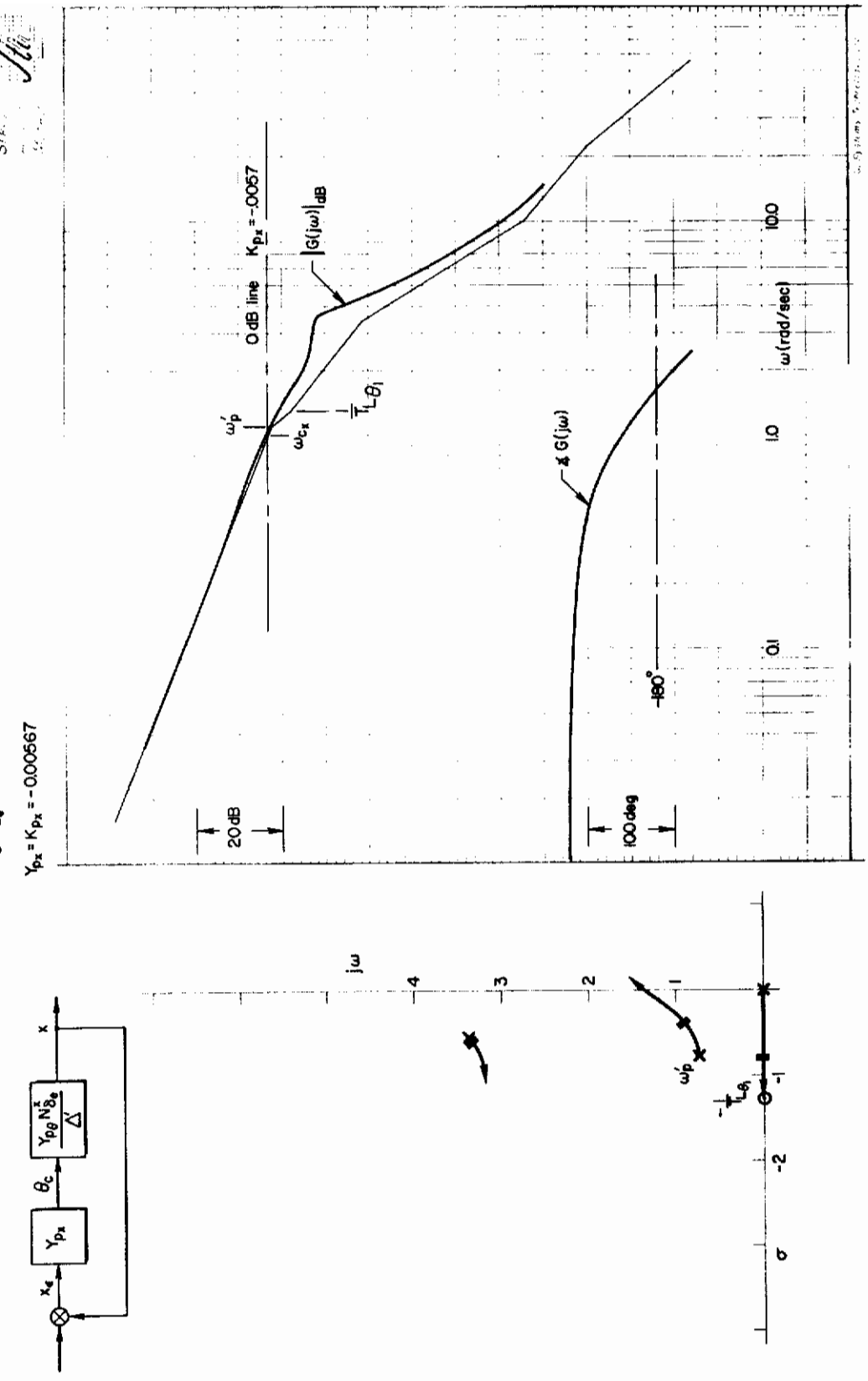

Figure 18. Position Loop Closure (x, $\theta \rightarrow \delta_e$) Unacceptable Condition, Configuration 1

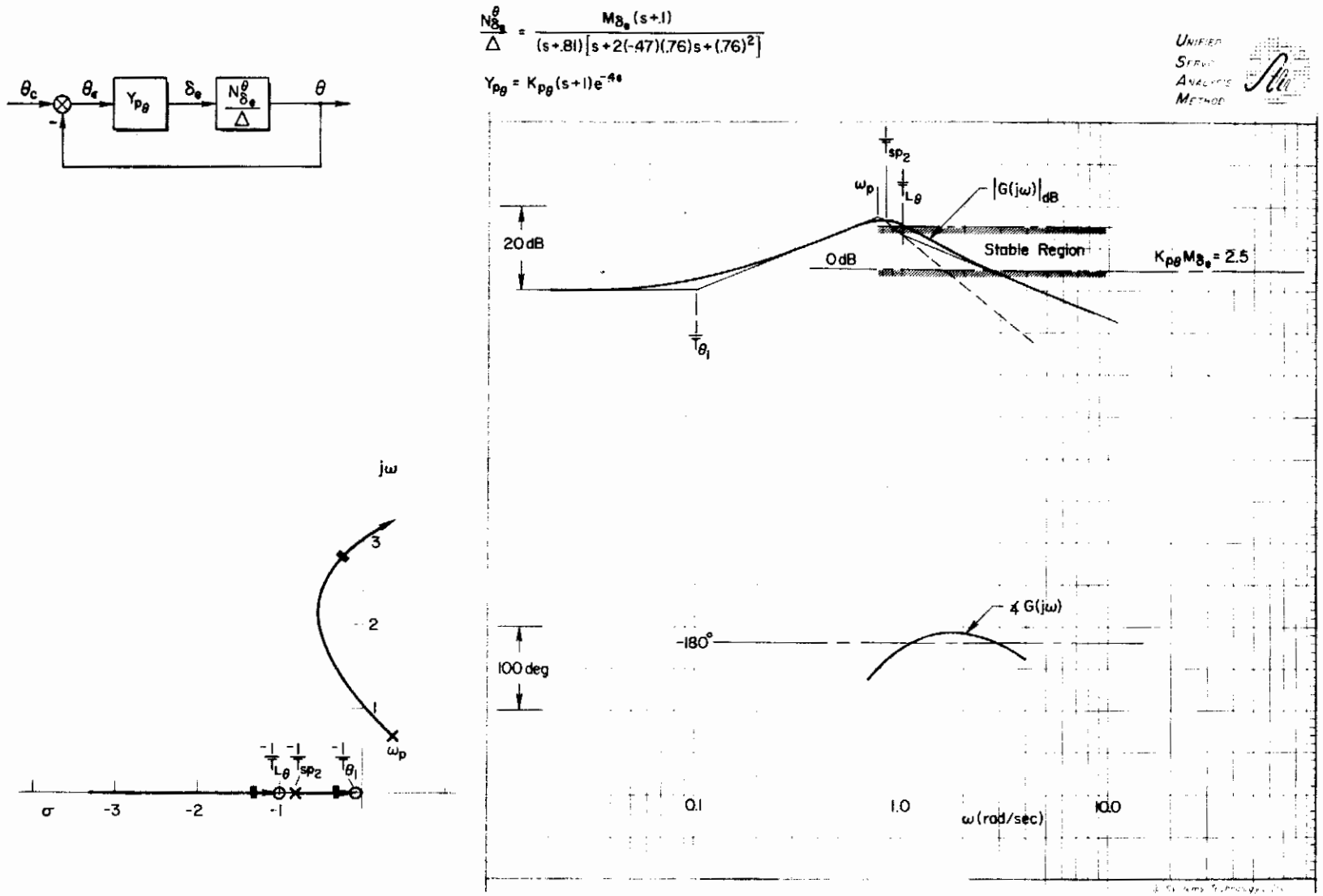

Figure 19. Attitude Loop Closure ($\theta \rightarrow \delta_e$) Unacceptable Condition, Configuration 2

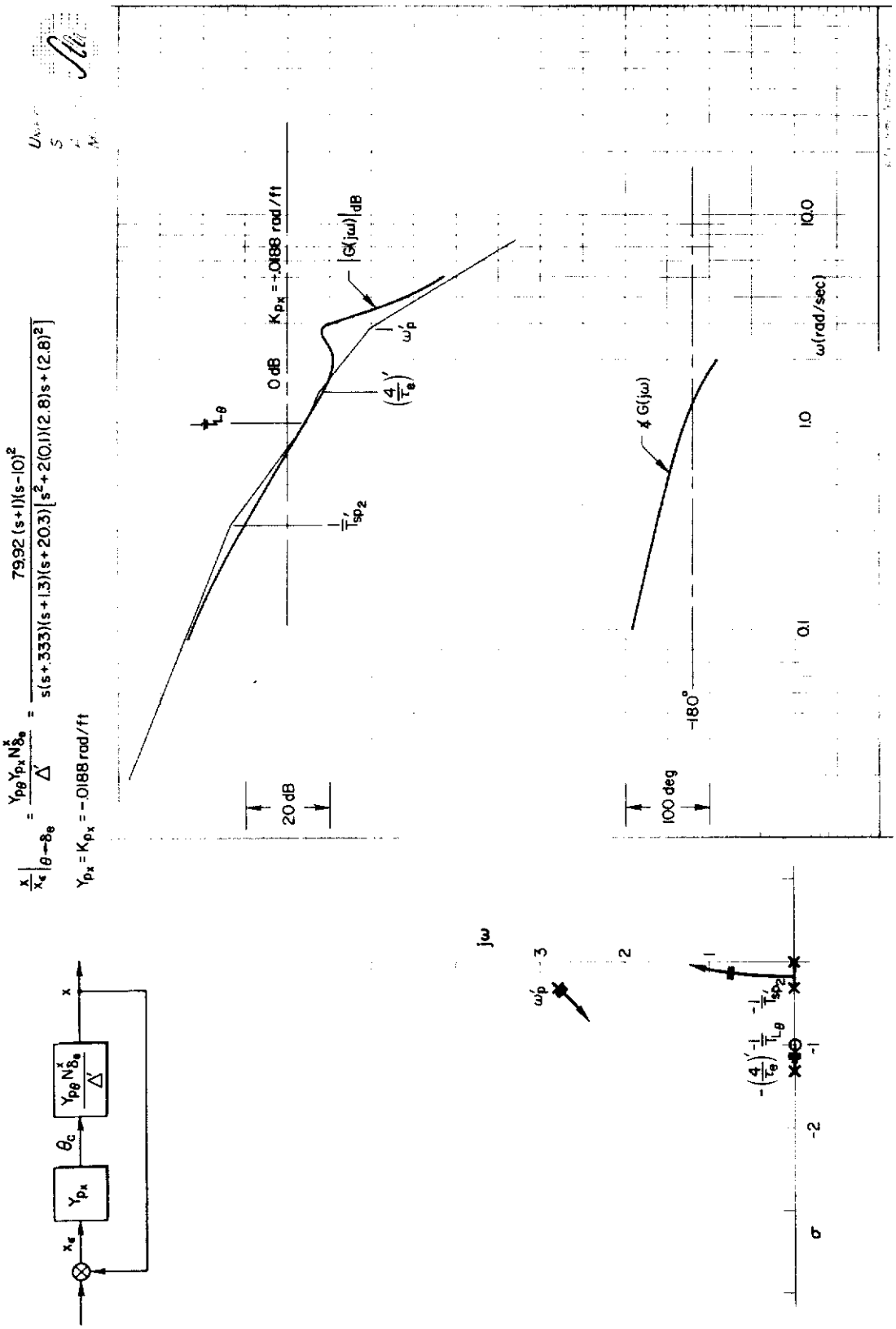

Figure 20. Position Loop Closure (x, θ → δe) Unacceptable Condition, Configuration 2

Figure 21 shows the results of the error analysis. The trend of the calculated values of $\sigma_\theta/\sigma_{u_g}$ and σ_x/σ_{u_g} with experimental pilot rating is quite different, but the difference does appear to reflect the closed-loop characteristics discussed previously. In particular, position error is relatively constant for all conditions, but the attitude error, $\sigma_\theta/\sigma_{u_g}$, rapidly increases with increasing rating above a rating of about 5.

Similar trends have been observed by Sadoff in the study of unstable second-order controlled elements (Ref. 18). Figure 22 shows the measured single-loop pilot's tracking score from this reference to illustrate the similarity of the present predictions and actual experience. Note that the tracking score shown here in percent is related to an integrated error squared function by the following equation

$$\underset{\text{(percent)}}{\text{Pilot Tracking Score}} = 100\left[1 - \left(\int \epsilon^2 dt / \int \theta_i^2 dt\right)\right]$$

It should be noted that the σ_x calculations are based for convenience on crossovers with K/s^2-like rather than K/s-like properties. However, since the outer x-loop did not radically change in the desired crossover frequency region among the various configurations, we would expect the foregoing comparisons to hold when suitable x-loop leads were used. The main effect of such leads would be to more-or-less uniformly increase the outer-loop crossover frequency and thereby reduce the levels of σ_x/σ_{u_g}. In fact, the results from Ref. 5 suggest that the pilot readily applies lead compensation in the x-loop to effect an improved σ_x performance.

2. Augmentation System Considerations

A preliminary study has been made of the closed-loop properties of the pilot-augmented-vehicle in the hover control situation. Clearly, the discussions in the foregoing sections have demonstrated that the overall pilot's control task is primarily related to the "effective" controlled element in the critical crossover region. Likewise, it has been equally well established that these "effective" dynamics depend upon the type and level of stabilization employed.

The "ultimate" stabilization system, which implies minimum pilot effort including the number of feedbacks, became evident from the work of Ellis and Carter (Ref. 11). A combination of M_θ and X_u augmentation was used in this hover control study and only the aircraft ground position was displayed to the pilot. In this case, with the inner attitude stabilized by the augmentation system, the compensatory pilot requires only the single position error signal, x_e, to stabilize and accurately hover. Basically, with this augmented form, the stabilized attitude-loop response becomes a well damped ($\zeta_p > 0.35$) second-order mode of moderately high frequency (i.e., $\omega_{c_\theta} > 2$ rad/sec) and appears to the pilot as a pure gain, K.

Two potential pilot closures are sketched in Fig. 23 for each of the apparently satisfactory control dynamics from this reference. In these single-loop closures, the pilot has the option of using a pure gain closure

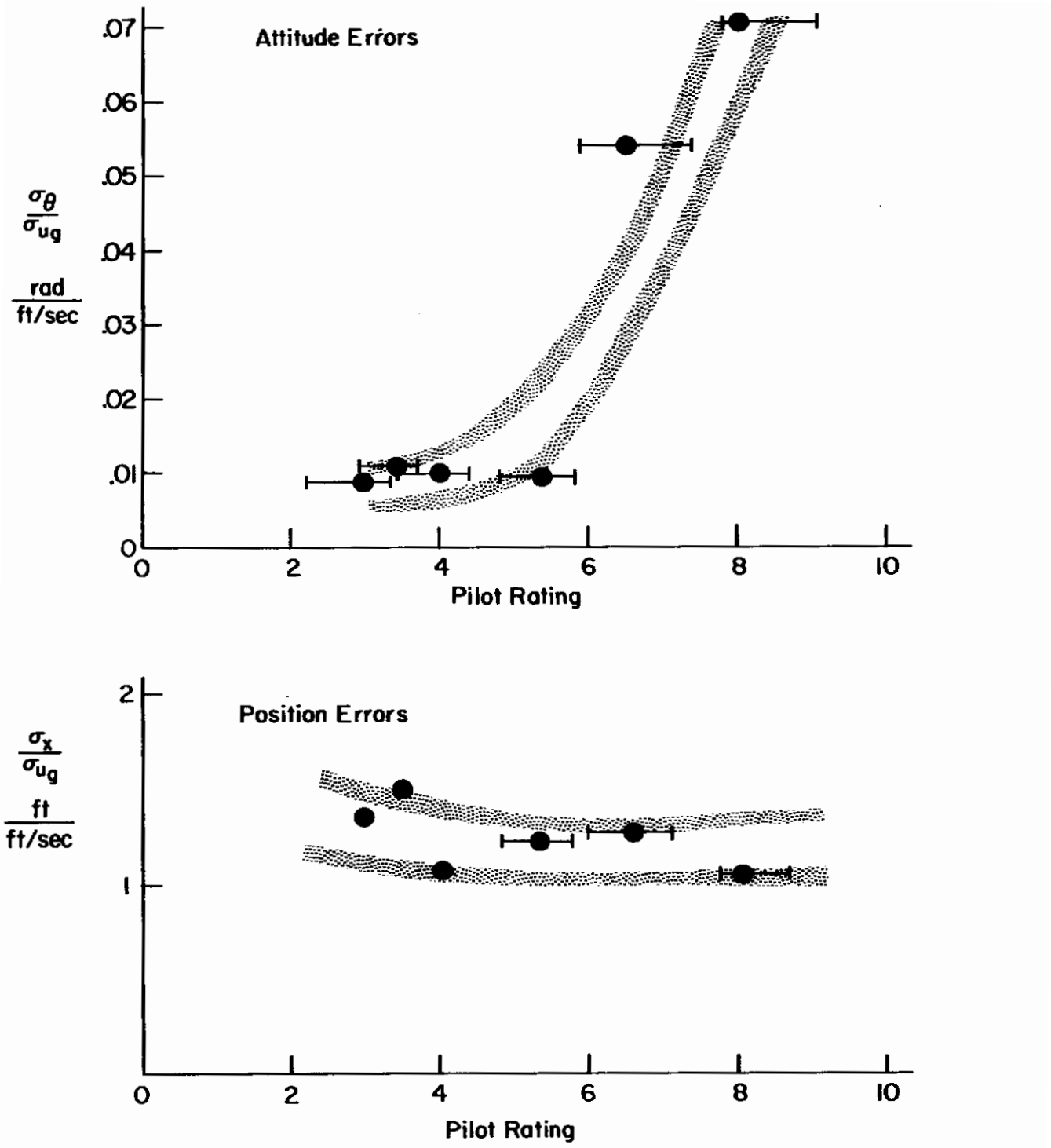

Figure 21. Predicted Normalized Performance Trends for Minimal Pilot Compensation Levels

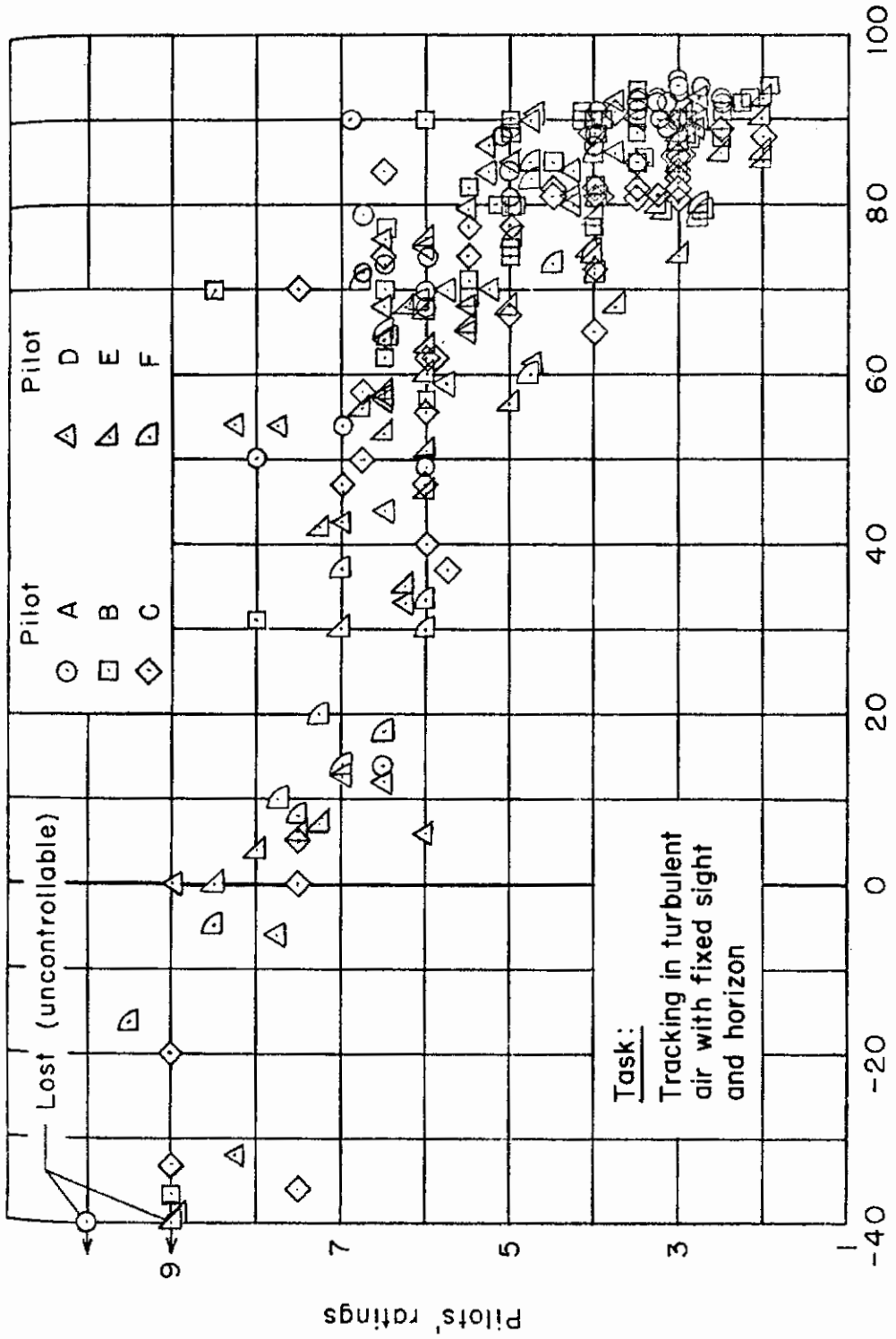

Figure 22. Interdependence of Pilots' Tracking Performance and Pilots' Opinion (Ref. 18)

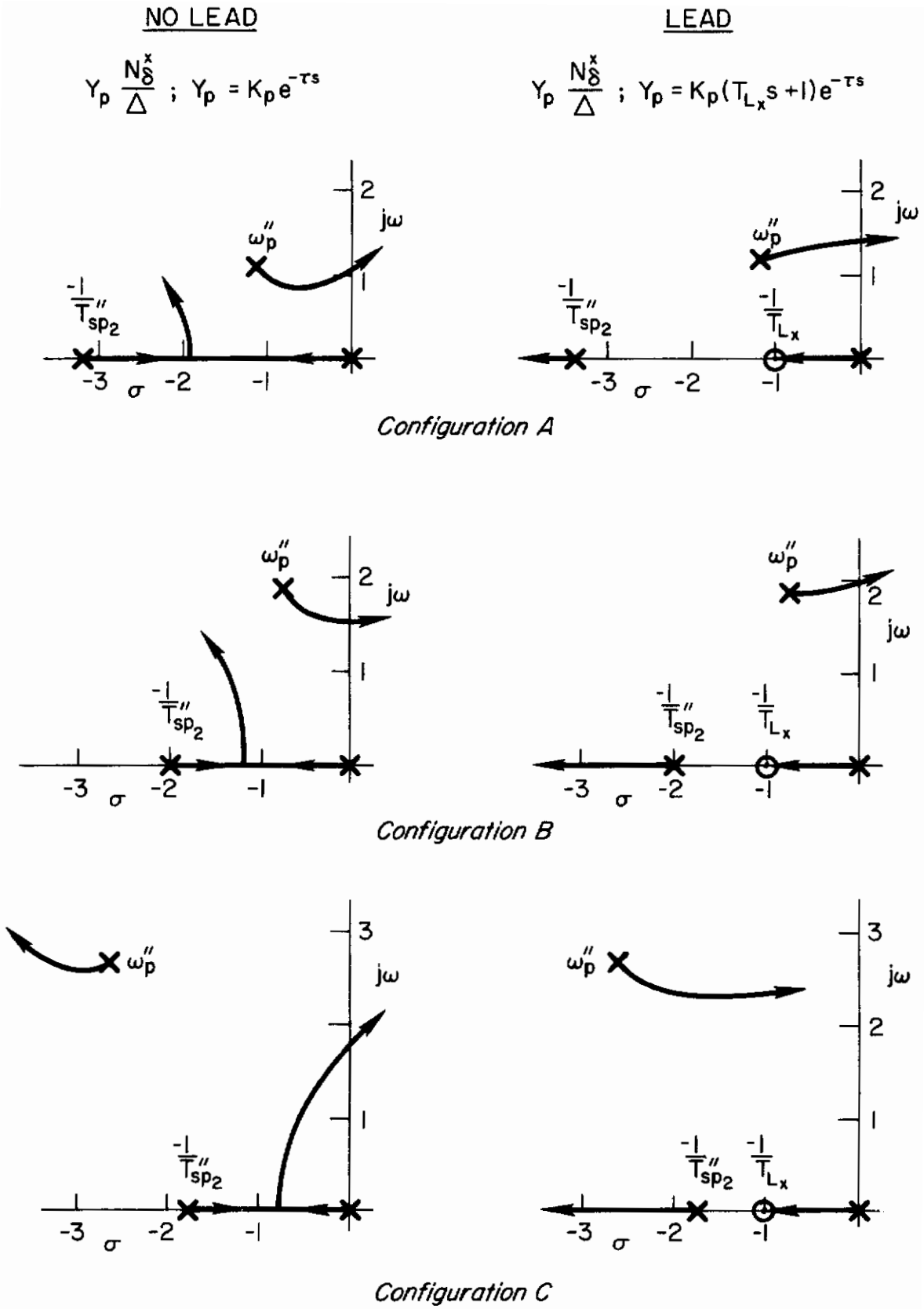

Figure 23. Potential Single-Loop Closure Characteristic for Combined Attitude and Translation Augmentation (Ref. 11)

for each of the systems; or he may increase bandwidth by adapting moderate leads ($1/T_L \doteq 1$ rad/sec). Obviously, x-loop control for either pilot compensation is clearly adequate ($\omega_{c_x} > 1.0$ rad/sec). Thus, the combined θ- and x-loop augmentation potentially results in minimal pilot control in hover.

The remaining discussion in this section will be directed toward the lesser augmentation system levels — the basic pitch attitude system and the translational velocity system.

a. Attitude Augmentation. Pilot control of the pitch attitude augmented vehicle is defined basically by whether the effective vehicle takes the form of "conventional" VTOL dynamics (i.e., feedback $|1/T_E| < |1/T_{sp_2}|$) with rate proportional to stick deflection or pitch attitude command (i.e., feedback $|1/T_E| > |1/T_{sp_2}|$). As already indicated in Section II.A.2.a, the former condition is adequately covered by conventional dynamics and warrants no additional consideration here.

The condition with $1/T_E > 1/T_{sp}$ provides the pilot with pitch attitude proportional to the control stick over some portion of the bandwidth ($1/T'_{sp_2} < \omega < \omega'_p$) as indicated in Section II.A.2.a. The dominant effective pitch control mode is the well damped ($\zeta_p > 0.25$) second-order phugoid of moderate frequency ($\omega_p > 2$ rad/sec). There are two basic options for SAS design, each of which reflects on the required pilot closures as follows:

1. The pilot closes both outer and inner loops, the latter with a moderate amount of pilot lead to extend the crossover frequency beyond the low-bandpass second-order controlled element (because of low ω'_p).

2. The pilot closes only the outer loop which has a K/s^2 form, with the stabilized pitch inner loop appearing as a pure gain.

Based on the fact that either of the foregoing requires less attention and effort on the pilot's part than conventional dynamics, it is obvious that either can be made satisfactory. However, there are potential problems with each option which will be briefly reviewed in the following paragraphs.

Option (1) — reduces the pilot's overall inner-loop stabilization efforts but some minimal lead generation in the inner loop is still necessary to obtain a good K/s region and crossover frequency, $\omega_{c_\theta} > 2$ rad/sec. The major potential disadvantage is the obvious reduction in control stick effectiveness resulting from the mechanization of the θ feedback (see Fig. 24). The pilot must employ larger than normal stick commands to offset the opposing SAS contribution. This type of mechanization is often employed in research studies (Ref. 19) and has been employed in the past (see Ref. 20) to stabilize helicopters.

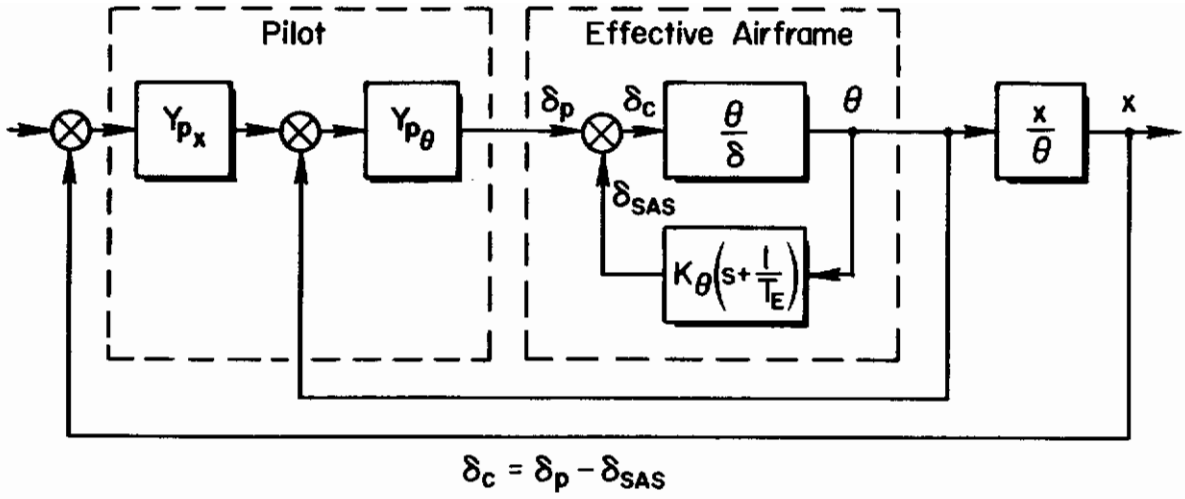

Figure 24. Attitude System Block Diagram

The problem noted above can be avoided by using an electrical bias signal to command θ directly at a rate proportional to control stick deflection. This electrical input signal ("fly-by-wire") is normally employed in parallel with the mechanical input (e.g., Ref. 10) when high-gain, large-authority feedbacks are used. The net effect of these combined electrical and mechanical input paths is to increase the control stick sensitivity. When the electrical signal is large the mechanization is often referred to as "command stick steering." We will, accordingly, assume that the stick commands the θ_{ref} (see Fig. 25 below) in the remaining discussions of attitude systems.

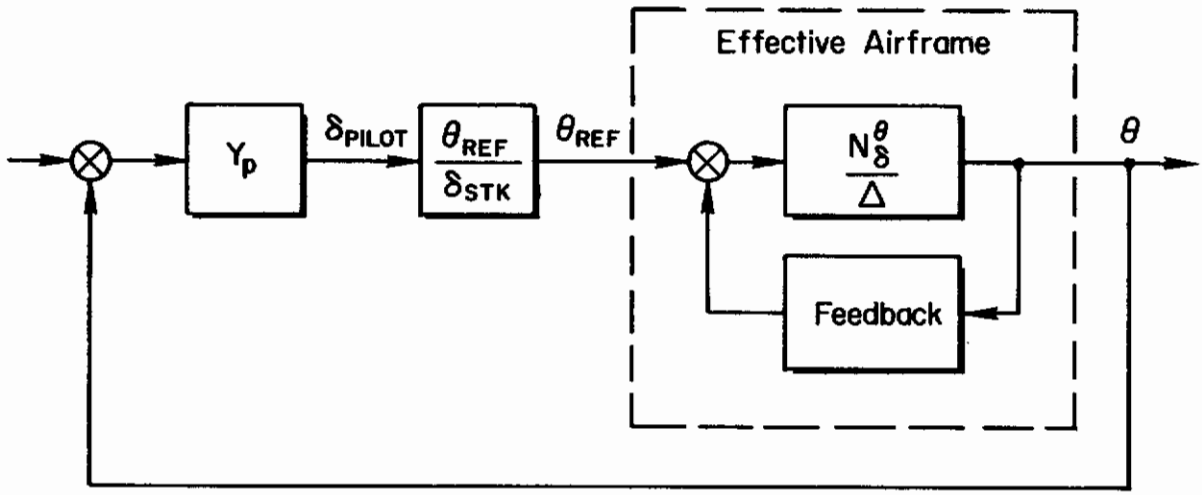

Figure 25. Attitude Command Scheme

Closure of the position loop with the above attitude loop augmentation is essentially the same as was indicated for the conventional VTOL dynamics.

Option (2) — The reduction of the multiloop hover task to the single-loop control situation is perhaps the major advantage of the pitch attitude stabilization system. The pilot is assumed to operate as a pure gain in pitch maneuvering control; regulation activities being relegated to the attitude stabilization system.

Figure 26 shows the closure of position loop with the pilot assumed to adopt lead compensation. The pilot can achieve good positional control and an adequate bandpass (i.e., $\omega_{c_x} > 1$ rad/sec) which responds directly to increasing gain and/or lead. The generally satisfactory character of closed-loop control exhibited in the Fig. 26 Bode sketches is consistent with the satisfactory system dynamics from Table V (i.e., $\omega_p > 2$, $1/T_{sp_2} \doteq 1/T_{\theta_1}$; $\zeta_p > 0.25$).

The unacceptable pitch stabilized systems are characterized by a lightly damped second-order mode. Figure 27 indicates the closures that can be expected for the same pilot generated leads (i.e., $1/T_L = 1.0$ and 0.2). The outstanding feature of this situation is the drastic reduction in the x-loop bandpass ($\omega_{c_x} << 1$ rad/sec) which results from the lightly damped pitch phugoid modes (see following sketch). The very low bandpass condition indicated by these closures appears to justify the unacceptable rating given by the pilot. Also, increased pilot lead reduces the available bandwidth and the maximum bandwidth corresponding to no lead is given by $\omega_{c_x} \doteq 2\zeta'_p\omega'_p/\sqrt{2\zeta'_p}$. Notice finally that increasing $1/T'_{sp_2}$, normally considered

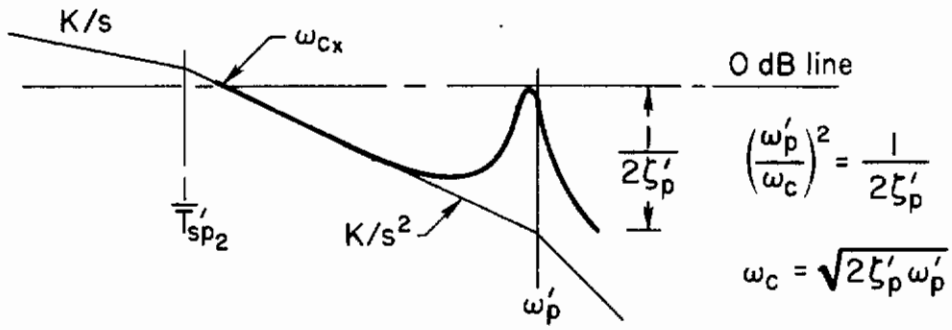

desirable, does not particularly improve crossover; i.e., increasing $1/T'_{sp_2}$ is equivalent to decreasing $1/T_L$. In the limit, for $1/T'_{sp_2}$ greater than the frequency region of interest, the K/s^2 slope in the above sketch would become K/s and the limiting ω_c would be given by $\omega_{cx} \doteq 2\zeta'_p\omega'_p$ (as in the sketch on page 57). For small ζ'_p as appropriate to this discussion, this is a smaller value than that given above.

The assumed independence of $\zeta'_p\omega'_p$ and $1/T'_{sp_2}$ in the foregoing discussion is, of course, incorrect. In fact they are connected by the augmentation system as discussed in Section II.A.2. Nevertheless, these simple considerations are useful as points of departure for considering potentially troublesome problems.

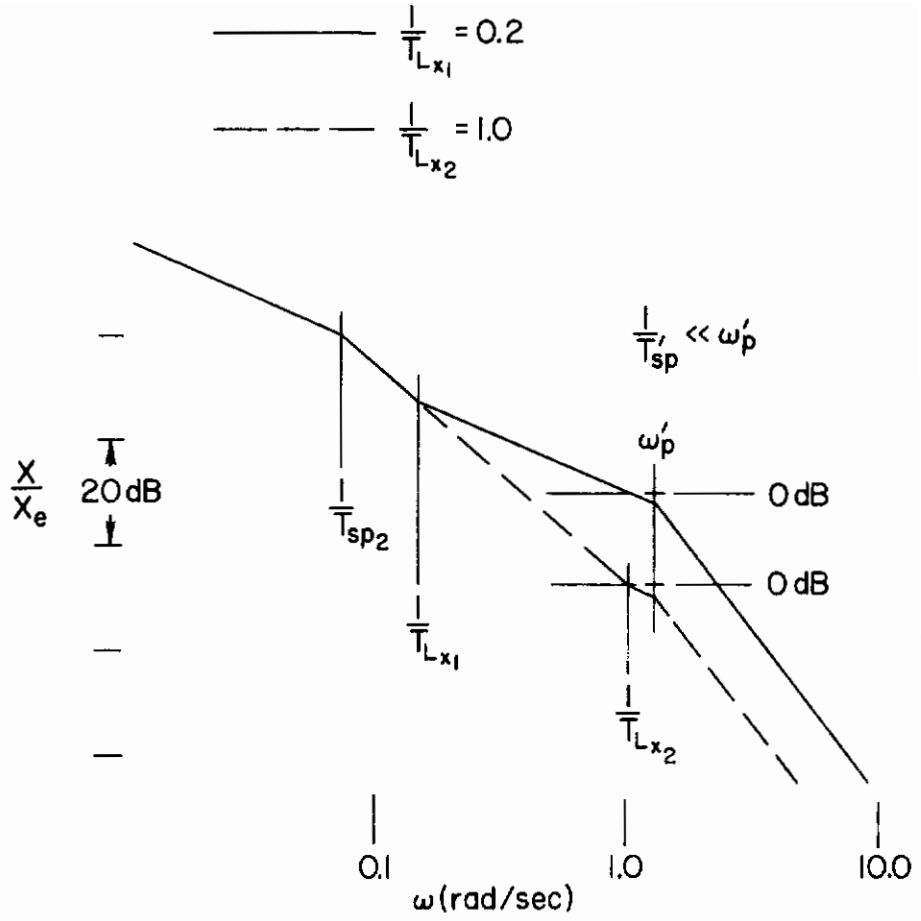

$$Y_p \frac{N'_x}{\Delta'} = \frac{-gM_\delta K_p \left(s + 1/T_{L_x}\right)}{s\left(s + 1/T'_{sp_2}\right)\left[s^2 + 2\zeta'_p\omega'_p s + \omega'^2_p\right]}$$

Figure 26. Translation Control with Pitch Stabilized Inner Loop; Hover

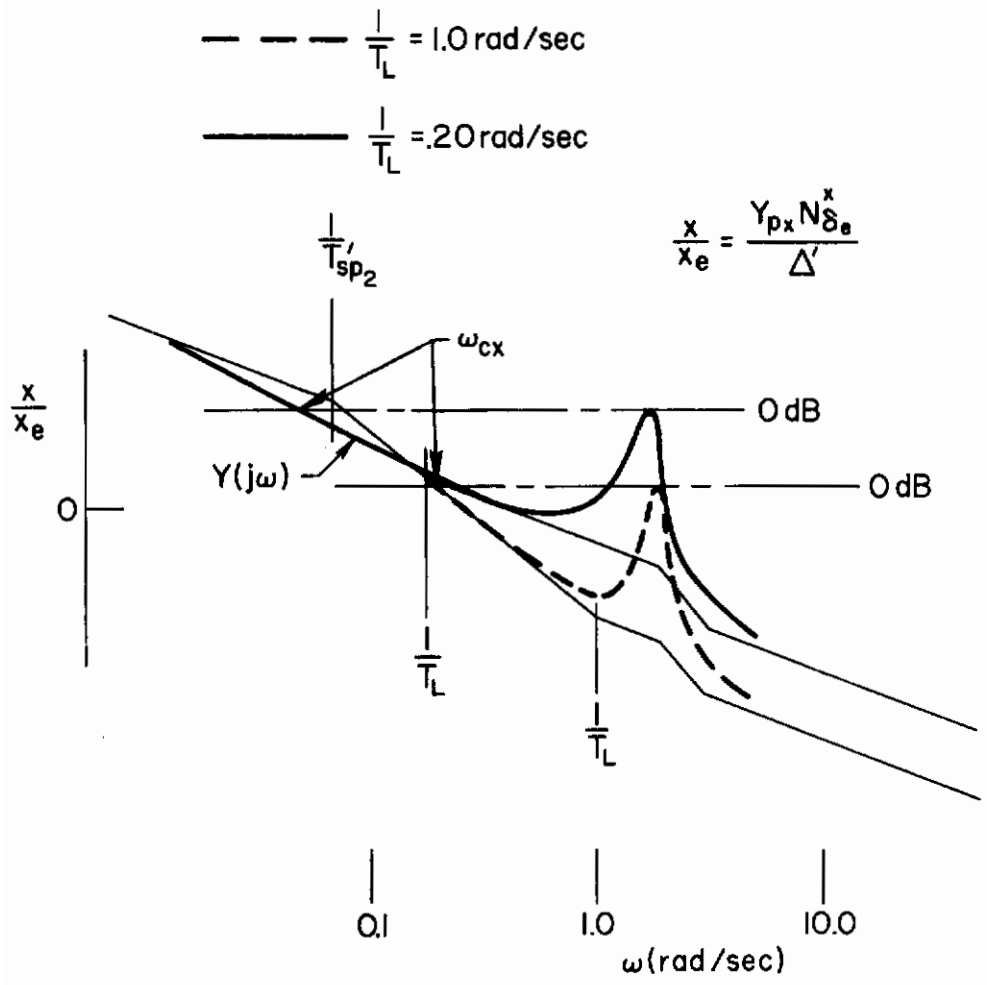

$$Y_p \frac{N'_x}{\Delta'} = \frac{-M_\delta g K_p \left(s + 1/T_L\right)}{s\left(s + 1/T'_{sp_2}\right)\left[s^2 + 2\zeta'_p \omega'_p s + \omega'^2_p\right]}$$

Figure 27. Position Loop Closure, Unacceptable Pitch-Stabilized System, Hover

b. Position Augmentation. In Subsection II.A.2.b, we noted how position loop augmentation was related to attitude augmentation and that using axial force feedback proportional to velocity was equivalent to modifying X_u or $1/T_{\theta_1}$. The resulting "effective" vehicle transfer function remained unchanged in form. Accordingly in this section the effect of the $1/T_{\theta_1}$ or X_u augmentation (with the attitude loop closed) was to extend the K/s region of the position loop.

Applying this background, we may observe that the basic restriction placed on the phugoid mode (i.e., $\zeta_p\omega_p > 0.25$) follows from consideration of the position-loop bandpass. For example, from the Bode figure below the x-loop

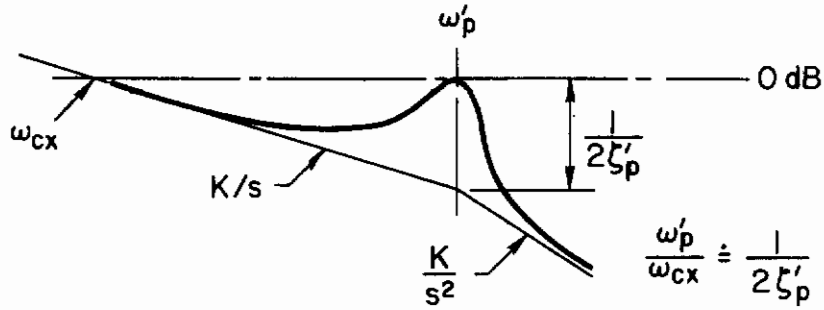

bandpass is again restricted by the effective phugoid damping. However, since the asymptotic region is K/s in form, the maximum bandwidth approaches $\omega_{c_x} \doteq 2\zeta'_p\omega'_p$. The closed-loop frequency restriction $\omega'_p > 1$ further insures the pilot of a good effective bandpass and overall control response features.

C. CONCLUSIONS

The results of the closed-loop analyses presented in the foregoing sections provide a fundamental basis for defining criteria governing manual control of the longitudinal mode during hover. From the closed-loop viewpoint, the following are the key aspects which relate to satisfactory control:

1. Attitude Loop

a. Low pilot lead compensation ($T_L < 1.0$ sec) with the proper sensitivity to lead variations (i.e., for an increased T_L, better error performance and stability). This basically sets the requirement for the minimum "effective" value of $1/T_{sp_2} \doteq -M_q > 1$ for conventional VTOL systems.

b. Good low-frequency gain characteristics to permit gust regulation. In conventional VTOL systems this leads to the requirement for $\omega_p < 0.5$, which in turn further defines the satisfactory M_q, M_u boundary.

c. Desired crossover frequencies near $\omega_{c_\theta} \doteq 2$ rad/sec. This permits good regulation for nominal dc gain; and for attitude augmentation systems leads to the requirement for $\omega_p > 2$ rad/sec.

2. Position Loop

a. In general, the position-loop features are not critical for conventional VTOL dynamics even though the dominant dynamic features are K/s^2 after the attitude-loop closure. Desired outer-loop crossovers are in the neighborhood of $\omega_{c_x} = 0.5$ rad/sec for no lead ($T_{L_x} = 0$); and, for attitude augmentation systems, this leads to requirements on the minimum phugoid mode damping ($\zeta_p \omega_p > 0.25$).

b. The "best" augmentation system provides a K/s outer, position loop and automatic inner-loop regulation, so that the pilot is relieved of one control loop. The K/s outer loop is of course "ideal" from the standpoint of manual control.

SECTION III

CONTROL POWER AND SENSITIVITY CONSIDERATIONS

The preceding section has correlated the available data with pilot opinion from the closed-loop point of view to show how the effective controlled element dynamics influence the pilot rating for near-optimum levels of control power and sensitivity. In this section, these data are further examined to determine the effects of changes in control power and sensitivity on pilot opinion rating, the closed-loop aspects again form the basis for the discussion.

A. CONTROL POWER

The use of the quasi-linear pilot describing function in estimating control power requirements for gust regulation is somewhat confounded by that portion of the pilot's output — the "remnant" — which is not linearly correlated with the input. The magnitude of the remnant will depend on the controlled element stability and crossover characteristics, and/or on the complexity of the task. For example, in the multiloop control situation under discussion (longitudinal hover), the pilot is observing two input errors (θ and x) and controlling with a single output (δ_e). The second error signal apparently decreases the remnant ratio, ρ, relative to the single-loop control situation — possibly because the pilot has more information available. As a result, the remnant is an even smaller part of the pilot's total output.

However, the remnant can represent a significant amount of the pilot's total output as measured by the rms control moment, $M_\delta \sigma_\delta$, or stick activity, σ_δ. For no input, the pilot's output is essentially all remnant by definition. However, as the input is increased (disturbances to the hover vehicle) the pilot remnant appears to remain constant, as indicated by limited analyses of UARL data and the work of Ref. 16. The rms value of the control moment or stick displacement for zero input could then be a rough measure of the remnant as, for example, the zero disturbance level of Fig. 28.

For the closed-loop control situation, it has been shown analytically in Ref. 1 that the correlated control power used, $M_\delta \sigma_\delta$, is approximately proportional to the disturbing moment, $M_u \sigma_{u_g}$, for small values of X_u. It appears reasonable to utilize this relation for formulating control power requirements for the closed-loop regulatory control task. Regardless of other control power requirements (e.g., large amplitude, largely precognitive maneuvers), the pilot must have available at least that much control power required for the regulatory task. The necessary relationship is given in mathematical form by,

$$M_\delta \sigma_\delta \doteq K M_u \sigma_{u_g} + M_R \qquad (2)$$

where M_R represents the fixed contribution due to pilot remnant. The constants in Eq. 2 are given on top of page 61, being based on the data of Fig. 28.

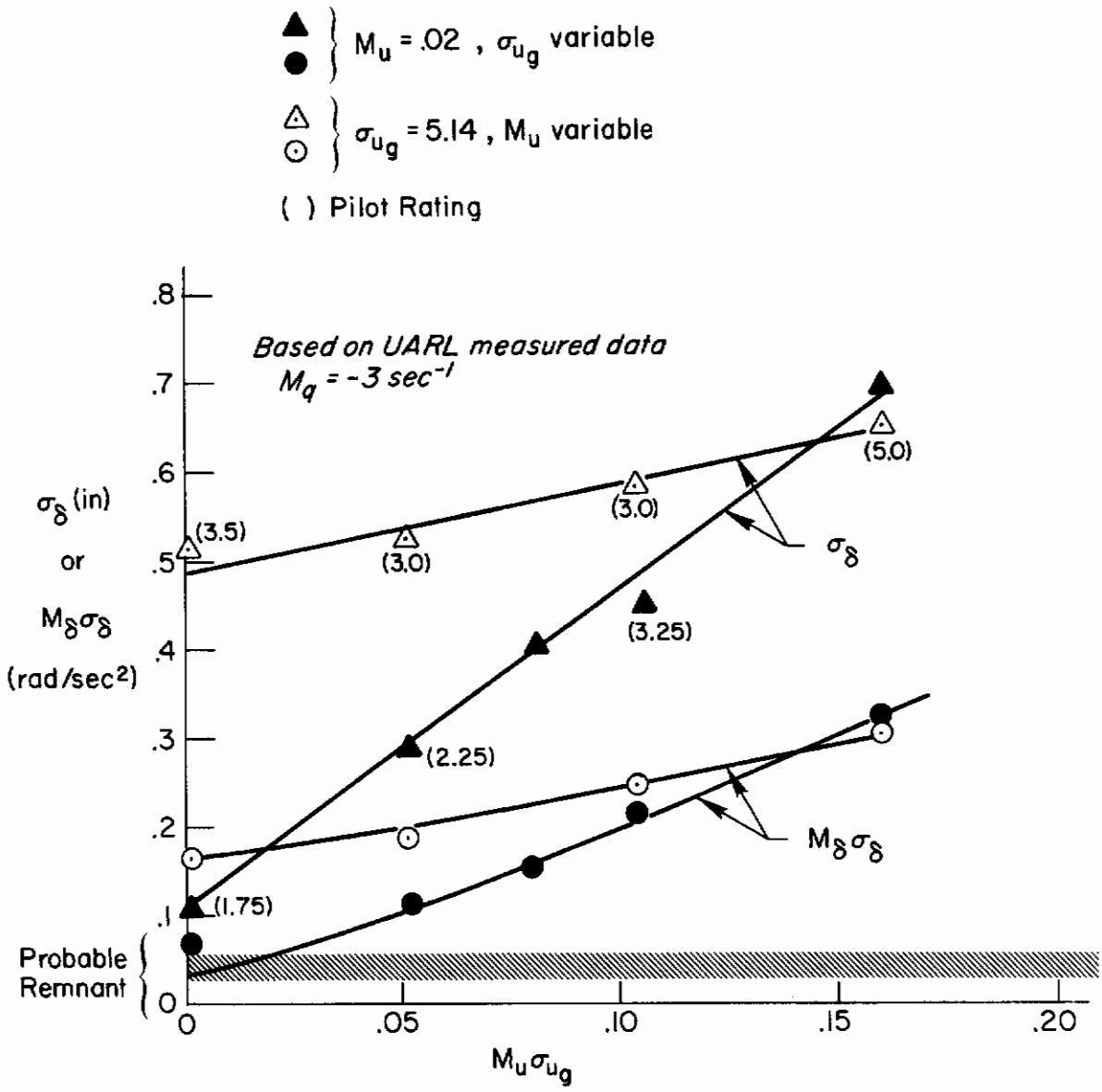

Figure 28. RMS Control Moment and Stick Deflection as a Function of Input Disturbance (UARL Data)

EMPIRICAL CONSTANTS FOR CALCULATION OF CONTROL POWER REQUIREMENTS

Data Set	Proportionality Constant, K	Remnant, M_R rad/sec^2
(a) Constant M_u	1.75	0.035
(b) Constant σ_{u_g}	1.0	0.17

Note that the 1.75 value of K is in fair agreement with closed-loop analytic predictions which range from 1.4 for low outer (position) loop crossover, $\omega_c \doteq 0.3$ (Ref. 1) to about 2.0 for high crossover, $\omega_c \doteq 1.0$.

In general, the approximate expression of Eq. 2 is considered difficult to define for low disturbance moments ($M_u\sigma_{u_g} < 0.1$) for two reasons:

1. The remnant becomes a large part of the pilot's output for low input magnitudes; further, it is a stronger function of the effective controlled element characteristics (e.g., stability) than of gust excitation upon which Eq. 2 is based.

2. There are additional disturbance factors not accounted for, e.g., X_u.

If the data are taken at constant M_u, the controlled-element dynamics are the same for all gust-magnitudes tested and the results tend to more closely match the approximate expression, whereas in the other set of data (constant σ_{u_g}) both the controlled-element dynamics and the disturbance to the aircraft, $M_u\sigma_{u_g}$, are changing. This consideration, as well as the better analytical correlation indicated above, strongly suggest data set (a) of the above listing to represent the better values for K and M_R.

The data given in Ref. 7 and replotted in Fig. 29 can be interpreted to apply directly to the question of control power requirements for gust regulation. In these tests the pilots were evaluating ease of control in combating gusts, and they were using large control inputs. The approximate control power level (as a function of gM_u) at which a satisfactory pilot rating is approached (PR < 4) is shown by the curve for estimated minimum $M(\delta)$ in Fig. 29. Control power is considered the primary variable influencing pilot rating here, because the rating shown in the figure is the "best rating" achieved for the given gust condition ($\sigma_{u_g} = 9$ fps) regardless of the level of the angular damping level, M_q, tested. Damping was the only other variable in this test. From the trend of Fig. 29, it is clear that the requirements for control power increase as the gM_u increases. This trend is closely equivalent to a plot of Eq. 2 [using the (a) data set above] as shown by the solid curve in Fig. 29. It may be noted that the trends given by the (b) set of constants do not fit the Ref. 7 experimental data. Both of these curves are closely equivalent to a control power equal to twice that necessary to balance the rms gust level, σ_{u_g}, i.e., a

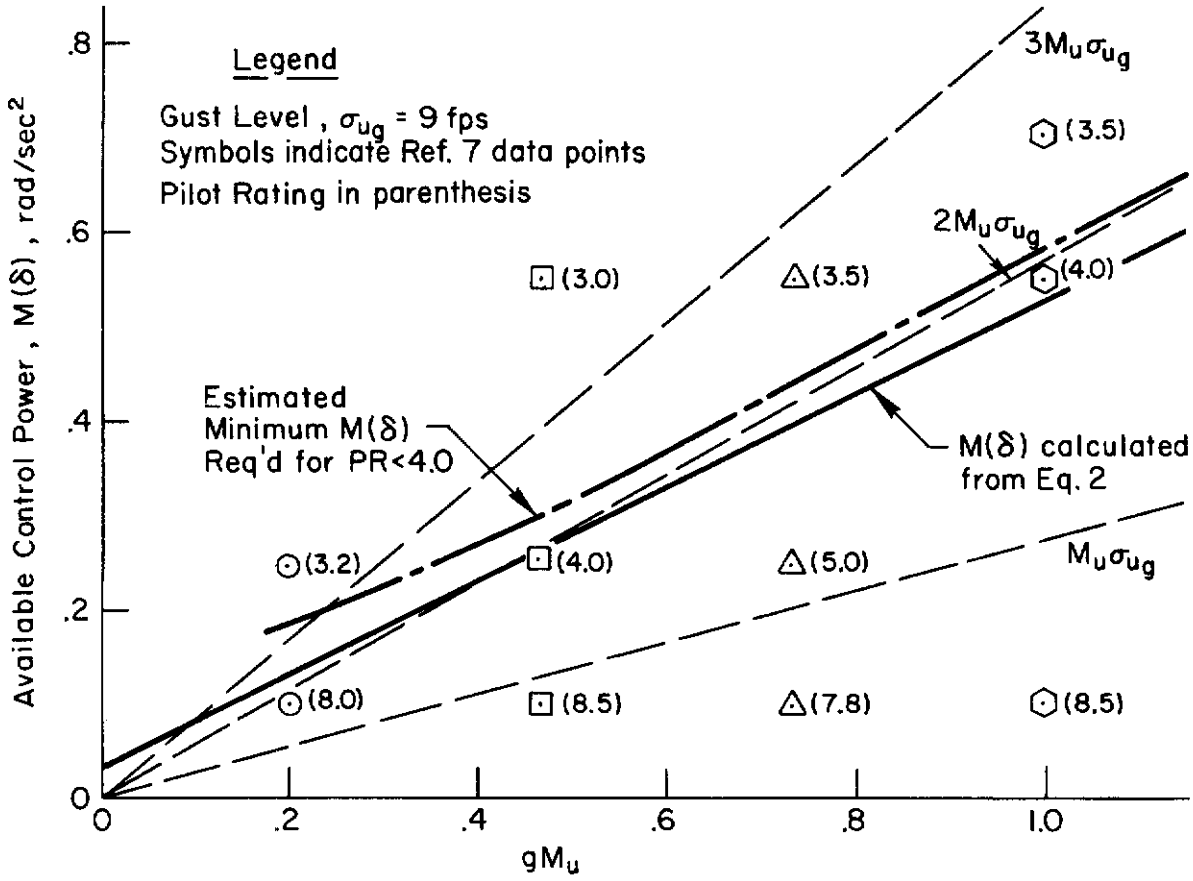

Figure 29. Minimal Control Power Requirement for Gust Regulation

level not exceeded 95 percent of the time for a Gaussian random process (see Fig. 29). If this control power is the maximum level, it means that the pilot is operating within the linear range 95 percent of the time, which seems to be a reasonable requirement for a marginally satisfactory rating. The rating, of course, improves as the available control power increases beyond this level, and degrades more rapidly for lower available control power.

B. SENSITIVITY

In hover-like attitude control situations [i.e., $Y_c \doteq M_\delta/s(s+M_q)$ in the region of crossover] where maximum control power is not required, pilot ratings are, for a given damping (M_q), strongly influenced by the gradient, or gain, M_δ. It has been established from the previous studies (e.g., Refs. 21 and 22) that such influences are best explained in terms of the pilot's gain required for closed-loop operation rather than in terms of the vehicle gain, M_δ. From Ref. 21, it was shown that the pilot gain in the crossover region is his chief concern for the simple attitude tracking task. That is,

$$\text{if} \qquad |Y_p(\omega_c)Y_c(\omega_c)| \doteq 1$$

$$\text{then} \qquad |Y_p(\omega_c)| = \frac{1}{|Y_c(\omega_c)|} = \frac{\omega_c\sqrt{T^2\omega_c^2+1}}{M_\delta T}$$

$$\text{where} \qquad \frac{1}{T} = -M_q \doteq \frac{1}{T_{sp_2}}$$

Thus for ω_c constant at roughly 2.5 rad/sec, the resulting values of $|M_\delta T Y_p(\omega_c)|$ depend on the damping term, T. The results showed that for $\omega_c T < 1$ the controlled element gain of most importance to the pilot is rate gain, $M_\delta T$. Furthermore, for high damping (low values of T) the controlled element is primarily a rate control, so that either gain or pitch angle response is proportional to the rate gain $M_\delta T$. On the other hand, for $\omega_c T > 1$, the acceleration gain, M_δ is most important. Here high values of T (low damping), control motions produce accelerations, so that the response or gain is proportional to the sensitivity, M_δ.

This concept of pilot gain selection and the equivalence between sensitivity and response time was extended in Ref. 1 to specifically cover hovering vehicle dynamics characteristics (i.e., include the effects of M_u). The results of this study showed that optimum control sensitivity corresponds to a constant attitude excursion in 1 sec, θ_1, of about 0.1 rad/in. of stick. However, we expect that for increasing gust inputs, $(M_u\sigma_{u_g})$, the pilot will want increased sensitivity to reduce his control activity to acceptable levels. The data of Fig. 30, taken in a compensatory hovering task with constant dynamics, show that the pilot-selected optimum sensitivity initially increases with increasing excitation but eventually becomes essentially constant for σ_{u_g} greater than about 5-1/2 ft/sec (usually considered a medium turbulent day).

The current explanation for this upper limit on M_δ is that it represents an incipient oversensitive response, i.e., the value of θ_1 is about 50 percent greater than that normally desired. Apparently the pilot is willing to trade off some oversensitivity to reduce his gust-regulating control activity, but he draws the line at about a 50 percent increase. Of course, as σ_{u_g} increases and σ_δ goes up (see Fig. 30) his rating also goes up (degrades), but apparently not as fast as it would if M_δ were higher (and σ_δ lower). The implication is that the pilot is more concerned with maneuver sensitivity than with "excessive" control activity for occasional very gusty air. In any event he still retains adequate control power up to the maximum σ_{u_g} tested because even at 3σ he never uses more than about 2-1/2 in. of control (from trim).

The foregoing data and analysis suggest a rationale for the variation of optimum control sensitivity with the governing parameters, M_u and M_q, as follows:

1. For a given M_u and σ_{u_g} the hovering control activity is given by $\sigma_\delta = KM_u\sigma_{u_g}/M_\delta$ where K is approximately 1.7 ±.3, depending upon pilot gain variations [see Ref. 1 and data set (a), page 61]. To keep σ_δ (control motions) within acceptable limits requires a minimum value of M_δ regardless of σ_{u_g}.

2. A given M_u also demands a minimum $-M_q$ (generally greater than 1.0) to give satisfactory dynamic characteristics, as discussed earlier (e.g., see Fig. 3).

3. The M_q and M_δ resulting from Items 1 and 2 must be compatible with a "desired" pitch response in 1 sec, θ_1, of about 0.1 rad/in. of stick. The pilot may compromise this value by no more than about 50 percent on the high side in deference to reducing Item 1 control activity.

An obvious question at this point, How do the optimum control sensitivities for a precision hover task (i.e., compensatory pilot control) compare with those selected for a rapid maneuver situation (i.e., precognitive or open-loop pilot control)? Results from a moving-base simulator study of the Short S.C.-1, which was conducted by Perry and Chinn (Ref. 23), can be used to partially answer this question and simultaneously lend some credence to the importance of closed-loop aspects. Figures 31a and b show the appraisal of lateral* control sensitivity on the conventional plots for the two control

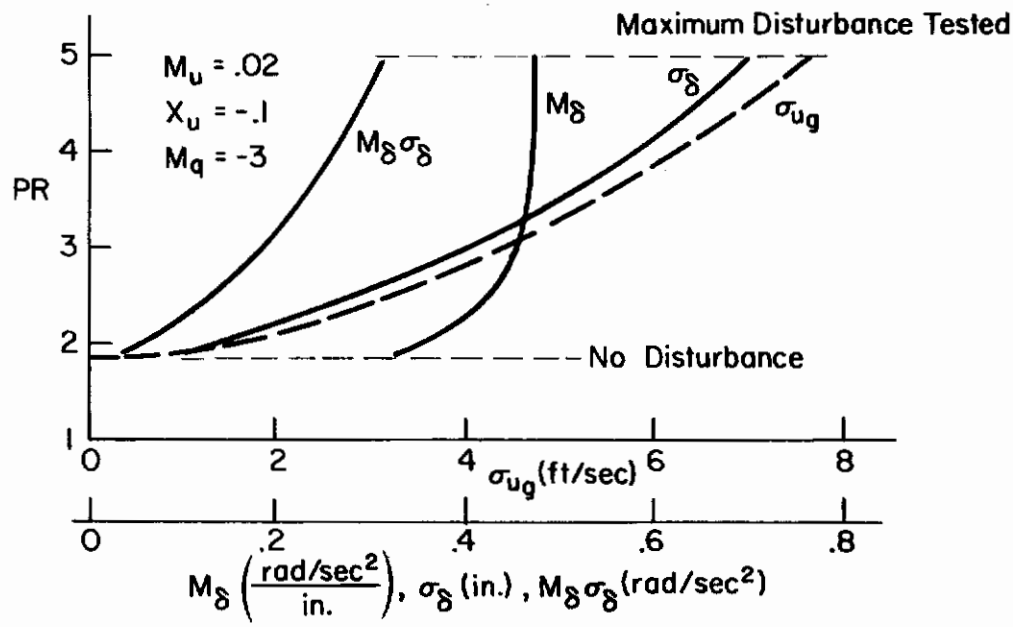

Figure 30. Control Measurements as a Function of Rating and Disturbance

*The form of the lateral and longitudinal hover dynamics are identical. In Figs. 31 and 32, L_δ and L_p may be interpreted as M_δ and M_q, respectively. with no loss of generality.

tasks — precision hover and quick stop maneuvers. The two control factors observed from the results of this experiment are:

1. The optimum response line for precision hover is approximately 0.1 rad in 1 sec and this response is suitable for rapid translational maneuvers, also.

2. The minimum damping requirements are the same for the two control tasks (i.e., the basic damping level required is unchanged regardless of the maneuver c).

When the "free from criticisms" boundaries for each of the control tasks are combined (Fig. 32), the final compromise sensitivity region selected by the pilots is formed by a lower boundary described by the optimum precision hover sensitivity and the upper boundary which is approximately 50 percent greater. Significantly, we see evidence to support the desired response in 1 sec of about 0.1 rad/in. of stick; furthermore, the pilot will compromise this value by no more than about 50 percent on the high side to obtain the desired maneuver control. This basic limitation again appears to be founded on the tendency at the higher sensitivities for the system to be oversensitive to the pilot in the precision hover (i.e., compensatory) control task.

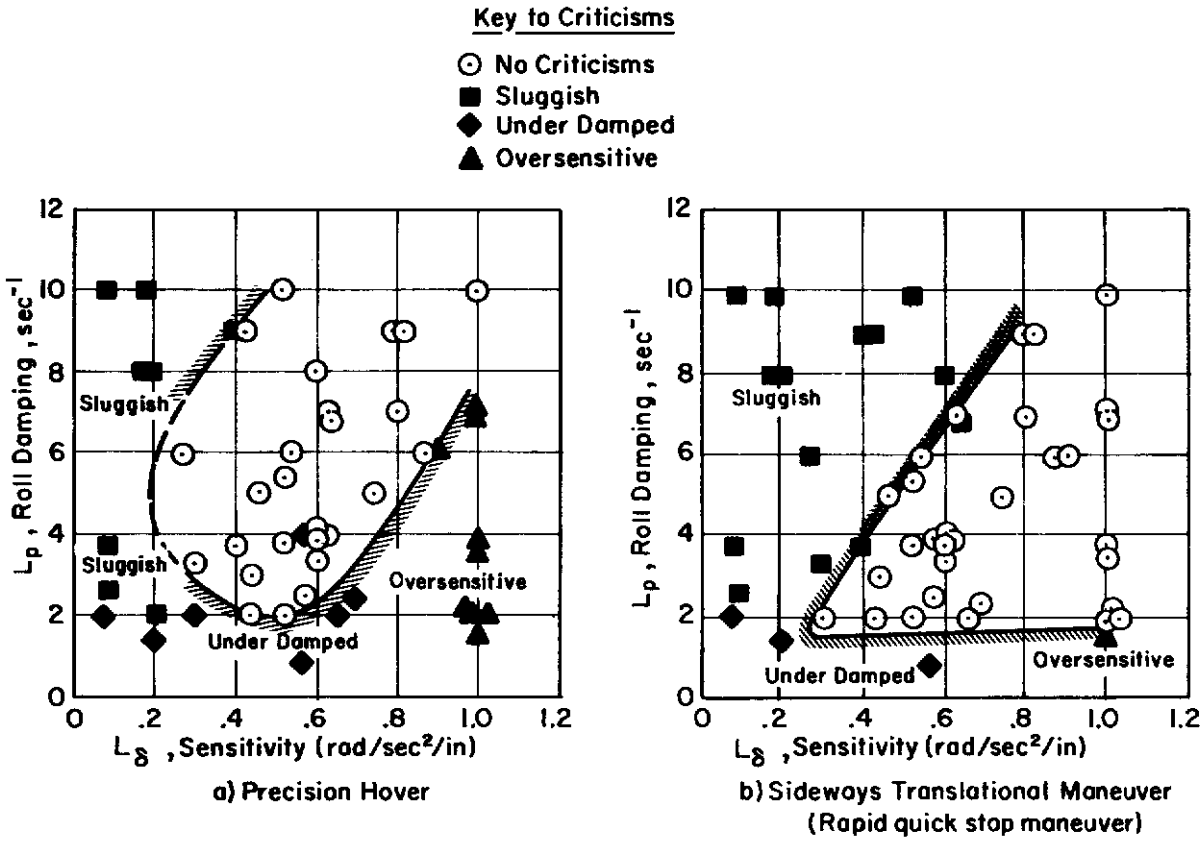

Figure 31. Summary of "Criticisms" for Precision Hovering and Lateral Quick Stop Translations

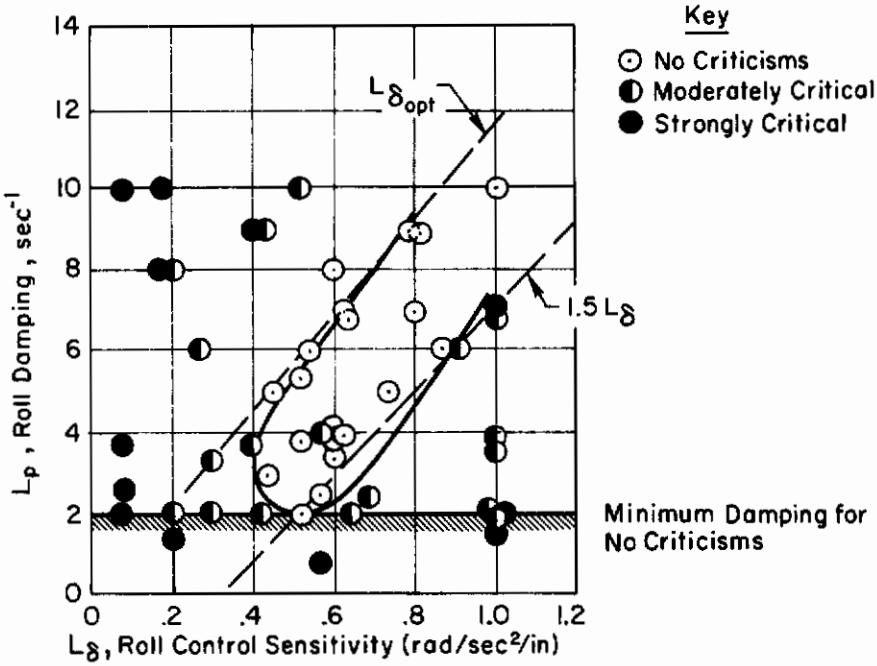

Figure 32. Roll Control Characteristics Which Were Free from Criticism for Both Hovering and Maneuvering

C. CONCLUSIONS

The results of this section suggest that consideration of the closed-loop aspects of the piloting task will define minimum levels of control power necessary for satisfactory pilot ratings although additional control power may be required for reasons of safety, rapid maneuvering, and the like. These minimum levels are dependent primarily upon the magnitude of the disturbances encountered, and pilot remnant. However, the latter represents a relatively small increment on the total power requirements for all except the low M_u cases — and generally speaking, such cases are of little practical concern from a gust regulation standpoint. The data discussed herein shows that a control power equal to two (or at most, three) times $M_u\sigma_{u_g}$ will suffice for gust regulation control in hover when X_u is small, substantiating the results of Ref. 1.

With regard to sensitivity, pilots generally prefer those levels yielding attitude responses in one second of approximately 0.1 rad/in. of stick travel. This response depends on not only the sensitivity, M_δ, but also on the dynamics of the controlled element. However, the sensitivity levels actually rated as "best" for a given vehicle configuration will cover a broad range depending upon the nature of the task (as well as pilot idiosyncrasies). In particular, as a greater premium is placed on the rapid maneuvering aspects of a mission, so will the preferred sensitivities increase — but only to a limited extent. Past this point, the vehicle will be termed "over sensitive," because of the fundamental necessity for the pilot to accomplish the precision control task.

SECTION IV

PRELIMINARY CONSIDERATIONS OF LONGITUDINAL CONTROL TECHNIQUES IN TRANSITION

This section presents the results of exploratory analyses to determine the probable piloting techniques for stability and control characteristics associated with transition flight. The identification of the control techniques and the delineation of the configuration-dependent derivatives which determine applicable techniques is an important part of understanding the transition maneuver. The preliminary results presented here show how certain dynamic and control properties in transition influence pilot control technique and potential augmentation systems.

The piloting techniques employed for longitudinal control during transition involve both trim and closed multiloop control. The primary control variables are pitch attitude, altitude, and airspeed, and the controls are longitudinal stick or cyclic, δ_e, throttle or collective, δ_c, and a conversion control such as wing tilt, i_w. In this analysis of closed-loop manual control, the prime concern is with the perturbation dynamics about trim conditions, and therefore, the conversion controller (e.g., wing incidence) is assumed to serve as a "trimmer" and not a primary control. This assumption is based upon recent comments by pilots of the CL-84 and XC-142 aircraft (Ref. 20) who state that wing tilt angle sets up the trim airspeed and is not changed unless it is desired to accelerate or decelerate. This is basic to the tilt wing concept, since wing incidence and airspeed are strongly related.

In this section, the effective control characteristics of a VTOL in the mid-transition flight regime are defined in subsection A. Subsection B considers various likely control schemes, i.e., various loop closure possibilities, and their relative merits and demerits. Subsection C extends the preceding results by examining the effects of VTOL configurational changes on the piloting techniques used. The results of all subsections are summarized in subsection D.

The "baseline" configuration for these analyses is the XC-142 tilt-wing configuration, for which considerable aerodynamic data exist at various operating points in the transition flight regime. The major differences in the longitudinal dynamics of this aircraft relative to other VTOL concepts originates in the location of the thrust vector and its method of rotation. Subsection C concerns itself with such configurational changes.

A. EFFECTIVE VEHICLE CONTROL CHARACTERISTICS

The pertinent vehicle dynamic features are the attitude, airspeed, and altitude responses to the two longitudinal controls — elevator, δ_e, and collective, δ_c. As in the previous study of hover control, we again assume that the pilot always controls the pitch attitude with the elevator (i.e., longitudinal stick). In other words, we envision that in transition he uses pitch control, the elevator, either to hold a preselected attitude or as the series inner command loop structure, to change attitude as necessary to operate on the outer-loop errors. As a preliminary to the more realistic

multiple-loop control situations implied from this latter statement, it is worthwhile to familiarize the reader both with the general properties of the pole/zero locations in transition and with the features of the simple single-loop closures. Both the elevator and collective are explored in the following subsections to relate how pilot's control might be affected by the "bare" airframe characteristics.

1. "Bare" Airframe Features

The attitude response will serve as the indicator of how the "bare" airframe characteristics change in the transition from aerodynamic (i.e., conventional) to thrust supported (i.e., VTOL-like) flight. The open-loop θ/δ_e frequency response sketched in Fig. 33 illustrates this change in both characteristic modes and control numerator factors. The three steady-state, trim level flight conditions shown are for hover, 60 and 80 knots. These response diagrams were derived from the transfer functions tabulated in Table XIV for the XC-142A aircraft.

The low frequency features associated with the phugoid mode dominate the dynamic response diagrams shown in Fig. 33. In fact, without the aid of the asymptotes shown in the diagrams it would be difficult to identify the significant changes in dynamics from only the amplitude characteristics of these plots. As such, a suitable identification is that the responses appear as low frequency, second-order modes which change from a stable lightly damped situation at 80 knots to an unstable situation below 60 knots.* A closer look at these dynamics as well as at the remaining transfer functions of Table XIV reveals the more subtle aspects of the dynamic changes. For example, at the 80 knot condition both short-period and phugoid modes are evident and the vehicle characteristics may be judged more or less quasi-conventional. At the 60 knot condition the static stability, defined by M_α, is essentially zero and the phugoid mode dynamics dominate entirely; that is, the speed stability term, M_u, dominates. Further, from the Table XIV transfer functions we see that at the 60 knot condition the vehicle heave response is essentially uncoupled from pitch by the almost exact cancellation of the numerator $(1/T_{\theta_2})$ and denominator $(1/T_{sp_1})$ terms, both strong functions of the effective lift curve slope. This characteristic cancellation was also evident in the hover mode analysis in Section II of this report. In fact, it was this aspect that we used to identify and classify the hover characteristics. Note, additionally, that the altitude numerator at 60 knots shows the vehicle to be on the front side of the drag or power required curve since the factor $1/T_{h_1}$ is positive. Front side operation at this high powered, high lift condition is unusual and is an artifact of the XC-142 configuration which is given more detailed consideration later in this section.

*The reader is reminded that for unstable (i.e., nonminimum phase condition) the phase angle features provide the means of determining stability from the Bode responses.

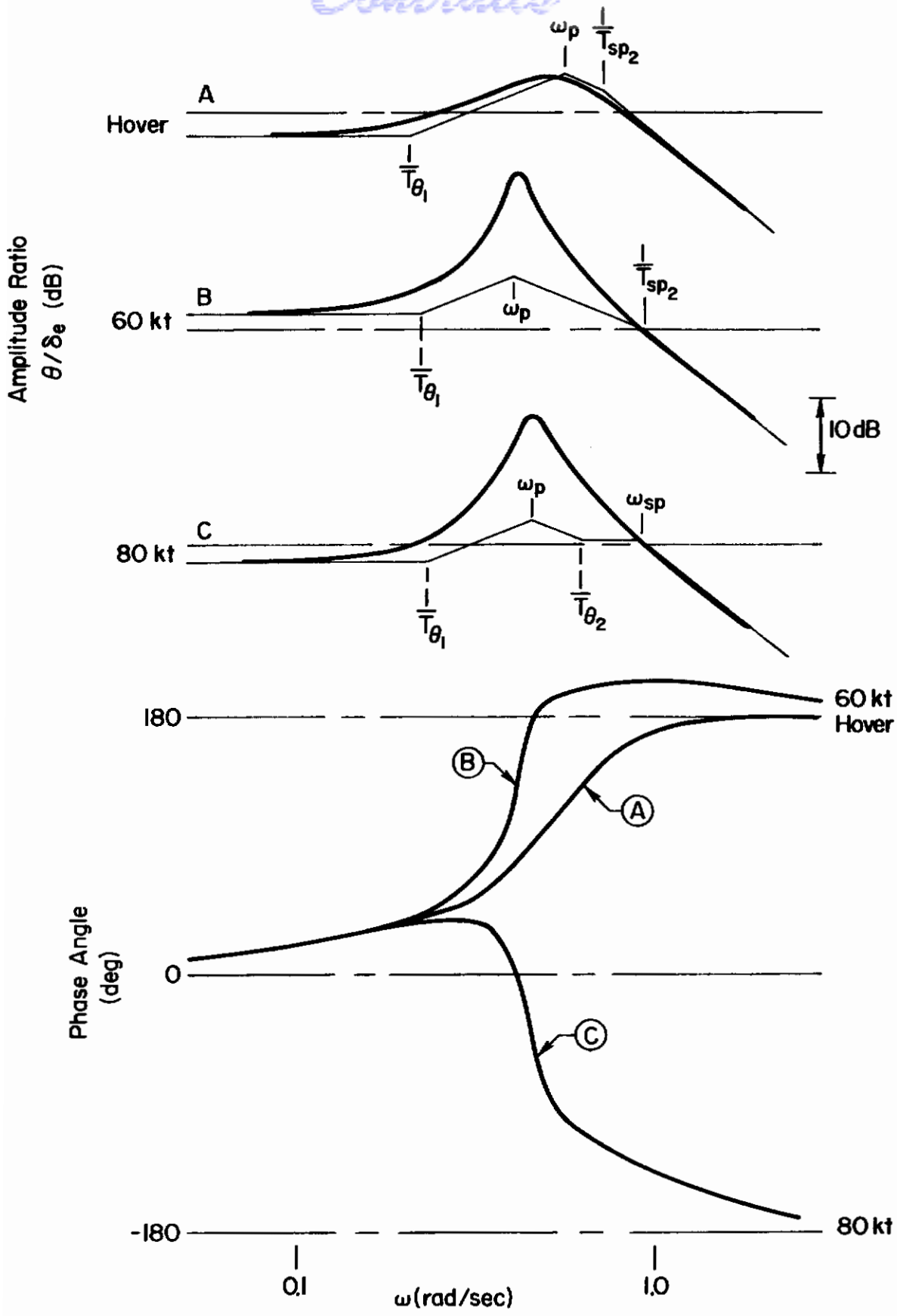

Figure 33. Attitude Dynamic Features for Steady-State Trim Condition in Transition

TABLE XIV

XC-142 — TRANSITION LONGITUDINAL DYNAMIC CHARACTERISTICS

		SPEED U_o (KNOTS)			
		40	60	80	120
DENOMINATOR	ω_{sp} ζ_{sp} ω_p ζ_p	$1/T_{sp_1} = 0.129$ $1/T_{sp_2} = 1.122$ 0.378 −0.279	$1/T_{sp_1} = 0.552$ $1/T_{sp_2} = 0.940$ 0.411 −0.109	0.942 0.745 0.459 0.104	1.60 0.624 0.352 0.306
ELEVATOR	$1/T_{\theta_1}$ $1/T_{\theta_2}$	0.193 0.509	0.225 0.566	0.234 0.635	0.241 0.798
	$1/T_{u_1}$ $1/T_{u_2}$ $1/T_{u_3}$	0.432 298.1 −	0.667 −13.5 14.9	0.918 −94.87 −	1.32 −12.6 15.6
	$1/T_w$ ω_w ζ_w	20.31 0.414 0.279	28.7 0.319 0.303	38.16 0.229 0.432	53.7 0.172 0.642
	$1/T_{h_1}$ $1/T_{h_2}$ $1/T_{h_3}$	−0.172 −2.59 3.45	0.0562 −3.72 4.47	0.142 −4.59 5.44	0.198 −6.0 7.16
COLLECTIVE	$1/T_w$ ω_w ζ_w	1.015 0.402 −0.258	3.63 0.332 0.154	3.21 0.328 −0.0132	11.924 0.219 −0.0104
	$1/T_{\theta_1}$ $1/T_{\theta_2}$	−1.15 0.379	−0.141 0.567	−0.136 0.534	−0.117 0.755
	$1/T_u$ ω_u ζ_u	1.198 0.454 −0.377	0.708 1.163 0.187	0.345 1.105 0.381	0.289 1.707 0.487
	$1/T_h$ ω_h ζ_h	1.102 0.339 −0.307	$1/T_{h_1} = 1.827$ $1/T_{h_2} = -0.135$ $1/T_{h_3} = -0.725$	1.71 0.539 −0.566	$1/T_{h_1} = 3.55$ $1/T_{h_2} = -0.242$ $1/T_{h_3} = -1.739$
COUPLING NUMERATORS	$N^{\theta\ u}_{\delta_e\delta_c}$	(s + 0.519)	(s + 0.538)	(s + 0.561)	(s + 0.781)
	$sN^{\theta\ h}_{\delta_e\delta_c}$	(s + 0.463)	(s + 0.382)	(s + 0.336)	(s + 0.538)
	$sN^{h\ u}_{\delta_e\delta_c}$	(s − 4.88)(s + 5.32)	(s − 4.96)(s + 5.57)	(s − 5.59)(s + 6.39)	(s − 6.18)(s + 7.33)

TABLE XIV (Concluded)

XC-142 HOVER DYNAMICS

Denominator

ζ_p	= −0.373	$1/T_{sp_1}$	= 0.0650
ω_p	= 0.570	$1/T_{sp_2}$	= 0.722

δ_e Numerators (Elevator)

$1/T_{\theta_1}$	= 0.210	$1/T_w$	= 0.834
$1/T_{\theta_2}$	= 0.0663	ζ_w	= −0.228
$1/T_{w_1}$	= 0.0663	ω_w	= 0.531
$1/T_{w_2}$	= —	$1/T_h$	= 0.731
$1/T_{w_3}$	= —	ζ_h	= −0.386
		ω_h	= 0.562

δ_c Numerators (Collective)

$1/T_{\theta_1}$	= −0.0457	ζ_w	= −0.375
$1/T_{\theta_2}$	= 0.210	ω_w	= 0.571
$1/T_{w_1}$	= −0.0457	$1/T_h$	= 0.722
$1/T_{w_2}$	= —	ζ_h	= −0.373
		ω_h	= 0.570

2. Single-Loop Control Characteristics

Because the hover-like qualities at 60 knots are not representative of conditions throughout transition, the 80 knot case was selected as the base for generic examination of the single-loop pilot/vehicle control aspects of transition flight. This examination starts with the elementary attitude/elevator loop and progresses through various other loops pertinent to the complete control situation. The closure features are illustrated by root locus diagrams assuming that the pilot function is a simple gain feedback with no additional compensation.

a. Pitch Attitude Control, $\theta \rightarrow \delta_e$. The $\theta \rightarrow \delta_e$ single-loop closure is sketched below. Although the short-period and phugoid mode are relatively close, the unequalized closure shows the conventional tendency for the attitude closure to stabilize the phugoid by driving the roots into the attitude numerator zeros $1/T_{\theta_1}$ and $1/T_{\theta_2}$. Because of the low frequency short period mode of the "bare" airframe, the closed-loop bandpass will be less than the desired 2.5 rad/sec. However, this condition (i.e., $\omega_c < 2.5$) is readily alleviated by the pilot's generation of a reasonable attitude lead, $1/T_{L_\theta}$.

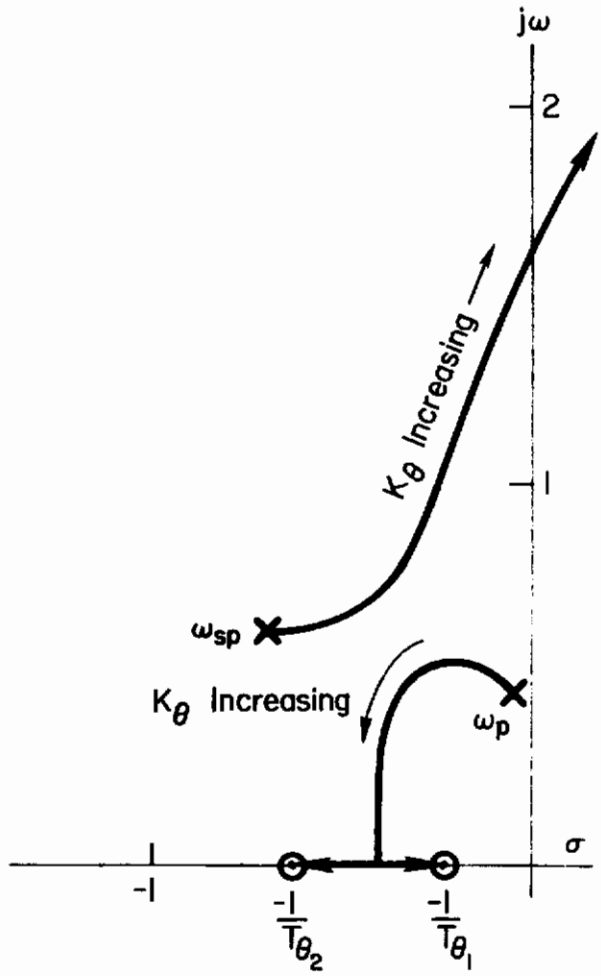

Attitude/Elevator Closed-Loop Control

b. Altitude Control, $h \rightarrow \delta_e$ or $h \rightarrow \delta_c$. The closure features of $h \rightarrow \delta_e$ and $h \rightarrow \delta_c$ single loops are shown below in the root loci sketches. Altitude control with the elevator indicates that this condition is on the front side of the drag curve (i.e., $1/T_{h_1} > 0$). Altitude control bandpass with the collective is limited by the unstable second-order zeros which are approximately equal to the phugoid mode. These unstable ω_{hc} zeros are due to the large thrust line offset (above the c.g.) in the XC-142. Note, also, that $1/T_{hc_1}$ is determined by thrust axis inclination, i.e., $X_{\delta_c}/Z_{\delta_c}$. In this closed-loop situation, the short period can also be driven unstable; however, since the short period is reasonably well damped ($\zeta_{sp} > 0.5$), no significant control problem exists in this respect. For both types of control, the limiting crossover frequency is set by the tendency to drive the phugoid unstable; obviously the countertendency of the attitude loop to stabilize the phugoid (preceding sketch) will be helpful in this respect when the multiple-loop situation is considered later.

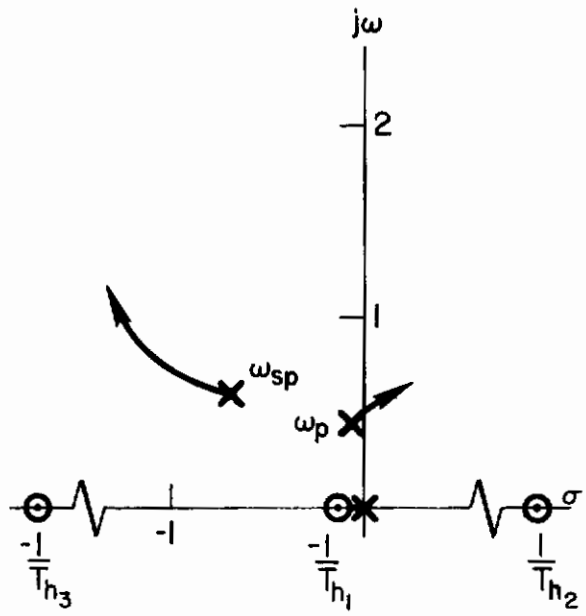

Altitude/Elevator Closed-Loop Control

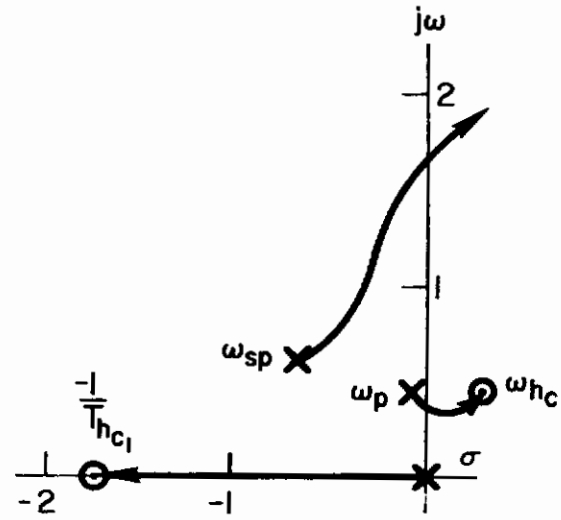

Altitude/Collective Closed-Loop Control

c. Airspeed Control, $u \rightarrow \delta_e$ or $u \rightarrow \delta_c$. The $u \rightarrow \delta_e$ and $u \rightarrow \delta_c$ single loops are shown in the following sketches. The $u \rightarrow \delta_e$ control, in effect, acts to increase M_u (i.e., increase ω_p), which results in a phugoid mode instability at very low gain. For collective control the large thrust offset displaces the $u \rightarrow \delta_c$ numerator second-order to a relatively high frequency. Feedback of the collective control thus increases the phugoid frequency and damping because of this high frequency zero, ω_{u_c}.

The right-half plane location sketched for the $u \rightarrow \delta_e$ zero, $1/T_{u_1}$, results from the positive X_w, in turn due to the combined high-power and lift necessary for trim level flight. That is, from the approximate expression for $1/T_{u_1}$ shown below, when $X_\alpha = U_o X_w$ is greater than g, the zero is unstable. However, its

$$\frac{1}{T_{u_1}} = -\frac{M_{\delta_e}(X_\alpha - g)}{Z_{\delta_e} X_w}$$

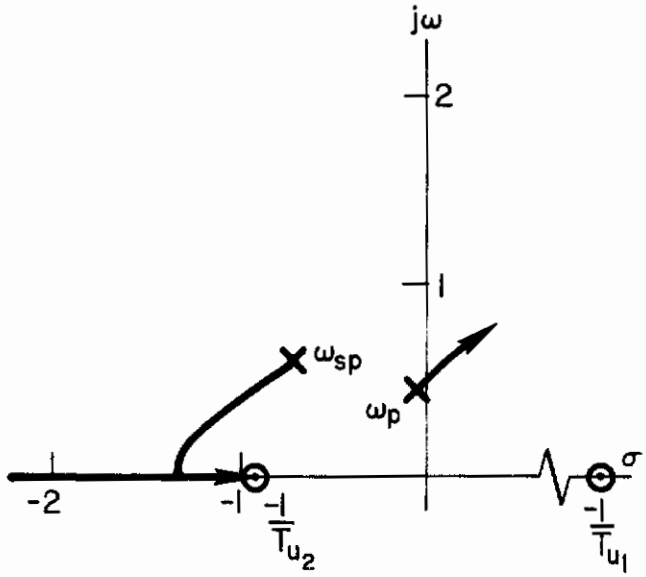

Airspeed/Elevator Single-Loop Control

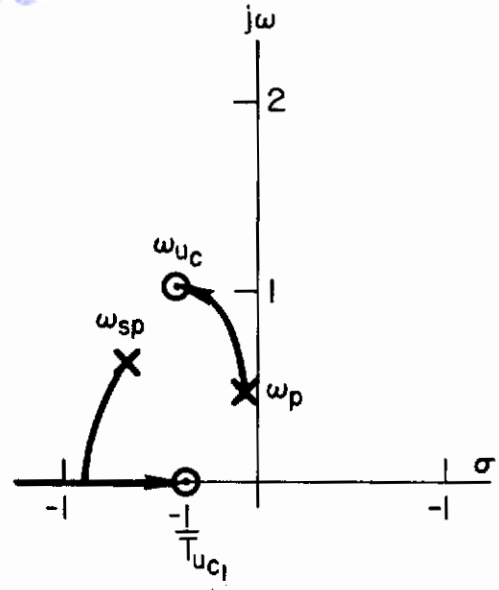

Airspeed/Collective Single-Loop Control

magnitude is generally too large (as in the present example) to be of concern in the frequency range of interest; and conventional elevator control piloting techniques are usually unaffected in the region $50 < U_o < 120$ by (negative) $1/T_{u_1}$ considerations. However, such considerations can become important for very short coupled (i.e., M_δ/Z_δ small) vehicles (e.g., jet lift or tilt duct aircraft where short tail arms may be desirable from engine failure considerations) or for high gain velocity feedback systems employing $u \rightarrow \delta_e$ feedback.

Although not indicated by the XC-142 transfer functions the X_w term may also modify the θ numerator and produce a similar nonminimum phase zero in the attitude loop. In this instance, the negative root ($1/T_{\theta_1}$) occurs when X_w is a large negative value, and the effective Z_w is low. The approximate expression below for small X_δ, Z_δ (see Appendix B) shows the dependence of the zero location on these two terms:

$$\frac{1}{T_{\theta_1}} \cdot \frac{1}{T_{\theta 2}} \doteq X_u Z_w - X_w Z_u$$

Obviously, then, $X_w Z_u > X_u Z_w$ is the condition for this unconventional location of the $1/T_{\theta_1}$ zero. The only apparent significance of this situation is related to a pitch attitude/rate stabilization system (see Section II). Because of the right-half plane zero, the resulting closed-loop phugoid for high gain will consist of two aperiodic modes, one of them slowly divergent.

In summary, the major problems of single-loop control are associated with the low frequency (phugoid) characteristics poles and with certain of the low frequency numerator zeros, some of which can be nonminimum phase (right half plane location) and thereby contribute to an instability near the phugoid mode when the loop is closed by the pilot. Because of this we can see that the modifications of these poles and zeros resulting from an inner-loop θ closure will constitute an important aspect in the appraisal of the multiloop control situation.

B. CLOSED-LOOP MANUAL CONTROL TECHNIQUES IN TRANSITION

By analyzing the possible loop structures the pilot might use we can determine the technique the pilot is most likely to employ, the probable reasons for his preference, the parameters that govern his choice, and the situations under which he might advantageously change to a different technique. This procedure is of advantage not only in preliminary design and specification activities, but also in clearly identifying problem areas and interpreting ground and flight simulation, or flight test, results. Our experience has shown that pilot are not generally fully aware of their flying technique at the detailed level available through such analyses. In fact, using the analyses as a base on which to frame proper questions to the pilot will make him more fully aware of his activities and control problems; and generally lead to better communication between him and the handling qualities or flight-control engineer.

The two multiloop control techniques studied here relate to the pilot's ability to control flight path using the available controls. Two competing control structures are considered in which the pilot is assumed to exercise a different closed-loop strategy. The conversion control (i.e., wing incidence) is not included because, as shown in the next subsection C, its characteristics are similar to those given by direct thrust variations. A study of these alternative techniques provides an effective basis upon which to judge the needs for manual control in transition and the consequences of variations in basic airframe stability and control derivatives. The two techniques involve either control of altitude with collective and airspeed with elevator or, conversely, altitude with elevator and airspeed with collective (or throttle). In either case, attitude control with elevator is the basic inner loop. The block diagrams in Fig. 34 illustrate schematically the control structures involved. To simplify the identification of these piloting techniques in the following discussions, we will utilize the variable being controlled directly by the collective (or throttle) as the key. Thus the control technique shown in Fig. 34a in which pilot's control of altitude is accomplished via attitude commands controlled with the elevator and airspeed with collective is denoted simply as airspeed/collective control.

The successive loop closures which are implied for each of the multiloop control situations follow the analysis techniques already discussed in preceding sections and are developed in detail in Ref. 24; however, for the readers' benefit, an example closure is presented in Appendix E.

1. Pitch Attitude Control, $\theta \rightarrow \delta_e$ Loop

As noted above, attitude control with elevator ($\theta \rightarrow \delta_e$) is the fundamental inner loop for the two control structures. Figure 35 shows the $\theta \rightarrow \delta_e$ closure for the 80 knot condition; note the shorthand convention used to designate the numerical open-loop transfer function. The phugoid and short-period frequencies are relatively closely coupled (i.e., $\omega_{sp} \doteq 2\omega_p$). The combined effect of the $2\omega_p \doteq \omega_{sp}$ condition and the closely related numerator terms, $1/T_{\theta_1}$ and $1/T_{\theta_2}$, is that, without pilot lead (T_{L_θ}), the Bode is similar to that of a lightly damped low frequency second order attitude system, as noted earlier (Fig. 33). The K/s^2 asymptote above ω_{sp} requires lead by the pilot to obtain the desired K/s crossover near 2.5 rad/sec; and Fig. 35 shows an appropriate lead of $1/T_{L_\theta}$

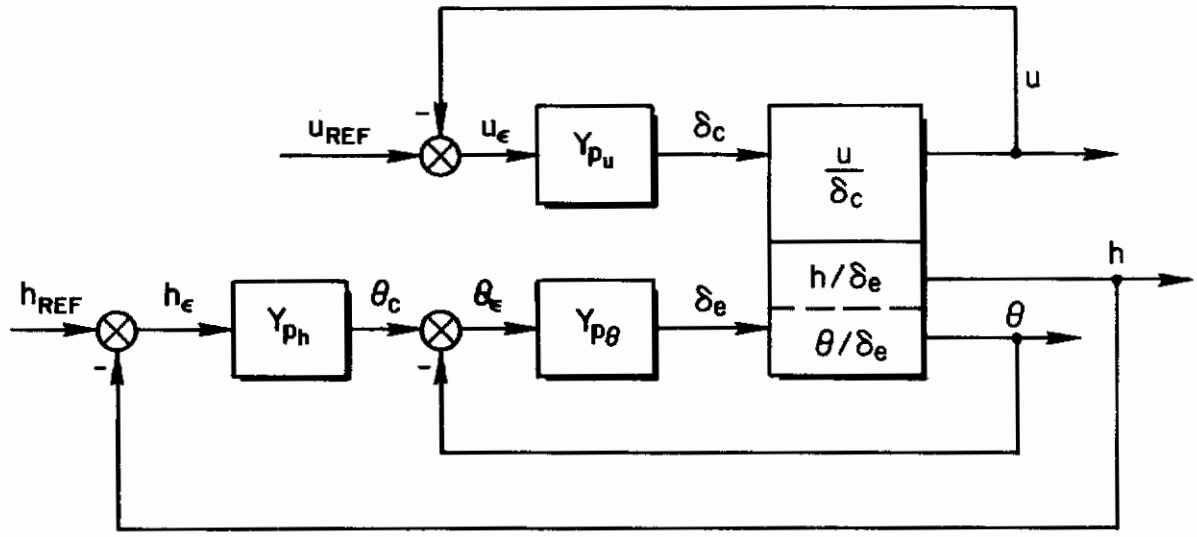

a) Airspeed / Collective Control

(h, $\theta \rightarrow \delta_e$, u $\rightarrow \delta_c$)

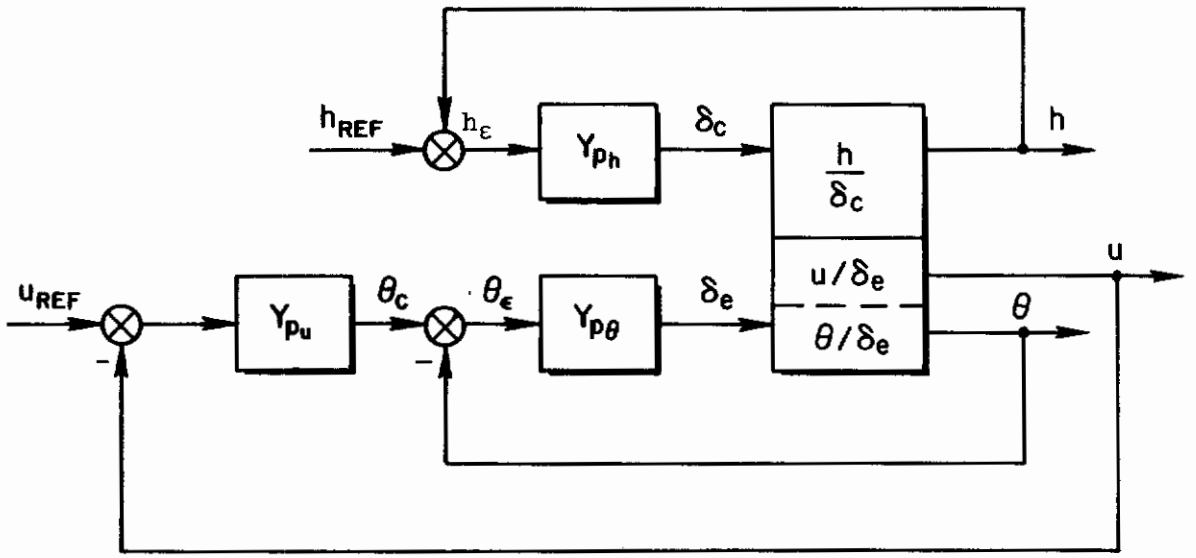

b) Altitude / Collective Control

(u , $\theta \rightarrow \delta_e$, h $\rightarrow \delta_c$)

Figure 34. Block Diagram for Closed-Loop Control Techniques

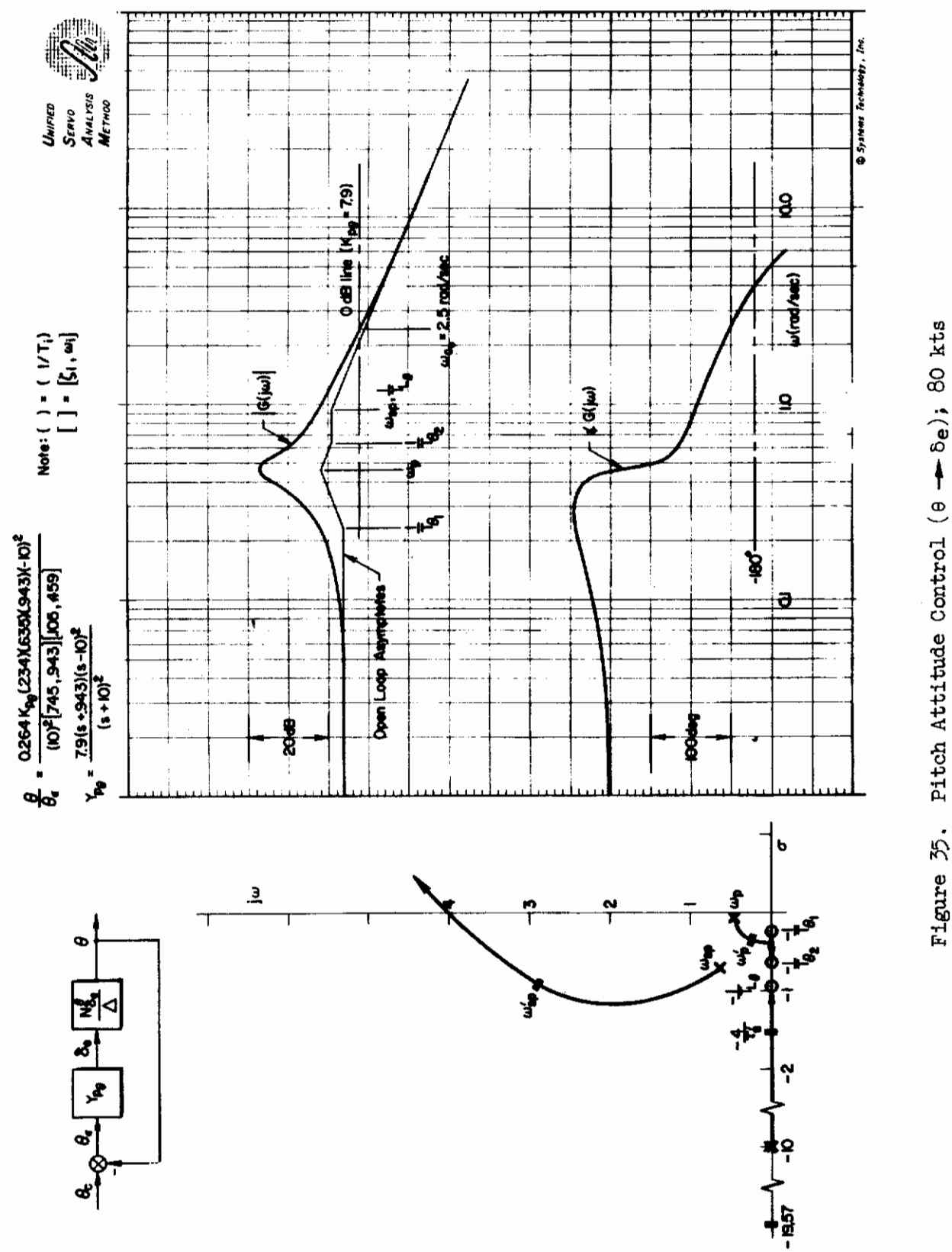

Figure 35. Pitch Attitude Control (θ → δe); 80 kts

approximately equal to ω_{sp}. This level of lead (i.e., $1/T_{L_\theta} \doteq 1$ rad/sec) is demanding but is not considered excessive for satisfactory pilot ratings. Note, however, that with this compensation regulatory control of attitude disturbances appears marginal because of the resulting low dc gain. The importance of having a tight attitude control loop as the basic inner loop and a high bandpass ($\omega_{c_\theta} \doteq 2.5$ rad/sec) "effective airframe" on which to erect the final multiloop flight path control structure will be more clearly demonstrated in the later phases of this survey.

2. Altitude Control Features

Altitude control with attitude and airspeed loops closed is shown for the airspeed/collective and altitude/collective in Figs. 36 and 37, respectively. These show the resulting altitude outer loop after <u>both</u> the attitude loop, just discussed, and the appropriate airspeed loops have been properly closed. Thus the open-loop factors appearing in Figs. 36 and 37 are double-primed, signifying that <u>two</u> loops (in this case, attitude and airspeed) have already been closed. The detailed process of getting from the single-primed factors resulting from the attitude-loop closure (Fig. 35) to the outer-loop double-primed factors is given in Appendix E for the Fig. 36 example. Such details would detract from the straightforward discussions and resulting conclusions sought here and they have therefore been deleted from the main text.

The final outer-loop characteristics displayed in Figs. 36 and 37 show a reasonably broad K/s-like range (e.g., K/s region $\omega \leq 0.7$ rad/sec) for both techniques with a somewhat higher maximum uncompensated system bandpass for the airspeed/collective technique. The near equivalence of the two techniques is somewhat unexpected since we would have anticipated from the pilot comments (Ref. 20) that collective control of altitude in a manner analogous to DLC (direct lift control) would be superior. The explanation, in this case, as to why altitude control with elevator appears equivalent if not superior, lies partly in the favorable interactions of the two intermediate closures — attitude with elevator and airspeed control with throttle. These interactions are traced in detail in Appendix E, and essentially consist of replacing the phugoid with two first orders near $1/T_{u_c}'$ and $1/T_{L_\theta}'$ [designated $1/T_{C_L}''$ and $(4/\tau_e'')_2$, respectively, in Fig. 36] because of the increased effective M_u and Z_u terms. The ω_p'', ω_h'' high frequency second-order dipole-pair shown in Fig. 36 is akin to a surface-actuator mode although ω_p'' does lie, in Fig. E-3 of Appendix E, on the locus emanating from ω_p'. In any event, these roughly cancelling factors are outside the frequency range of most interest and exert little influence on the final closure shown in Fig. 36. However, the reduction in ζ_{sp}'' attending the $u \rightarrow \delta_c$ closure is important and tends to detract from the beneficial effects on the phugoid which basically stem from the influence of the thrust line offset characteristics of the tilt wing XC-142 configuration. An extremely tight closure (high gain closure for intermediate $u \rightarrow \delta_c$) of airspeed is indicated here which has a very broad bandpass airspeed control ($\omega_{c_u} > 2$ rad/sec) (e.g., see Fig. 38). Such tight control of airspeed is not considered representative of normal pilot control; however, this somewhat unrealistic situation does not detract from the validity of the foregoing discussion.*

*The reader may verify this conclusion from the loci of the $u \rightarrow \delta_c$ closure of Fig. E-3 of Appendix E, where it is evident that, while a lower pilot gain would reduce the bandpass, the basic closed-loop characteristics are not modified.

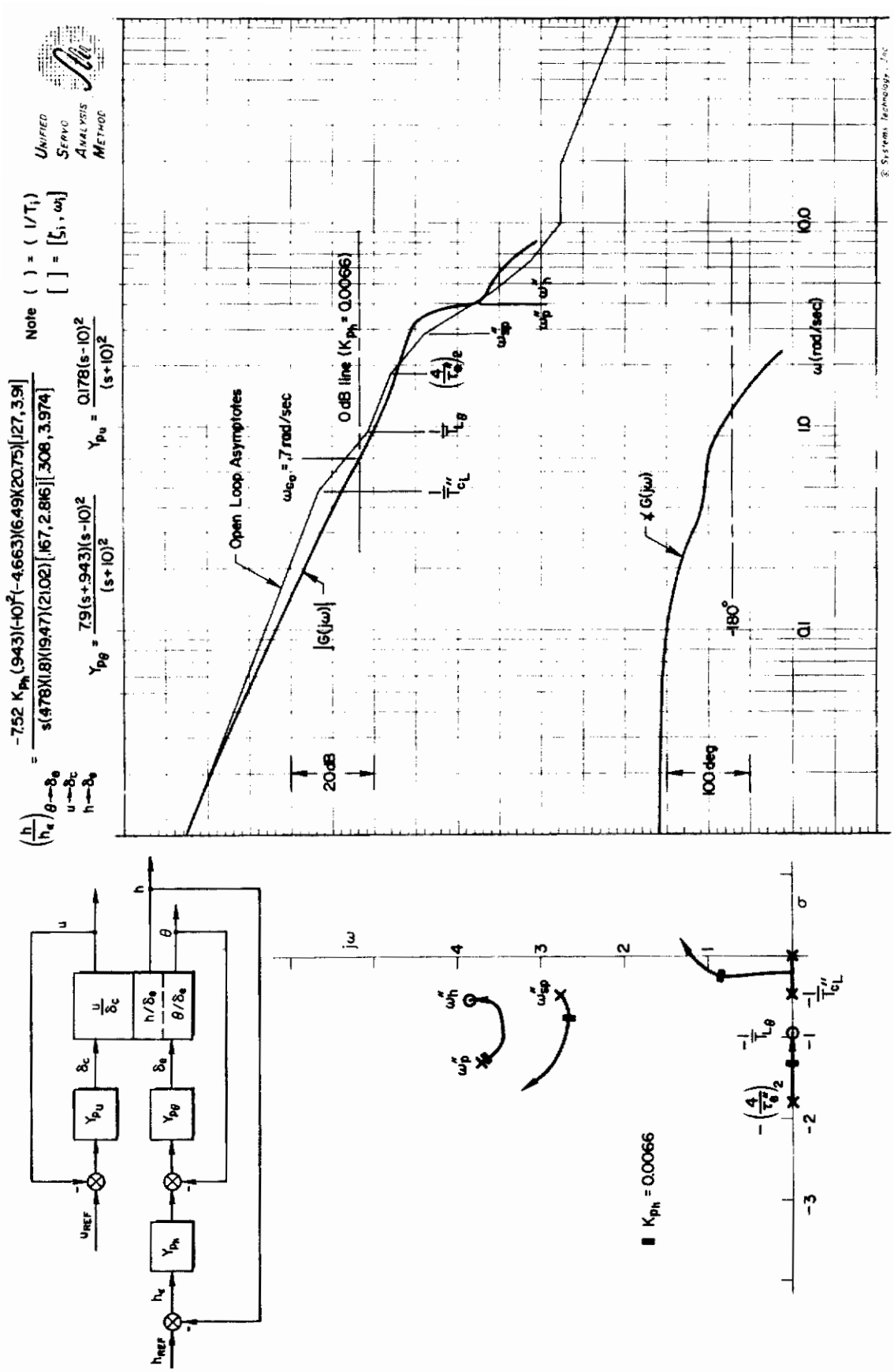

Figure 36. Airspeed/Collective Closed-Loop Control; h, θ → δe, u → δc (Altitude)

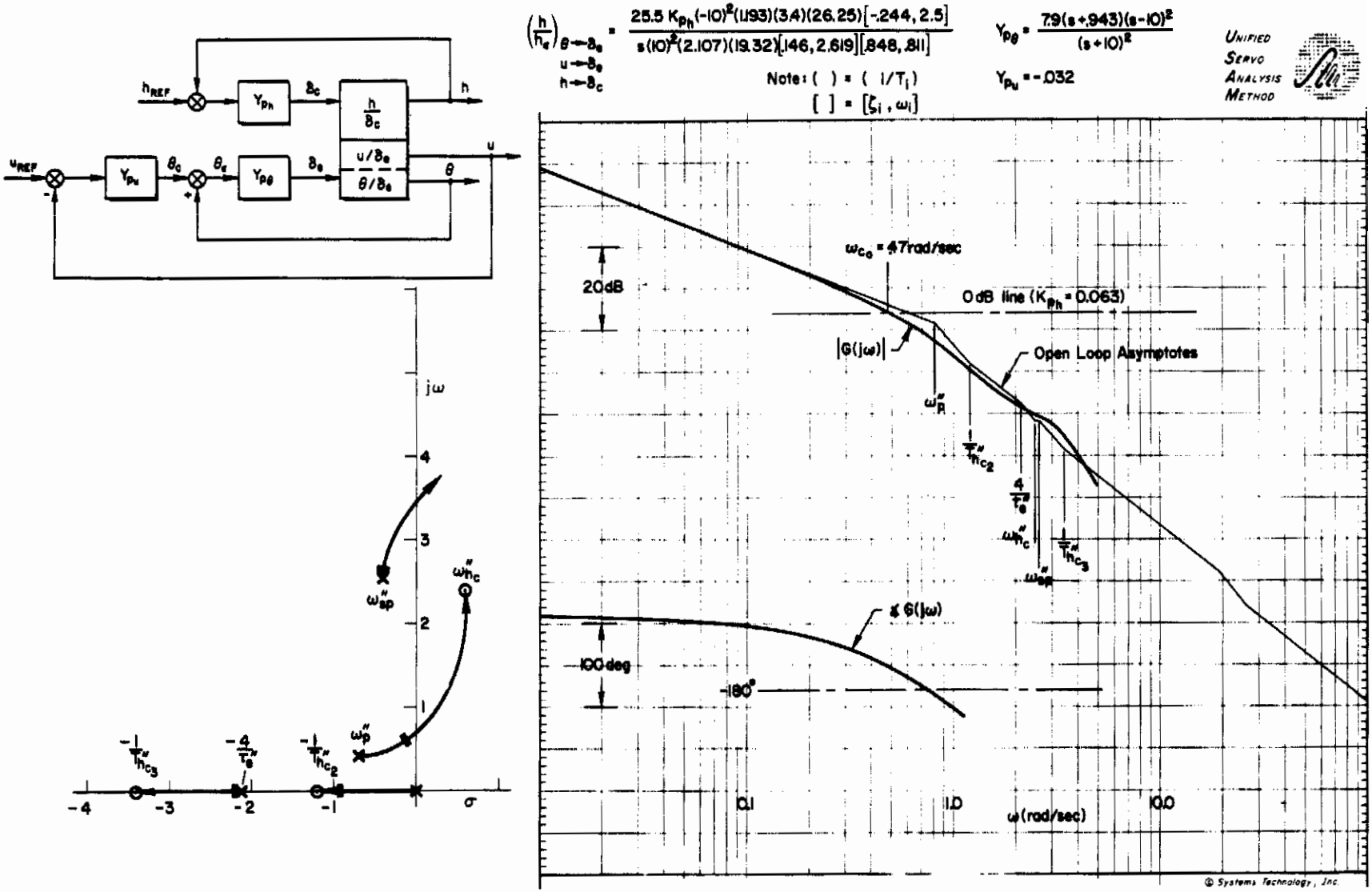

Figure 37. Altitude/Collective Closed-Loop Control, u, $\theta \rightarrow \delta_e$, h $\rightarrow \delta_c$

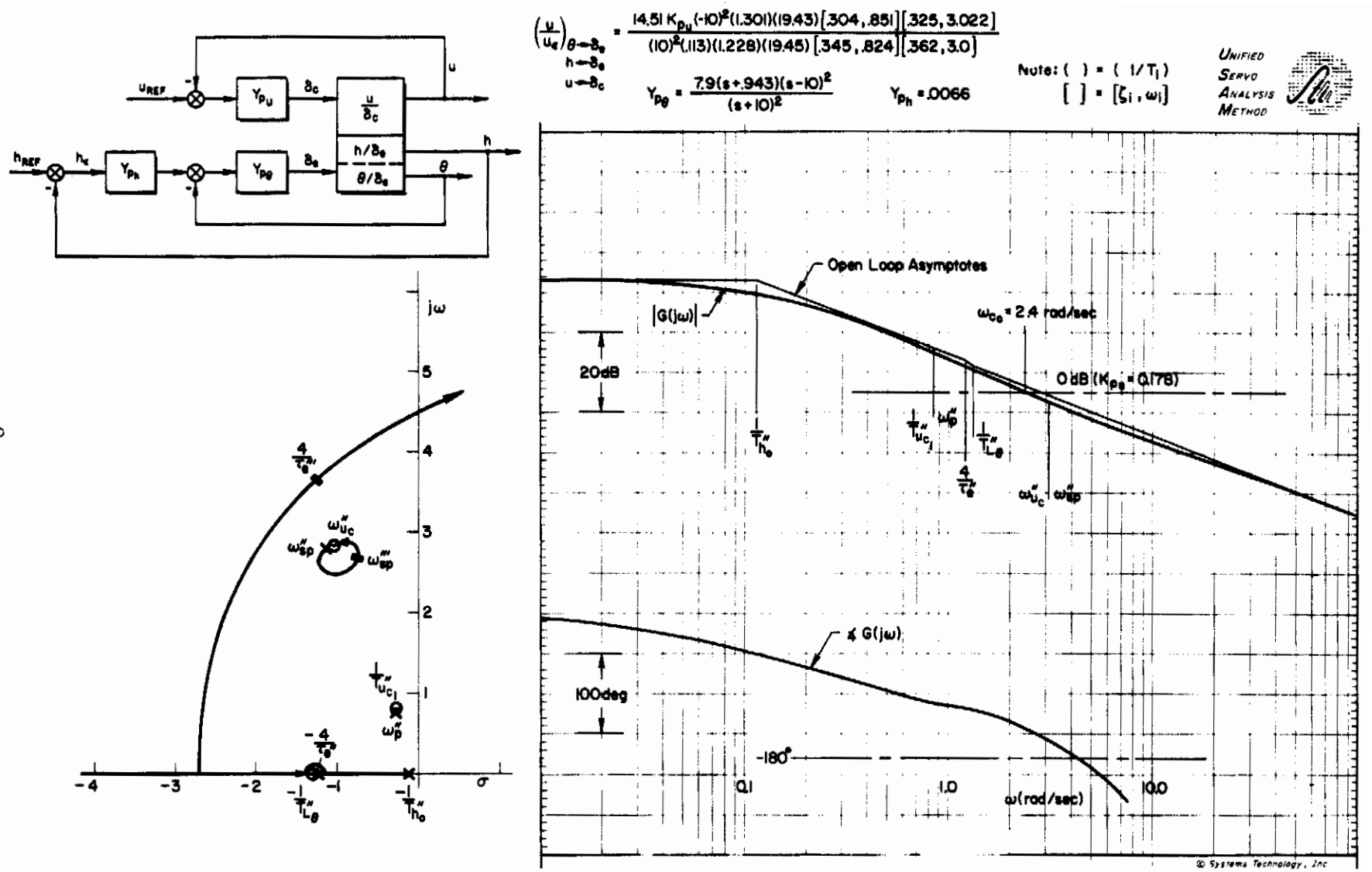

Figure 38. Airspeed/Collective Closed-Loop Control; h, $\theta \rightarrow \delta_e$, u $\rightarrow \delta_c$ (Airspeed)

In fact, if collective control of airspeed ($u \rightarrow \delta_c$) were eliminated, altitude control with the elevator would remain essentially unchanged, as shown in Fig. 39. Note here that the altitude bandpass is established by the ω_p'' root instead of the two first-order roots [$1/T_{C_L}''$ and $(4/\tau_e'')_2$] cited in the case where the collective control is employed (see Fig. 36). In either case these situations are similar to those discussed in the carrier approach studies of Ref. 25. This study showed that the altitude bandpass with the elevator is restricted by the closed-loop phugoid mode (ω_p'') which is approximately equal to the value of $1/T_{\theta 2}$. Here the intermediate closed-loop, ω_p' (Fig. 35), is strongly influenced by the attitude numerator zero, $1/T_{\theta 2}$; and the final ω_p'' is, again, nearly equal to $1/T_{\theta 2}$.

Even with the beneficial effects of the intermediate airspeed control loop eliminated, altitude control with elevator (Fig. 39) is still at least as good as that for the complete altitude/collective technique (Fig. 37). However, we can improve the latter by eliminating the intermediate airspeed/elevator control loop which now has a detrimental effect on altitude control. Altitude/collective characteristics without airspeed control as displayed in Fig. 40 are much superior (e.g., higher crossover) to those with airspeed control shown in Fig. 37. The potential instabilities exhibited in Fig. 37 (e.g., numerator ω_{h_T}'' located in right half plane) are not present when the airspeed control loop is eliminated. Furthermore, the available bandwidth is about the same as that attainable with elevator control of altitude (Fig. 39).

On the basis of the foregoing analyses and considerations, the simplest and best technique for control of altitude is to pay little, if any, attention to airspeed, hold and regulate attitude tightly with elevator, and control altitude separately (as with DLC) with the collective. This conforms with pilot commentary, but still leaves the question of airspeed control unresolved.

3. Airspeed Control

On the basis of the loop closures and sketches thus far considered, it is clear that airspeed control with collective is superior to that with elevator. That is, the comparative sketches for single-loop control of airspeed on p. 74 indicate stability problems for elevator control that don't exist for collective control. Also, the foregoing exercise shows that multiple-loop control of altitude is degraded by elevator control, but unchanged by collective control, of airspeed. Figure 41 solidifies this tentative conclusion by showing very broad K/s-like characteristics and high available crossovers for airspeed — collective control, regardless of whether or not the inner, attitude loop is closed.

But if the pilot tries to control airspeed with collective, what happens to his preferred technique for collective control of altitude? Figure 42 shows that, if anything, his control of altitude is improved over that without collective control of airspeed (compare with Fig. 40). However, we note that the lightly damped closed-loop short-period mode, ω_{sp}'', which is a consequence of the high gain $u \rightarrow \delta_c$ closure mentioned previously, does tend to restrict the potential bandpass somewhat. Of course, the time-shared usage of collective to alternately control altitude and airspeed would theoretically imply that both loops cannot be closed simultaneously; therefore, the applicability of Fig. 42 to the real-life situation could be questioned. However, we should recognize that pilot describing functions are necessarily a smoothed-over view

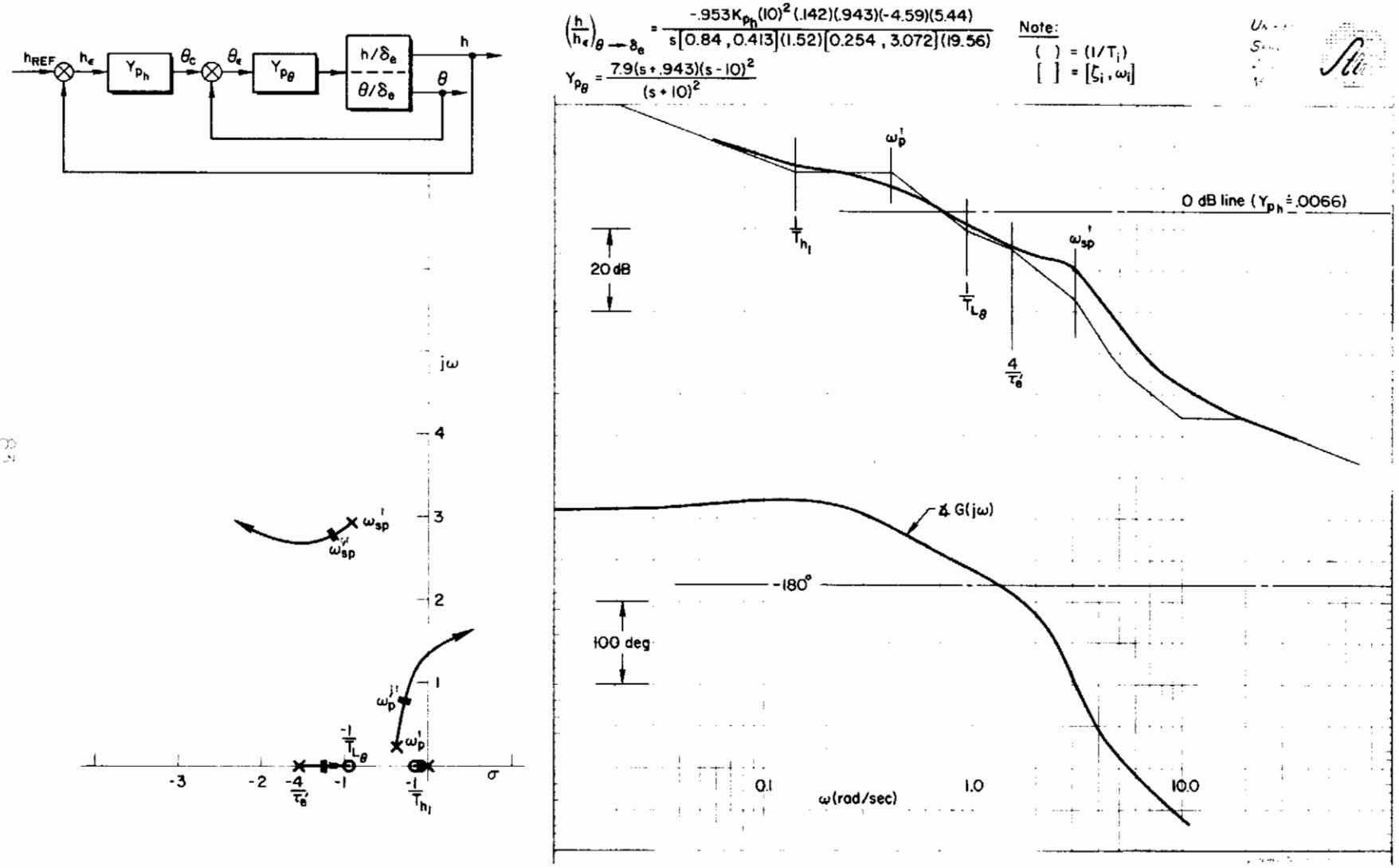

Figure 39. Altitude/Elevator Control Without Airspeed Regulation, h, $\theta \rightarrow \delta_e$

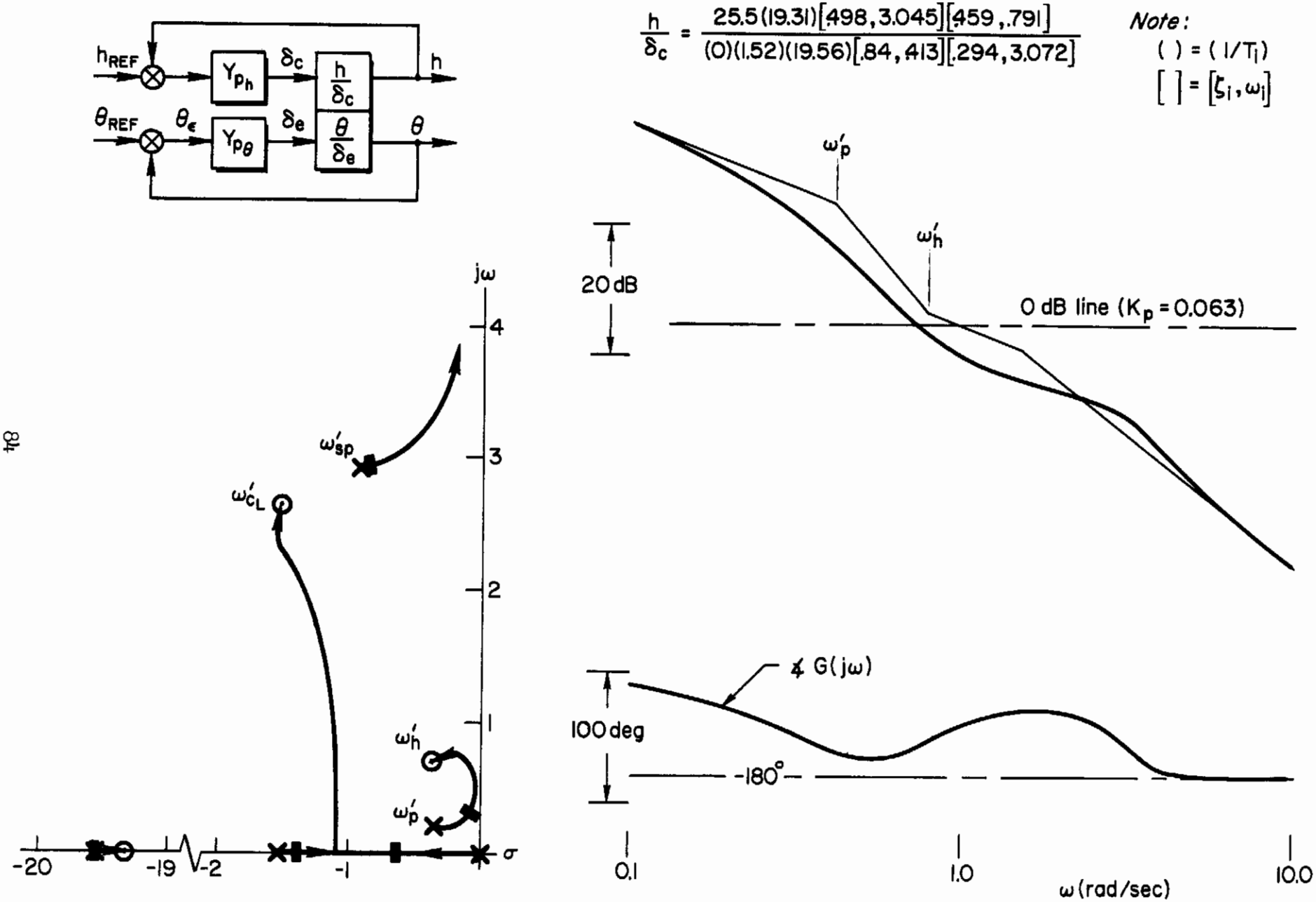

Figure 40. Altitude Control with Collective ($\theta \rightarrow \delta_e$, $h \rightarrow \delta_c$)

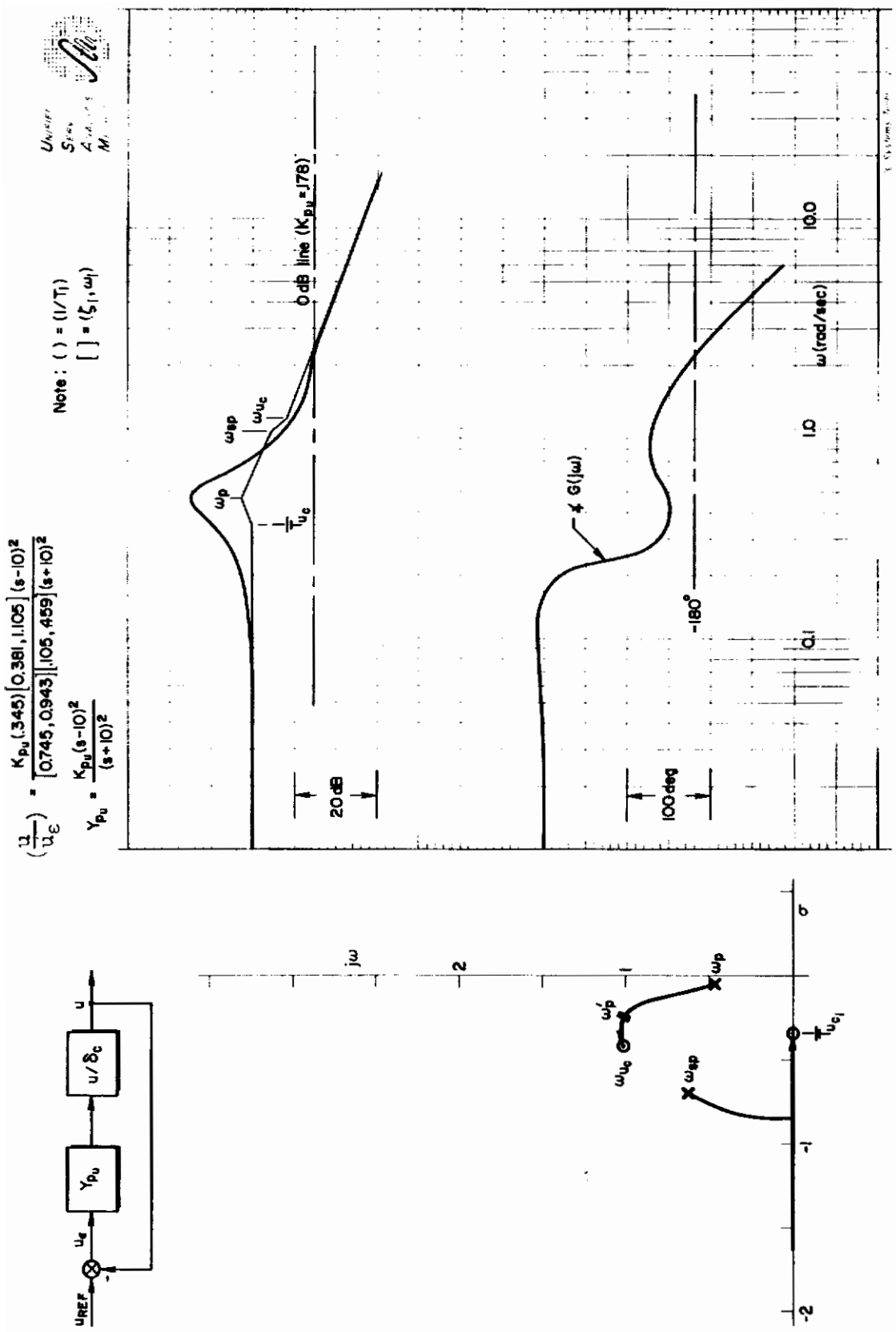

Figure 41. Airspeed/Collective Single-Loop Control Without Attitude Control; $u \rightarrow \delta_c$

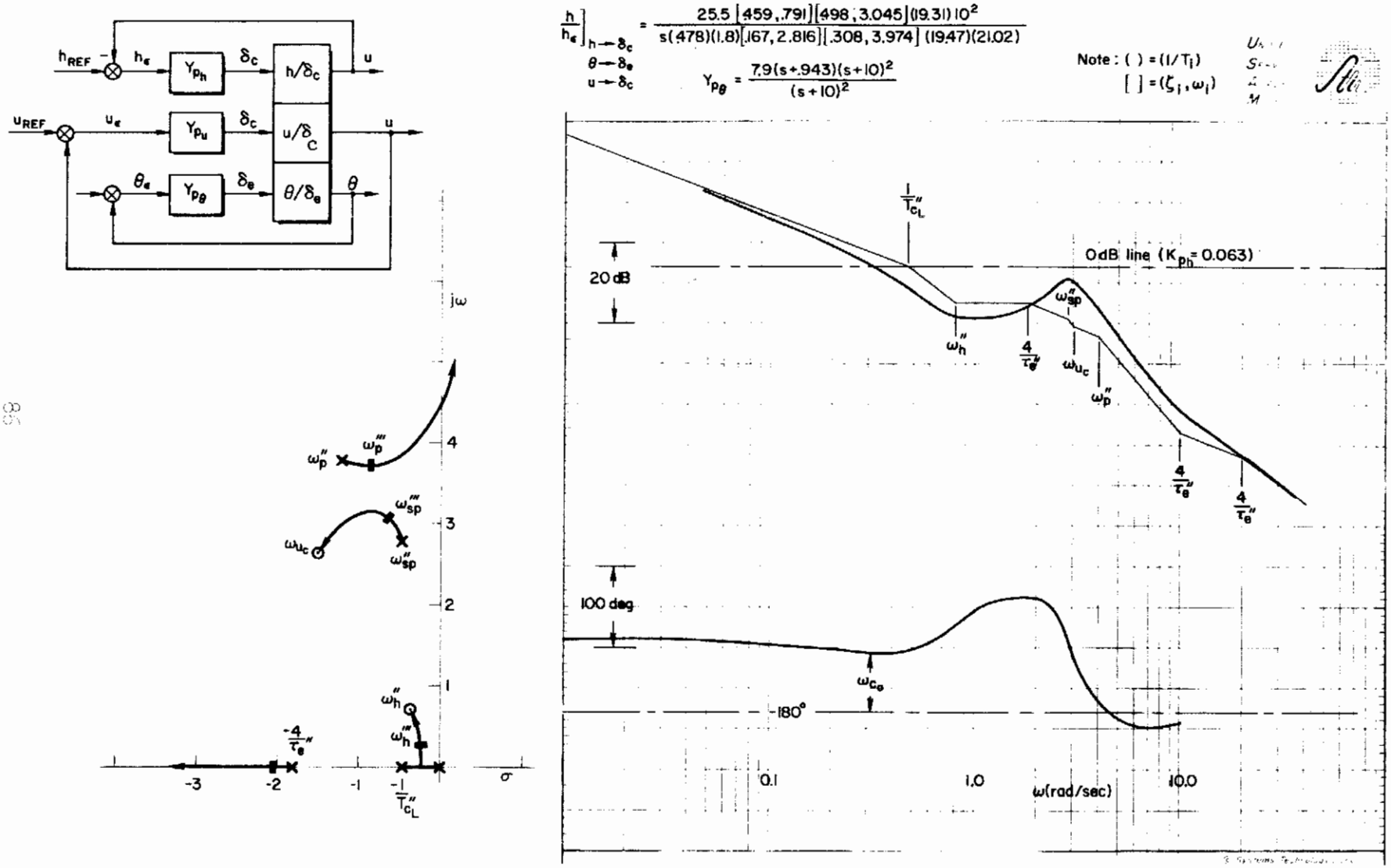

Figure 46. Collective Control of Airspeed and Altitude with Attitude Control; $u \rightarrow \delta_c$, $h \rightarrow \delta_c$, $\theta \rightarrow \delta_e$

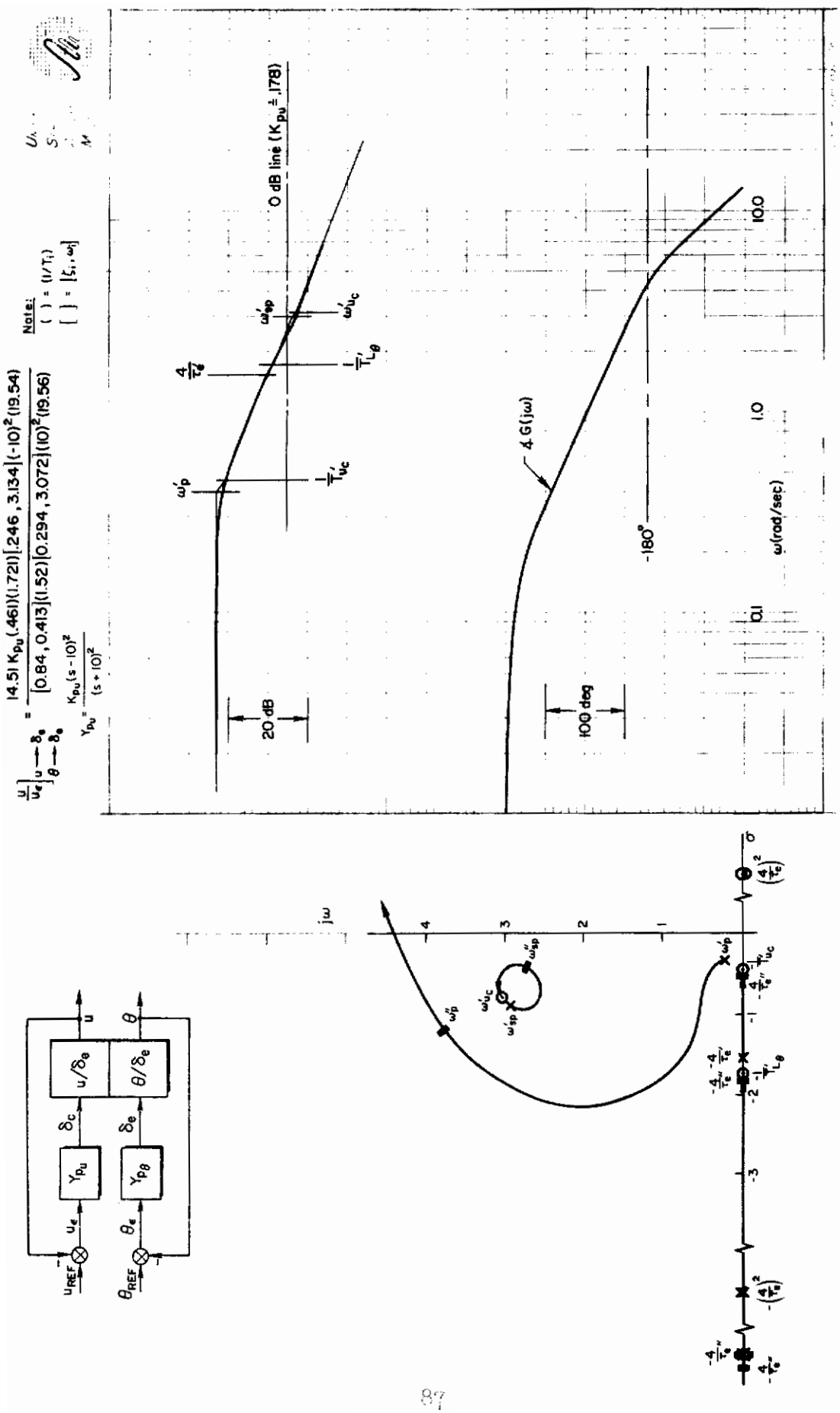

Figure 43. Airspeed/Collective Control with Attitude Control; $u \rightarrow \delta_c$, $\theta \rightarrow \delta_e$

of the pilot's experimentally-observed behavior, rather than a second-by-second, time-history description. Therefore, it is valid, for the relatively low activity involved (i.e., low gains in both loops) to consider that on the average the pilot is in fact closing both loops simultaneously.

Fortunately, in the present case, we can eliminate the above argument by noting that wing tilt is essentially equivalent to collective control (as shown later). Therefore, the pilot can use wing tilt to control airspeed, collective to control altitude, and elevator to regulate attitude. This complete separation of control function yields the very good performance corresponding to Figs. 40 and 43 and avoids the requirement for parallel control of two motion parameters (altitude, airspeed) with a single input device (collective).

4. Inner-Loop ($\theta \rightarrow \delta_e$) Compensation Effects and Implication for Desired Augmentation

The preceding analyses assumed that pilot compensation in the attitude loop was sufficient to cancel the adverse phase effects of the short-period mode and provide an attitude bandpass in the region of 2.5 rad/sec. This required a substantial, but not unreasonable, amount of pilot lead compensation ($1/T_{L_\theta} \doteq 1$ rad/sec) which suggests a relatively high degree of concentration. We will now reexamine the two basic control techniques to consider the effects on closed-loop performance of eliminating pilot compensation in the attitude loop (i.e., the simple-gain describing function form $Y_{p_\theta} = K_{p_\theta} e^{\tau s}$ will be used). From these results an assessment can be made of the relative effort the pilot must devote to the inner-loop task.

Figures 44-45 show the final outer-loop closures for the two original control techniques to permit direct comparison with Figs. 36 and 37. The distinctive feature of these closures is the fact that closed-loop short-period stability considerations now limit the gain and crossover frequencies. Furthermore, the overall superiority of the collective control of altitude (i.e., $h \rightarrow \delta_c$) is clearly evident from a comparison of the resulting bandpasses shown in Figs. 44 and 45; the $h \rightarrow \delta_c$ control (Fig. 45) shows almost twice the bandpass even with the detrimental effect of including $u \rightarrow \delta_e$.

The presence of the lightly damped short-period mode in both cases could lead to a PIO type of condition when the pilot attempts to obtain a "tighter" control of altitude. For example, if we assume that the pilot is operating with a small lag in the altitude control (e.g., smoothing the control inputs) the pilot may increase his gain, which correspondingly increases the altitude bandpass. With this lagged control technique the system is stable; however, if this lag is removed (i.e., abrupt rather than smooth inputs), for this same gain setting the h-loop is unstable. In exerting this tighter control, the pilot/vehicle instabilities or PIO oscillations are then possible at frequencies close to the closed-loop short-period (ω_{sp}''). This situation is caused by the low bandpass characteristics of the attitude loop which resulted from the inadequate lead compensation. Neither the $u \rightarrow \delta_c$ nor the $u \rightarrow \delta_e$ closures improves the damping of the short-period mode (the critical factor).

In summary, the overall task of longitudinal flight path control in transition is critically dependent on the performance of the inner pitch attitude loop. Generation of the required lead compensation in the attitude loop

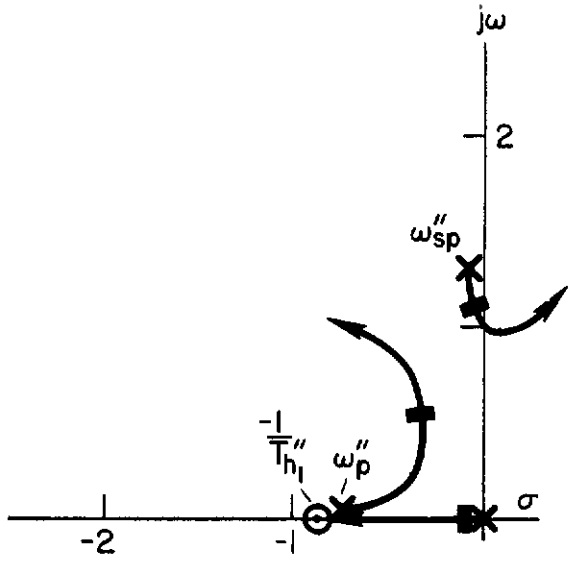

$$Y_{p_\theta} = \frac{4.8(s-10)^2}{(s+10)^2}$$

$$Y_{p_h} = 0.005$$

$$Y_{p_u} = \frac{.026(s-10)^2}{(s+10)^2}$$

$$\left(\frac{h}{h_\epsilon}\right)_{\substack{\theta \to \delta_e \\ u \to \delta_c \\ h \to \delta_e}} = \frac{-4.57K_{p_h}(-10)^2(.853)(-4.61)(4.79)(9.18)(17.76)}{s(8.617)(17.87)[.994,.726][.058,1.292][.985,10.69]}$$

Note:

$(\ ) = (1/T_i)$

$[\ ] = [\zeta_i, \omega_i]$

Amplitude/Phase Characteristics

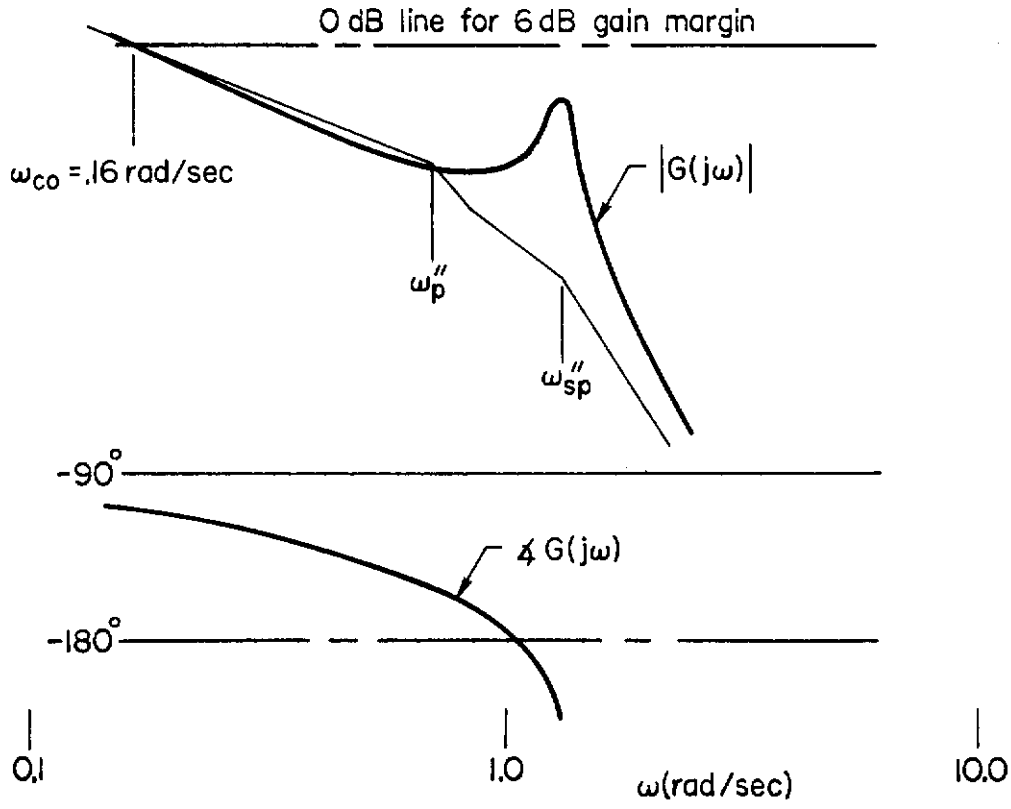

Figure 44. Altitude Control — Airspeed/Collective Technique, h, $\theta \rightarrow \delta_e$, u $\rightarrow \delta_c$

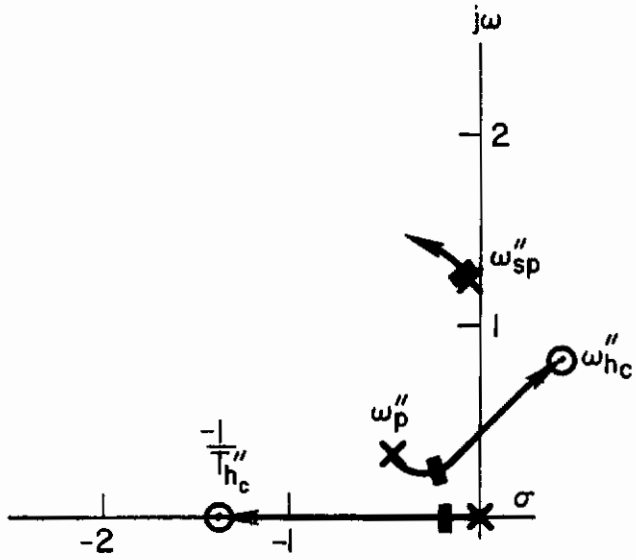

$$Y_{p_\theta} = \frac{4.8(s-10)^2}{(s+10)^2}$$

$$Y_{p_h} = \frac{.0025(s-10)^2}{(s+10)^2}$$

$$Y_{p_u} = -0.0073$$

$$\left(\frac{h}{h_\epsilon}\right)_{\substack{\theta \to \delta_e \\ u \to \delta_e \\ h \to \delta_c}} = \frac{25.5\,K_{p_h}(-10)^2(1.41)\left[-.33, 1.03\right]\left[.99, 10.68\right]}{s(10)^2\left[.803, .597\right]\left[.061, 1.24\right]\left[.99, 10.64\right]}$$

Note:

$(\ ) = (\ 1/T_i)$

$[\ ] = [\zeta_i, \omega_i]$

Amplitude Phase Characteristics

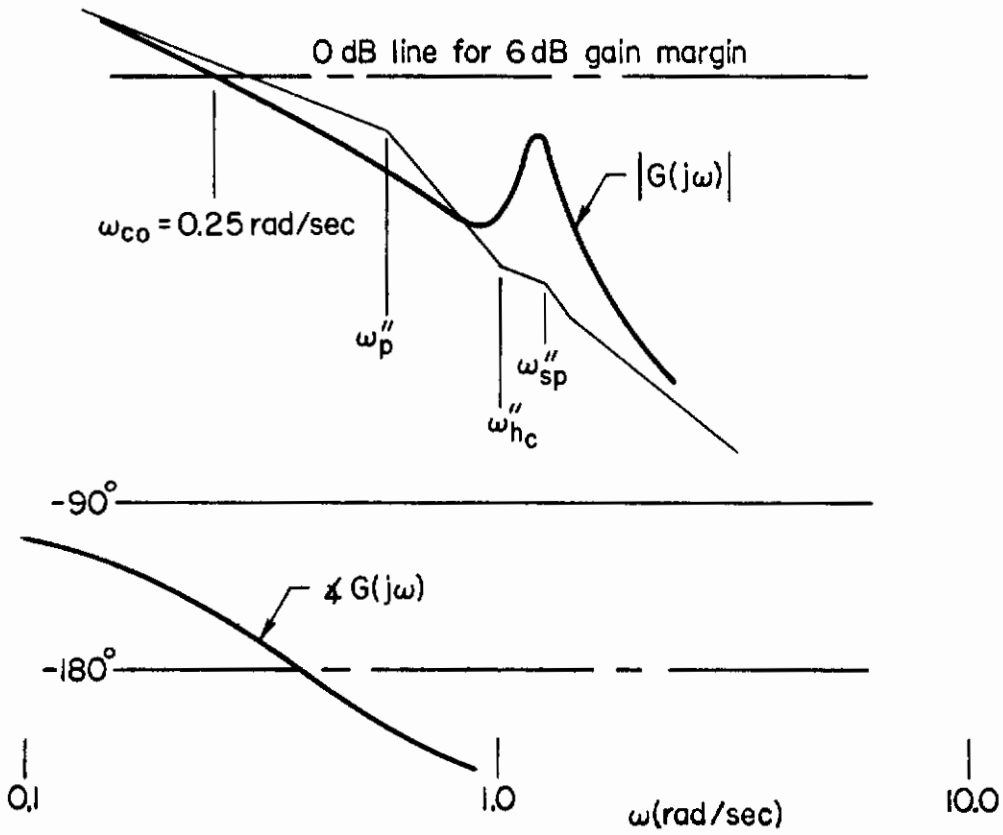

Figure 45. Altitude Control — Altitude/Collective Technique, $u, \theta \rightarrow \delta_e$, $h \rightarrow \delta_c$

appears to be essential. Judging from the overall dependence on attitude control, augmentation for the longitudinal axis should include both attitude and attitude rate feedbacks. In general, without pitch augmentation the manual flight path control task appears excessive from a closed-loop control viewpoint for the transition configuration below 60 knots because the outer-loop control functions are relatively intolerant of changes in the θ-loop

C. EFFECTS OF THRUST AXIS CONFIGURATION ON PILOT CONTROL

From the foregoing closed-loop analyses it is evident that the thrust axis configuration of the particular VTOL is the underlying physical situation determining the appropriate manual control technique. In the conversion from aerodynamic lift to the thrust support configuration, all VTOL vehicles have in common the rotation of the thrust vector from horizontal to approximately a vertical position. The position of this vector relative to the vehicle center of gravity is the single configuration variable which may change significantly throughout transition (i.e., at a given inclination) or may vary between vehicles due to the individual geometry of each (e.g., power plant location). For the generic surveys to follow, we will consider the thrust inclination to affect the relative magnitude of the lift and axial forces, and the thrust offset to affect the control pitching moment.* The variation in control dynamics due to the thrust offset will be considered first and then the thrust inclination aspects briefly reviewed.

It is worthwhile recalling from the preceding analyses that the uncompensated vehicle modes are dominated by relatively low frequency dynamics which are marginal for good manual control; thus the pilot's primary task is to utilize the available controls (e.g., collective, elevator, etc.) to achieve the desired higher bandwidth characteristics. The 60 knots dynamic features are used as representative characteristics since at this flight condition (as previously noted in Section IV.A) the vehicle exhibits a decoupled attitude control, $\theta \rightarrow \delta_e$, characteristic associated with hover; and front-side-of-minimum-drag features usually expected for aerodynamic flight conditions — i.e., it's halfway between hover and cruise in characteristics as well as speed.

1. Effects of Thrust Offset on Control

The effects of thrust-offset arm, z_T, on the airspeed and altitude control responses are analyzed by isolating the z_T-dependent terms in the pertinent numerator equations defined in Appendix C and plotting the locus of numerator zeros for variations in z_T.

a. Altitude Control. The root locus illustrations of the thrust line offset effect on the location of the collective control zeros is shown in Fig. 46 with and without the attitude inner loop closed.

The $N^h_{\delta_c}$ zeros without the attitude loop are shown in Fig. 46a. When the thrust line is above the c.g., as it is for the XC-142, the zeros are all real and two zeros are located in the right half plane. This limits pilot control

*The change in the basic airframe derivative, M_u, due to thrust offset is omitted.

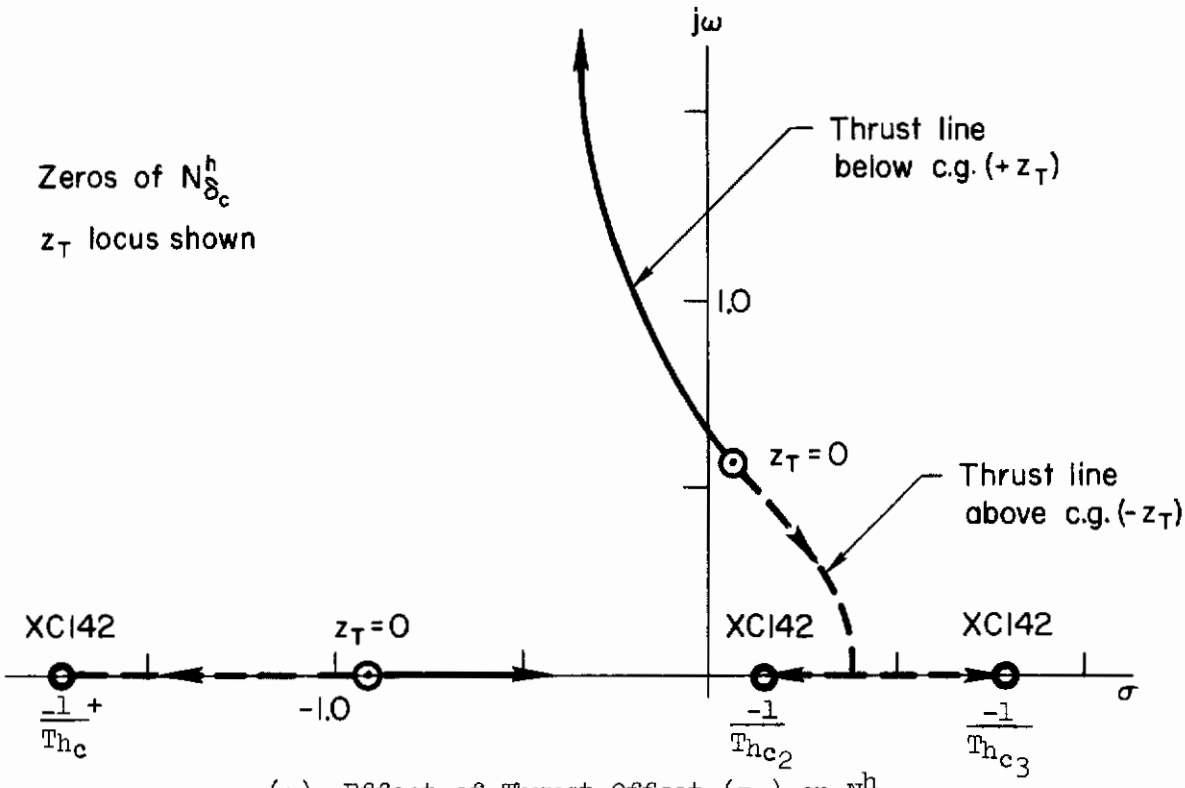

(a) Effect of Thrust Offset (z_T) on $N^h_{\delta_c}$

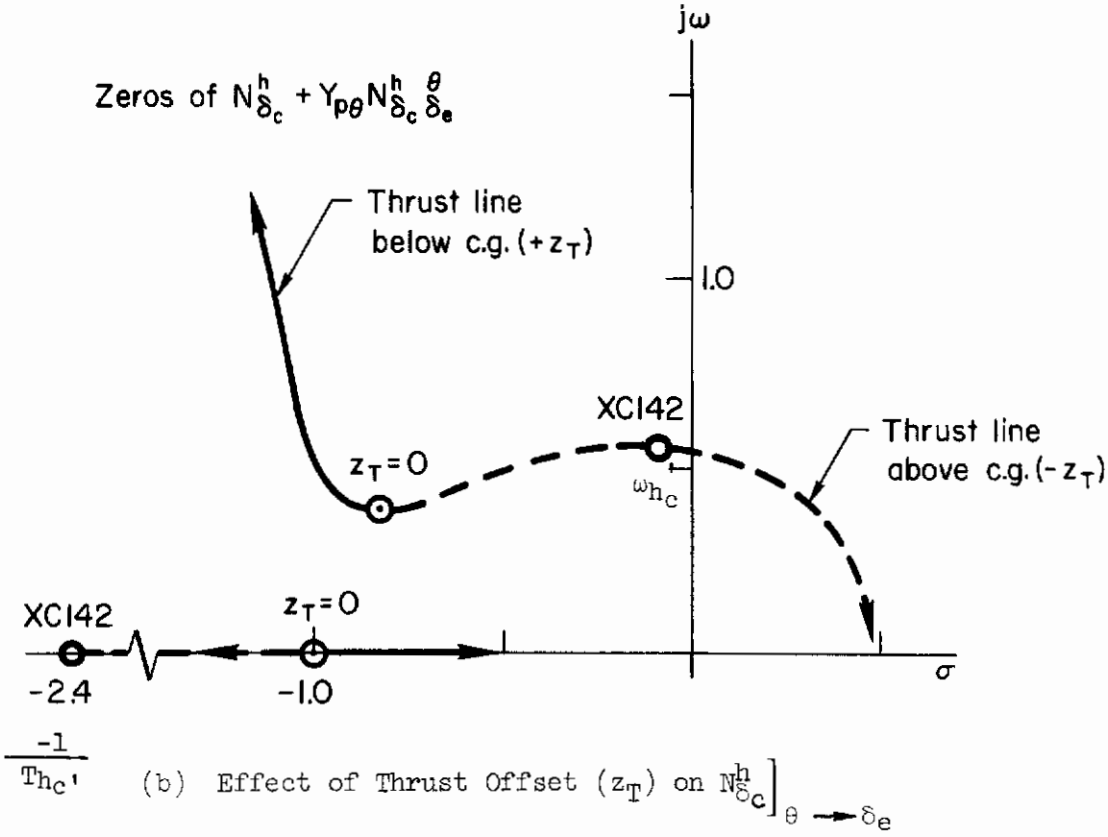

(b) Effect of Thrust Offset (z_T) on $N^h_{\delta_c}\Big]_{\theta \rightarrow \delta_e}$

Figure 46. Effects of Thrust Offset on Altitude Numerators

of altitude because the $h \rightarrow \delta_c$ closure tends to drive the phugoid mode toward these unstable zeros. The location of basic XC-142 numerator zeros is determined primarily by the combination of thrust offset affected terms (i.e., M_{δ_c} and M_u) and the thrust inclination terms (i.e., X_δ/Z_δ ratio) for this flight condition (i.e., 60 knots). This can be seen from the approximations for the three numerator zeros which are indicated below:

$$\frac{1}{T_{h_c}} \doteq -X_u - \frac{gZ_\delta M_u}{U_o M_\delta Z_w} - \frac{X_\delta}{M_\delta} M_u$$

$$\omega_{h_c}^2 \quad \text{or} \quad \frac{1}{T_{h_{c2}}} \frac{1}{T_{h_{c3}}} \doteq - \frac{U_o M_\delta Z_w}{Z_\delta}$$

$$2\zeta_h \omega_h \quad \text{or} \quad \frac{1}{T_{h_{c2}}} + \frac{1}{T_{h_{c3}}} = -M_q$$

The above approximate factors are reasonably valid (Ref. 2) since the static stability term, M_w, is small and the wing incidence (thrust inclination) is much greater than zero.

Thrust line location below the c.g. as might occur in a jet lift or vectored thrust vehicle potentially improves the control of altitude with the collective by increasing the frequency and damping of the numerator zeros. This suggests that proper control of offset or vertical c.g. position during transition may provide a means for aiding pilot control.

Effect of z_T variation on the roots of $(N^h_{\delta_c})_{\theta \rightarrow \delta_e}$ are shown in Fig. 46b. Closure of the $\theta \rightarrow \delta_e$ loop is essential to good altitude control because it has a stabilizing effect on the numerator zeros. The pertinent numerator equation becomes

$$(N^h_{\delta_c})_{\theta \rightarrow \delta_e} = N^h_{\delta_c} + Y_{p_\theta} N^{h\ \theta}_{\delta_c \delta_e} \quad ,$$

where Y_{p_θ} is of the form $K_{p_\theta}(s + 1/T_{L_\theta})e^{-\tau s}$. For the nominal XC-142 offset ($z_T = -2.6$) all zeros are stable and altitude control with collective is easily accomplished without outer-loop closures or additional pilot compensation, as already noted. As thrust offset decreases to zero, the damping of the complex zeros increases, indicating further improvement in control with smaller values of offset. For thrust below the c.g., the complex zeros again move out to high frequency and the real zero moves toward the origin. An interesting point is that with sufficiently large values of offset below the c.g., the real zero, $1/T_{h_c}$, becomes dominant. For a well damped short-period mode this lead term would negate some of the (short-period) phase lag and permit a higher bandpass in altitude control. However, for a lightly damped short-period mode, the effective $1/T_{h_c}$ lead term can be detrimental to the bandpass of the altitude loop because it accentuates the peaking of the short-period mode.

b. **Airspeed Control.** The effect of z_T on the basic vehicle numerator, $N^u_{\delta_c}$, is shown in Fig. 47a. For thrust line above the c.g. (as in the XC-142), all numerator roots are stable, whereas for the thrust line below the c.g. there exists an unstable zero ($1/T_{u_1}$) which becomes increasingly divergent as offset distance is increased. Because of the stable location of the $u \rightarrow \delta_c$ zeros, single-loop control of airspeed with throttle appears acceptable for negative z_T such as tilt-wing type vehicles.

The effect of z_T on the closed-loop numerator, $N^u_{\delta_c} + Y_{p_\theta} N^{u\ \theta}_{\delta_c \delta_e}$, is shown in Fig. 47b. Closure of the $\theta \rightarrow \delta_e$ loop, as in the altitude control case, again has a stabilizing effect on the numerator zeros, especially for the thrust line above the c.g., and to some extent for relatively small values of offset below the c.g. For large positive (i.e., below c.g.) values of thrust offset, a divergent root exists which would be detrimental to the $u \rightarrow \delta_c$ closure because of the tendency of the phugoid to drive toward the zeros. For this reason control of airspeed with collective may be a more desirable control technique for tilt-wing vehicles than for jet-lift type.

2. Effect of Thrust Line Incidence on Control

A simple isolation of thrust line incidence effects on the collective altitude and airspeed numerators is somewhat colored by the similarity between either small variations in thrust or incidence. For example, in the sketches of Fig. 48 the similarity at intermediate wing incidences ($i_w < 45^\circ$) is made quite apparent. The results are not identical because of the fact that an increase in thrust provides an increase in both the Z and X components, whereas a corresponding positive incidence change increases the Z force but reduces the X force; X_λ is negative while X_δ is positive.

The similarity means that some analogy may be drawn between the control with collective and control using thrust (wing) incidence. As previously noted from Ref. 20, the pilots consider wing incidence the primary means of controlling speed. Thus we may use the control response features of the collective at various wing incidence to gain some appreciation of the thrust line effects.

The attitude-loop-modified airspeed numerator zeros remain relatively unchanged for variations in the thrust line incidence, as shown in Fig. 49b. This is confirmed by the collective numerator zeros tabulated in Table XIV for the steady-state level trim points in transition. Closure of the u-loops with either collective or thrust line incidence results in a stable closure as sketched on page 98 so long as the thrust axis is inclined slightly, which means that the real root, $1/T_{u_1}$, remains stable.

The effect of thrust incidence on the modified altitude/throttle numerator is shown in Fig. 49a. Relatively small increases in λ result in a large change in the $1/T_{h_c}$ root. The increase in vertical force component, Z_{δ_c}, as the incidence is increased, stabilizes the altitude second-order numerators, and as a result the collective control of altitude ($h \rightarrow \delta_c$) improves as wing tilt increases, i.e., becomes akin to "pure" DLC — a not-unexpected result.

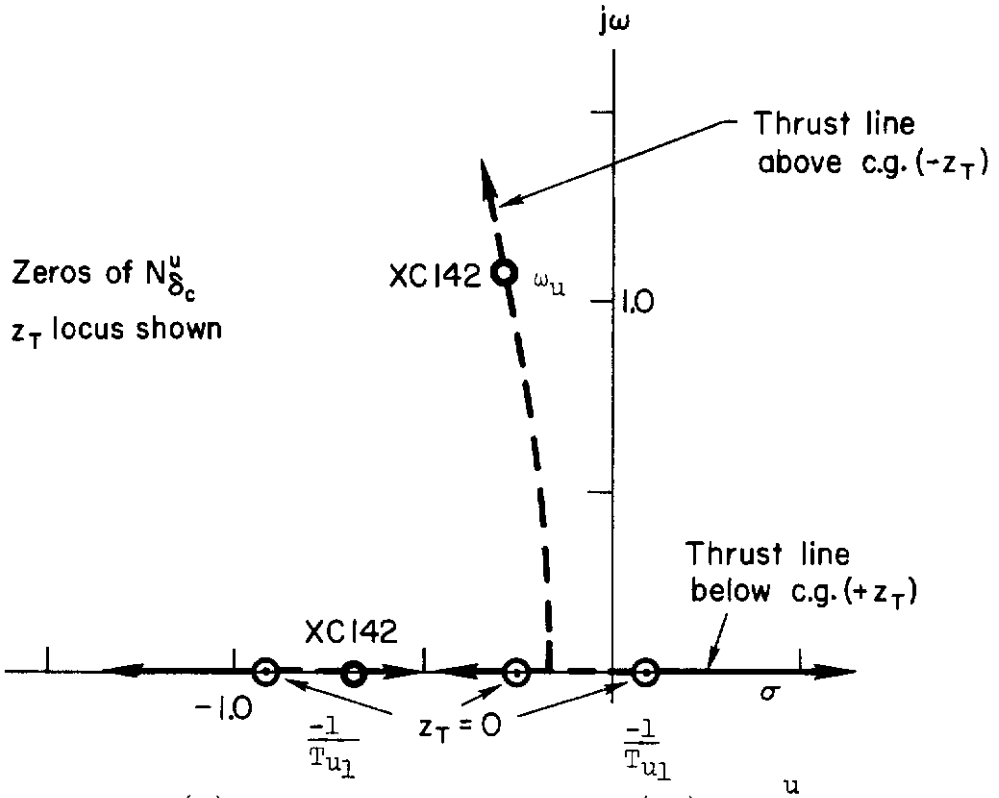

(a) Effect of Thrust Offset (z_T) on $N^u_{\delta_c}$

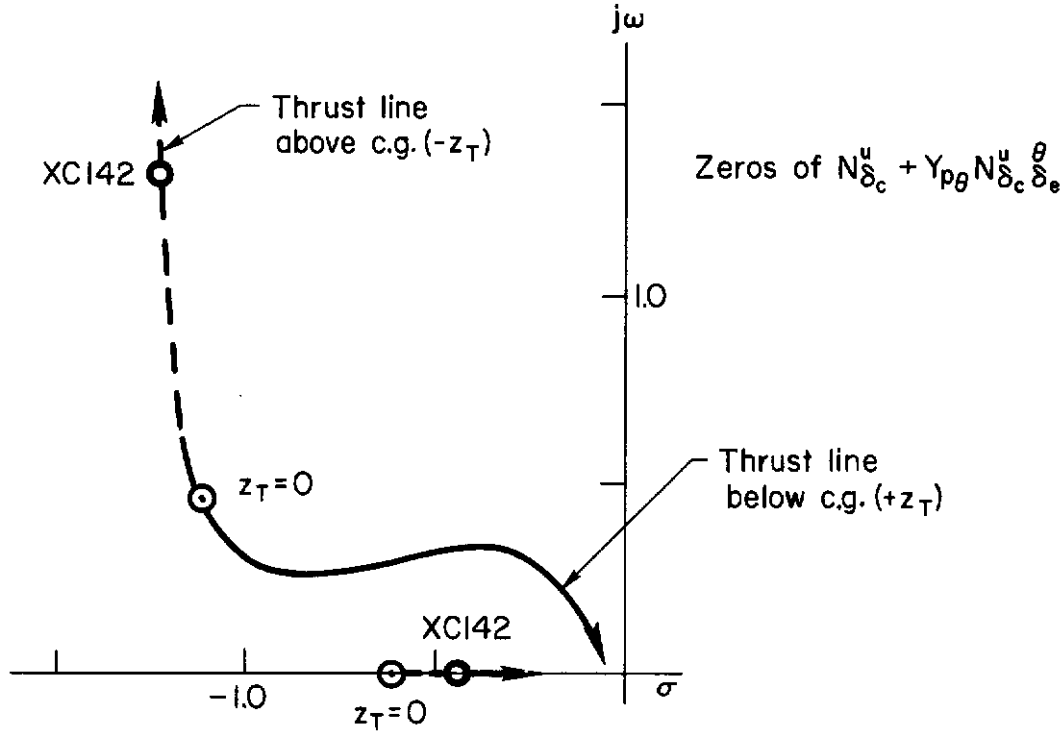

(b) Effect of Thrust Offset (z_T) on $N^u_{\delta_c}\Big]_{\theta \rightarrow \delta_e}$

Figure 47. Effect of Thrust Line Offset on Airspeed Numerators

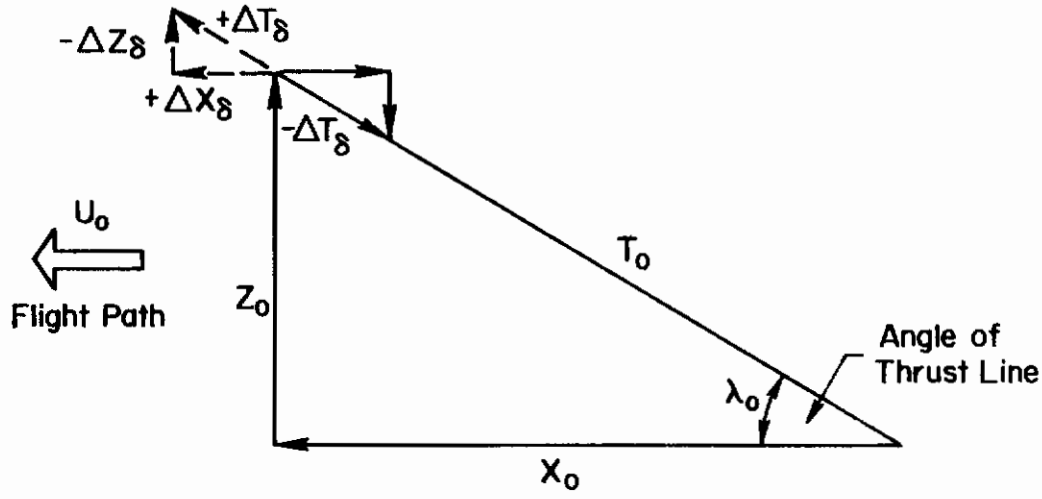

(a) Perturbation Control Using Collective Inputs

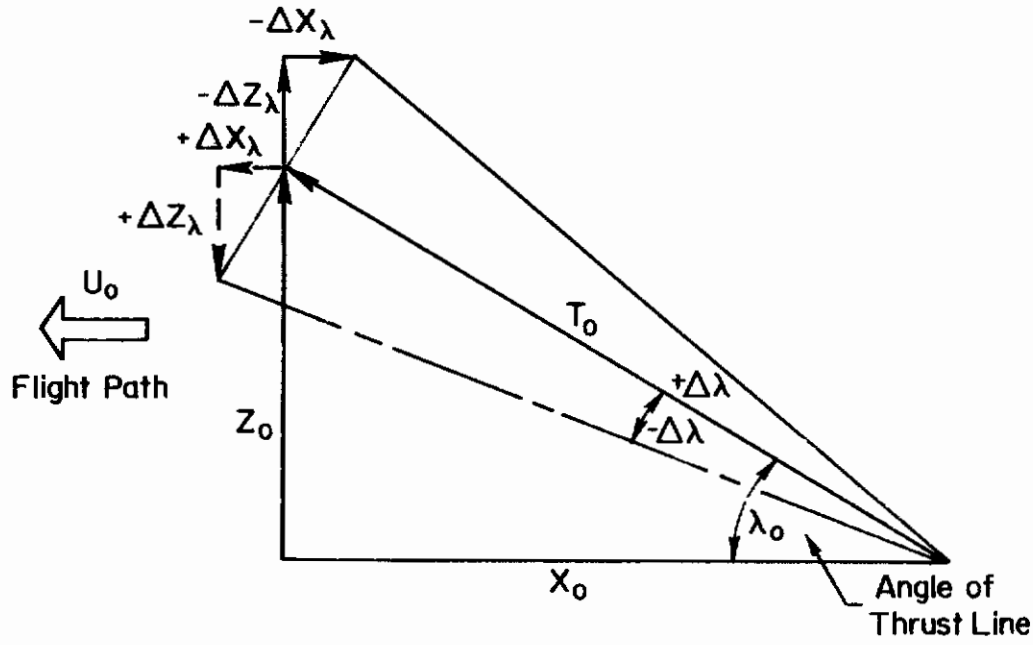

(b) Perturbation Control Using Thrust Vector Angle

Figure 48. Similarity of Control with Thrust Magnitude and Incidence

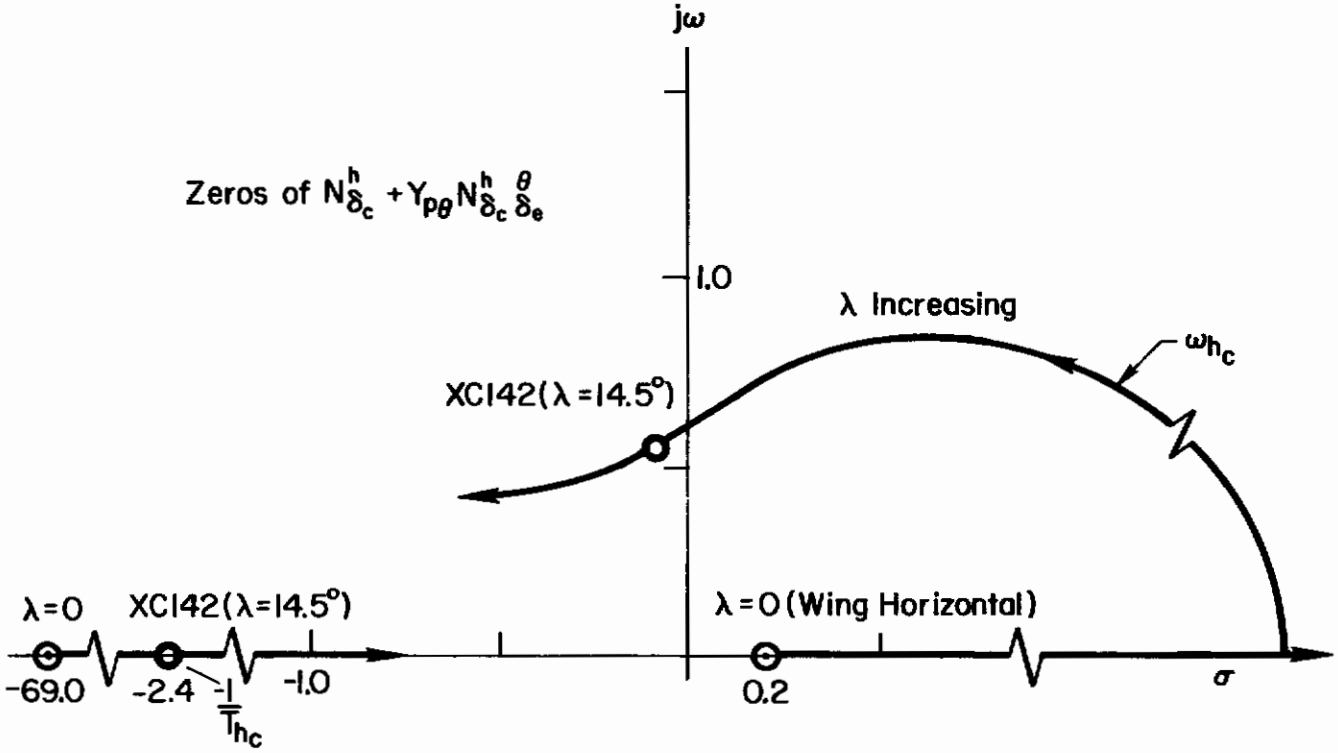

(a) Effect of Thrust Line Angle of Incidence (λ) on $N^h_{\delta c}\Big]_{\theta \to \delta_e}$

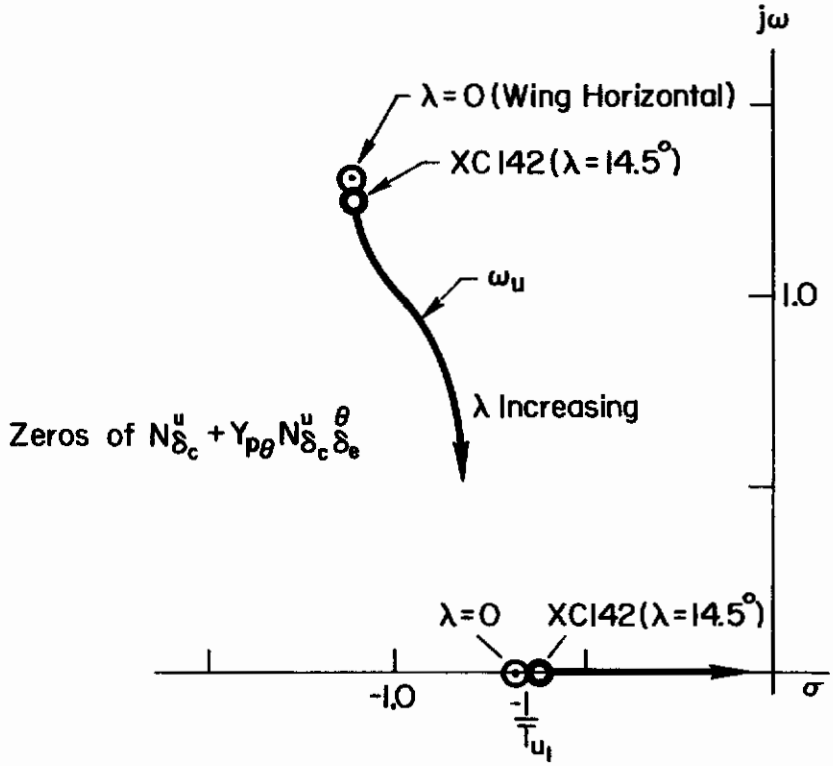

(b) Effect of Thrust Line Angle of Incidence (λ) on $N^u_{\delta c}\Big]_{\theta \to \delta_e}$

Figure 49. Effect of Thrust Line Angle on Numerator Characteristics

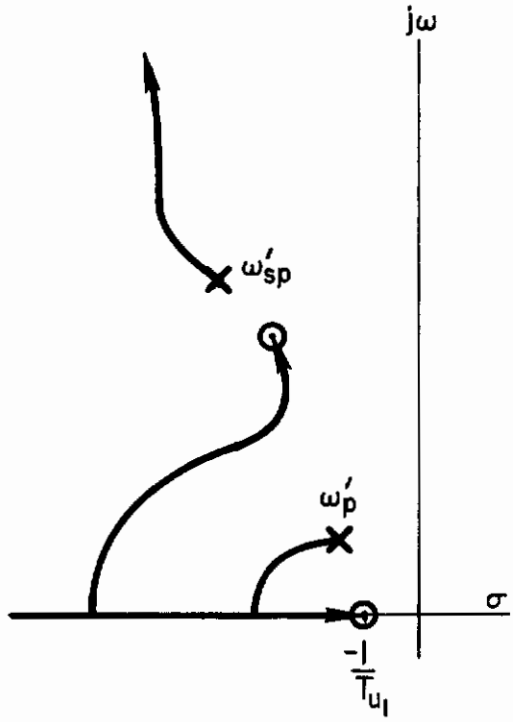

Pilot Closure of the u → δ_c or u → λ Loop
(θ-Loop Closed)

D. CONCLUSIONS

The system analyses presented in this section have shown that a key factor influencing the handling qualities in the transition regime is the effective low frequency pitch attitude characteristic, which tends to be dominated by the phugoid mode dynamics. Furthermore, the appropriate piloting technique and multiloop control structure for flight path control are traceable to configuration-related aspects, in particular, thrust-offset and inclination. For the XC-142, the fundamental control task is pitch attitude control, which serves the purpose of providing compensation for the outer control loops. To provide a clear division of control functions between the three available controllers: elevator, collective, and wing incidence, the pilot control of either altitude or airspeed is achieved with the inner, pitch attitude, loop closed. Thus the multiloop control structure during transition is similar to hover, i.e., the inner, attitude, loop is closed.

The pilot desire for separation of control functions may well be the major factor underlying the control problems associated with transition. This being the case, future experimental efforts should emphasize the control situations in which complex control interactions and couplings are involved.

While these analyses have established attitude-loop features which appear as fundamental requirements for compensatory pilot control, it is worth noting that other noncompensatory control techniques or functions may be substituted

by the pilot. For example, the primary function of the attitude-loop closure for the XC-142 is to equalize the thrust offset effect on the $h \rightarrow \delta_c$ numerator (i.e., cancel the thrust moment term, M_δ, in $N^h_{\delta_c}$). This function could be accomplished by the pilot's crossfeeding between collective and elevator without closing the attitude loop. Such crossfeed control possibilities represent a potential area for additional studies.

Specific results related to the XC-142A vehicle are:

1. Flight path control at a fixed-wing incidence can be achieved with the collective, although a moderately tight closure of the θ-loop is necessary. Control of airspeed with thrust incidence (wing incidence) is superior and suggests that the conversion controller serves a primary role in airspeed regulation.

2. Because of the large negative thrust offset (i.e., thrust line above the c.g.) and compensating effects of the intermediate closures of attitude and airspeed, a piloting control technique employing airspeed to collective appears feasible. This would allow the pilot to control altitude with the elevator at speeds somewhat below 80 knots for the "frozen" configuration (i.e., wing tilt angle fixed). The ability to control altitude in such a frozen configuration by conventional use of the elevator is significant. This implies that employment of airspeed to collective or throttle has application to STOL vehicles having a configuration similar to the XC-142A.

3. Airframe stability derivatives having a prime effect on the closed-loop dynamics are those associated with the collective control, since in general the characteristic dynamic modes are dominated by low frequency phugoid features similar to the hover mode.

SECTION V

SUMMARY OF CONCLUSIONS

A. LONGITUDINAL HOVER DYNAMICS

Based on correlations and study of available ground-simulated and flight-tested configurations (about 100 considered in detail) "satisfactory" ($3 < PR < 4$) characteristics for the general transfer function forms

$$\frac{\theta}{\delta_e} = \frac{M_{\delta_e}(s + 1/T_{\theta_1})}{(s + 1/T_{sp_2})(s^2 + 2\zeta_p\omega_p s + \omega_p^2)}$$

$$\frac{x}{\delta_e} = \frac{-gM_{\delta_e}}{s(s + 1/T_{sp_2})(s^2 + 2\zeta_p\omega_p s + \omega_p^2)}$$

are connected primarily with the existence of K or K/s asymptotes in θ/δ_e near $\omega_{c_\theta} \doteq 2$ rad/sec. Such characteristics are consistent with good closed-loop pilot control of θ; i.e., adequate gain and phase margins, noncritical lead requirements ($T_L < 1$), good error performance (i.e., low frequency gain near 1). In addition the outer, x-loop must have reasonable crossover characteristics (i.e., no worse than K/s^2) in the neighborhood of 0.5 rad/sec, but these are seldom an issue (see Section II, Conclusions). The distinction between satisfactory and unsatisfactory ($6 < PR < 7$) characteristics is clearly evident on the basis of the exemplary closed-loop situations illustrated in the text which show very low inner-loop dc gain and resulting poor error (σ_θ) performance because of adverse sensitivity to lead which in effect makes system performance dependent on the pilot's neuromuscular lags.

The foregoing general conclusions have been more specifically related to a variety of satisfactory and unacceptable pole/zero combinations for the above, "effective vehicle" transfer functions (for $M_u\sigma_{u_g} < 0.1$ to avoid extreme gust effects), as shown in Table III for conventional dynamics and tabulated in Tables V and VI for attitude and/or position augmentation. The satisfactory dynamic situations can be summarized as follows:

1. For $0 < 1/T_{\theta_1} < \omega_p/2$ — Results in "conventional" low dc θ/δ_e gain
   Also applies for "low-stiffness" attitude augmentation

   $\omega_p < 0.5$ rad/sec — Implies $|gM_u/M_q^3| < 1$ and $\omega_p^2 \doteq -gM_uT_{sp_2}$

   $\zeta_p\omega_p > -0.25$

   $1/T_{sp_2} > 1$

2. For $1/T_{\theta_1} > \omega_p$ e.g., for X_u augmentation; results in high dc θ/δ_e gain

$\omega_p' > 1$ rad/sec

$\zeta_p'\omega_p' > 0.3$, $\zeta_p' > 0.25$

$1/T_{sp_2}' > \omega_p'$ or $1/T_{\theta_1}'$; $1/T_{sp_2}' > 2.0$

3. For $1/T_{\theta_1} \doteq 1/T_{sp_2}$ e.g., for M_θ augmentation; results in high dc θ/δ_e gain

$2 \leq \omega_p' \leq 5$ rad/sec

$\zeta_p' > 0.25$

It seems obvious from the above diverse situations that a specification written in terms of the above parameters and classifications would, although feasible, be fairly complicated. This is particularly true if one notes that the variety of possible SAS configurations indicated here is not necessarily all-inclusive. This complication is not greatly alleviated by considering the requirements in terms of the basic aerodynamic derivatives, M_q, M_u, and X_u, because the boundaries shift between conditions 1 and 2; and must be expanded to include M_θ for condition 3. The really bright spot in this is that such diverse results can all be consolidated and explained in terms of the closed multiple-loop situation, which also yields an appreciation for the effects of practical SAS design considerations such as control system lag.

B. LONGITUDINAL CONTROL POWER AND SENSITIVITY

1. Sensitivity

Analysis of extant data leads to the following rationale for pilot's selection of optimum control sensitivity; M_δ for longitudinal control.

a. For a given M_u and σ_{ug} the hovering control activity is given by $\sigma_\delta = KM_u\sigma_{ug}/M_\delta$ where K is approximately 1.7 ± 0.3 depending on pilot gain variations; to keep σ_δ within acceptable limits (say, 1/2 in.) requires a minimum value of M_δ.

b. A given M_u also demands a minimum $-M_q$ (generally greater than 1.0) to give satisfactory dynamic characteristics, e.g., Fig. 3.

c. The M_q and M_δ resulting from a and b must be compatible with a "desired" pitch response in 1 sec (θ_1) of about 5 deg per in. of stick. The pilot may compromise this compensatory value level by no more than about 50 percent on the high side in deference to reducing Item a, control activity. However, open-loop tasks such as "quick-stop" maneuvers may result in a broad range of control sensitivity selections which are considerably in excess of the compensatory or precision tracking requirements, but not less than the "desired."

2. Control Power

Must be adequate for trim, gust regulation and necessary maneuvering. The requirements for trim and gust regulation in closed-loop tasks can be easily checked (e.g., by considering a 2σ or 3σ value to be adequate coverage for maximum gusts). However the maneuvering requirement as a function of mission or size is presently poorly defined. As a practical matter it seems that 3 in. of stick travel at the optimum M_δ corresponding to $\theta_1 \doteq 5$ deg is generally adequate.

C. PRELIMINARY CLOSED-LOOP ANALYSIS OF TRANSITION

System analysis of the multiple-loop aspects of manual pilot control in transition has yielded insight into the problems associated with flight where thrust provides a significant amount of vehicle lift. Theoretically, the appropriate flight path control technique is traceable to configuration-related factors, in particular, thrust offset and inclination; however, the key piloting control deficiency in this flight region stems from the inadequacy of the short-period attitude control features (i.e., low ω_{sp}). More specific conclusions derived from the transition analyses are summarized as follows:

1. Flight path control at a fixed configuration (i.e., fixed-wing incidence, $i_w > 0$) in transition is clearly adequate ($\omega_{ch} \doteq 0.75$ rad/sec) with the collective. However, while the height control with the collective is analogous to DLC, a moderately tight closure of the θ-loop (e.g., $\omega_{c\theta} \doteq 2.5$ rad/sec) either by the pilot or a suitable augmentation system is essential. Control of airspeed with thrust incidence (e.g., wing incidence) appears more desirable than using the elevator.

2. Generically, a control technique employing the collective for airspeed control (i.e., h, $\theta \rightarrow \delta_e$, u $\rightarrow \delta_c$) also appears feasible for the XC-142. The primary reason is that with the large negative thrust offset (i.e., thrust line above the c.g., $M_u >> 0$) the u $\rightarrow \delta_c$ closure greatly stiffens the phugoid mode ($\omega_p' >> \omega_p$), eliminating the bandpass restriction on the h $\rightarrow \delta_e$ control which is normally imposed by this mode.

3. The airframe stability and control derivatives depend primarily on the combined high-power (thrust level), thrust inclination, and lift condition required for trimmed flight. The derivatives' effect on the dynamic features is shown by the unstable numerator factors (i.e., zeros in the right half plane) of the altitude and airspeed response for collective input and the attitude response for the elevator inputs.

4. Whether or not the conversion controller (e.g., the wing incidence) should be considered as a primary compensatory control for airspeed as suggested by pilot comments in lieu of the trimmer function appears to be a moot point as the results of this study have shown that: There is generically

some equivalence between the effects produced by thrust-angle control and the thrust manipulator (e.g., collective) insofar as closed-loop control is concerned.

5. From this analytical treatment some appreciation of the pilot's manual control problems in transition which will affect all VTOL configurations, not just the tilt-wing, has been gained.

REFERENCES

1. Walton, R. P. and I. L. Ashkenas, Analytical Review of Military Helicopter Flying Qualities, Systems Technology, Inc., TR-143-1, Nov. 1965.

2. Stapleford, R. L., J. Wolkovitch, R. E. Magdaleno, et al, An Analytical Study of V/STOL Handling Qualities in Hover and Transition, Air Force Flight Dynamics Laboratory, Wright-Patterson Air Force Base, Ohio, AFFDL-TR-65-73, Oct. 1965.

3. Wolkovitch, J., and R. P. Walton, VTOL and Helicopter Approximate Transfer Functions and Closed-Loop Handling Qualities, Systems Technology, Inc., TR-128-1, Jan. 1965.

4. Miller, David P., and E. Wayne Vinje, Flight Simulator Studies of Some Factors Which Influence VTOL Handling Qualities, United Aircraft Research Labs. Rept. E110129-1, Oct. 1966.

5. Vinje, Edward W., and David P. Miller, Interpretation of Pilot Opinion by Application of Multiloop Models to a VTOL Flight Simulator Task, United Aircraft Research Labs. Rept. UAR-F20, Mar. 1967.

6. Cooper, George E., "Understanding and Interpreting Pilot Opinion," Aero. Eng. Rev., Vol. 16, No. 3, Mar. 1957, pp. 47-51, 56.

7. Breul, H. T., A Simulator Study of Low Speed VTOL Handling Qualities in Turbulence, Grumman Aircraft Engineering Copr. Research Rept. RE-238, Feb. 1966.

8. Craig, S. J., Assembly of Bode Features for VTOL Aircraft, Systems Technology, Inc., WP-171-2 (to be published).

9. Miller, David P., and Edward W. Vinje, Fixed-Base Flight Simulator Studies of VTOL Aircraft Handling Qualities in Hovering and Low Speed Flight, Air Force Flight Dynamics Laboratory, Wright-Patterson Air Force Base, Ohio, AFFDL-67-152, Jan. 1968.

10. Shields, M. E., Estimated Flying Qualities XC-142A V/STOL Assault Transport, LTV Vought Aeronautics Division Rept. No. 2-53310/4R939, 22 May 1964.

11. Ellis, David R., and Gregory A. Carter, A Preliminary Study of the Dynamic Stability and Control Response Desired for V/STOL Aircraft, Princeton University Rept. No. 611, June 1962.

12. A'Harrah, R. C., and S. F. Kwiatkowski, "A New Look at V/STOL Flying Qualities," Aero. Eng., Vol. 20, No. 7, July 1961, pp. 22, 23, 86-92; Kwiatkowski, S. F., Experimental Conditions for V/STOL Handling Qualities Study, letter dated 1963.

13. Stapleford, Robert L., and Samuel J. Craig, Measurement of Pilot Describing Functions in Single-Controller Multiloop Tasks, Systems Technology, Inc., TR-167-1, Aug. 1967.

14. McRuer, Duane, Dunstan Graham, Ezra Krendel, and William Reisener, Jr., Human Pilot Dynamics in Compensatory Systems: Theory, Models, and Experiments with Controlled Element and Forcing Function Variations, Air Force Flight Dynamics Laboratory, Wright-Patterson Air Force Base, Ohio, AFFDL-TR-65-15, July 1965.

15. Jex, H. R., J. D. McDonnell, and A. V. Phatak, A "Critical" Tracking Task for Man-Machine Research Related to the Operator's Effective Delay Time. Part I. Theory and Experiments with a First-Order Divergent Controlled Element, NASA CR-616, Nov. 1966.

16. McDonnell, J. D., and H. R. Jex, A "Critical" Tracking Task for Man-Machine Research Related to the Operator's Effective Delay Time. Part II. Experimental Effects of System Input Spectra, Control Stick Stiffness, and Controlled Element Order, NASA CR-674, Jan. 1967.

17. Seckel, E., J. J. Traybar, and G. E. Miller, Longitudinal Handling Qualities for Hovering, Princeton University, Dept. of Aeronautical Engineering, Rept. No. 594, Dec. 1961.

18. Sadoff, Melvin, and Norman M. McFadden, A Study of Longitudinal Control Problems at Low and Negative Damping and Stability with Emphasis on Effects of Motion Cues, NASA TN D-348, Jan. 1961.

19. Wolkovitch, Julian, and Donald E. Johnston, Automatic Control Considerations for Helicopters and VTOL Aircraft with and without Sling Loads, Systems Technology, Inc., TR-138-1, Nov. 1965.

20. "Development of VTOL Handling Qualities Design Criteria," CAL Summary of Notes from VTOL Meetings at Wright Field, 10-24 Oct. 1966.

21. Ashkenas, I. L., A Study of Conventional Airplane Handling Qualities Requirements. Parts I and II, Air Force Flight Dynamics Laboratory, Wright-Patterson Air Force Base, Ohio, AFFDL-TR-65-138, Nov. 1965.

22. Lollar, Thomas A., A Rationale for the Determination of Certain VTOL Handling Qualities Criteria, AGARD Rept. 471, July 1963.

23. Perry, D. H. and H. W. Chinn, A Preliminary Flight Simulation Study of Jet-Borne VTOL Aircraft Handling Qualities, Aeronautical Research Council C.P. No. 902, June 1965.

24. McRuer, D. T., I. L. Ashkenas and H. R. Pass, Analysis of Multiloop Vehicular Control Systems, Aeronautical Systems Division, Wright-Patterson Air Force Base, Ohio, ASD-TDR-62-1014, Mar. 1964.

25. Durand, Tulvio S., Theory and Simulation of Piloted Longitudinal Control in Carrier Approach, Systems Technology, Inc., TR-130-1, Mar. 1965.

26. Salmirs, Seymour and Robert J. Tapscott, The Effects of Various Combinations of Damping and Control Power on Helicopter Handling Qualities During Both Instrument and Visual Flight, NASA TN D-58, Oct. 1959.

27. Madden, J., J. Kroll, and D. Neil, A Study of VTOL/STOL Flying Qualities Requirements, Bell Aircraft Corp., Rept. 2023-917001, 10 Aug. 1960.

28. McRuer, D. T., L. G. Hofmann, H. R. Jex, et al, New Approaches to Human-Pilot/Vehicle Dynamic Analysis, Air Force Flight Dynamics Laboratory, Wright-Patterson Air Force Base, Ohio, AFFDL-TR-67-150, Feb. 1968.

29. Stapleford, R. L., D. T. McRuer, and R. Magdaleno, Pilot Describing Function Measurements in a Multiloop Task, NASA CR-542, Aug. 1966.

30. Magdaleno, R. E., and D. T. McRuer, Effects of Manipulator Restraints on Human Operator Performance, Air Force Flight Dynamics Laboratory, Wright-Patterson Air Force Base, Ohio, AFFDL-TR-66-72, Dec. 1966.

31. McRuer, D. T., R. E. Magdaleno, and G. P. Moore, "A Neuromuscular Actuation System Model," Third Annual NASA-University Conference on Manual Control, NASA SP-144, 1967, pp. 281-304.

APPENDIX A

DATA COMPARISONS AND FACTORS INFLUENCING HANDLING QUALITY RATING

Intersource correlations and comparisons were made using the four primary data sources listed in Table A-II. These sources are documented in Refs. 7, 9, 12, and 17. The experimental conditions differ somewhat for each source, and some variance and overlapping between rating levels were anticipated. To judge the extent of the differences, direct comparisons were made between the results for tested control situations having essentially the same controlled element dynamics. The effects of three subjective factors, environmental conditions (e.g., gust level), task, and type of simulation, were determined and expressed as an effective change in the level of pilot rating.

The basic procedure used in the comparison effort was first to make a detailed review of the nature of the documented experiment noting the piloting task involved, instruction to the pilots, and the type of simulation facility. Then, in the second step, the effects of control power and sensitivity were minimized by selecting only the optimum and/or the best rating given for the specific control element dynamics. This involved cross plotting the "raw" opinion data for constant dynamics and disturbance levels versus either control power or sensitivity. The final step involved the specific comparisons and determination of the separate effects.

DISCUSSION OF TEST DATA

The distinguishing features derived from the detailed review of documented experiments are presented in the following paragraphs:

a. A'Harrah and Kwiatkowski, Ref. 12

The experiment was conducted on a fixed-base six degree of freedom visual presentation flight simulator. The pilots rated each of the more than seventy longitudinal dynamic characteristics separately in still air and then gave an overall rating in slightly turbulent

air (rms gust velocity of 5 ft/sec). These evaluations were conducted primarily in precision hovering task, but included discrete low speed flight and takeoff and landings. Thus the rating given by the pilot included consideration of the vehicle dynamics and the performance aspects; however, the weighting placed by the pilot on his effort and resulting performance is unknown. One may conclude that his still air capabilities were emphasized because a greater percentage of the testing was done without turbulence.

The one unique feature of this experiment is that the values of X_u and M_q were interchanged for fixed levels of M_u. The characteristic dynamics remained unchanged from those associated with the M_q variations, because the characteristic equation is $[s(s-X_u)(s-M_q)+gM_u]$. The attitude numerator term is modified by the X_u term. The higher levels of X_u (e.g., $-0.5 > X_u \geq -5$) are considered representative of velocity damping augmentation in the position loop.

Introduction of the large X_u values does increase the vehicle response to gusts and may have negated any potential advantage of the translational damping term. The results do suggest that the combined effects of the higher pitch damping ($-M_q > 2$) and the emphasis placed on still air handling qualities compensated for the increased gust sensitivity due to X_u. In fact, it should be recognized that the inner-loop damping level suggested for a satisfactory rating by the authors (i.e., $\zeta_p\omega_p > 0.25$) may well have been influenced by the additional gust sensitivity for the high X_u conditions.

b. Breul, Ref. 7

These experiments were conducted using a visual reference system in conjunction with pitch and roll moving-base simulator. In Breul's experiments the test condition matrix covers slightly more than 80 different longitudinal dynamic configurations out of the approximately 300 control configurations evaluated.

The unusual aspects of this experiment were the flight control task and the basic philosophy for handling quality rating. The flight task was a minimal type of mission envisioned and required the pilot to hover over a spot, move smoothly to another point and establish a new hover (e.g., an air taxi maneuver). The pilots were instructed as follows: "... to evaluate each vehicle with emphasis on the ease with which they could get it from one spot to another, and not on the precision with which they could control hover." By de-emphasizing the

precision hover control and performance aspects in general, the major factors reflected by the opinion data are vehicle stability and closed-loop regulatory control. The above conclusion is partially supported by the rating trends derived from cross plots of the pilot rating and the primary variables in the experiment (i.e., $M(\delta)$, M_q, M_u, and σ_{ug}). Also, the closed-loop analysis presented in Section II of the text further substantiates this assessment. The trend resulting from the cross plots is shown schematically in the three dimensional matrix of Fig. A-1. Here a constant rating level (PR $\doteq$ 3.5) is defined by the surface composed of various combinations of aerodynamic parameters. This iso-opinion surface is independent of the gust level (i.e., $0 \leq \sigma_{ug} \leq 9$ ft/sec). We note, also, that no aerodynamic parameter is singularly indicative of the opinion level. However, the combinations do represent various dynamic properties from which a valid correlating parameter, the characteristic phugoid mode frequency, ω_p, can be identified. Figure A-2, also, shows that this frequency is near ω_p = 0.5 rad/sec.

The correspondence of the phugoid frequency and the satisfactory opinion level is associated with the pilot's ability to maintain good attitude-loop stability (see Section II) and to regulate against low-frequency disturbances such as gust. Two factors may be cited for the lack of opinion change with gust:

1. The pilot was instructed to neglect precision performance as a merit.
2. For satisfactory vehicle dynamics, the gust levels tested are not a significant factor in the pilot's rating.

c. Seckel, Ref. 17

These tests were conducted in a variable stability helicopter where the task consisted of precision hovering and low speed air taxi maneuvers under moderate gust condition (i.e., σ_{ug} = 6.3 ft/sec). An overall pilot rating was given by the pilots which was to consider stability, performance, and environmental factors. No weighing of these factors was suggested to the pilots.

The sensitivity of pilot rating to disturbance level was demonstrated in the test by interchanging the gust response levels. The major point was that the precision hover rating may be degraded by changing the gust sensitivity factor, $M_u\sigma_{ug}$. Thus the importance of attitude-loop regulatory control was confirmed. In addition, the correlations of gM_u and M_q presented in this reference strongly supported the dependency of pilot opinion on the basic vehicle phugoid mode properties (i.e., $\omega_p \doteq 0.5$ rad/sec) derived from Breul's results (see Fig. A-3).

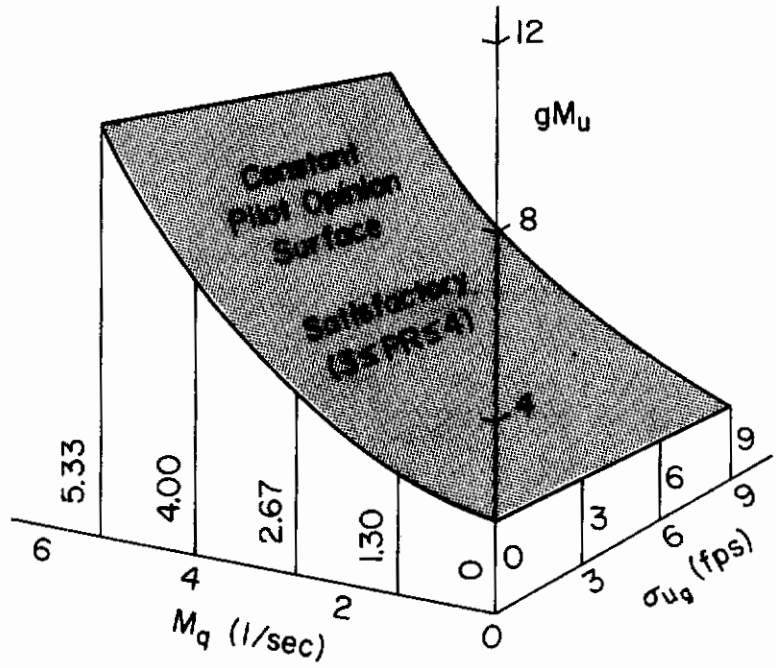

Figure A-1. Schematic of Rating Trends as a Function of Primary Variables

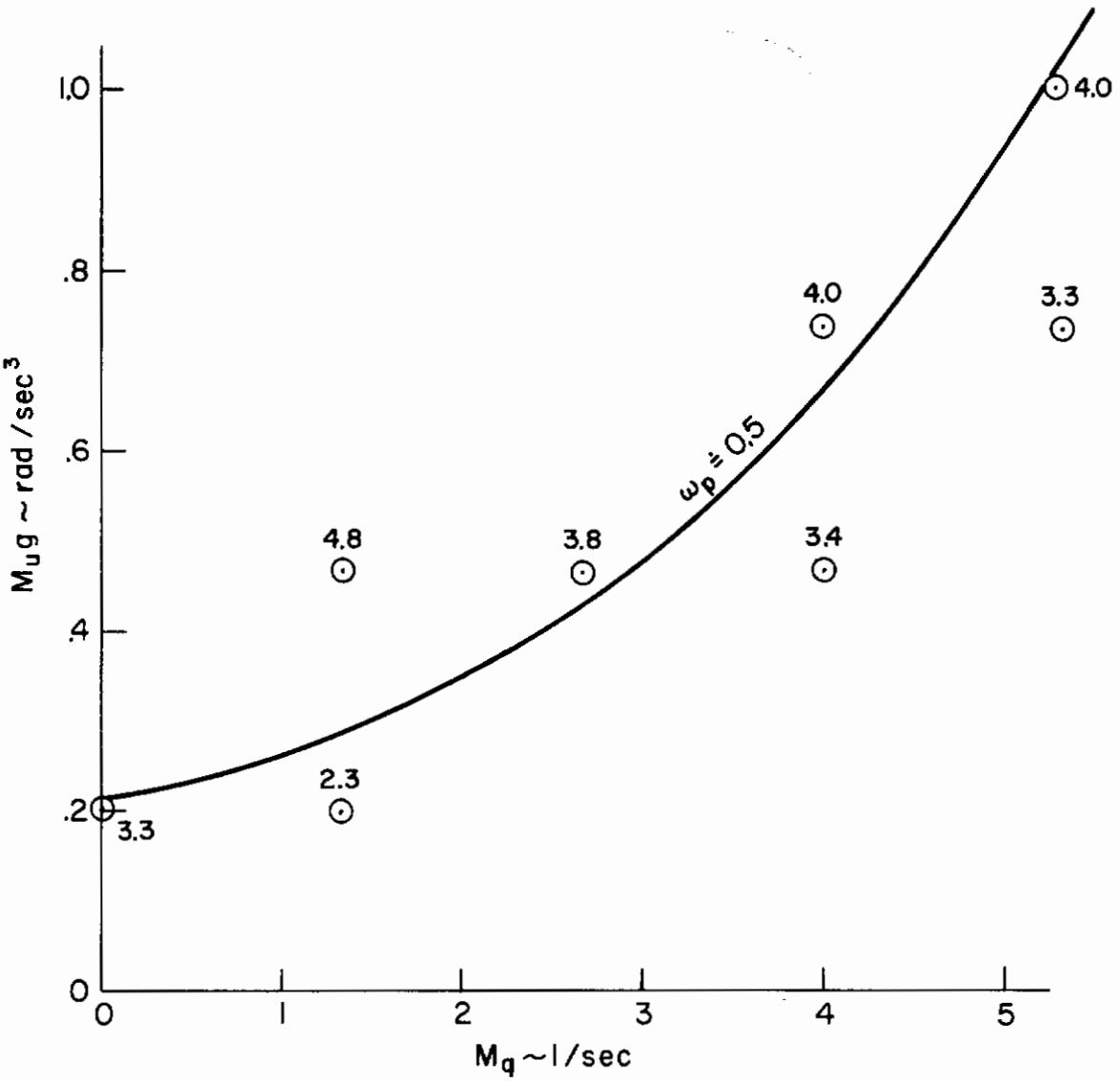

Figure A-2. Phugoid Frequency Correlation with Satisfactory Dynamics

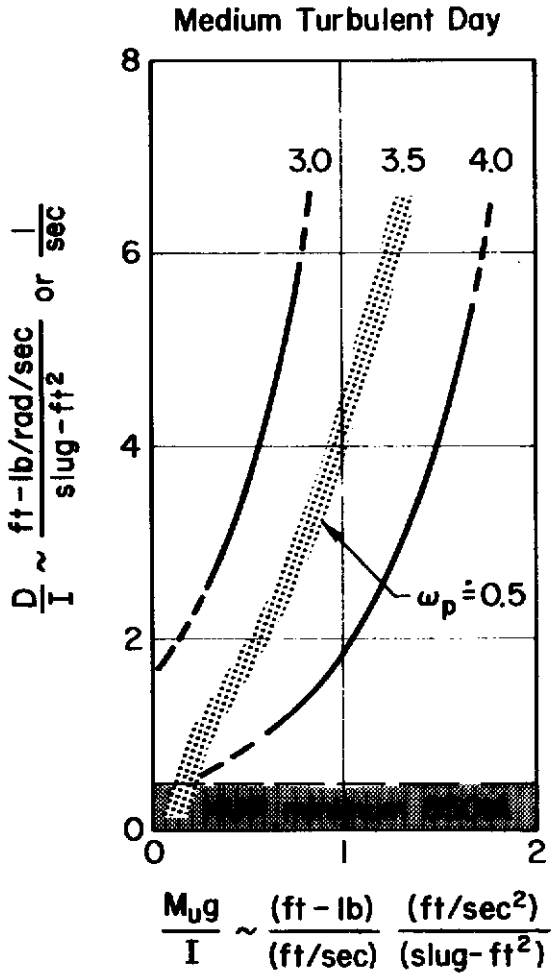

Figure A-3. Correlation of Pilot Rating and Dynamic Characteristics (Ref. 17)

d. Miller, et al, Refs. 5 and 9

These most recent VTOL experiments were conducted using a contact analog visual display and a fixed-base simulation. Precision hover and low speed air taxi maneuvers were stressed and the overall pilot ratings were given under various gust levels and vehicle dynamics.

The major aspect of these results was the rating correlations established between vehicle dynamics, error performance merits (e.g., σ_θ, σ_x), pilot effort, σ_δ, and gust level. In addition the pilot compensation features which were derived from the error measurement data have supported, in general, trends given in ratings due to changes in either gust or vehicle dynamics. The separation of the rating due to gust aspects suggests a strong dependency of rating on the performance achieved. Data showed almost a near linear dependency of pilot rating on gust level for dynamics rated good in still air.

EFFECTS OF SIMULATION TECHNIQUE ON RATINGS

The pilot rating variances which are attributed to the differences in simulation technique are considered broadly as either:

1. Intersource variances of the fixed-base experiments. References 12 and 9.

2. Intersource variance between the above fixed-base experiments and the moving-base and flight test in Refs. 7 and 17.

This description of our approach to the data compilation has been used to illustrate general trends and thus avoid accounting for the detailed differences in the display and simulation facilities.

1. Comparison Between Fixed-Base Results

A direct comparison has been made between the results of the fixed-base experiments from Refs. 12 and 9. For convenience Ref. 12 data are superimposed on the contours of the average ratings derived from Ref. 9. The resulting comparisons are shown in Figs. A-4 and A-5. With some extrapolation of the contours, a direct comparison of seven dynamic conditions is obtained. Note that the extrapolation of the contours has generally followed the constant frequency, ω_p, conditions.

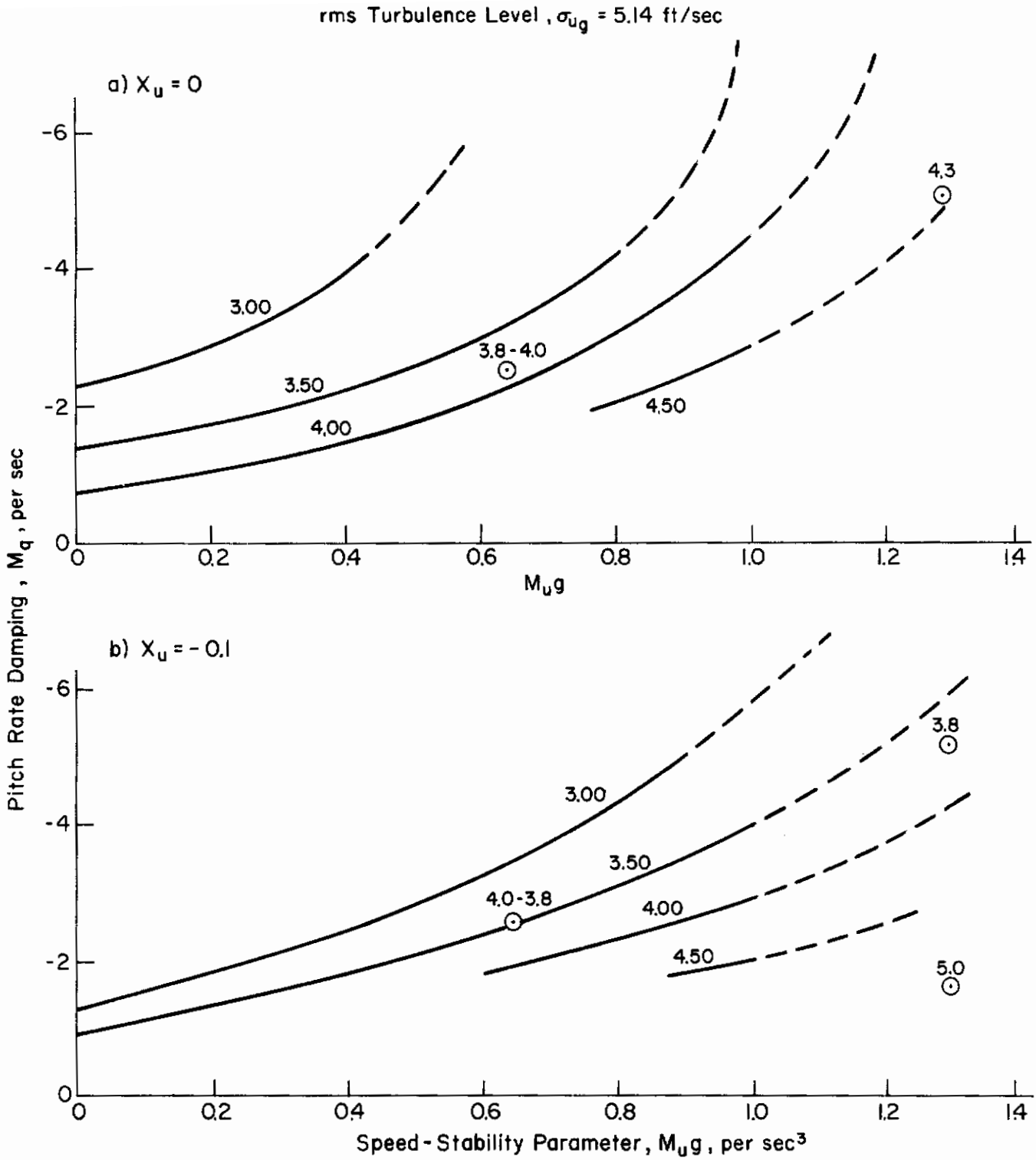

Figure A-4. Contours of Average Pilot Ratings Derived from Flight Simulation Data

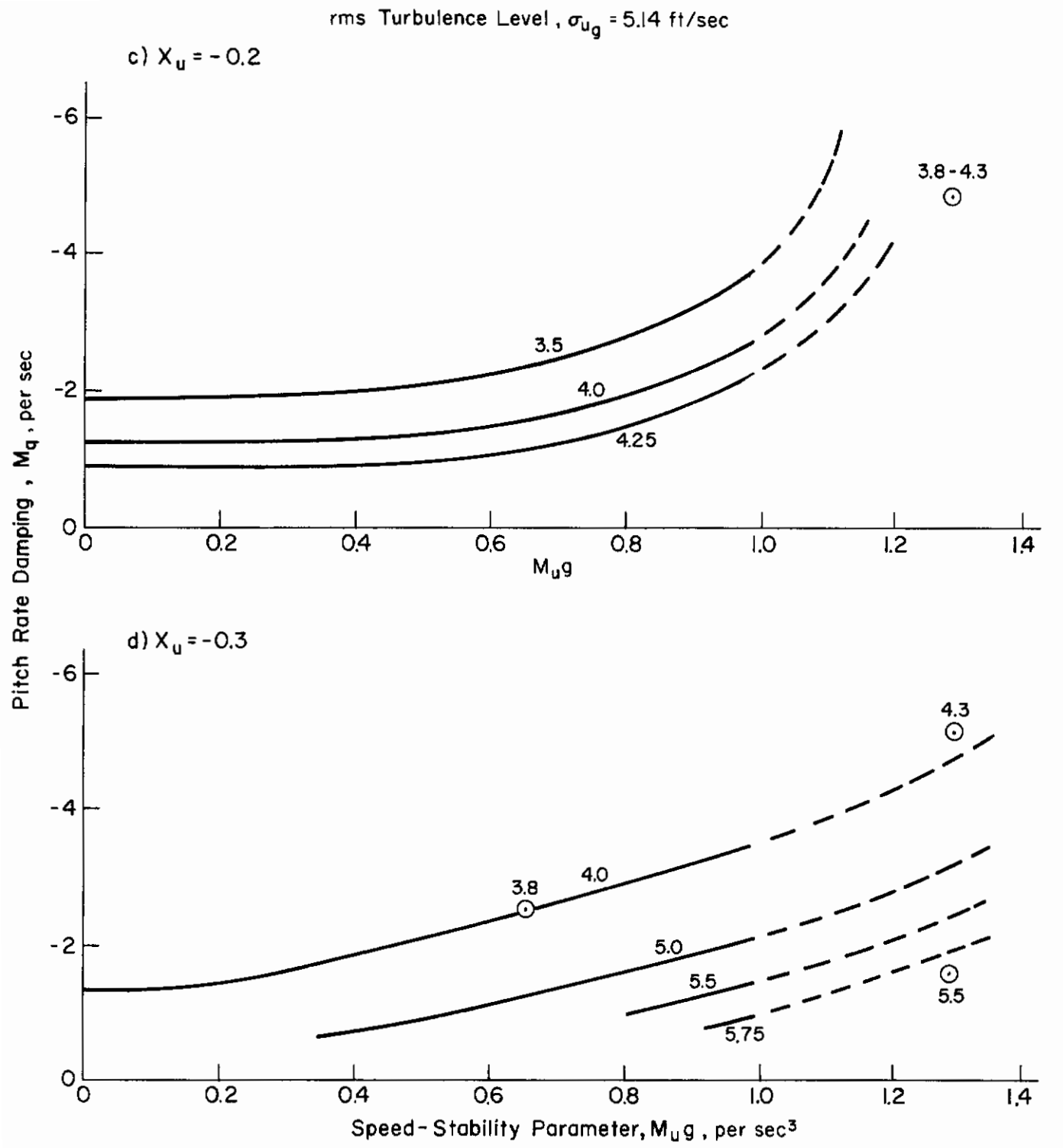

Figure A-5. Contours of Average Pilot Ratings Derived from Flight Simulation Data

Basically, no discernible difference is indicated in the level of rating given by the pilots from the two sources. Additional comparisons for different dynamic conditions would be desirable, but these limited results do suggest that with all other factors being equal, good correlations can be expected for fixed-based results. Certainly in the present case this is true. It is also apparent that good comparisons were obtained at the higher gust response conditions (i.e., $M_u\sigma_u > 0.1$) even though the exact use of gust input ($\sigma_{u_g} = 5$ ft/sec) for each condition and the specific influence on pilot ratings is not indicated in Ref. 12.

2. Rating Variance Due to Moving-Base and/or Flight Test Versus Fixed-Base

Of course, motion cues are the major factor contributing to rating differences between the fixed- and moving-base experiments where VTOL vehicles are concerned. In general, the motion effects have been somewhat avoided in the present survey by considering primarily the satisfactory pilot rating data. However, the satisfactory dynamics of Table III do indicate that less stable dynamic properties are acceptable where motion cues are available.

The effects of motion become more obvious when the vehicle dynamics approach the marginal control regions. These marginally stable or slightly unstable vehicles require more lead compensation than that easily generated by pilots visually, which partially accounts for the rating differences.

3. Satisfactory Ratings

Figure A-6 shows that the cutoff point for the fixed-base data appears to be the aperiodic mode $1/T_{sp_2} \doteq 1$ rad/sec which is approximately $M_q \doteq -1$, whereas, the satisfactory boundary for moving-base data appears to follow the condition that $\omega_p \doteq 1/T_{sp_2}$ as the vehicle dynamic properties collapse into an effective inertial body (i.e., $\theta/\delta = K/s^2$).

In this region of low-frequency aperiodic and phugoid modes, the conventional dynamics modes become equal and a direct function of gM_u (i.e., $\omega_p \doteq 1/T_{sp_2} \doteq \sqrt{gM_u}$). The damping ratio, ζ_p, approaches a

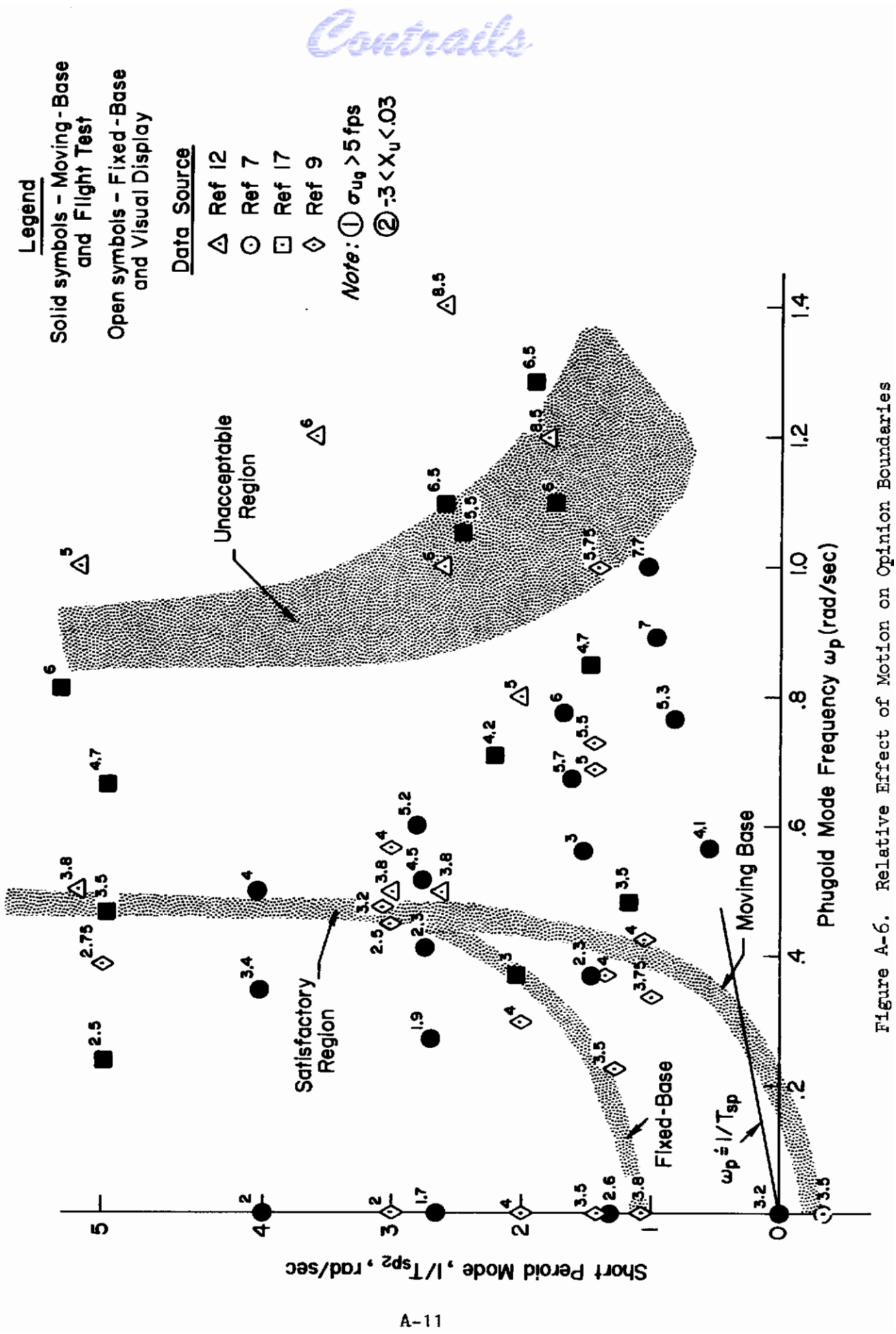

Figure A-6. Relative Effect of Motion on Opinion Boundaries

constant, $\zeta_p = -0.5$. Under these conditions the vehicle dynamics are classically unstable and K/s^2 in appearance in the crossover region. This difference between fixed and moving base is shown in the following s-plane sketch of the characteristic root of the attitude mode. Note that this difference is reflected by the phugoid mode damping, i.e., $\zeta_p \doteq 0$ for fixed base and $\zeta \doteq -0.5$ for moving. Thus, motion cues apparently account for the inclusion of slightly more unstable control situations for the satisfactory ratings. Also, with motion, a marginally satisfactory rating can be maintained as the vehicle aerodynamic properties are eliminated.

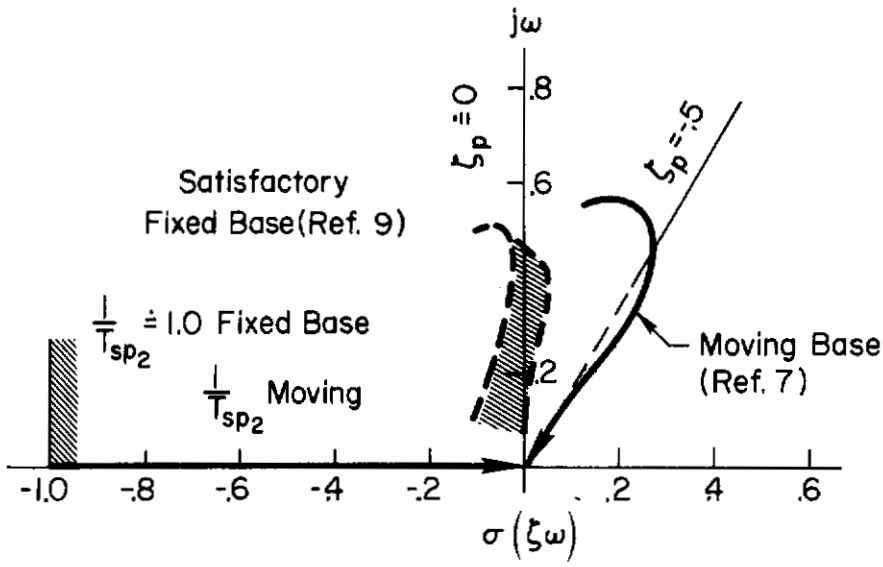

By excluding the above small region of vehicle dynamics (i.e., where $1/T_{sp_2} < 1$ and $\omega_p \doteq 1/T_{sp_2}$), the effective change in pilot rating between fixed- and moving-base results amounts to about ±1/2 point in rating at the satisfactory conditions.

4. Unacceptable Ratings

Significant rating differences are evident between fixed- and moving-base results from Fig. A-6 in the region of unacceptable dynamics. However, the rating difference between fixed- and moving-base results is not clearly pictured in this figure (i.e., $1/T_{sp_2}$ versus ω_p) because the divergence properties of the phugoid mode are not identified. A moderately high

frequency phugoid mode (i.e., $\omega_p \geq 0.8$) is characteristic of the unacceptable rating indicated in the figure.

A selective comparison of data from the primary sources is shown in Table A-I for evaluating fixed- and moving-base differences. In these comparisons, both characteristic dynamic properties (i.e., ω_p, $1/T_{sp_2}$, and ζ_p) and the aerodynamic features (M_u, X_u, and M_q) have been matched as closely as possible using the available data. Basically, the unacceptable dynamics from Refs. 12 and 17 correspond to high M_u and $M_u\sigma_u$ conditions; therefore, the ratings are possibly clouded by the gust response aspects. Based strictly on the few case comparisons shown, motion cues apparently account for better rating for the highly unstable dynamic situations (i.e., $\zeta_p > -0.2$) but at the lightly damped (i.e., $\zeta_p \doteq 0$) conditions motion doesn't appear significant.

Logically from these limited data, we can conclude only that for the very unstable, moderately high frequency dynamics ($\omega_p > 1.0$) the rating increment between fixed and moving base approaches ± 1.3 rating points.

EFFECTS OF GUST

As a starting point, the data assembled for the present study was specifically restricted to conditions of low gust sensitivity, $M_u\sigma_{u_g}$. These "base line" data were defined as having a gust sensitivity, $M_u\sigma_{u_g} < 0.1$. Figure A-7 identifies the available data relative to this gust response merit. It will be noted that several dynamic conditions (indicated by gM_u level) from each source fall in this region; in fact, the data conditions from Ref. 7 were all tested at low gust levels.

Generally speaking, the desirable VTOL dynamics identified in the text have application to gust conditions greater than $M_u\sigma_u = 0.1$, but we are unable to establish the level at which gust aspects dominate. Some general conclusions concerning the effects of disturbance level have been observed as a result of the present efforts, and these are reviewed in the following:

TABLE A-I

FLIGHT TEST, MOVING-BASE, AND FIXED-BASE DATA COMPARISON OF RATING FOR UNACCEPTABLE CONTROLLED ELEMENTS

REFERENCE SOURCE	$1/T_{sp_2}$	ζ_p	ω_p	X_u	GUST FACTOR $M_u\sigma_{u_g}$	PR
Seckel	1.90	−0.30	1.28	−0.15	0.66	6.5
A'Harrah	1.80	−0.29	1.20	−0.24	0.40	8.5
Seckel	2.60	−0.19	1.10	−0.15	0.66	6.0
A'Harrah	2.60	−0.17	1.00	−0.05	0.40	6.0
A'Harrah	2.60	−0.25	1.40	−0.075	0.80	8.5
Seckel	5.30	−0.06	0.81	−0.15	0.66	6.0
A'Harrah	4.04	0	0.80	−0.16	0.40	4.5−5.0
A'Harrah	5.2	−0.087	1.00	−0.20	0.50	5.0−5.5
Seckel	2.4	−0.17	0.95	−0.085	0.436	6
A'Harrah	2.6	−0.17	1.00	−0.05	0.40	6
Miller	1.4	−0.112	0.736	−0.36	<0.1	5.75
Breul	1.69	−0.175	0.767	−0.25	<0.1	6.0

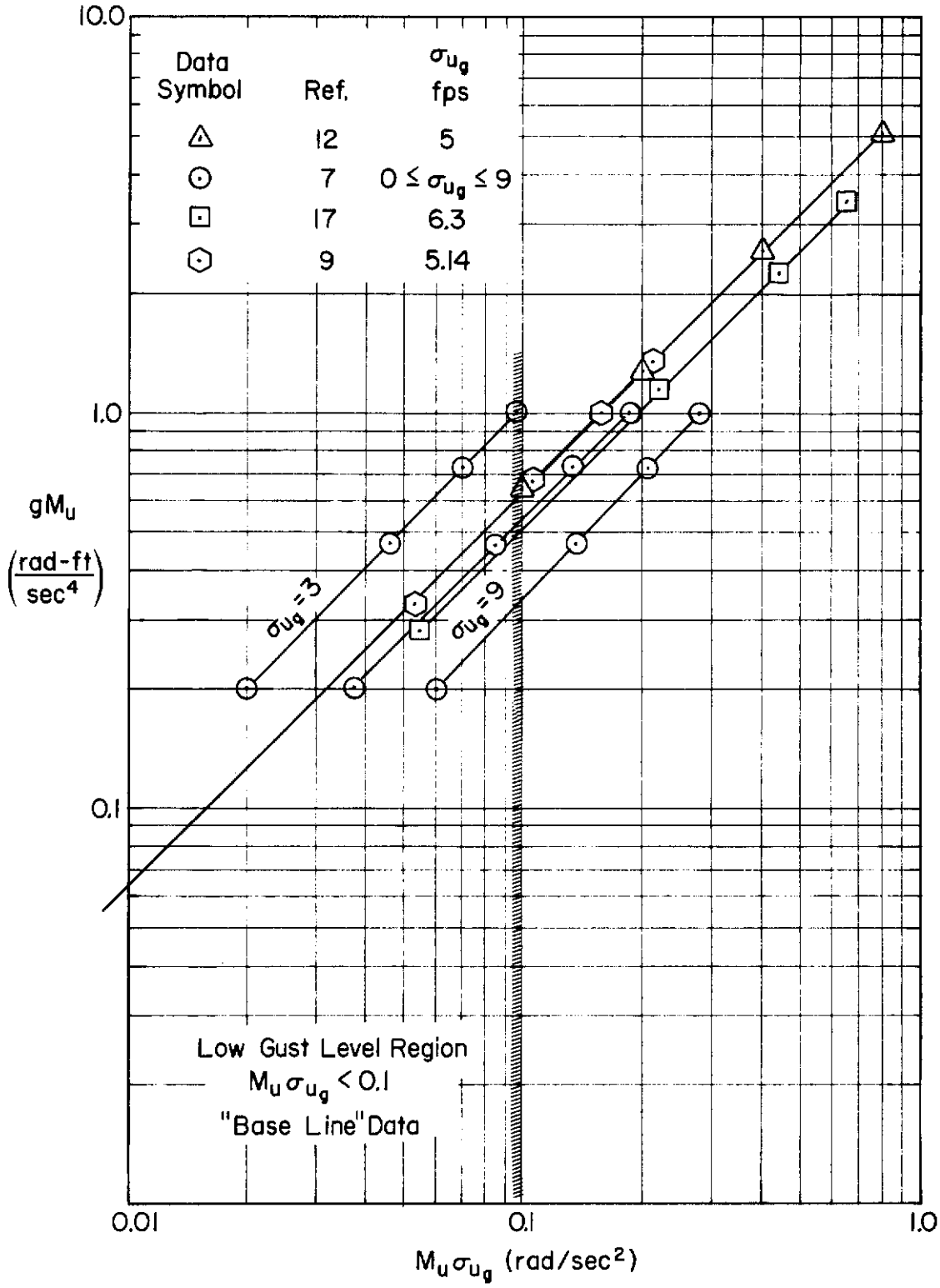

Figure A-7. Data Selection for Gust Sensitivity Effects

a. Relation of Closed-Loop Regulatory Control and Gust Response Level

Results of the flight test of Ref. 17 are shown in the table below. We note here that a satisfactory precision hover rating deteriorates to a marginally

					Pilot Rating Gust Sensitivity, $M_u\sigma_{ug}$			Crossover Point Freq.
gM_u	M_q	ω_p	$-\zeta\omega_n$	$1/T_{sp}$	Low	Medium	High	$1/T_L \doteq \omega_p$
0.28	−0.99	0.48	0.091	1.19	3.7			0.48
0.28	−1.98	0.37	0.024	2.05	3.2			0.37
1.13	−1.98	0.71	0.107	2.21		4.1		0.71
3.38	−1.98	1.13	0.259	2.52	3.2*		6.6	1.13
3.38	−4.95	0.81	0.056	5.08			6.0	0.81

*PR = 4.5 for low-speed maneuvering task

acceptable rating in medium turbulence. In addition, the high M_u case ($gM_u = 3.38$) in precision hover (low disturbance) is rated satisfactory and becomes unacceptable for high gust response. While these results confirm the correlation of the pilot opinion with the attitude response factor, $M_u\sigma_{ug}$, the crossover point frequency ($1/T_L \doteq \omega_p$) which is indicative of poor attitude loop low frequency regulatory control is equally as good. The crossover point as described in the text (Section II.B) as the frequency at which the pilot does not improve his performance by increased lead compensation.

b. Pilot Rating Trends for Various Dynamics

Reference 1 data presented in Fig. A-8 provides a good indication of the trend resulting as the gust intensity is increased for constant dynamics. Basically, a poorer rating corresponds to a deterioration in mean-square error performance level and an increase in pilot effort. These results indicate that either hovering accuracy or effort can become a major factor in the pilot's rating of a vehicle.

EFFECTS OF TASK DIFFERENCES

Task differences appear to be reflected only in the results from Ref. 7. In these results, the pilot was instructed not to consider the precision hover task or hovering accuracy in rating the handling qualities. The pilot's task is obviously less demanding if he doesn't strive to maintain good hover performance. Furthermore, since the gust

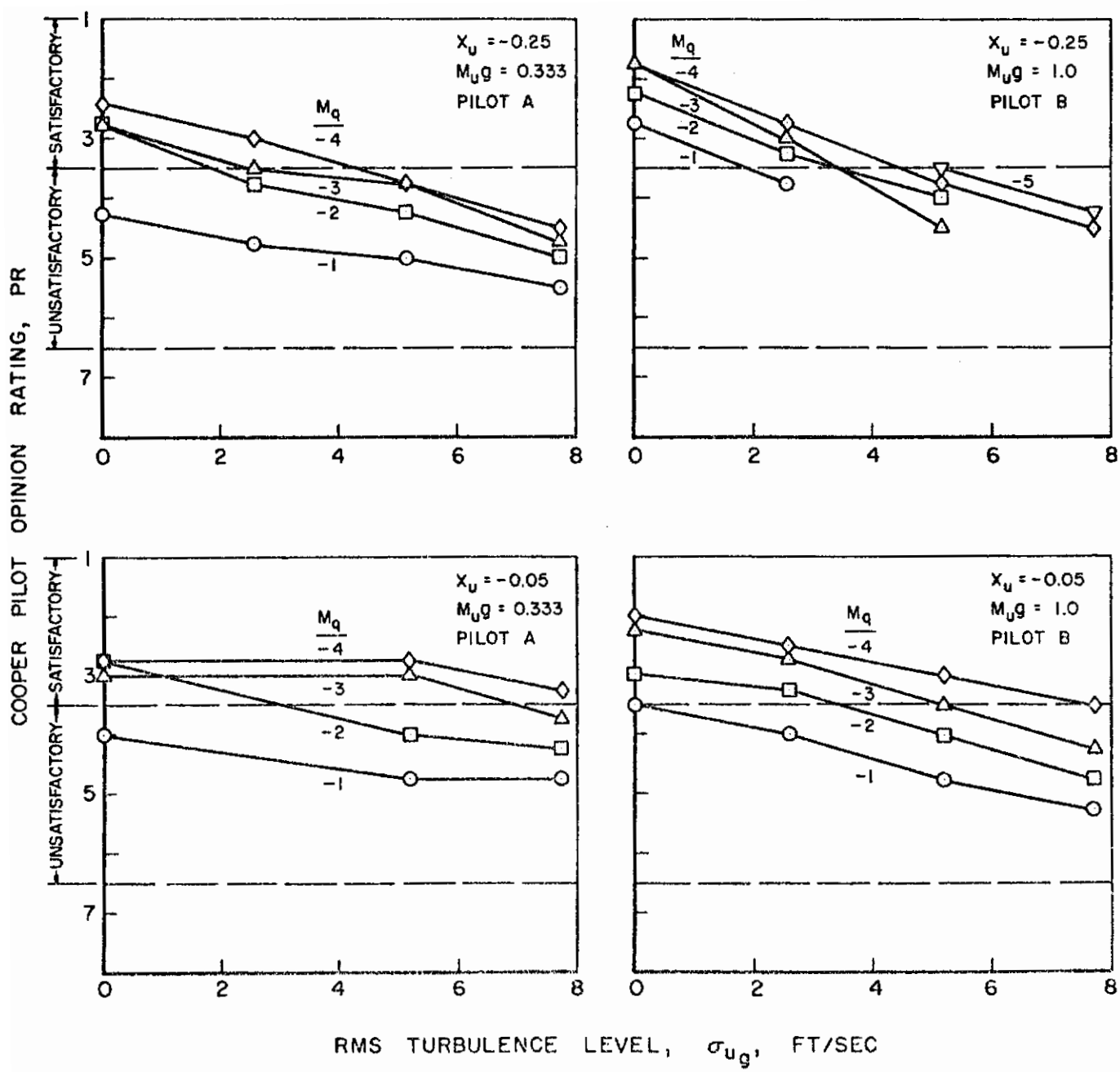

Figure A-8. Effect of Turbulence on Pilot Opinion of Longitudinal Handling Qualities (Ref. 9), Hovering, and Low-Speed Maneuvering Task

level primarily affects performance and the change in rating basically follows the deterioration in performance (as noted in the preceding paragraph), we can anticipate that the gust level will have had less effect on the pilot ratings in Breul's experiments. Although it is difficult to say conclusively that this task aspect alone is the dominant factor, the carpet plot constructed using best rating data in Fig. A-9 does reflect this conclusion. No change is indicated as the gust level is increased regardless of the level of vehicle dynamics or gust sensitivity factor $M_{u_g}\sigma_{u_g}$.

Thus, when task performance merits are eliminated in judging a vehicle, the pilot does appear to be less sensitive to gust disturbance level based on the somewhat limited results.

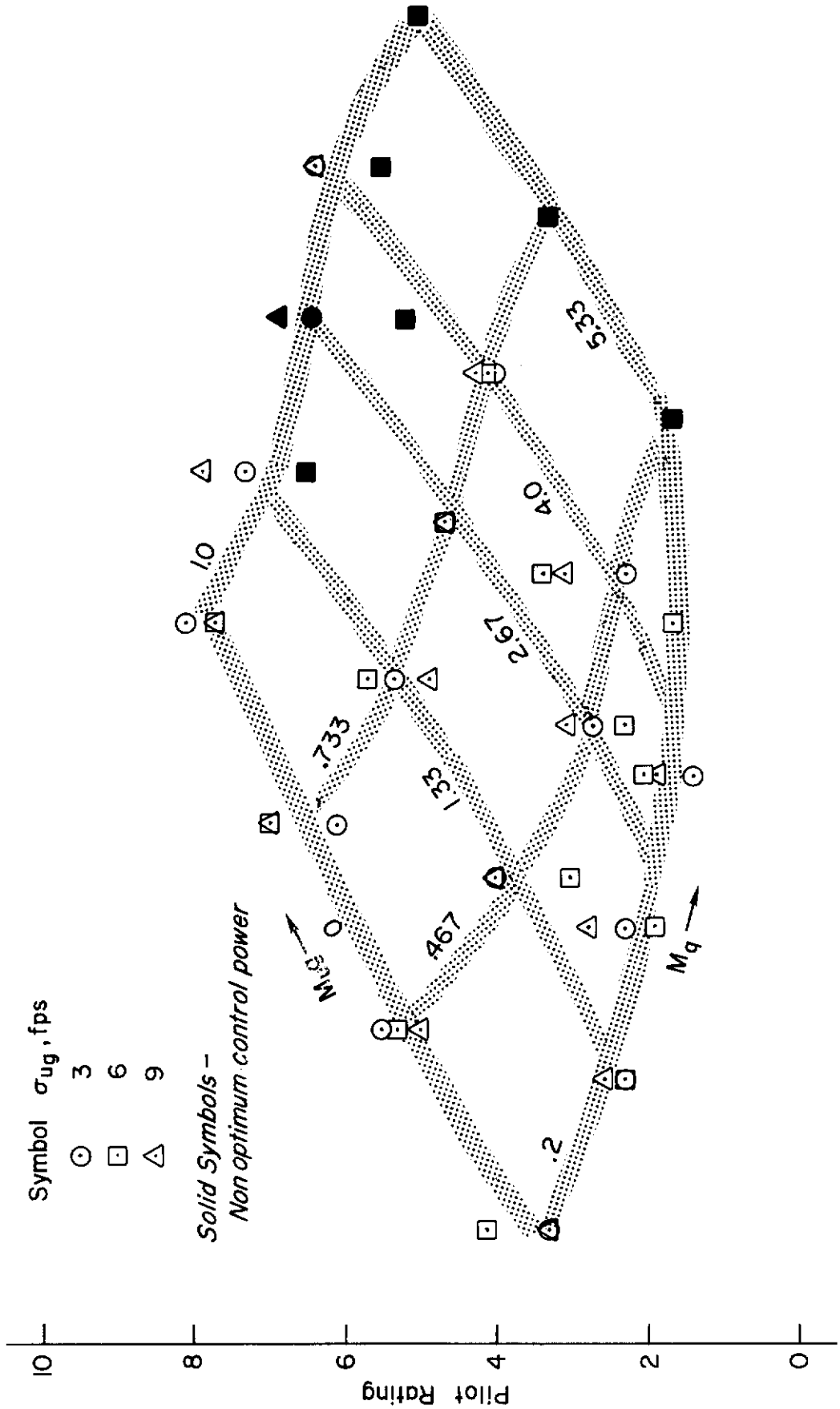

Figure A-9. Rating Trends Under Gust Conditions (Ref. 7)

APPENDIX B

LONGITUDINAL DYNAMIC CHARACTERISTICS, TRANSFER FUNCTIONS, AND STABILITY DERIVATIVES DERIVED FROM VTOL EXPERIMENTS

The data contained in this appendix represents a partial listing of aerodynamic parameters and transfer function expressions derived from this review of VTOL handling qualities experiments. From the listing in Tables B-I, B-III, and B-IV the vehicle dynamic response characteristics and Bode diagrams discussed in the text were calculated. Optimum control sensitivities or power, "best" pilot rating, disturbance conditions (e.g., gust rms levels), and experimental condition are included in the tables in this appendix. For convenience, the data from each source are listed as a group.

TABLE B-I. CONVENTIONAL VTOL DYNAMIC CHARACTERISTICS REVIEWED DURING STUDY

TEST COND. NO.	STABILITY DERIVATIVES							EFFECTIVE OPEN-LOOP DYNAMIC FACTORS						REFERENCE SOURCE
	AIRFRAME				CONTROL			CHARACTERISTIC FACTORS				ATTITUDE, θ		
	X_u sec^{-1}	M_u $(ft\text{-}sec)^{-1}$	Z_w sec^{-1}	M_q sec^{-1}	M_δ	X_δ	$M(\delta)$ (X_δ/M_δ)	$1/T_{sp_2}$ (ζ_{sp})	$1/T_{sp_1}$ (ω_{sp})	ζ_p	ω_p	$1/T_{\theta_1}$	$1/T_{\theta_2}$	
1	−0.10	0	−0.3906	0	varied	0	varied	0.1	0.391	0	0	0.1	0.391	Breul, Ref. 7
2		0.0062						0.620		−0.458	0.568			
3		0.0145						0.811		−0.468	0.759			
4		0.0228						0.936		−0.473	0.885			
5		0.0311						1.00		−0.500	1.00			
6	−0.10	0		−1.33				1.33		0.1	0			
7		0.0062						1.43		−0.006	0.373			
8		0.0145						1.54		−0.100	0.551			
9		0.0228						1.64		−0.146	0.671			
10		0.0311						1.70		−0.175	0.767			
11	−0.10	0		−2.67				2.67		0.1	0			
12		0.0062						2.70		0.131	0.272			
13		0.0145						2.74		0.043	0.412			
14		0.0228						2.77		0.0008	0.515			
15		0.0311						2.80		−0.027	0.597			
16	−0.10	0		−4.00				4.00		0.1	0			
17		0.0062						4.01		0.195	0.223			
18		0.0145						4.03		0.104	0.340			
19		0.0228						4.06		0.064	0.426			
20		0.0311						4.06		0.038	0.496			
21	−0.10	0		−5.33				5.33		0.1	0			
22		0.0062						5.33		0.24	0.19			
23		0.0145						5.34		0.14	0.29			
24		0.0228						5.36		0.10	0.370			
25		0.0311						5.37		0.0748	0.4317	0.1		
26	0	0		0			varied	0		0	0	0		
27	−0.03	0		−1.33				1.33		0	0	0.03		
28	−0.25	0		−1.33				1.33		0	0	0.25		
29	−0.03	0.0145		−1.33				1.534		−0.155	0.554	0.03		
30	−0.25			−1.33				1.534		0.044	0.554	0.25		
31	−0.03			−2.67				2.55		0.186	0.428	0.03		
32	−0.25	0.0145	−0.3906	−2.67	varied	0	varied	2.55	0.391	0.445	0.428	0.25	0.391	

TABLE B-I (Continued)

TEST COND. NO.	STABILITY DERIVATIVES: AIRFRAME X_u sec^{-1}	M_u $(ft\text{-}sec)^{-1}$	Z_w sec^{-1}	M_q sec^{-1}	CONTROL M_δ	X_δ	$M(\delta)$ (X_δ/M_δ)	EFFECTIVE OPEN-LOOP DYNAMIC FACTORS: CHARACTERISTIC FACTORS $1/T_{sp_2}$ (ζ_{sp})	$1/T_{sp_1}$ (ω_{sp})	ζ_p	ω_p	ATTITUDE, θ $1/T_{\theta_1}$	$1/T_{\theta_2}$	REFERENCE SOURCE
33	−0.0276	0.0087	−0.82	−0.99	varied	varied	(−1.88)	1.17	0.82	−0.22	0.48	−0.044	0.82	Seckel;
34	↓	↓	↓	−1.98	↓	↓	↓	2.04	↓	−0.13	0.37	−0.044	↓	Traybar,
35	↓	↓	↓	−4.95	↓	↓	↓	4.95	↓	−0.10	0.24	−0.044	↓	Miller
36	−0.0198	0.0351	↓	−0.99	↓	↓	↓	1.45	↓	−0.27	0.84	−0.047	↓	Ref. 17
37	↓	↓	↓	−1.98	↓	↓	↓	2.2	↓	−0.15	0.71	↓	↓	
38	↓	↓	↓	−4.95	↓	↓	↓	4.95	↓	−0.07	0.47	↓	↓	
39	−0.085	0.0698	↓	−0.99	↓	↓	↓	1.75	↓	−0.29	1.10	↓	↓	
40	↓	↓	↓	−1.98	↓	↓	↓	2.4	↓	−0.17	0.95	↓	↓	
41	↓	↓	↓	−4.95	↓	↓	↓	4.95	↓	−0.06	0.66	↓	↓	
42	−0.150	0.105	↓	−0.99	↓	↓	↓	1.90	↓	−0.30	1.28	↓	↓	
43	↓	↓	↓	−1.98	↓	↓	↓	2.60	↓	−0.19	1.10	↓	↓	
44	↓	↓	↓	−4.95	↓	↓	↓	5.30	↓	−0.06	0.81	↓	↓	
45	−0.0198	0.0351	↓	−6.65	↓	↓	↓	6.9	↓	−0.06	0.41	−0.047	↓	
46	−0.0276	0.0087	−0.82	−6.65	varied	varied	(−1.88)	6.9	0.82	−0.13	0.20	−0.044	0.82	
47	−0.23	0.0398	N.A.*	−5.1	varied	0	N.A.	5.14	N.A.*	0.174	0.5	0.23	N.A.*	A'Harrah;
48	−0.28	0.0199	↓	−2.5	↓	↓	↓	2.6	↓	0.175	0.496	0.28	↓	Kwiatkowski
49	−0.35	0.0795	↓	−3.9	↓	↓	↓	4.05	↓	0.11	0.795	0.35	↓	Ref. 12
50	−0.17	0.0398	↓	−1.65	↓	↓	↓	1.980	↓	−0.11	0.805	0.17	↓	
51	−0.05	0.0795	↓	−2.2	↓	↓	↓	2.55	↓	−0.35	1.0	0.05	↓	
52	−0.06	0.159	↓	−3.2	↓	↓	↓	3.6	↓	−0.145	1.2	0.06	↓	
53	−0.1	0.0398	↓	−2.5	↓	↓	↓	2.6	↓	−0.06	0.68	0.1	↓	
54	−0.075	0.159	↓	1.88	↓	↓	↓	2.67	↓	−0.253	1.385	0.075	↓	
55	−0.24	0.0795	↓	−0.86	↓	↓	↓	1.32	↓	−0.219	1.60	0.24	↓	
56	−0.16	0.0795	↓	−0.4	↓	↓	↓	4.15	↓	0.004	0.79	0.16	↓	
57	−0.06	0.0398	↓	5.1	↓	↓	↓	5.13	↓	0.03	0.50	0.06	↓	
58	−0.26	0.08	↓	−2.15	↓	↓	↓	2.6	↓	−0.087	1.0	0.26	↓	
59	−0.26	0.16	N.A.	−3.16	varied	0	N.A.	3.6	N.A.	−0.072	1.2	0.26	N.A.	

*Not available.

TABLE B-I (Concluded)

TEST COND. NO.	STABILITY DERIVATIVES: AIRFRAME X_u sec^{-1}	M_u $(ft\text{-}sec)^{-1}$	Z_w sec^{-1}	M_q sec^{-1}	CONTROL M_δ	X_δ	$M(\delta)$ (X_δ/M_δ)	EFFECTIVE OPEN-LOOP DYNAMIC FACTORS: CHARACTERISTIC FACTORS $1/T_{sp_2}$ (ζ_{sp})	$1/T_{sp_1}$ (ω_{sp})	ζ_p	ω_p	ATTITUDE, θ $1/T_{\theta_1}$	$1/T_{\theta_2}$	REFERENCE SOURCE
60	Derivatives not given				varied	N.A.	N.A.	(0.94)	(0.717)	−0.25	0.410	0.051	0.761	Tapscott Ref. 26
61					↓	↓	↓	(0.939)	(0.833)	−0.127	0.349	↓	↓	
62								(0.985)	(1.085)	0.015	0.0041			
63					varied	N.A.	N.A.	(1.085)	(1.285)	0.039	0.0091	0.051	0.761	
64	−0.126	0.0361	N.A.	0	varied	0	N.A.	1.09	N.A.	−0.478	1.036	−0.126	N.A.	Madden Ref. 27
65	−0.1	0.0207	N.A.	−1.0	varied	0	N.A.	1.4	N.A.	−0.202	0.694	0.1	N.A.	Miller and Vinje UARL Ref. 9
66	↓	0.0207	↓	−3.0	↓	↓	↓	3.1	↓	0.028	0.471	↓	↓	
67		0.0207		−5.0				5.0		0.098	0.379			
68		0		−3.0				3.0		0.028	0.472			
69		0.0103		↓				3.0		0.069	0.453			
70		0.0207						3.1		0.028	0.472			
71	−0.1	0.0311						3.1		−0.007	0.570	0.1		
72	0	0.0207						3.0		−0.054	0.335	0		
73	−0.05	↓						3.1		−0.0276	0.471	0.05		
74	−0.1							↓		0.0280	0.472	0.1		
75	−0.2									0.124	0.500	0.2		
76	−0.3	0.0207						3.1		0.245	0.463	0.3		
77	−0.05	0.0103		−3.0				3.04		0.0604	0.308	0.05		
78	−0.2	0.0414		−3.0				3.14		0.087	0.644	0.2		
79	−0.1	0.0103		−1.0				1.24		−0.255	0.519	0.1		
80	−0.025	0.0103		−1.0				1.23		−0.386	0.521	0.025		
81	−0.10	0.0103		−3.0				3.04		−0.284	0.308	0.1		
82	−0.025	0.0103		−3.0				3.04		−0.0518	0.308	0.025		
83	−0.09	0.0622		−1.0				1.16		−0.206	0.417	0.09		
84	−0.36	0.0248	N.A.	−1.0	varied	0	N.A.	1.48	N.A.	−0.112	0.736	0.36	N.A.	

TABLE B-II. CONVENTIONAL VTOL DYNAMICS EXPERIMENTAL CONDITIONS FOR HANDLING QUALITY BOUNDARIES

HANDLING QUALITIES BOUNDARY	TEST COND. NO.*	SIMULATION TECHNIQUE AND DESCRIPTION	PILOT RATING CONSIDERATIONS						CONTROL			REFERENCE
			GUST LEVELS; σ_{ug}, fps			TASK		OVERALL RATING	SENSITIVITY	POWER	FORCE	
			$0<\sigma_{ug}<3$	$3<\sigma_{ug}<6$	$\sigma_{ug}>6$ $(6\leq\sigma_{ug}\leq9)$	PRECISION HOVER	LOW-SPEED FLIGHT		M_δ, $\frac{rad/sec^2}{in.}$	$M(\delta)$ rad/sec^2	$K_P \sim$ lb/in.	
Satisfactory $3 \leq PR \leq 4$	2	Cockpit with motion in pitch and roll and optical visual display of motion in remaining four degrees of freedom. Controls; stick, collective and pedals.	✓				✓	3.3	nonlinear	0.7	1 → 1/2	Breul Ref. 7
	2			✓			✓	4.0		0.7		
	2				(✓)		✓	3.1		0.7		
	8		✓				✓	3.0		0.55		
	8			✓			✓	4.0		0.55		
	12				(✓)		✓	3.2		0.7		
	14				(✓)		✓	3.2		0.7		
	18			✓			✓	3.2		0.7		
	18				(✓)		✓	3.4		0.7		
	19		✓				✓	4.0		0.7		
	19			✓			✓	4.0		0.7		
$5.5 \leq PR \leq 7$	3		✓				✓	5.5		0.55		
	4		✓				✓	6.2		0.7		
	4			✓			✓	7.0		0.7		
	4				(✓)		✓	7.0		0.55		
	9			✓			✓	5.7		0.55		
	10			✓			✓	6.5		0.7		
	15		✓				✓	6.3		0.7		
	15				(✓)		✓	6.9		0.7		
	20		✓				✓	7.0		0.7		
	20				(✓)			6.3	nonlinear	0.7	1 → 1/2	
$3 < PR < 4$	33	Actual flight test in variable stability HUP-1 helicopter where M_q, M_u, X_u, and M_δ were allowed to vary. Pilot control about longitudinal axis in near hover situations. Motion about other axes was optimally stabilized by autopilot.			(✓)	✓	✓	3.5	0.41	N.A.	1.0	Seckel; Traybar, Miller Ref. 17
	34				(✓)	✓	✓	3.0	0.41			
	37				(✓)	✓	✓	4.0	0.41			
	38				(✓)	✓	✓	3.5	0.41			
	45				(✓)	✓	✓	3.5	0.41			
	46				(✓)	✓	✓	3.5	0.72			
	43		✓			3.2	4.5		0.41			
	38				(✓)	✓	✓	3.5	0.63			
$5.5 < PR < 7.0$	39				(✓)	✓	✓	5.5	0.41			
	40				✓	✓	✓	5.5	0.41			
	42				✓	✓	✓	6.5	0.41			
	43				✓	6.6	6.6	6.6	0.41			
	44				✓	✓	✓	6.0	0.41	N.A.	1.0	

TABLE B-II (Concluded)

HANDLING QUALITIES BOUNDARY	TEST COND. NO.*	SIMULATION TECHNIQUE AND DESCRIPTION	PILOT RATING CONSIDERATIONS						CONTROL			REFERENCE
			GUST LEVELS; σ_{ug}, fps			TASK		OVERALL RATING	SENSITIVITY	POWER	FORCE	
			$0<\sigma_{ug}<3$	$3<\sigma_{ug}<6$	$\sigma_{ug}>6$ $(6\leq\sigma_{ug}\leq9)$	PRECISION HOVER	LOW-SPEED FLIGHT		M_δ, $\frac{rad/sec^2}{in.}$	$M(\delta)$ rad/sec^2	K_F – lb/in.	
3 < PR < 4	47	Fixed-base; visual presentation which used closed-circuit television system for simulation of six-degree-of-freedom motion over terrain.		✓		✓	✓	3.8		0.35	1.5	A'Harrah and Kwiatkowski Ref. 12
	48			✓		✓	✓	3.8				
	49			✓		✓	✓	3.8				
	53			✓		✓	✓	3.9				
	54			✓		✓	✓	3.8				
	57			✓		✓	✓	3.8				
	58			✓		✓	✓	3.8				
5.5 < PR < 8.5	50			✓		✓	✓	5.5				
	51			✓		✓	✓	6.0				
	52			✓		✓	✓	6.0				
	55			✓		✓	✓	8.5				
	56			✓		✓	✓	8.5				
	59			✓		✓	✓	5.5				
	60			✓		✓	✓	5.5				
	61			✓		✓	✓	6.0		0.35	1.5	
3 < PR < 4	73	Fixed-base visual presentation which uses a contact analog display system for simulation of five degrees of freedom.		✓		✓		3.5	0.49			Miller and Vinje Ref. 9
	69			✓		✓		3.0	0.431			
	70			✓		✓		3.25	0.493			
	71			✓		✓		3.5	0.33			
	72			✓		✓		3.0	0.36			
	76			✓		✓		4.0	0.467			
	78				✓	✓		4.0	0.32			
	79		✓			✓		3.5	—			
	80			✓		✓		3.5	0.25			
	84		✓			✓		3.5	0.34			
5.5 < PR < 6.5	81				✓	✓		6.50	0.26			

*See Table B-I

TABLE B-III

VTOL ATTITUDE STABILIZATION SYSTEM DYNAMICS REVIEWED DURING THE PRESENT STUDY

DATA NO.	BASIC AIRFRAME DERIVATIVES				STABILIZATION SYSTEM FEATURES		EFFECTIVE OPEN-LOOP DYNAMICS FACTORS						PILOT RATING	REFERENCE
							CHARACTERISTICS FACTORS				ATTITUDE, θ			
	X_u	M_u	M_q	Z_w	ATTITUDE POSITION K_θ OR M_θ EFFECTIVE	ATTITUDE RATE PLUS POSITION $s + K_\theta/K_{\dot\theta}$	$1/T'_{sp_2}$ (ζ_{sp})	$1/T_{sp_1}$ (ω_{sp})	ζ'_p	ω'_p	$1/T_{\theta_1}$	$1/T_{\theta_2}$		
1	−0.126	0.0361	0	N.A.	−24	s + 24	−0.17	N.A.	0.11	4.92	−0.126	N.A.	2	Madden
2	↓	↓	↓	↓	−16	s + 64	−0.13	↓	0.025	4.03	↓	↓	6	Ref. 27
3	−0.126	0.0361	0	N.A.	−8	s + 8	−0.26	N.A.	0.20	2.53	−0.126	N.A.	4	
1	−0.22	0.010	−0.10	−0.14		s + 0.5	(0.45)	(4.3)	0.45	0.45	0.237	0.142	2 → 3	Shaw
2	−0.153	0.0096	−0.203	−0.165	−2.4	s + 0.511	(0.70)	(3.8)	0.751	0.45	0.237	0.142	2 → 3	Ref. 20
3														
1	−0.05	0.0311	−0.5	N.A.	−8	s + 1.6	0.191	N.A.	0.897	2.71	0.05	N.A.	2.0	Miller
2		0.0104	−1.0		−1	s + 1.0	0.492		0.318	0.881			4.9	and Vinje
3					−2	s + 2.0	0.236		0.3	1.37			4.7	Ref. 9
4					−3	s + 3.0	0.166		0.26	1.70			4.0	
5	↓	↓			−4	s + 4.0	0.136		0.23	1.99	↓		4.5	
6	−0.05	0.0104			−5	s + 5.0	0.117		0.21	2.22	0.05		4.5	
7	−0.20	0.0311			−2	s + 2.0	0.75		0.16	1.37	0.20		4.7	
8	↓	↓			−3	s + 3.0	0.57		0.19	1.68	↓		4.0	
9			↓		−4	s + 4.0	0.46		0.18	1.97			4.5	
10			−1.0		−5	s + 5.0	0.42		0.17	2.22			4.5	
11			−2.0		−2	s + 1.0	0.75		0.47	1.1			4.3	
12	↓	↓	↓		−3	s + 1.5	0.55		0.5	1.54	↓		3.8	
13	−0.20	0.0311	−2.0		−4	s + 2.0	0.48		0.45	1.88	0.20		4.3	
14	−0.1	0.0207	−1.0		−3	s + 3.0	0.345		0.23	1.68	0.10		3.5	
15	−0.1	0.0207	−1.0	N.A.	−5	s + 5.0	0.24	N.A.	0.198	2.21	0.10	N.A.	4.0	

TABLE B-IV

TRANSLATIONAL STABILIZATION SYSTEM DYNAMICS

DATA NUMBER	BASIC AIRFRAME DERIVATIVES				EFFECTIVE OPEN-LOOP DYNAMICS FACTORS						PILOT RATING	REFERENCE
					CHARACTERISTIC FACTORS				ATTITUDE, θ			
	X_u	M_u	M_q	Z_w	$1/T_{sp_2}$	$1/T_{sp_1}$	ζ_p	ω_p	$1/T_{\theta_1}$	$1/T_{\theta_2}$		
1	−0.82	0.02	−2.5	N.A.	3.0	N.A.	0.70	0.5	0.82	N.A.	3	A'Harrah and Kwiatkowski Ref. 12
2	−0.75	0.04	−5.1	↓	5.2	↓	0.70	0.5	0.75	↓	3	
3	−0.95	0.04	−1.4	↓	2.02	↓	0.21	0.8	0.95	↓	4.2	
4	−0.87	0.08	−3.9	↓	4.04	↓	0.44	0.8	0.87	↓	3	
5	−0.95	0.08	−2.0	↓	2.6	↓	0.173	1.0	0.95	↓	4.0	
6	−0.87	0.16	−3.06	↓	3.6	↓	0.144	1.2	0.87	↓	3.5	
7	−1.33	0.16	−2.95	↓	3.6	↓	0.29	1.2	1.33	↓	3	
8	−0.926	0.16	−4.93	↓	5.2	↓	0.35	1.0	0.926	↓	3	
9	−5.1	0.04	−0.23	↓	5.14	↓	0.174	0.5	5.10	↓	3	
10	−2.5	0.02	−0.28	↓	2.6	↓	0.174	0.5	2.50	↓	3	
11	−3.9	0.08	−0.35	↓	4.05	↓	−0.11	0.8	3.90	↓	3.8	
12	−1.65	0.04	−0.17	↓	2.0	↓	−0.11	0.805	1.65	↓	5.5	
13	−2.20	0.08	−0.05	↓	2.6	↓	−0.35	1.00	2.20	↓	6.0	
14	−3.2	0.16	−0.06	↓	3.6	↓	−0.145	1.20	3.20	↓	6.0	
15	−1.88	0.16	−0.075	N.A.	2.67	N.A.	−0.253	1.385	1.88	N.A.	8.5	

APPENDIX C

EQUATIONS OF MOTION AND APPROXIMATE FACTORS

EQUATIONS OF MOTION, HOVER

When terms which are usually negligibly small are omitted, the longitudinal equations of motion can be written:

$$\begin{bmatrix} s - X_u & 0 & g \\ -Z_u & s - Z_w & 0 \\ -M_u & 0 & s^2 - M_q s \end{bmatrix} \begin{Bmatrix} u \\ w \\ \theta \end{Bmatrix} = \begin{Bmatrix} X_\delta \\ Z_\delta \\ M_\delta \end{Bmatrix} \delta - \begin{Bmatrix} X_u \\ Z_u \\ M_u \end{Bmatrix} u_g \qquad (C\text{-}1)$$

The control-fixed motion of the VTOL-type aircraft in hover consists of one mode, described by $s = Z_w$, which involves only the w-degree of freedom plus two other modes involving only u and θ.

The characteristic equation is:

$$\Delta(s) = (s - Z_w)\left[s^3 - (X_u + M_q)s^2 + X_u M_q s + g M_u\right] = 0 \qquad (C\text{-}2)$$

The $(s - Z_w)$ factor characterizes the plunging mode, which is controlled with the throttle or collective pitch. The other factor is called the "hovering cubic" and characterizes a motion which is controlled with the attitude control.

The lateral hover equations are generally identical in form to Eq. C-1 with the following changes in symbols:

$u \rightarrow v$	$w \rightarrow r$	$\theta \rightarrow \varphi$
$X_u \rightarrow Y_v$	$g \rightarrow -g$	$Z_u \rightarrow N_v$
$Z_w \rightarrow N_r$	$M_u \rightarrow L_v$	$M_q \rightarrow L_p$
$X_\delta \rightarrow Y_\delta$	$Z_\delta \rightarrow N_\delta$	$M_\delta \rightarrow L_\xi$

TRANSFER FUNCTIONS AND LITERAL EXPRESSIONS

All the approximate factors are for straight and level flight and for stability axis derivatives. If the conditions of validity are met, the approximate factors should be within ±10 percent of the magnitude of the root (real or imaginary part).

CHARACTERISTIC EQUATION ("HOVERING CUBIC")

The approximate factors for the "hovering cubic" which may be applied to relate root factors to specific stability derivatives are reviewed below for the two pertinent damping regimes.

Regime I: High damping conditions

$$\left|\frac{gM_u}{M_q^3}\right| < 1.0 \quad ; \quad M_q \gg X_u$$

Then

$$\frac{1}{T_{sp_1}} \doteq -Z_w$$

$$\frac{1}{T_{sp_2}} \doteq \frac{-3M_q}{4} + \sqrt{\frac{M_q^2}{16} - \frac{gM_u}{2M_q}}$$

$$2\zeta_p\omega_p \doteq -X_u - \frac{M_q}{4} - \sqrt{\frac{M_q^2}{16} - \frac{gM_u}{2M_q}}$$

$$\omega_p^2 \doteq gM_uT_{sp_2}$$

If $M_q > 1.0$, these expressions may be reduced to

$$\frac{1}{T_{sp_2}} \doteq -M_q$$

$$2\zeta_p\omega_p \doteq -X_u$$

$$\omega_p^2 \doteq \frac{gM_u}{-M_q}$$

and in the s-plane, associated root locations are:

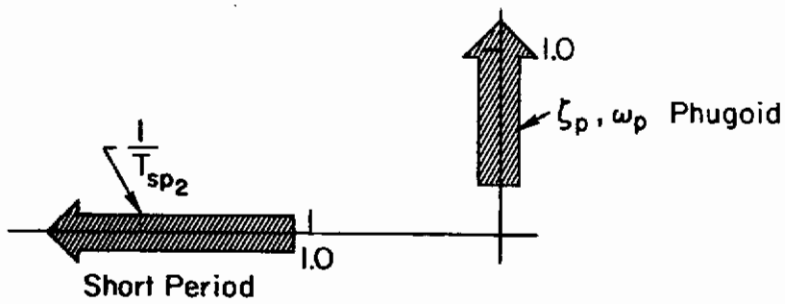

CONTROL RESPONSE FUNCTIONS

The appropriate numerator factors for attitude and speed response to longitudinal control inputs are as follows.

1. Attitude Numerator: $N^{\theta}_{\delta_e}$

$$N^{\theta}_{\delta_e} = \kappa_\theta \left(s + \frac{1}{T_{\theta_1}}\right)\left(s + \frac{1}{T_{\theta_2}}\right)$$

where: $\kappa_\theta = M_\delta$

$$\frac{1}{T_{\theta_1}} \doteq \frac{X_\delta(M_u Z_w - Z_u M_w) + Z_\delta(X_u M_w - M_u X_w) + M_\delta(Z_u X_w - X_u Z_w)}{Z_w M_\delta}$$

$$\frac{1}{T_{\theta_2}} \doteq -Z_w$$

when

$$\left|\frac{1}{T_{\theta_1}}\right| \ll \left|\frac{1}{T_{\theta_2}}\right|$$

2. Velocity Numerator: $N^{u}_{\delta_e}$

$$N^{u}_{\delta_e} = \kappa_u \left(s + \frac{1}{T_{u_1}}\right) \underbrace{\left(s + \frac{1}{T_{u_2}}\right)\left(s + \frac{1}{T_{u_3}}\right)}_{\text{or}} \quad (s^2 + 2\zeta_u\omega_u s + \omega_u^2)$$

where $\kappa_u = X_\delta$

$$\frac{1}{T_u} \doteq -Z_w$$

$$\omega_u^2 \doteq \frac{-g}{X_\delta}\left(M_\delta - Z_\delta \frac{M_w}{Z_w}\right)$$

$$2\zeta_u\omega_u \doteq -M_q$$

Note: $N^{x}_{\delta_e} = \dfrac{N^{u}_{\delta_e}}{s}$

Regime II: Low damping conditions

$$\left|\frac{gM_u}{M_q^3}\right| > 1.0 \quad ; \quad U_o M_w \ll Z_w M_q$$

$$\left|\frac{gM_u}{X_u}\right| > 1.0 \quad ; \quad X_u \to 0$$

Thus,

$$\frac{1}{T_{sp_1}} \doteq -Z_w \qquad \text{or if } M_q = X_u = 0$$

$$\frac{1}{T_{sp_2}} \doteq \sqrt[3]{gM_u} + \frac{-X_u - M_q}{3} \qquad \frac{1}{T_{sp_2}} \doteq \sqrt[3]{gM_u}$$

$$2\zeta_p\omega_p \doteq -\sqrt[3]{gM_u} + \frac{2}{3}\left(-X_u - M_q\right) \qquad 2\zeta_p\omega_p \doteq -\sqrt[3]{gM_u}$$

$$\omega_p^2 \doteq gM_u T_{sp_1} \qquad \omega_p^2 \doteq \frac{gM_u}{\sqrt{gM_u}} \doteq gM_u^{2/3}$$

Practically speaking, the gM_u term is the dominant factor in this situation. If the boundary condition $|gM_u| = |M_q^3|$ is used, the root locations as traced in the s-plane by Regime II are:

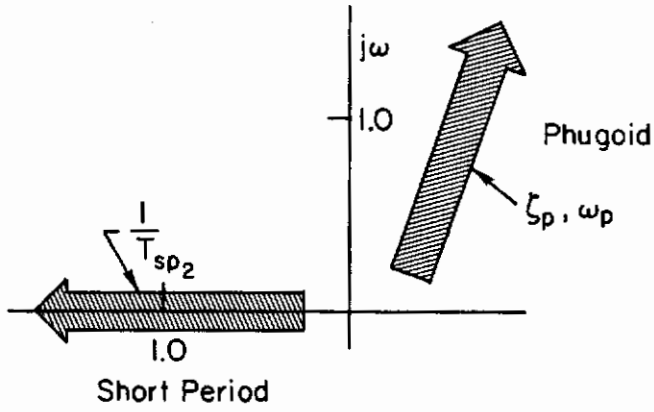

Alternate presentation — after derivative of numerator factors, whence the "pole and zero" locations of the "attitude dynamics" are given below — same applies to diagram on p. C-2.

In this regime the attitude and velocity numerator factors are as follows.

1. **Attitude Numerator:** $N^{\theta}_{\delta_e}$

$$\frac{1}{T_{\theta_1}} + \frac{1}{T_{\theta_2}} \doteq \frac{X_\delta}{M_\delta}(Z_u M_{\dot{w}} + M_u) + \frac{Z_\delta}{M_\delta}(M_w - X_u M_{\dot{w}}) - (X_u + Z_w)$$

$$\frac{1}{T_{\theta_1}}\frac{1}{T_{\theta_2}} \doteq \frac{X_\delta}{M_\delta}(Z_u M_w - Z_w M_u) + \frac{Z_\delta}{M_\delta}(M_u X_w - M_w X_u) + (Z_w X_u - X_w Z_u)$$

when $|Z_\delta M_{\dot{w}}| \ll |M_\delta|$

2. **Velocity Numerator:** $N^{u}_{\delta_e}$

$$\kappa_u = Z_\delta X_w$$

$$\frac{1}{T_{u_1}} \doteq \frac{-gM_\delta}{Z_\delta X_w}$$

$$\frac{1}{T_{u_2}} \doteq \frac{g\left(Z_w - \frac{Z_\delta}{M_\delta} M_w\right)}{(U_o X_w - g)} \doteq -Z_w$$

GUST RESPONSE FUNCTIONS

The gust response numerators for both Regimes I and II are:

1. **Attitude:** $N^{\theta}_{u_g} \doteq -M_u s$

2. **Position:** $N^{x}_{u_g} = \frac{-X_u}{s}\left(s^2 - M_q s - \frac{gM_u}{X_u}\right)$

3. **Coupling:** $N^{\theta\ x}_{u_g \delta_e} = -N^{x\ \theta}_{u_g \delta_e} = \frac{X_u M_\delta}{s}$

HOVER TRANSFER FUNCTIONS FOR MULTILOOP CONTROL AND FOR GUST INPUTS

The pilot/vehicle system most often assumed in the longitudinal hover studies is given by the block diagram of Fig. C-1. The transfer functions required in the closed-loop analyses are given in Table C-I.

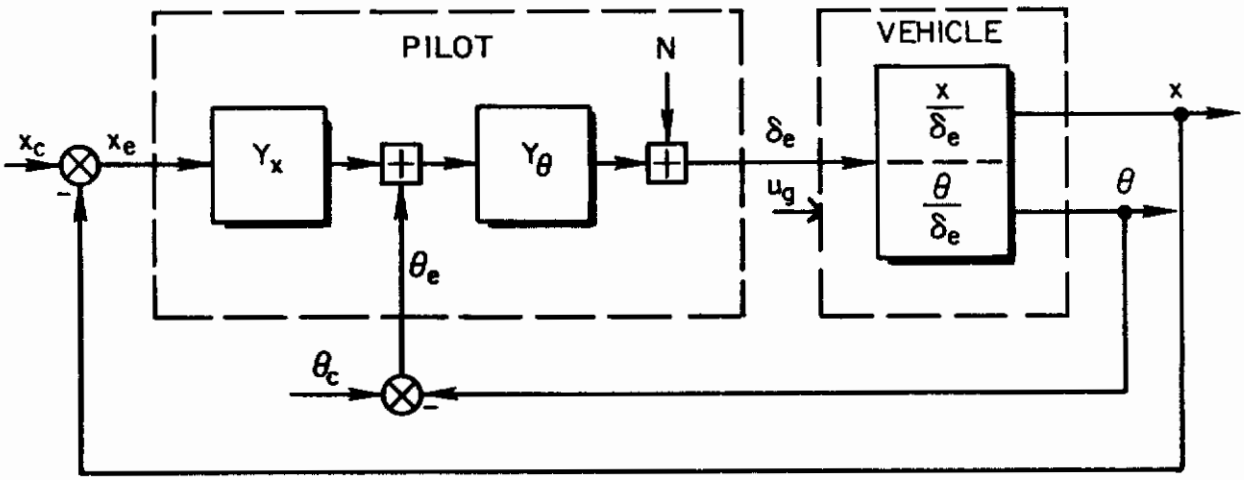

Figure C-1. Pilot Control Structure for the x, $\theta \rightarrow \delta_e$ "Series" Closure

TRANSFER FUNCTIONS AND LITERAL APPROXIMATE FUNCTIONS — TRANSITION

Due to the large variation in approximate factors for the transition flight regime between vehicle configurations, they are presented in Tables C-II and C-III without derivation for reasons of brevity. Their derivations are given in Ref. 3. These literal expressions provide a basis for identifying the relationship between aerodynamic derivatives and transfer function pole/zeros location for most types of vehicles at representative transition conditions.

TABLE C-I. CLOSED-LOOP RELATIONSHIPS[1,2] FOR $\theta \rightarrow \delta_e$ AND $x \rightarrow \delta_e$ CLOSURES IN "SERIES" FOR VTOL-TYPE AIRCRAFT IN HOVER

INPUT	OUTPUT	TRANSFER FUNCTIONS
θ_c	θ	$\frac{N^{\theta}_{\theta_c}}{\Delta''} = \frac{Y_\theta N^{\theta}_{\delta_e}}{\Delta + Y_\theta N^{\theta}_{\delta_e} + Y_x Y_\theta N^{x}_{\delta_e}}$
	θ_e	$\frac{N^{\theta''_e}_{\theta_c}}{\Delta''} = \frac{\Delta + Y_x Y_\theta N^{x}_{\delta_e}}{\Delta''}$
	x	$\frac{N^{x''}_{\theta_c}}{\Delta''} = \frac{Y_\theta N^{x}_{\delta_e}}{\Delta''}$
	x_e	$\frac{N^{x''_e}_{\theta_c}}{\Delta''} = \frac{-Y_\theta N^{x}_{\delta_e}}{\Delta''}$
	δ_e	$\frac{N^{\delta''_e}_{\theta_c}}{\Delta''} = \frac{Y_\theta \Delta}{\Delta''}$
x_c	θ	$\frac{N^{\theta''}_{x_c}}{\Delta''} = \frac{Y_x Y_\theta N^{\theta}_{\delta_e}}{\Delta''}$
	θ_e	$\frac{N^{\theta''_e}_{x_c}}{\Delta''} = \frac{-Y_x Y_\theta N^{\theta}_{\delta_e}}{\Delta''}$
	x	$\frac{N^{x''}_{x_c}}{\Delta''} = \frac{Y_x Y_\theta N^{x}_{\delta_e}}{\Delta''}$
	x_e	$\frac{N^{x''_e}_{x_c}}{\Delta''} = \frac{\Delta + Y_\theta N^{\theta}_{\delta_e}}{\Delta''} = \frac{\Delta'}{\Delta''}$
	δ_e	$\frac{N^{\delta''_e}_{x_c}}{\Delta''} = \frac{Y_x Y_\theta \Delta}{\Delta''}$
u_g	θ	$\frac{N^{\theta''}_{u_g}}{\Delta''} = \frac{N_{u_g} + Y_x Y_\theta N^{\theta\ x}_{u_g \delta_e}}{\Delta''}$
	θ_e	$\frac{N^{\theta''_e}_{u_g}}{\Delta''} = -\frac{1}{\Delta''}\left[N^{\theta''}_{u_g}\right]$
	x	$\frac{N^{x''}_{u_g}}{\Delta''} = \frac{N^{x}_{u_g} + Y_\theta N^{x\ \theta}_{u_g \delta_e}}{\Delta''}$
	x_e	$\frac{N^{x''_e}_{u_g}}{\Delta''} = \frac{-N^{x''}_{u_g}}{\Delta''}$
	δ_e	$\frac{N^{\delta''_e}_{u_g}}{\Delta''} = \frac{-Y_\theta}{\Delta''}\left[N^{\theta''}_{u_g} + Y_x N^{x''}_{u_g}\right]$

[1] Signs shown correspond to "Negative Feedback" of both loops.
[2] Inputs θ_c, x_c, u_g are considered one at a time.

TABLE C-II

AVAILABILITY AND KEY TO LOCATION OF APPROXIMATE FACTORS FOR HOVER AND TRANSITION

				TILT-WING		HELICOPTER				TILT-DUCT		TILT-ROTOR
						SINGLE-ROTOR		TANDEM-ROTOR				
				LOW SPEED[1,3]	HIGH SPEED[2,3]	Hover ($U_o \doteq 0$)	High Speed ($U_o > 50$ fps)	Hover ($U_o \doteq 0$)	High Speed ($U_o > 40$ fps) ($U_o < 120$ fps)	Hover ($U_o \doteq 0$)	High Speed ($U_o > 100$ fps)	All Speeds
LONGITUDINAL	Denominator			AA	AB	AC	AB	AC	AD	AA	AB	AB
	NUMERATORS	Elevator (Pitching Moment Control)	θ	BB	BB	BC	BC	BC	BC	BB	BB	BC
			w	None	CC	Zero	CD	Zero	CD	None	CC	CD
			u	DD	DD	DE	DE	DE	DE	DD	DD	DE
			$\dot{h}$	None	None	Zero	EF	Zero	EF	None	EE	None
		Throttle (Thrust Control)	θ	BB	BB	Zero	FF	Zero	FG	Zero	BB	BB
			w	None*	None	None*	GG	None*	GG	None*	None	None
			u	None	None	Zero	HH	Zero	HI	Zero	None	None
			$\dot{h}$	None*	None	None*	None	None*	II	None*	None	None

Notes: [1] Including range of speed for which wing incidence is within 45 deg of wing incidence at hover.

[2] Wing incidence greater than 45 deg from incidence at hover.

[3] The separation of high and low speed factors by wing incidence is empirical.

* Although there is not an approximate factor available, the numerator factors will cancel with denominator factors to give a known transfer function.

"None" indicates approximate factors not available.

"Zero" indicates response is approximately zero.

Letters indicate appropriate approximate factor from Table C-III

TABLE C-III

APPROXIMATE FACTORS REFERRED FROM TABLE C-II

	FIRST COEFF.	APPROXIMATE FACTORS	CONDITIONS OF VALIDITY
AA	1	$\frac{1}{T_{sp_1}} \doteq -Z_w$ $\frac{1}{T_{sp_2}} \doteq \sqrt[3]{gM_u} + \frac{-X_u - M_q}{3}$ $2\zeta_p\omega_p \doteq -\sqrt[3]{gM_u} + \frac{2}{3}(-X_u - M_q)$ $\omega_p^2 \doteq gM_uT_{sp_1}$	$\lvert U_oM_w \rvert \ll \lvert Z_wM_q \rvert$ $\lvert \frac{gM_u}{M_q^3} \rvert > 1$ $\lvert \frac{gM_u}{X_u^3} \rvert > 1$
AB	1	$\frac{1}{T_{sp_1}}\frac{1}{T_{sp_2}}$ or $\omega_{sp}^2 \doteq Z_wM_q - U_oM_{\dot{w}}$ $\frac{1}{T_{sp_1}} + \frac{1}{T_{sp_2}}$ or $2\zeta_{sp}\omega_{sp} \doteq -Z_w - M_q - U_oM_{\dot{w}}$ $\frac{1}{T_{p_1}}\frac{1}{T_{p_2}}$ or $\omega_p^2 \doteq \frac{g(M_wZ_u - M_uZ_w)}{Z_wM_q - U_oM_w}$ $\frac{1}{T_{p_1}} + \frac{1}{T_{p_2}}$ or $2\zeta_p\omega_p \doteq -X_u - \frac{M_u(X_wU_o - g)}{Z_wM_q - U_oM_w}$	ω_{sp}^2 or $\lvert \frac{1}{T_{sp_1}}\frac{1}{T_{sp_2}} \rvert > 4\omega_p^2$ or $4\lvert \frac{1}{T_{p_1}}\frac{1}{T_{p_2}} \rvert$ $\lvert X_u \rvert \ll \lvert M_q + Z_w + U_oM_{\dot{w}} \rvert$ $\lvert X_u(M_q + Z_w + U_oM_{\dot{w}}) \rvert \ll \lvert M_qZ_w - U_oM_w \rvert$ $\lvert Z_u(gM_{\dot{w}} + X_wM_q) \rvert \ll \lvert M_u(g - U_oX_w) - X_u(Z_wM_q - U_oM_w) \rvert$
AC	1	$\frac{1}{T_{sp_1}} \doteq -Z_w$ $\frac{1}{T_{sp_2}} \doteq \frac{-3M_q}{4} + \sqrt{\frac{M_q^2}{16} - \frac{gM_u}{2M_q}}$ $2\zeta_p\omega_p \doteq -X_u - \frac{M_q}{4} - \sqrt{\frac{M_q^2}{16} - \frac{gM_u}{2M_q}}$ $\omega_p^2 \doteq \frac{gM_u}{\frac{-3M_q}{4} + \sqrt{\frac{M_q^2}{16} - \frac{gM_u}{2M_q}}}$	$\lvert M_q \rvert \gg \lvert X_u \rvert$ $\lvert \frac{gM_u}{M_q^3} \rvert < 1$ If $\lvert X_u \rvert \gg \lvert M_q \rvert$ and $\lvert \frac{gM_u}{X_u^3} \rvert < 1$ interchange X_u and M_q in equations

TABLE C-III (Continued)

	FIRST COEFT.	APPROXIMATE FACTORS	CONDITIONS OF VALIDITY
DD	$Z_\delta X_w$	$\frac{1}{T_{u_1}} \doteq \frac{M_\delta(U_o X_w - g)}{Z_\delta X_w}$ $\frac{1}{T_{u_2}} \doteq \frac{g\left(Z_w - \frac{Z_\delta}{M_\delta} M_w\right)}{(U_o X_w - g)}$	$\lvert Z_\delta(gM_{\dot{w}} + M_q X_w)\rvert \ll \lvert M_\delta(U_o X_w - g)\rvert$ $\left\lvert\frac{X_w Z_\delta}{X_\delta}\right\rvert \gg \left\lvert\frac{1}{T_{u_2}}\right\rvert \gg \left\lvert\frac{1}{T_{u_1}}\right\rvert$ For $U_o \doteq 0$, $\frac{1}{T_{u_2}} \doteq -Z_w$, $\frac{1}{T_{u_1}} \to \infty$
EE	X_δ	$\frac{1}{T_u} \doteq -Z_w$ $\omega_u^2 \doteq \frac{g}{X_\delta}\left(M_\delta - Z_\delta \frac{M_w}{Z_w}\right)$ $2\zeta_u\omega_u \doteq -M_q$	$\lvert X_\delta(M_q + Z_w)\rvert \gg \lvert U_o X_\delta M_{\dot{w}} - Z_\delta X_w)\rvert$ $\lvert X_\delta Z_w M_q - gM_\delta\rvert \gg \lvert U_o(X_w M_\delta - X_\delta M_w) - Z_\delta(gM_{\dot{w}} + X_w M_q)\rvert$
FF	$-Z_\delta$	$\frac{1}{T_{h_1}} \doteq -X_u + (U_o X_w - g)\frac{M_u - \frac{M_\delta}{Z_\delta} Z_u}{U_o\left(M_w - \frac{M_\delta}{Z_\delta} Z_w\right)}$ $-\frac{1}{T_{h_2}} \doteq \frac{1}{T_{h_3}} \doteq \sqrt{U_o\left(M_w - \frac{M_\delta}{Z_\delta} Z_w\right)}$	$\left(\frac{1}{T_{h_2}}\right)^2 \gg \left\lvert\left(X_u - \frac{X_\delta Z_u}{Z_\delta}\right)(M_q + U_o M_{\dot{w}})\right\rvert$ $\left\lvert\frac{1}{T_{h_1}}\frac{1}{T_{h_2}}\frac{1}{T_{h_3}}\right\rvert \gg \left\lvert\frac{X_\delta}{Z_\delta} U_o(Z_w M_u - Z_u M_w)\right\rvert$ For $U_o \doteq 0$, $\dot{h} \doteq -w$
GF	$-Z_\delta$	$\frac{1}{T_h} \doteq -\frac{gZ_u}{U_o Z_w} + \frac{Z_\delta}{M_\delta}\frac{gM_u}{U_o Z_w} + \frac{X_\delta}{M_\delta}\left(M_u - \frac{M_w Z_u}{Z_w}\right)$ $\omega_h^2 \doteq \frac{M_\delta U_o Z_w}{Z_\delta}$ $2\zeta_h\omega_h \doteq -M_q - U_o M_{\dot{w}}$	$\left\lvert\frac{1}{T_h}\right\rvert \ll \omega_h$ $\lvert M_w Z_\delta\rvert \ll \lvert Z_w M_\delta\rvert$ $\left\lvert\frac{1}{T_h}\omega_h^2\right\rvert \gg U_o\left\lvert(M_u X_w - M_w X_u) + \frac{M_\delta}{Z_\delta}(X_u Z_w - X_w Z_u)\right\rvert$
HF	M_δ	$\frac{1}{T_{\theta_1}} \doteq -X_u - \frac{M_u(Z_w X_\delta - X_w Z_\delta)}{M_w Z_\delta - Z_w M_\delta}$ $\frac{1}{T_{\theta_2}} \doteq -Z_w + \frac{M_w Z_\delta + M_u X_\delta}{M_\delta} \doteq -Z_w + \frac{M_w}{M_\delta} Z_\delta$	$\left\lvert\frac{1}{T_{\theta_1}}\right\rvert \ll \lvert Z_w\rvert$ $\left\lvert\frac{1}{T_{\theta_1}}\right\rvert \ll \left\lvert\frac{1}{T_{\theta_2}}\right\rvert$ $M_\delta \neq 0$

TABLE C-III (Continued)

	FIRST COEFF.	APPROXIMATE FACTORS	CONDITIONS OF VALIDITY
AD	1	$\frac{1}{T_{sp_1}} \doteq -\left(\frac{M_q + Z_w + U_o M_{\dot{w}}}{2}\right) + \sqrt{\left(\frac{M_q + Z_w + U_o M_{\dot{w}}}{2}\right)^2 + U_o M_w - M_q Z_w}$ $\frac{-1}{T_{sp_2}} \doteq \omega_p \doteq -\left[g T_{sp_1}(M_w Z_w - M_u Z_w)\right]^{1/3}$ $2\zeta_p \omega_p \doteq -X_u - \frac{1}{T_{sp_2}}$	$\left\|\frac{1}{T_{sp_1}}\right\| > 5\left\|\frac{1}{T_{sp_2}}\right\|$ $\|gM_u\| \gg \|-X_u(M_q Z_w - U_o M_w) - M_u U_o X_w + M_q X_w Z_u + g Z_u M_{\dot{w}}\|$ If M_u is too small to satisfy this condition, use AB
AB	M_δ	$\frac{1}{T_{\theta_1}} + \frac{1}{T_{\theta_2}} \doteq \frac{X_\delta}{M_\delta}(Z_u M_{\dot{w}} + M_u) + \frac{Z_\delta}{M_\delta}(M_w - X_u M_{\dot{w}}) - (X_u + Z_w)$ $\frac{1}{T_{\theta_1}}\frac{1}{T_{\theta_2}} \doteq \frac{X_\delta}{M_\delta}(Z_u M_w - Z_w M_u) + \frac{Z_\delta}{M_\delta}(M_u X_w - M_w X_u) + (Z_w X_u - X_w Z_u)$	$\|Z_\delta M_{\dot{w}}\| \ll \|M_\delta\|$
BC	M_δ	$\frac{1}{T_{\theta_1}} \doteq \frac{X_\delta(M_u Z_w - Z_u M_w) + Z_\delta(X_u M_w - M_u X_w) + M_\delta(Z_u X_w - X_u Z_w)}{Z_w M_\delta}$ $\frac{1}{T_{\theta_2}} \doteq -Z_w$	$\left\|\frac{1}{T_{\theta_1}}\right\| \ll \left\|\frac{1}{T_{\theta_2}}\right\|$
CC	Z_δ	$\frac{1}{T_w} \doteq \frac{U_o M_\delta}{Z_\delta}$ $\omega_w^2 \doteq \frac{g}{U_o}\left(\frac{M_u Z_\delta}{M_\delta} - Z_u\right)$ $2\zeta_w \omega_w \doteq -X_u$	$\|Z_\delta(M_q + X_u) - X_\delta Z_u\| \ll \|U_o M_\delta\|$ $\|X_\delta(U_o M_u - Z_u M_q)\| \ll \|X_u(Z_\delta M_q - U_o M_\delta)\|$
CD	Z_δ	$\frac{1}{T_w} \doteq \frac{U_o M_\delta}{Z_\delta}$ $\omega_w^2 \doteq \frac{g}{U_o}\left(\frac{M_u Z_\delta}{M_\delta} - Z_u\right)$ $2\zeta_w \omega_w \doteq \frac{1}{U_o M_\delta}\left[U_o(X_\delta M_u - X_u M_\delta) + M_q(X_u Z_\delta - X_\delta Z_u) - Z_\delta \omega_w^2\right]$	$\left\|\frac{1}{T_w}\right\| \gg \|M_q\|$ $U_o \neq 0$ (at $U_o = 0$, $Z_\delta = 0$) $\left\|\frac{1}{T_w}\right\| \gg \omega_w$ $\|U_o M_\delta\| \gg \|X_u Z_\delta\|$

TABLE C-III (Concluded)

	FIRST COEFF.	APPROXIMATE FACTORS	CONDITIONS OF VALIDITY
FG	$Z_\delta M_{\dot{w}}$	$\frac{1}{T_{\theta_1}} \doteq \frac{M_w}{M_{\dot{w}}}$ $\frac{1}{T_{\theta_2}} \doteq -X_u + M_u \frac{X_w}{M_w}$	$M_{\dot{w}} \neq 0$ $\lvert M_\delta \rvert \ll \lvert Z_\delta M_{\dot{w}} \rvert$ $\lvert X_\delta \rvert \ll \lvert Z_\delta \rvert$ $U_o \neq 0$
GG	Z_δ	$\frac{1}{T_{w_1}} \doteq -M_q$. $\frac{1}{T_{w_2}} \frac{1}{T_{w_3}}$ or $\omega_w^2 \doteq \frac{gM_u}{-M_q}$ $\frac{1}{T_{w_2}} + \frac{1}{T_{w_3}}$ or $2\zeta_w\omega_w \doteq -X_u - \frac{gM_u}{M_q^2}$	$U_o \neq 0$ $\left[\text{for } U_o = 0, \frac{w(s)}{\delta(s)} = \frac{Z_\delta}{s - Z_w}\right]$ $\lvert X_u \rvert \ll \lvert 1/T_w \rvert$ $\lvert X_u \rvert \ll \lvert \omega_w \rvert$ $\lvert X_\delta \rvert \ll \lvert Z_\delta \rvert$ $\lvert U_o M_\delta \rvert \ll \lvert Z_\delta M_q \rvert$
HH	X_δ	$\frac{1}{T_u} \doteq -Z_w + X_w \frac{Z_\delta}{X_\delta}$ $\omega_u^2 \doteq \frac{-gM_\delta}{X_\delta}$ $2\zeta_u\omega_u \doteq -M_q$	$X_\delta \neq 0$ (Note: $X_\delta = 0$ at $U_o = 0$) $\lvert X_w Z_\delta \rvert < \lvert Z_w X_\delta \rvert$
II	$Z_\delta X_w$	$\frac{1}{T_{u_1}} \frac{1}{T_{u_2}} \doteq \frac{-gM_w}{X_w}$ $\frac{1}{T_{u_1}} + \frac{1}{T_{u_2}} \doteq -M_q - \frac{gM_{\dot{w}}}{X_w}$	$X_\delta = M_\delta = 0$ $U_o \neq 0$
KK	$-Z_\delta$	$\frac{1}{T_{h_1}} \doteq X_u + (g - U_o X_w) \frac{M_u}{U_o M_w}$ $\frac{1}{T_{h_2}} + \frac{1}{T_{h_3}}$ or $2\zeta_h\omega_h \doteq -M_q$ $\frac{1}{T_{h_2}} \frac{1}{T_{h_3}}$ or $\omega_h^2 \doteq -U_o M_w$	$U_o \neq 0$ $\left[\text{for } U_o = 0, \frac{\dot{h}(s)}{\delta(s)} = \frac{-Z_\delta}{s - Z_w}\right]$ $\lvert Z_u \rvert \ll \lvert U_o Z_w \rvert$ $\lvert M_u \rvert \ll \lvert U_o M_w \rvert$ $X_\delta = M_\delta = 0$

APPENDIX D

PILOT MODEL CONSIDERATIONS FOR VTOL AIRCRAFT CONTROLLED ELEMENTS

The selection and formulation of the pilot model features used throughout these studies are adapted from the concepts presented in Refs. 14 and 28. The basic models stem from the so-called "crossover" model concept which has had wide application to single-loop feedback control situations. However, more recent experiments with multiloop control structures (Refs. 13 and 29) have illustrated the concept's application to more complex multiloop situations.

The VTOL hovering task involves the pilot in a single controller multiloop task analogous to the situation in Ref. 13. The pilot describing function data derived in this reference has direct application to the VTOL control task. In particular, both control tasks require stabilizing or compensation for an inner attitude-loop to set up a good outer-loop control situation for tracking. Also, since these results indicated that the inner-loop (attitude) closures are quite similar to the single-loop attitude closures, we may apply the adjustment rules presented in Ref. 14. These rules for the human pilot model are reviewed in the following discussion. Some implications and apparent restriction imposed by neuromuscular systems dynamic are shown, in connection with VTOL controlled elements having unacceptable dynamics.

In controlling a system having several degrees of freedom, some of which are directly sensed within the general visual field and some of which are observed via visual displays, the human pilot evolves, during a learning and skill development phase, a particular multiloop control structure. The feedback structure he chooses will be similar to that selected by a skilled controls designer who has available certain system variables to use for control of the system's fixed characteristics; and who also has available a relative preference guide for the selection of those variables. The fixed characteristics include controlled element dynamics, forcing function and disturbance properties, and actuation characteristics. System variable characteristics comprise sensing channels for each of the feedback possibilities available to the pilot

and possible equalization in each loop which is tailored from a flexible but restricted class of equalization form.

The loops selected will have the following characteristics:

- To the extent possible, the feedback loops selected and equalizer adjustments made will be such as to allow wide latitude and variation in pilot characteristics.
- The loop and equalization structure selected will exhibit the highest pilot rating of all practical loop closure possibilities.
- Sampling is minimized; i.e., the information used will come from the following sources, in order of preference:

  General visual field

  Integrated displays

  Separately displayed quantities

A. GENERAL DESCRIBING FUNCTION FORM

For visual inputs each loop will have a pilot element which has the general describing function form*

$$Y_p \doteq \underbrace{KK_T\left(\frac{a_T}{\sigma_T}\right)}_{K_p} e^{-j\omega\tau}\left(\frac{T_L j\omega+1}{T_I j\omega+1}\right)\left\{\underbrace{\left(\frac{T_K j\omega+1}{T_K' j\omega+1}\right)}_{e^{-j\alpha/\omega}} \underbrace{\frac{1}{\left(T_{N_1} j\omega+1\right)\left[\left(\frac{j\omega}{\omega_N}\right)^2+\frac{2\zeta_N}{\omega_N}j\omega+1\right]}}_{\left(\frac{1}{T_N j\omega+1}\right)\ \text{or}\ e^{-j\omega T_N}}\right\} \qquad (D\text{-}1)$$

where

K = open-loop gain

K_p = human pilot gain

τ = reaction time delay (transport lag)

*Terms in the second line are simplified approximations for the more exact forms shown in Eq. D-1.

$\left(\frac{T_L j\omega + 1}{T_I j\omega + 1}\right)$ = equalization characteristic

$K_T\left(\frac{a_T}{\sigma_T}\right)$ = indifference threshold describing function $\left[1 - \sqrt{2/\pi}\ (a_T/\sigma_T) \text{ when } a_T/\sigma_T \ll 1\right]$

T_K, T_K' = lead and lag time constants in precision model of human pilot describing function

$\frac{1}{\left(T_{N_1} j\omega + 1\right)\left[\left(\frac{j\omega}{\omega_N}\right)^2 + \frac{2\zeta_N}{\omega_N} j\omega + 1\right]}$ = neuromuscular system characteristic

T_N = first-order lag time constant approximation of the neuromuscular system

α = low frequency phase approximation parameter

The describing function is written in terms of the frequency operator, $j\omega$, instead of the Laplace transform variable, s, to emphasize that this describing function is valid only in the frequency domain and exists only under essentially stationary conditions. For instance, it cannot be used to compute the system response to a discrete input, e.g., a step response. For conditionally stable loops, an appropriate simplified version of Eq. D-1 is

$$Y_p \doteq K_p\left(\frac{T_L j\omega + 1}{T_I j\omega + 1}\right) e^{-j\left[\omega(\tau + T_N) + \alpha/\omega\right]} \qquad (D-2)$$

For loops essentially unaffected by the low frequency phase lag term, $e^{-j\alpha/\omega}$, Eq. D-2 can be simplified to

$$Y_p \doteq K_p\left(\frac{T_L j\omega + 1}{T_I j\omega + 1}\right) e^{-j\omega(\tau + T_N)} \qquad (D-3)$$

This simplified version of the human pilot describing function is the one adopted in the analyses of this report; however, the Eq. D-2 is used for discussion of certain unacceptable control situations. Equation D-3 has a considerable range of validity for a variety of operators, forcing

functions, controlled elements, and manipulators. Reference 13 discusses some of the properties of Eq. D-3:

"Most of the parameters in the describing function are adjustable as needed to make the system output follow the forcing function— i.e., the parameters as adjusted reflect the pilot's efforts to make the over-all system (including himself) stable and the error small.

"The pure time delay represented by the $e^{-j\omega\tau}$ term is due to sensor excitation (the retina in the visual case), nerve conduction, computational lags, and other data processing activities in the central nervous system. It is closely related to, but not identical with, certain kinds of classical reaction times. τ is currently taken to be a constant because it appears to be essentially invariant with forcing function and controlled element dynamics for either single or dual random-appearing input tasks. However both inter- and intra-subject τ variations occur. Observed τ's run as low as about 0.1 sec and as high as 0.2 sec.

"The neuromuscular lag, T_N, is partially adjustable for the task. The nature of the adjustment is somewhat obscure due to the lack of high frequency data, although the general trend is a monotonic decrease in T_N with increasing forcing function bandwidth (see Table 13, Ref. 14). The observed variation of T_N with forcing function bandwidth ranges from less than 0.1 sec to somewhat greater than 0.6 sec....

"The equalizing characteristics, $(T_L j\omega + 1)/(T_I j\omega + 1)$, coupled with the gain K_p are the major elements in that adaptive capability of the human which allows him to control many differing dynamic devices. Their function is the modification of the stimulus signal into a suitable neuromuscular command which is properly scaled and phased for suitable over-all man-machine system operation. For given input and controlled element characteristics, the form of the equalizer is adapted to compensate for the controlled element dynamics and the pilot's reaction time delay.

"The describing function adjustment rules are not simply stated since they depend intimately on interactions of the elements in the man-machine system. In general, the adjustments can artificially be divided into two categories —adaptation and optimalization. Broadly speaking, adaptation is the selection by the operator of a specific form (lag-lead, lead-lag, pure lead, pure lag, or pure gain) for the equalization characteristics; and optimalization is the adjustment of the parameters of the selected form to satisfy some internally generated criteria. The result of the adaptation process is fairly well understood, since the form selected is one compatible with good low frequency, closed-loop response and the absolute stability of the system. The internal optimalizing criteria are not known, although they appear to be generally compatible with the minimization of the rms error (Refs. 14, 28)."

B. ADJUSTMENT RULES FOR OUTER (COMMAND) LOOP

The following adjustment rules are adopted from Refs. 14 and 28.

1. Equalization Form Selection and Adjustment

A particular equalization is selected from the general form $K_p(T_L j\omega + 1)/(T_I j\omega + 1)$ such that the following properties are attained:*

- **a.** The system can be stabilized by proper selection of gain, preferably over a very broad region.
- **b.** $|Y_p Y_c|$ has approximately a −20 db/decade slope in the crossover region — that frequency band centered on the crossover frequency, ω_c.
- **c.** $|Y_p Y_c| \gg 1$ at low frequencies to provide good low frequency closed-loop response to system forcing functions (commands).

2. Effective Time Delay

After the appropriate equalization form has been adopted, the net effect in the region of crossover of high-frequency (relative to crossover) leads and lags can be approximated by replacing these terms in Eqs. D-1, D-2, or D-3 with a pure time delay term, $e^{-j\omega\tau_e}$. The effective time delay, τ_e, is the sum of all the human pilot's pure time delays and high-frequency lags less the high-frequency leads, i.e.,

$$\tau_e \doteq \tau + T_N - T_{L_{hi}} \qquad \text{(D-4)}$$

The notation $T_{L_{hi}}$ implies that only those T_L's used to compensate partially for high-frequency phase lags (e.g., see Table D-I) are involved here; otherwise $T_{L_{hi}} = 0$. In general τ_e depends on both the controlled element dynamics and the forcing-function bandwidth, ω_i. These dependencies are approximately serial, viz,

$$\tau_e(Y_c, \omega_i) = \tau_o(Y_c) - \Delta\tau_e(\omega_i) \qquad \text{(D-5)}$$

where $\Delta\tau_e(0) = 0$.

---

*Y_c is the controlled element (vehicle) transfer function for the outer loop with the inner loops closed.

TABLE D-I. EQUALIZER ADJUSTMENTS VERSUS CONTROLLED ELEMENT TRANSFER FUNCTION IN CROSSOVER REGION

CONTROLLED ELEMENT APPROX. TRANSFER FUNCTION IN CROSSOVER REGION	PILOT EQUALIZER FORM	EQUALIZER ADJUSTMENTS		
		Low Freq. ($\omega \ll \omega_c$)	Mid-freq. (ω_c Region)	High Freq. ($\omega > \omega_c$)
K_c	Lag/lead	$\frac{1}{T_I}$	—	T_L to partially offset $\tau + T_N$
$\frac{K_c}{j\omega}$	High freq. lead	—	—	T_L to partially offset $\tau + T_N$ ($T_L\omega_c < 1$)
$\frac{K_c}{(j\omega)^2}$	Low freq. lead	$\frac{1}{T_L}$	—	T_L not avail. to offset $\tau + T_N$
$\frac{K_c}{j\omega(Tj\omega + 1)}$	Mid-freq. lead ($T > \tau$)	—	$T_L \doteq T$	—
	High freq. lead ($T < \tau$)	—	—	T_L to partially offset $\tau + T_N + T$
$\frac{K_c}{\left(\frac{j\omega}{\omega_n}\right)^2 + \frac{2\zeta}{\omega_n}j\omega + 1}$	Low freq. lead ($\omega_n \ll 1/\tau$)	$\frac{1}{T_L}$	—	—
	Lag/lead ($\omega_n \gg 1/\tau$)	$\frac{1}{T_I}$	—	T_L to partially offset $\tau + T_N$

a. **Estimation of τ_o for continuous control situations.** For one-handed spring-restrained stick control, τ_o can be estimated from the effective order of Y_c in the crossover region using the data of Table D-II.

b. **τ_o increment for other actuation modes.** If another mode of actuation is used, an incremental $\Delta\tau_o$ is added to that found above. This $\Delta\tau_o$ is the difference between the step reaction times for the actuation mode and for hand actuation.

c. **τ_o increment due to display sampling.** When the display situation is such that either eye movements are required or several displays must be sampled, an additional increment, τ_s, the effective time delay due to sampling behavior, is added to τ_o.

TABLE D-II. τ_o ESTIMATE VERSUS EFFECTIVE ORDER OF Y_c IN CROSSOVER REGION

Y_c	$\left[\frac{d\lvert Y_c\rvert_{db}}{d \ln \omega}\right]_{\omega \doteq \omega_c}$ (db/decade)	τ_o (sec)
K_c	0	0.33
$\frac{K_c}{j\omega}$	−20	0.36
$\frac{K_c}{(j\omega)^2}$	−40	0.52

d. Incremental τ_e due to forcing function. The portion of τ_e given by τ_o is all there is when the forcing-function bandwidth, ω_i, is zero or very small. As ω_i is increased, however, the neuromuscular lag, T_N, or the equalizer lead $T_{L_{hi}}$ is adjusted to reduce the net lag. A first-order approximation for this effect, good for all controlled elements in continuous control tasks, is

$$\Delta\tau_e \doteq 0.08\,\omega_i \qquad (D\text{-}6)$$

where $\Delta\tau_e$ is in seconds and ω_i in radians/second.*

3. Continuous Control Crossover Frequency

a. Basic crossover frequency, ω_{co}. The basic continuous control crossover frequency for tasks where ω_i is zero or very small, denoted as ω_{co}, is found by adding the phase angle, $-\omega\tau_o$, due

*"Forcing function bandwidth" is a vague term unless the forcing function spectrum is low pass and rectangular in shape. For other spectral shapes the effective bandwidth can be defined as follows:

$$\omega_{i_e} = \frac{\left[\int_o^\infty \Phi_{ii}\, d\omega\right]^2}{\int_o^\infty (\Phi_{ii})^2\, d\omega}$$

to the high-frequency phase lag to that of the controlled element and the previously estimated Y_p equalizer characteristics. Estimates for the basic crossover frequency, ω_{c_o}, and the continuous control gain are then made by determining the conditions for neutral stability.*

b. ω_c invariance properties.

(1) **$\omega_c - K_c$ independence.** After initial adjustment, changes in controlled element gain, K_c, are offset by changes in pilot gain, K_p; i.e., system crossover frequency, ω_c, is invariant with K_c.

(2) **$\omega_c - \omega_i$ independence.** System crossover frequency depends only slightly on forcing function bandwidth for $\omega_i < 0.8\,\omega_{c_o}$.

(3) **ω_c regression.** When ω_i nears or becomes greater than $0.8\,\omega_{c_o}$, the crossover frequency regresses to values much lower than ω_{c_o}.

(4) **Phase margin adjustment with ω_i.** Since ω_c is essentially independent of ω_i and $\Delta\tau_e$ is directly proportional to ω_i, the system phase margin, Φ_M, is directly proportional to ω_i. This strong dependence of phase margin on the forcing function bandwidth is associated with the linear variation of $\Delta\tau_e$ with ω_i, and is essentially an alternate statement of Eq. D-5.

C. ADJUSTMENT RULES FOR INNER LOOP

Ordinarily the inner loops provide subsidiary feedbacks which act as equalization for subsequent loops, or provide feedbacks or crossfeeds which suppress subsidiary degrees of freedom which have undesirable effects on subsequent loops. Because the role of the inner loops is so dependent on outer-loop requirements, the rigid rules given above are not generally applicable, e.g., even stability may not be

---

*In the present study of manual control of VTOL aircraft, the basic crossover frequencies, ω_{c_o}'s, were taken as 2 rad/sec for the inner loop (attitude) and 1 rad/sec for the outer loop (position). The pilot's effective time delay was held constant at a nominal 0.35 sec.

required. The types of inner loops closed and the equalization selected will generally be compatible with one or all of the following considerations:

- Outer loop adjustments per the outer-loop adjustment rules become more feasible, e.g., $|Y_pY_c|$ can be made approximately −20 db/decade with less outer-loop equalization.
- The sensitivity of the closed-loop characteristics to changes in either inner or outer loop pilot characteristics is reduced from that in an outer-loop-only situation. This includes the improvement of gain and phase margins.
- The loop structure and equalization selected are those for which total pilot rating is the best obtainable.
- Sampling is minimized.

D. CROSSOVER FREQUENCY RANGE

The crossover frequencies estimated using the above rules are maximum values for ground simulators without motion feedbacks. These will ordinarily be considerably reduced in flight, or when full attention is not demanded. The maximum extent of this reduction can be readily estimated for conditionally stable systems on the basis of stability alone.

1. Full-Attention Flight

To obtain an estimate of the full-attention flight value, consideration should be given to

- Gain reduction (longitudinally) between flight and simulator
- τ_e increase due to conflicting demands
- τ_e increase due to manipulator, especially when holding trim loads
- "Natural" statistical variation in ω_c

2. Intermittent Control

In many simulated and actual flying situations the pilot's regulation of control activity is only intermittent, so the average ω_c's will invariably be less than those estimated for full-attention flight. (This reduction is due primarily to an increase in indifference threshold, and hence will not constitute much of a reduction for large amplitude motions.) A matter of some importance is the spread between the highest and lowest

ω_c values possible (the lowest often merges with the unattended condition), which is a measure of the degree of configuration forgiveness. This or an associated measure also implies limitations on indifference threshold, sampling, minimum and maximum average movements per second, minimum and maximum information rates, etc.

E. PILOT RATING PENALTIES

In the iterative process of determining the likely inner loop structure and both inner and outer loop equalization estimates, the key design criteria are not confined to the objective considerations outlined above; they also include consideration of subjective pilot ratings. Although all the connections between pilot ratings and pilot/vehicle dynamics and performance are not yet firmly established, enough are available to provide a relative preference guide.

1. Single-Axis Penalties

The pilot rating penalties associated with gain variations are perhaps the best defined. For fixed controlled element dynamics pilot gain will be inversely proportional to controlled element gain (crossover frequency is constant). The optimum (best pilot rating) gain will depend on the manipulator characteristics and possibly on other factors such as controlled element dynamic characteristics. The degradations in pilot ratings for nonoptimum gains are shown in Fig. D-1.

In addition to gain, pilot ratings depend on the system closed-loop performance and the sensitivity of the performance to variations in elements of the pilot's describing function. For good ratings the pilot must be able to obtain satisfactory performance with a relatively broad set of characteristics. Ratings will be degraded if good performance can be obtained only with a tightly constrained set of pilot characteristics.

There is also some evidence that pilot rating may depend directly on the amount of lead he is required to generate (see Ref. 4). For example, rating variations with T_R for controlled elements of the form $Y_c = K/j\omega(T_R j\omega + 1)$ are shown in Fig. D-2. As shown in Table D-I, for this type of controlled element the pilot adopts a lead which nearly

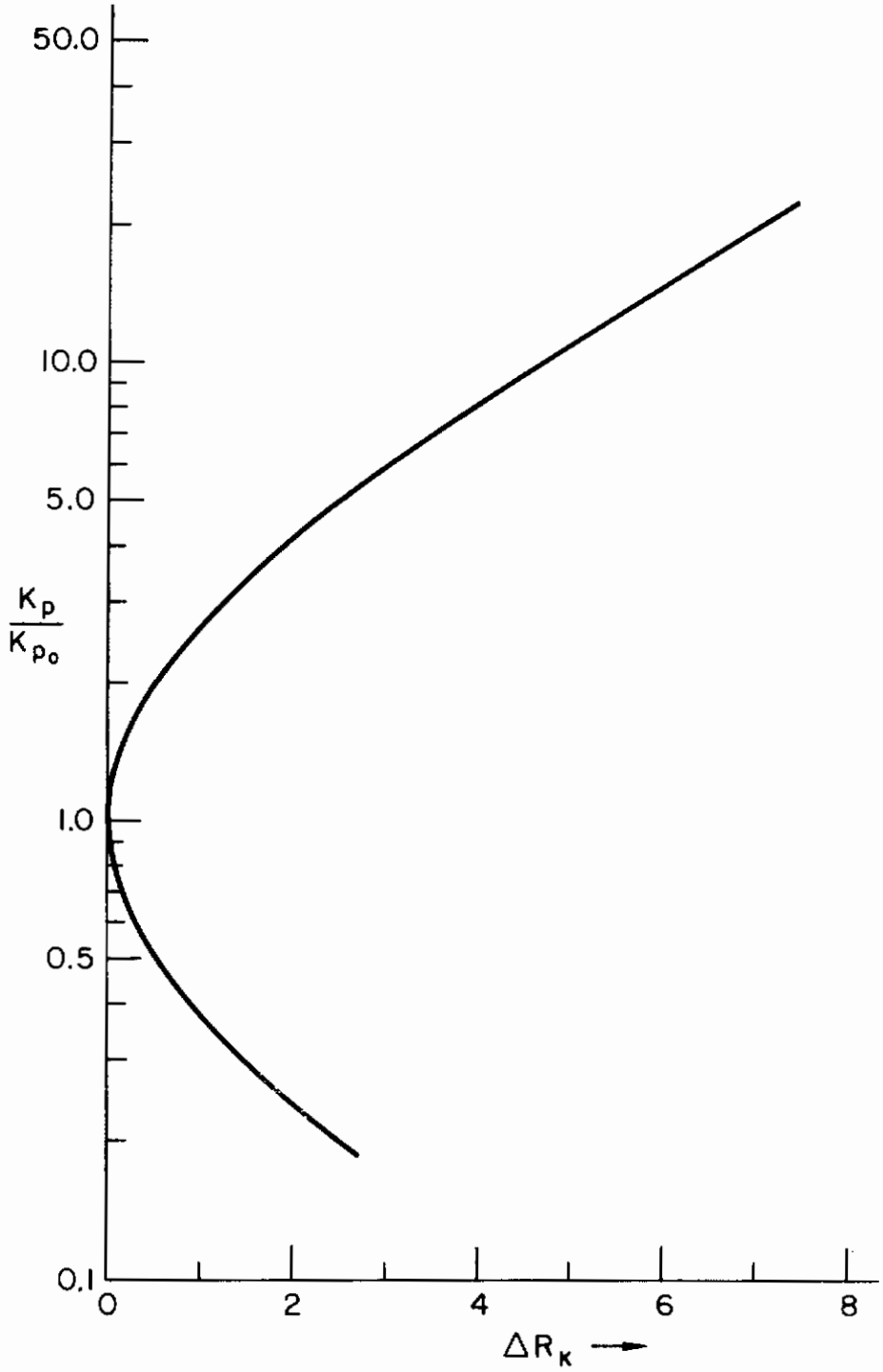

Figure D-1. Degradation of Pilot Opinion Rating for Nonoptimum Gains

cancels the lag, i.e., $T_L \doteq T_R$. Whether the rating increments shown in Fig. D-2 are due to the changes in average performance, sensitivity to pilot characteristics, or pilot lead directly cannot be determined at this time. Consequently Fig. D-2 should not be interpreted as the rating penalty for lead operation by substituting T_L for T_R.

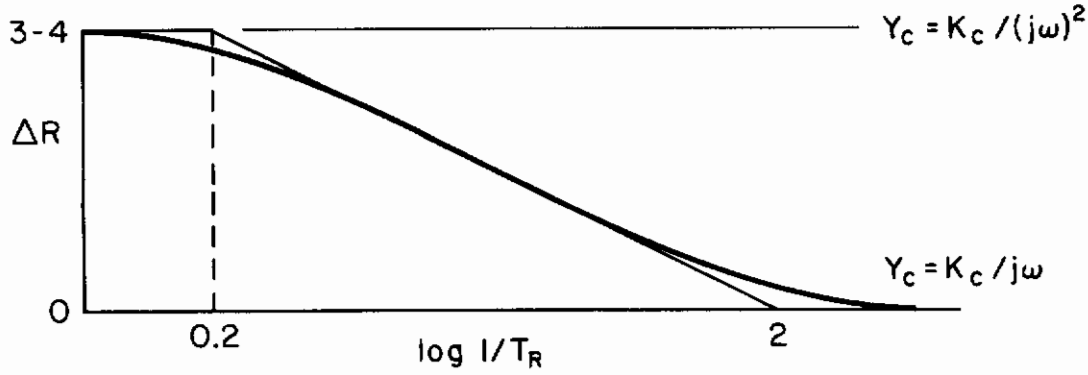

Figure D-2. Degradation of Pilot Opinion Rating Versus Pilot-Generated Lead

2. Conversion of Single-Axis Increments to Multiaxis Ratings

The above rating penalties are based on single-axis data. A simple approximation (Ref. 5) to the total system rating can be made using a "base" multiaxis rating and adding incremental single-axis ratings. The base rating is that given by the pilot for the multiaxis control task made up of the easiest-to-control (or best rated) single axes. Equation D-7 describes the relation:

$$PR_m = ER_{m_{best}} + \sum_{i=1}^{N} \Delta R_i \qquad \text{(D-7)}$$

where PR_m = predicted pilot rating for the multiaxis situation

$ER_{m_{best}}$ = actual pilot rating for the multiaxis situation consisting of the best rated single axes (experimentally determined)

ΔR_i = increment between the actual pilot rating for control of the ith single axis and the best pilot rating for the ith axis

Reference 5 states that "...this technique predicts multiaxis ratings quite well, with only a gradual tendency to predict higher numerical ratings as the vehicle dynamics become more difficult to control."

F. ADDITIONAL CONSIDERATIONS OF MANIPULATOR AND NEUROMUSCULAR SYSTEM EFFECTS

Recent experiments in Ref. 30 have provided a basis for qualitatively considering the effects of pressure, free-moving, and spring-restrained type controls for the compensatory control task. Conventionally, VTOL aircraft have very light spring-restrained type controls which approach free-moving systems. For free-moving type control, the inertial properties of the manipulator can become a factor in the pilot's closed-loop compensatory control. This aspect can be indicated by using the crossover model form given below:

$$Y_p Y_c = \frac{\omega_c e^{-j(\tau_e \omega + \alpha/\omega)}}{j\omega}$$

where

ω_c = crossover frequency

$\tau_e = \tau + T_N - T_{L_{hi}}$

α = approximate to low frequency terms

Thus, the T_N component of τ_e contains the first-order effects of the neuromuscular system within the measured bandwidth, i.e.,

$$T_N = \underbrace{T_{N_1}}_{\text{actuation lag}} + \underbrace{\frac{2\zeta_N}{\omega_N}}_{\substack{\text{effective time constant of the second order terms of motor load dynamics}}}$$

Therefore, τ_e will tend to be increased by increases in inertia and decreases in spring rate (i.e., load). The overall effects of these changes in τ_e must be considered in light of each controlled element and pilot closure features.

Unfortunately, the present reference data did not include unstable controlled elements in the survey of manipulatory effects with various controlled elements. The K/s^2 controlled element result can be used only to estimate the appropriate first-order trends for the neuromuscular system. In Figs. D-3 and D-4 the effects of spring restraint and inertia load on the neuromuscular components are indicated by the effective change in the Bode diagrams of Y_pY_c. For our purposes, we may summarize the effects of these manipulator features on the neuromuscular system dynamics as follows:

1. $Y_c = K_c/s^2$ Spring (Fig. D-3)

   Crossover frequency is constant except for a slight decrease for the stiffest spring while τ_e decreases slightly as spring rate increases. The τ_e decreases indicate that the spring increases help push the second-order neuromuscular lag to higher frequencies. In addition, the best of the pressure controller configurations had lower gain at low frequency. This is offset by a lower τ_e in the crossover region.

   The basic trend in the data is that k ↑ causes τ_e ↓ which correlates with the findings of the various manipulators experiments.

2. $Y_c = K_c/s^2$ Inertia (Fig. D-4)

   Inertia increases cause steady decline in gain, increase in σ_e/σ_i and an increase in τ_e. There is a resonance at high frequency for the larger inertias. Clearly the inertia increases are reducing ω_N of the second-order neuromuscular lag which affects τ_e and for the larger inertias the break point is within the measurement bandwidth. Here, without question, the position loop of the neuromuscular system plays a central role in retaining the characteristic Y_pY_c features since the lead equalization capabilities are used up at low frequencies to compensate for the controlled element.

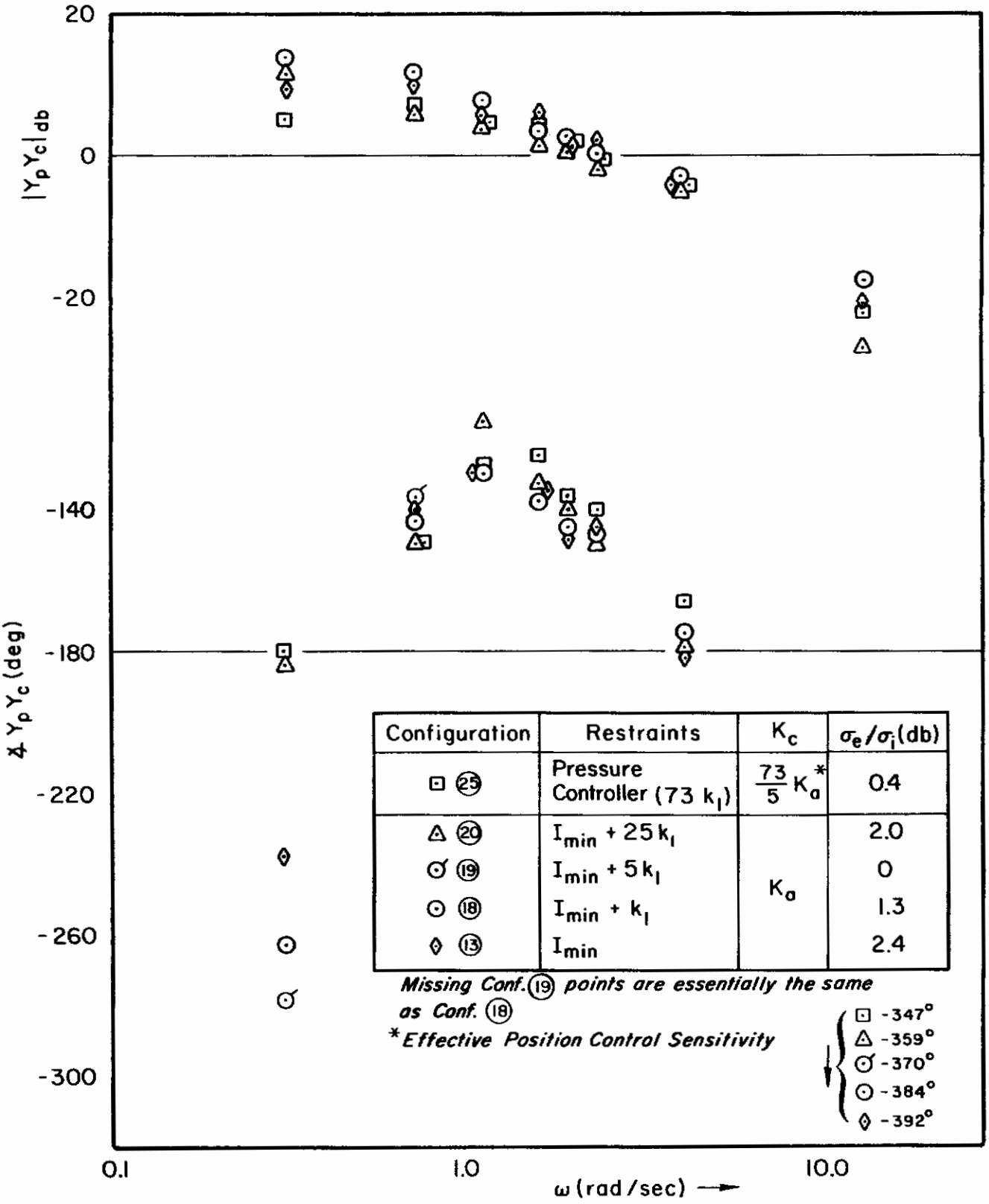

Figure D-3. Averaged Open-Loop Describing Functions for $Y_c = K_c/s^2$ with Spring Rate as Parameter

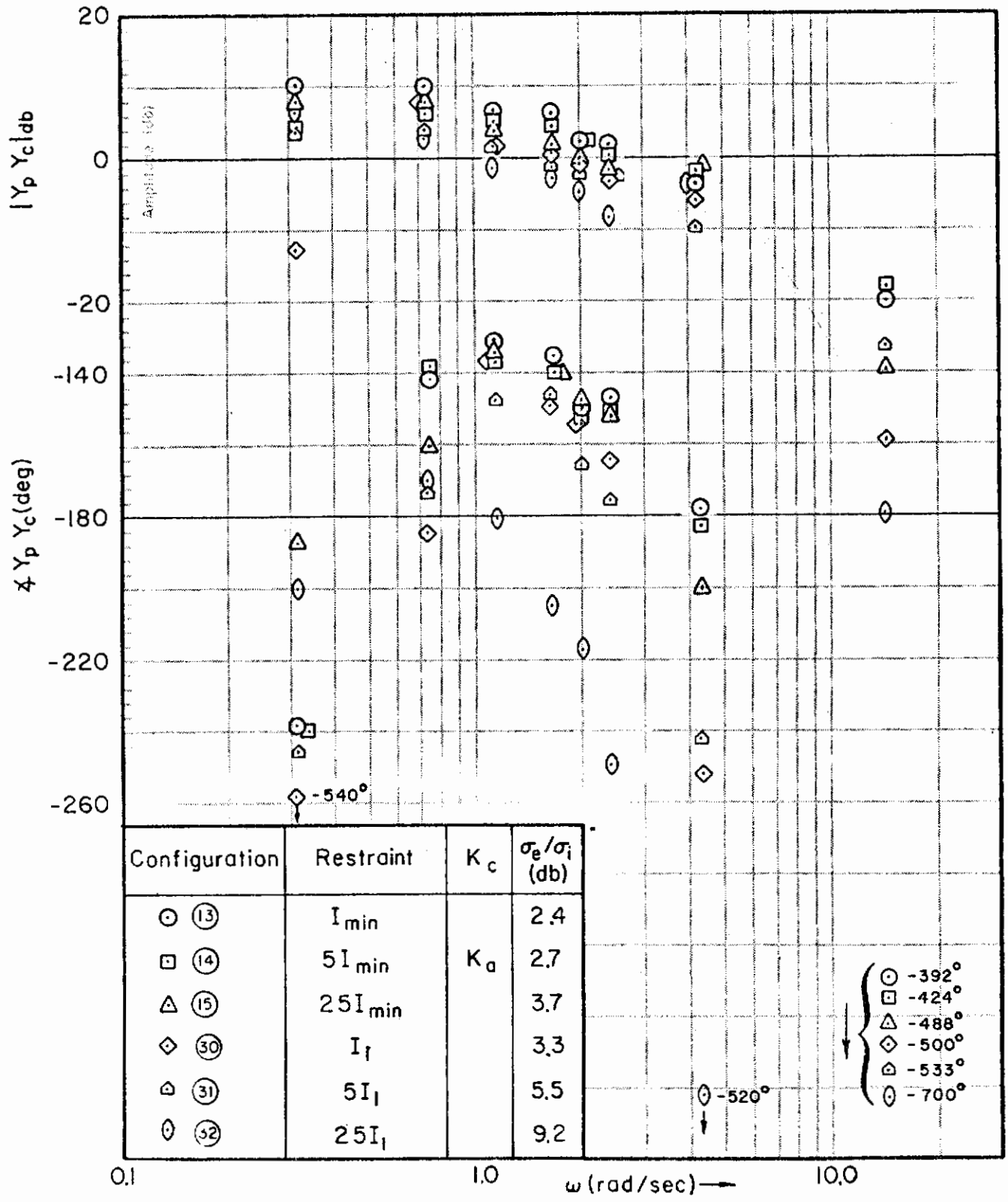

Configuration	Restraint	K_c	σ_e/σ_i (db)
⊙ (13)	I_{min}		2.4
⊡ (14)	$5I_{min}$	K_a	2.7
△ (15)	$25I_{min}$		3.7
◇ (30)	I_I		3.3
⌂ (31)	$5I_I$		5.5
⊙ (32)	$25I_I$		9.2

Figure D-4. Averaged Open-Loop Describing Functions for $Y_c = K_c/s^2$ with Inertia as Parameter

The basic effects to note are (neglecting the highly variable phase data at the lowest frequency)

$$I \uparrow \text{ causes } \omega_c \downarrow,\ \tau_e \uparrow,\ \alpha \uparrow$$

Both the low frequency term, α, and the equivalent time delay, τ_e, quantities contained in the phase descriptor term, $e^{-j(\omega\tau_e + \alpha/\omega)}$ of the neuromuscular system are involved in pilot control of conditionally stable systems. In general, the conventional VTOL dynamic features described in Section II are an example of these systems. Figure D-5 illustrates the nature of pilot describing function data and application as descriptors of a conditional control situation. The typical data shown are from a so-called subcritical task involving the control of a first-order divergence $\left[Y_c = K_c/(s-\lambda)\right]$. The α and τ_e aspects do not affect the amplitude ratio at all, although they are clearly shown in the phase. The $\omega\tau_e$ phase due to time delay dominates the high frequencies, whereas the α/ω phase lag is the major low frequency effect. Their joint action tends to make the phase look like an umbrella, with α controlling the left side and τ_e the right side, i.e., changes in τ_e shift the right side of the umbrella, while changes in α shift the left. Simultaneous increases in both α and $1/\tau_e$ shift the umbrella to the right, whereas decreases shift it to the left. (See Fig. D-6.)

Some idea of the variation of α and τ_e and their connections is provided in Ref. 31. Figure D-7, which is taken from Ref. 31, indicates that α and $1/\tau_e$ vary together for the experiments considered there. In terms of the describing function phase curve shown in Fig. D-5, both ends of the umbrella are shifted together in an adaptive response to forcing function bandwidth, ω_i, changes $\left[\text{for } Y_c = K_c/(s)^2\right]$ or controlled element divergent time constant, T, changes $\left[\text{for } Y_c = K_c/s(s-1/T)\right]$.

One implication from the preceding discussion is that the level of tension has an important part in the pilot's ability to reduce the effective neuromuscular time constant, τ_e. In fact, Ref. 14 noted that for unstable elements the neuromuscular system can be forced to its

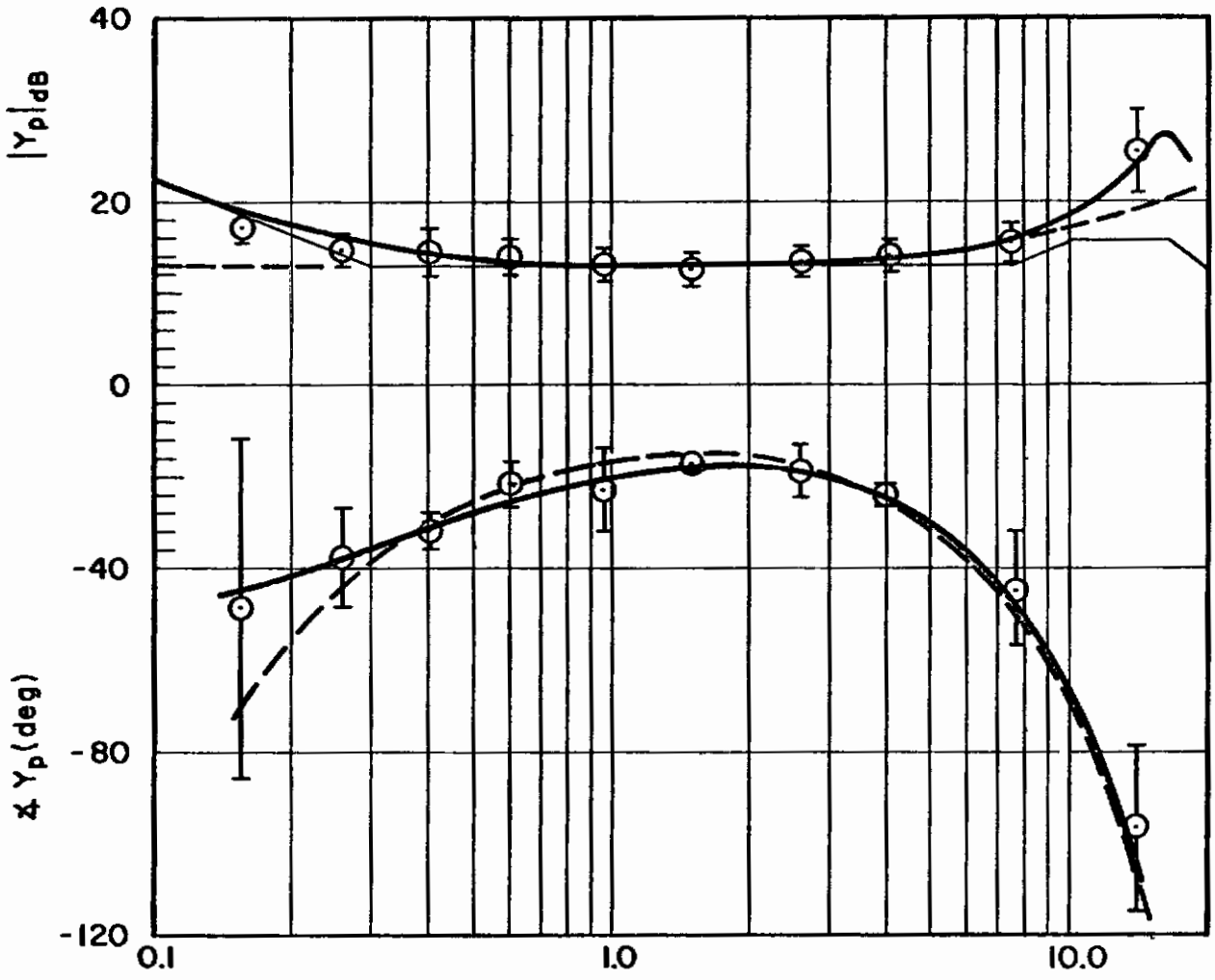

Precision Model (———)

$$Y_p = (25.1)\left(\frac{j\omega}{7.8}+1\right)e^{-0.09\,j\omega}\left\{\left(\frac{\frac{j\omega}{0.3}+1}{\frac{j\omega}{0.05}+1}\right)\frac{1}{\left(\frac{j\omega}{10}+1\right)\left[\left(\frac{j\omega}{16.5}\right)^2+\frac{2(0.12)}{16.5}\,j\omega+1\right]}\right\}$$

Approximate Model (— — —)

$$Y_p = (4.2)\left(\frac{j\omega}{7.8}+1\right)e^{-1[0.21\,\omega+(0.19/\omega)]}$$

Figure D-5. Typical Pilot Describing Function Data and Models ($Y_c = K_c/(s-2)$; $\omega_i = 4.0$ rad/sec)

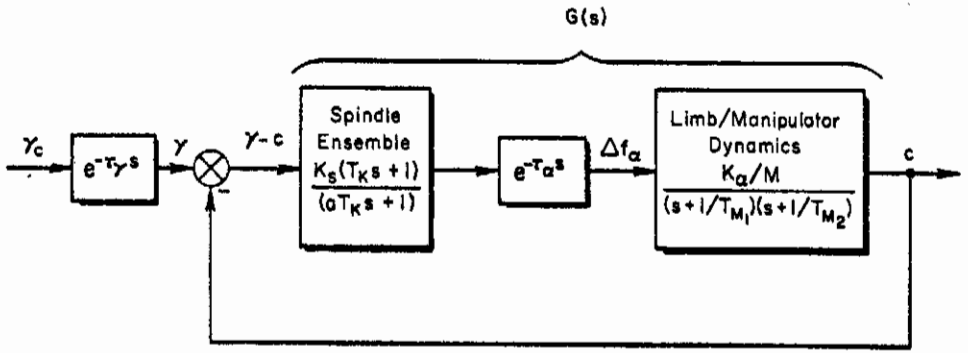

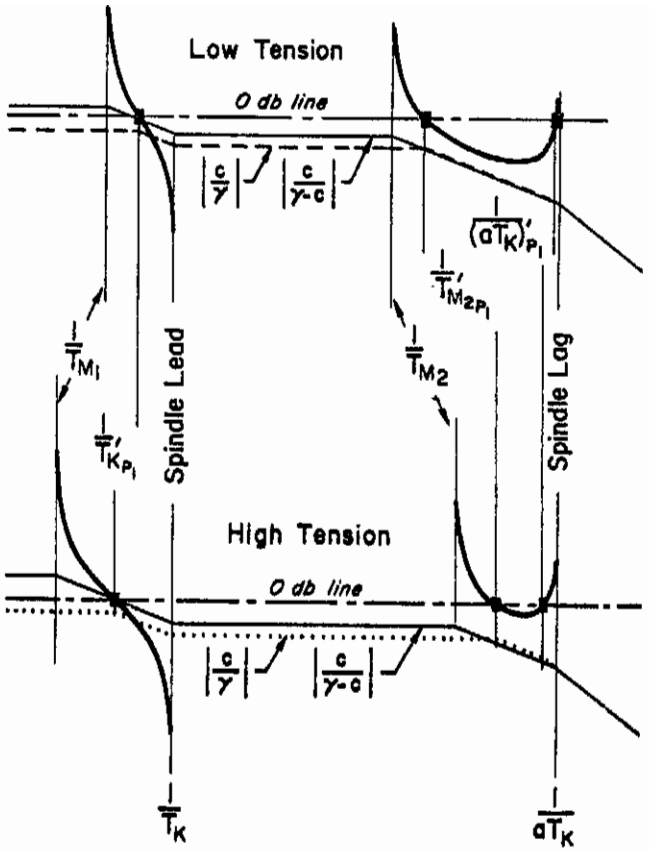

a) Amplitude Ratios

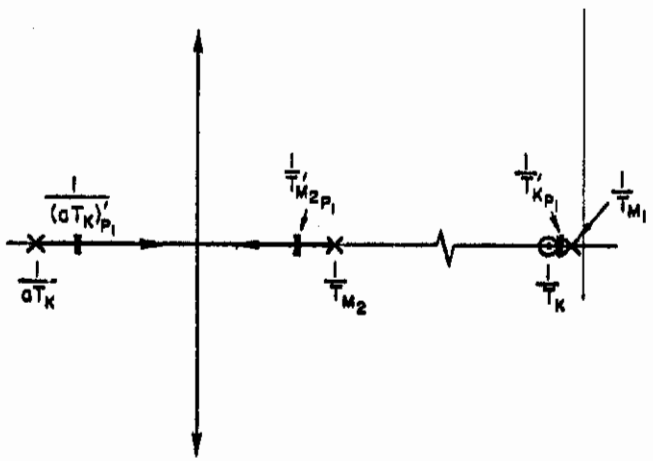

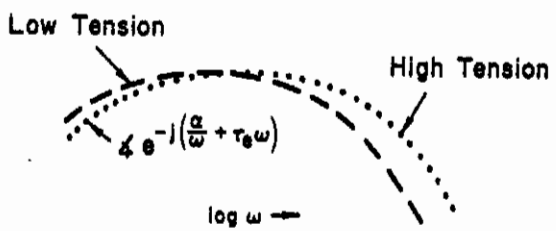

b) Approximate Phases

Figure D-6. Root Loci of Neuromuscular Subsystem Dynamics with Two Levels of Tension

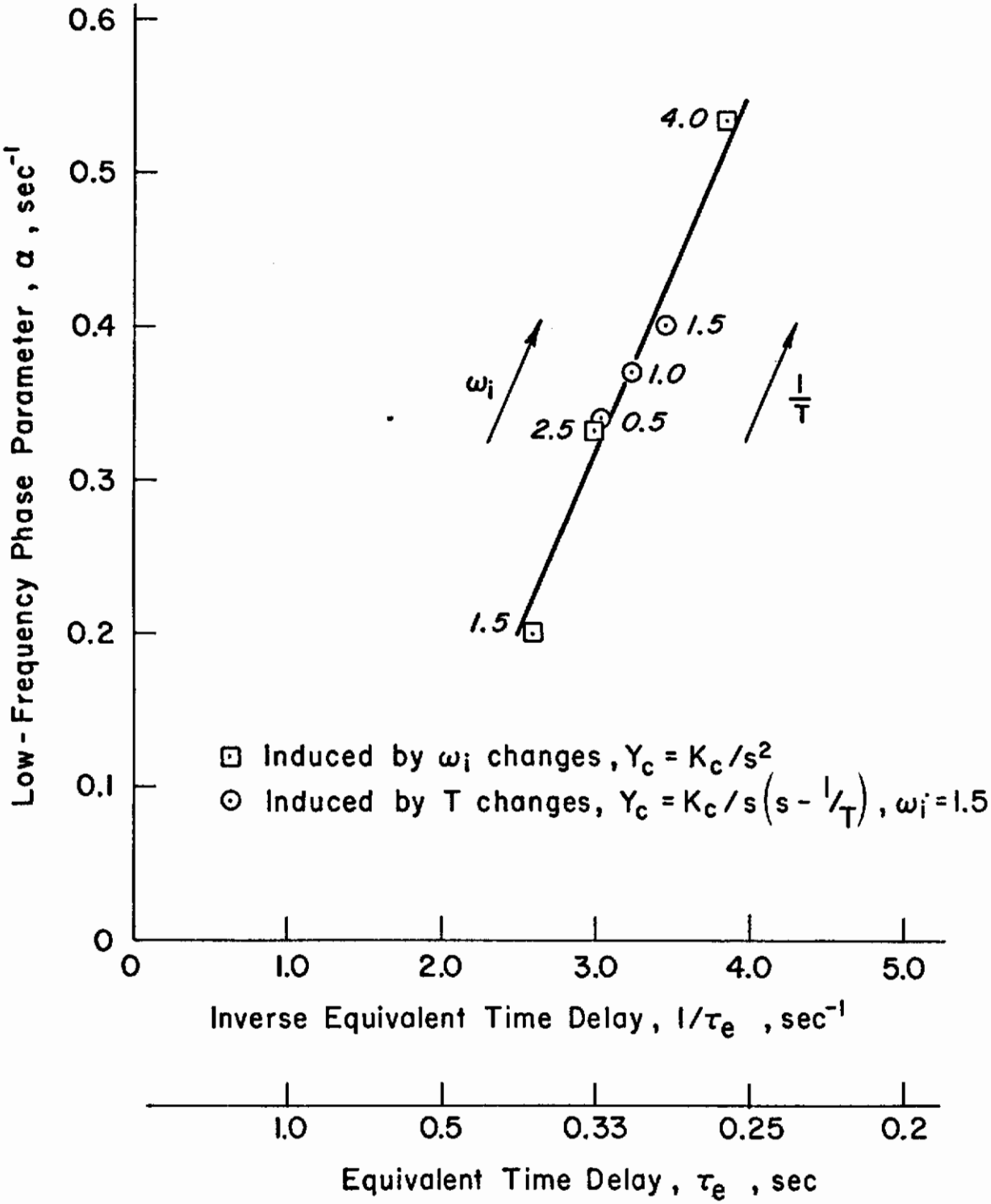

Figure D-7. Connection Between Equivalent Time Delay and Low-Frequency Phase Lag

tightest mode of operation to achieve minimum neuromuscular contributions to τ_e.

G. CONSIDERATION OF SPECIFIC VTOL CONTROL ELEMENTS

In the preceding discussions, we have identified the features of the pilot model and now have some appreciation of the factors influencing the individual components of the model. Basically, the model features illustrate that the pilot's control capabilities are limited by the properties of the neuromuscular system. As the control element dynamics become more complex, the pilot is taxed heavily by adapting the proper compensation needed for a stable closed-loop situation. The conventional VTOL dynamics described as unacceptable in Section II will be examined here to illustrate the limiting aspect of the neuromuscular system.

Figure D-8 indicates by the Bode and root locus plots the effect of time delay term, τ_e, on the potential region for closing the attitude loop. The controlled element dynamics used are Configuration 2 taken from Section II of the text. It is obvious that reducing τ_e will greatly expand the frequency region for stable control and reduce the supplemental lead compensation required for establishing a stable closure with a desired crossover frequency and phase margin. Figure D-9 verifies that the potential closure region is quite large for the low τ_e and nominal lead condition (i.e., $\tau_e = 0.15$ sec and $1/T_L = 1.28$ rad/sec).* We note, however, that the stable gain region is reduced by applying excessive lead compensation (i.e., $1/T_L < \omega_p$). We can conclude tentatively that a reduction in the time delay, τ_e, is a more effective means of improving the pilot's control situation than increasing his lead.

The apparent advantage of the τ_e is subject to some qualification because of the connection between equivalent time delay and low-frequency phase lag, α. An exemplary tradeoff study of consequences of the α term

*The value of time delay (i.e., $\tau_e = 0.15$) should not be considered typical since available measured data suggest that a minimal τ_e of 0.25 is more appropriate.

may be considered by assuming a linear relation between α and τ_e, which is implied from the data in Fig. D-9. An α value of 0.6 second is assumed for the $\tau_e \doteq 0.15$ condition. If the first-order approximation to the phase characteristics of the α term is used, the stable gain region is somewhat reduced. The net result indicated here is that the α effects do not greatly change the overall closed-loop situations. However, the pilot will have a difficult time improving this low frequency region because of the α term.

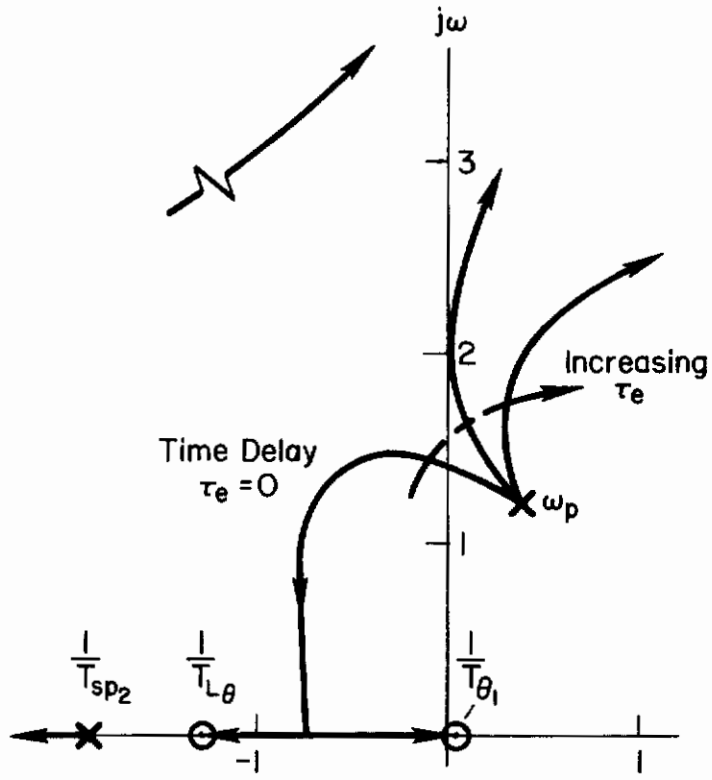

Figure D-8. Effect of Pilot Time Delay τ_e on Attitude Loop

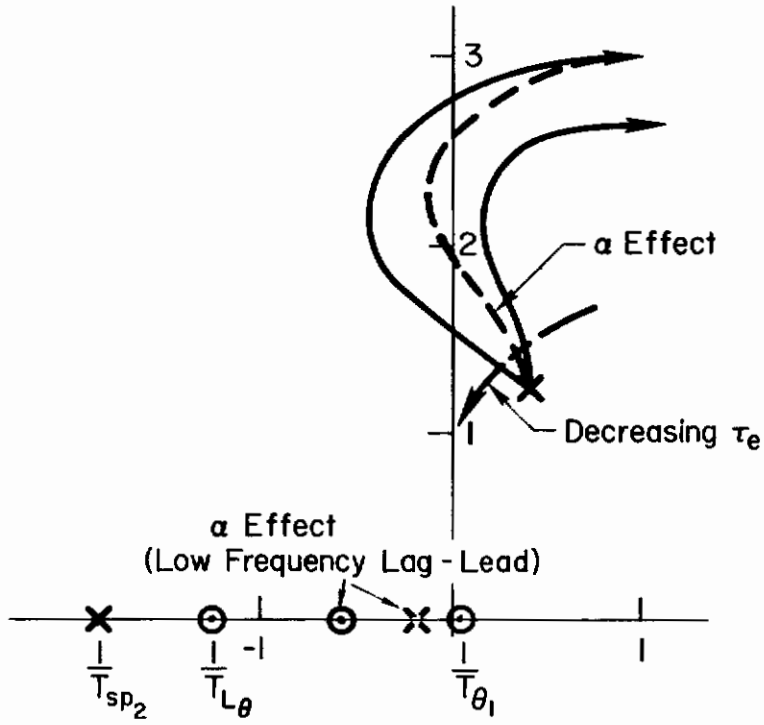

Figure D-9. Attitude Loop ($\theta \rightarrow \delta_e$) Closure Possibilities for Low τ_e

APPENDIX E

APPLICATION OF MULTILOOP ANALYSIS TECHNIQUE TO TRANSITION CONTROL

The purpose of this appendix is to illustrate the multiloop analysis technique employed in the study of longitudinal flight path control tasks in transition. The problem of controlling altitude and attitude control with elevator, airspeed control with collective will be considered. The appropriate dimensional stability derivatives and aircraft transfer functions are listed in Table E-I.

Altitude control outer loop transfer function with attitude and airspeed loops closed is:

$$\left.\frac{h}{h_\epsilon}\right]_{\substack{\theta\to\delta_e \\ u\to\delta_c \\ h\to\delta_e}} = \frac{Y_{p_h} Y_{p_\theta}\left[N^h_{\delta_e} + Y_{p_u} N^{h\ u}_{\delta_e \delta_c}\right]}{\underbrace{\Delta + Y_{p_\theta} N^{\theta}_{\delta_e}}_{\Delta'} + Y_{p_u}\left(N^u_{\delta_c} + Y_{p_\theta} N^{\theta\ u}_{\delta_e \delta_c}\right)}$$

Δ''

Loop closures will be taken in sequence and their effects on the altitude control transfer function numerator and denominator terms will be examined in detail.

$\theta \to \delta_e$ LOOP CLOSURE

Pitch attitude loop closure characteristics are shown in Fig. E-1. Closed-loop roots are given by the equation*

$$\Delta' = \Delta + Y_{p_\theta} N^{\theta}_{\delta_e}$$

$$\Delta' = [0.745\ ,\ 0.943][0.105\ ,\ 0.459] + \frac{K_{p_\theta}(0.943)(-10)^2(0.234)(0.635)}{(10)^2}$$

when $K_{p_\theta} = 7.9$

$$\Delta' = \frac{[0.84\ ,\ 0.413][0.294\ ,\ 3.072](1.52)(19.56)}{(10)^2}$$

*The notation $(1/T_1) = (s + 1/T_1)$; $[\zeta_i\ ,\ \omega_i] = [s^2 + 2\zeta_i\omega_i s + (\omega_i)^2]$.

Closure of the $\theta \rightarrow \delta_e$ loop has no effect on the outer loop altitude numerator since in this case both attitude and altitude are controlled by elevator.

TABLE E-I

CHARACTERISTICS OF XC-142 AT 80 KTS

Dimensional Stability Derivatives

$X_w = 0.065$		$Z_w = -0.68$		$M_w = -0.004$	
$X_u^* = -0.2$		$Z_u^* = -0.198$		$M_u^* = 0.0074$	
$X_{\delta_c} = 14.51$		$Z_{\delta_e} = 0.953$		$M_{\dot{w}} = -0.00127$	
$X_{\delta_e} = 0$		$Z_{\delta_c} = -25.5$		$M_q = -0.62$	
		$Z_{\dot{w}} = 0$		$M_{\dot{u}} = 0$	
				$M_{\delta_c} = -0.429$	
				$M_{\delta_e} = 0.265$	

$U_o = 135$ ft/sec $h = 0$ ft $m = 1{,}160$ slugs

$I_x = 5{,}950$ slug ft^2

Aircraft Transfer Functions

$$\Delta = [s^2 + 2(0.745)(0.943)s + 0.943^2][s^2 + 2(0.105)(0.459)s + 0.459^2]$$

$$N_{\delta_e}^{\theta} = 0.264(s + 0.234)(s + 0.635)$$

$$N_{\delta_e}^{h} = \frac{-0.953(s - 4.59)(s + 0.142)(s + 5.438)}{s}$$

$$N_{\delta_c}^{u} = 14.51(s + 0.345)[s^2 + 2(0.381)(1.105)s + (1.105)^2]$$

$$N_{\delta_e\delta_c}^{\theta\ u} = 3.83(s + 0.561)$$

$$N_{\delta_e\delta_c}^{h\ u} = \frac{-13.83(s - 5.6)(s + 6.38)}{s}$$

$$\Delta' = \Delta + Y_{p_\theta} N^{\theta}_{\delta_e}$$

$$Y_{p_\theta} = \frac{K_{p_\theta}(s+.943)(s-10)^2}{(s+10)^2}$$

$$\Delta' = \frac{(1.52)(19.56)[.84, .413][.294, 3.072]}{(10)^2}$$

Note:

( ) = $(1/T_i)$

[ ] = $[\zeta_i, \omega_i]$

■ $K_{p_\theta} = 7.9$

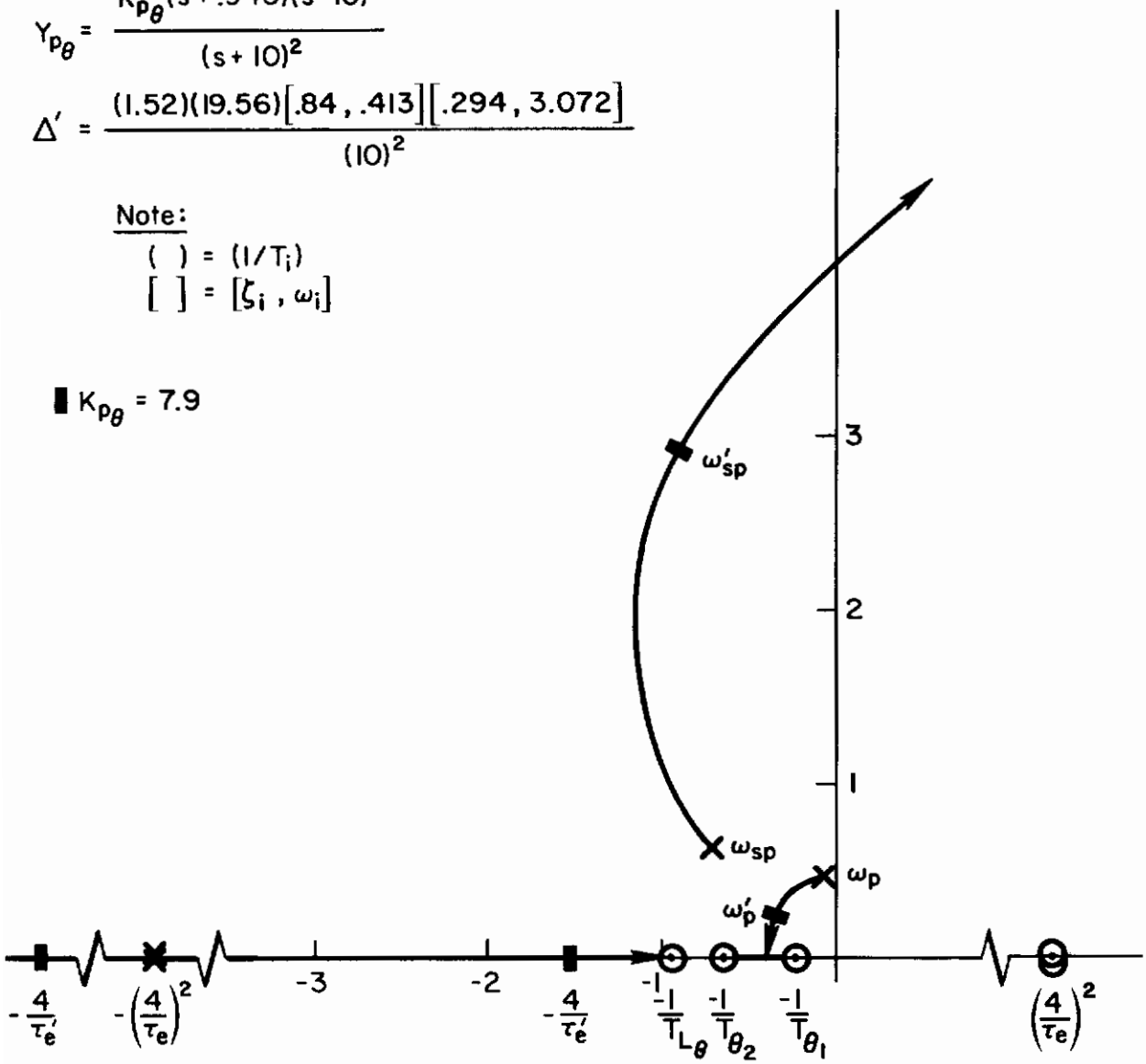

Figure E-1. $\theta \rightarrow \delta_e$ Loop Closure

$u \rightarrow \delta_c$ LOOP CLOSURE

The appropriate transfer function for the $u \rightarrow \delta_c$ closure with the $\theta \rightarrow \delta_e$ loop closed is:

$$\left(\frac{u}{u_\epsilon}\right)_{\theta \rightarrow \delta_e} = \frac{Y_{p_u}\left(N^u_{\delta_c} + Y_{p_\theta} N^{u\ \theta}_{\delta_c \delta_e}\right)}{\Delta + Y_{p_\theta} N^{\theta}_{\delta_e}}$$

$$N^u_{\delta_c} + Y_{p_\theta} N^{u\ \theta}_{\delta\ \delta_e} = 14.51(0.345)[0.381\ ,\ 1.105] + \frac{7.9(0.943)(-10)^2}{(10)^2} \times 3.83(0.561)$$

Factorization of this polynomial in root locus form is shown in Fig. E-2.

$$N^u_{\delta_c} + Y_{p_\theta} N^{u\ \theta}_{\delta_c \delta_e} = \frac{14.51(0.461)(1.721)(19.54)[0.246\ ,\ 3.134]}{(10)^2}$$

$u \rightarrow \delta_c$ closure characteristics with the $\theta \rightarrow \delta_e$ loop closed are shown in Fig. E-3.

$$\left(\frac{u}{u_\epsilon}\right)_{\theta \rightarrow \delta_e} = \frac{14.51 K_{p_u}(-10)^2(0.461)(1.721)(19.54)[0.246\ ,\ 3.134]}{(10)^2(1.52)(19.56)[0.84\ ,\ 0.413][0.294\ ,\ 3.072]}$$

Closed-loop roots for $(u/u_c)_{\theta \rightarrow \delta_e}$ are given by

$$\Delta'' = \underbrace{\Delta + Y_{p_\theta} N^{\theta}_{\delta_e}}_{\Delta'} + Y_{p_u}\left(N^u_{\delta_c} + Y_{p_\theta} N^{\theta\ u}_{\delta_e \delta_c}\right)$$

For $K_{p_u} = 0.178$ (30° φ_M, 5 dB K_M)

$$\Delta'' = \frac{(0.478)(1.8)(19.47)(21.02)[0.167\ ,\ 2.816][0.308\ ,\ 3.974]}{(10)^4}$$

These are the denominator roots of the outer-loop altitude control transfer function.

$$Y_{p_\theta} = \frac{K_{p_\theta}(s + .943)(s - 10)^2}{(s + 10)^2}$$

$$N^{u}_{\delta_c} + Y_{p_\theta} N^{\theta\ u}_{\delta_e\ \delta_c} = \frac{14.51\,(.461)(1.72)(19.54)[.246,\ 3.154]}{(10)^2}$$

Note:
( ) = $(1/T_i)$
[ ] = $[\zeta_i, \omega_i]$

$K_{p_\theta} = 7.9$

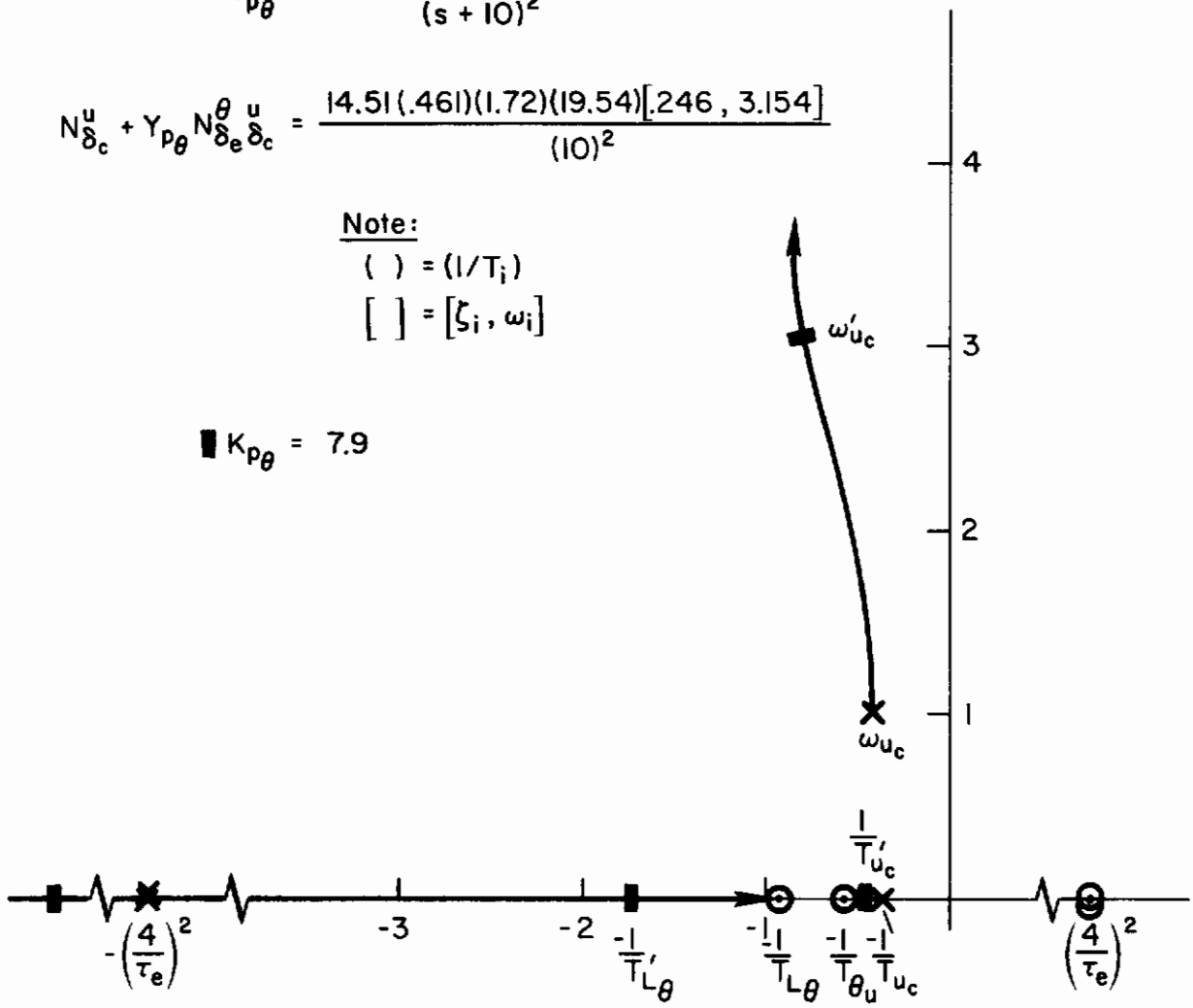

Figure E-2. Factorization of $N^{u}_{\delta_c} + Y_{p_\theta} N^{\theta\ u}_{\delta_e\ \delta_c}$

$$\Delta'' = \Delta' + Y_{p_u}\left(N^{u}_{\delta_c} + Y_{p_\theta} N^{\theta\ u}_{\delta_e \delta_c}\right)$$

$$= \frac{(.478)(1.8)(19.47)(21.02)[.167, 2.816][.308, 3.974]}{(10)^4}$$

$$Y_{p_u} = \frac{K_{p_u}(s-10)^2}{(s+10)^2}$$

Note:

( ) = $(1/T_i)$

[ ] = $[\zeta_i, \omega_i]$

■ $K_{p_u} = 0.178$

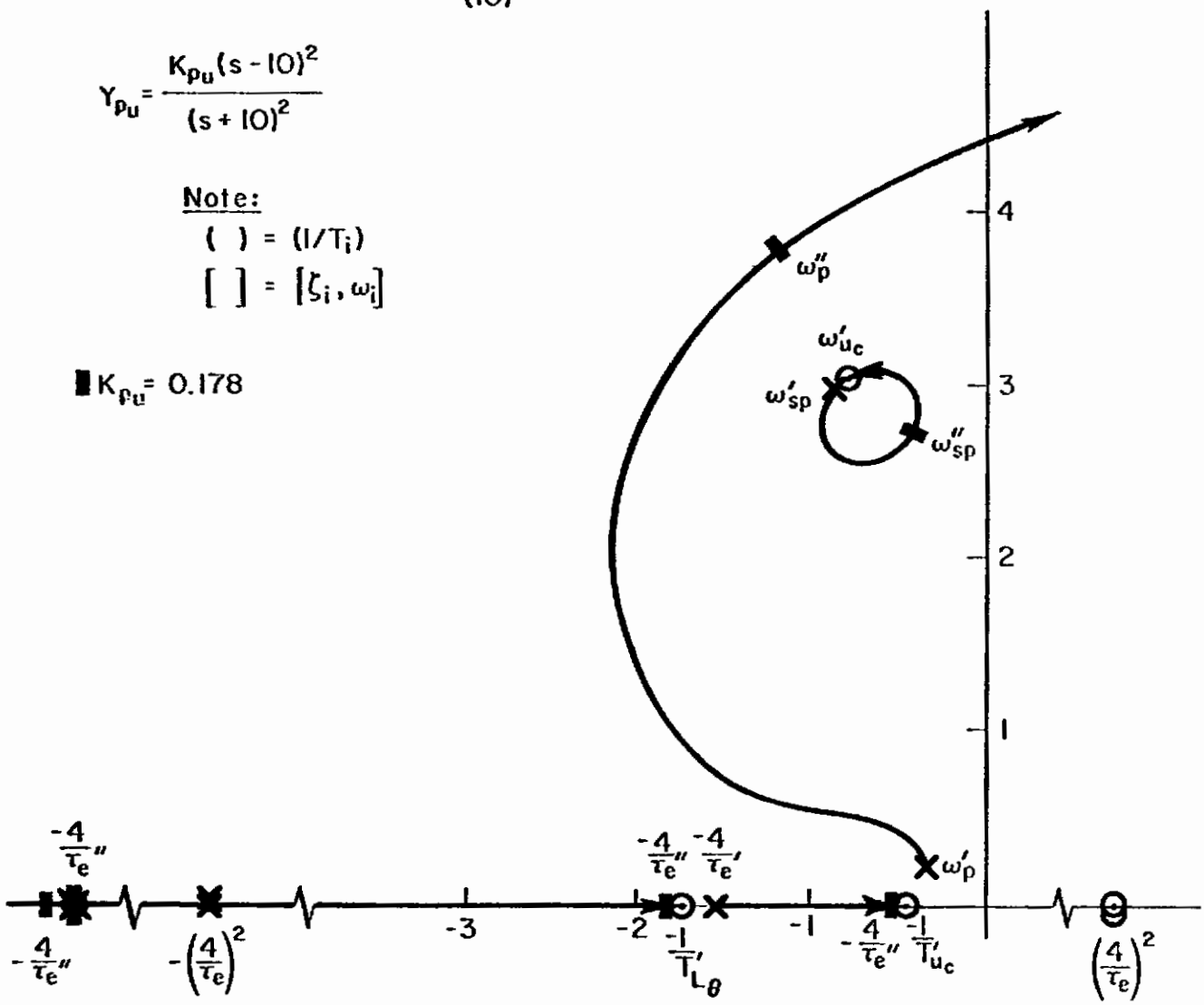

Figure E-3. $u \rightarrowtail \delta_c$ Closure with $\theta \rightarrowtail \delta_e$ Loop Closed

$u \rightarrow \delta_c$ closure modifies the numerator of the outer-loop altitude control transfer function by adding to the basic airframe altitude numerator ($N^h_{\delta_e}$) a coupling term, $Y_{p_u} N^{h\ u}_{\delta_e \delta_c}$.

$$N^h_{\delta_e} + Y_{p_u} N^{h\ u}_{\delta_e \delta_c} = \frac{-0.953(-4.59)(0.142)(5.438)}{s} + \frac{K_{p_u}(-10)^2}{(10)^2} \times \frac{-13.83(-5.6)(6.38)}{s}$$

Factorization of this polymonial in root locus form is shown in Fig. E-4.

For $K_{p_u} = 0.178$

$$N^h_{\delta_e} + Y_{p_u} N^{h\ u}_{\delta_e \delta_c} = \frac{-0.953(-4.663)(6.487)(20.75)[0.127\ ,\ 3.906]}{(10)^2 s}$$

Final altitude control open-loop transfer function with $\theta \rightarrow \delta_e$ and $u \rightarrow \delta_c$ loops closed is given by

$$\left(\frac{h}{h_c}\right)_{\substack{\theta \rightarrow \delta_e \\ u \rightarrow \delta_c \\ h \rightarrow \delta_e}} = \frac{Y_{p_h} Y_{p_\theta} \left[N^h_{\delta_e} + Y_{p_u} N^{h\ u}_{\delta_e \delta_c}\right]}{\Delta''}$$

$$= \frac{K_{p_h} K_{p_\theta} (0.943)(-10)^2}{(10)^2} \times \frac{-0.953(-4.663)(6.487)(20.75)[0.127\ ,\ 3.906]}{(10)^2 s}$$

$$\times \frac{(10)^4}{(0.478)(1.8)(19.47)(21.02)[0.167\ ,\ 2.816][0.308\ ,\ 3.974]}$$

$$= \frac{-7.52 K_{p_h}(-10)^2 (0.943)(-4.663)(6.487)(20.75)[0.127\ ,\ 3.906]}{s(0.478)(1.8)(19.47)(21.02)[0.167\ ,\ 2.816][0.308\ ,\ 3.974]}$$

Final altitude control loop closure characteristics are shown in Fig. E-5.

$$Y_{pu} = \frac{K_{pu}(s - 10)^2}{(s + 10)^2}$$

$$N^h_{\delta_e} + Y_{pu} N^{h\ u}_{\delta_e \delta_c} = \frac{-.953(-4.663)(6.487)(20.75)[.127, 3.906]}{(10)^2 s}$$

Note:

( ) = $(1/T_i)$

[ ] = $[\zeta_i, \omega_i]$

$K_{pu} = 0.178$

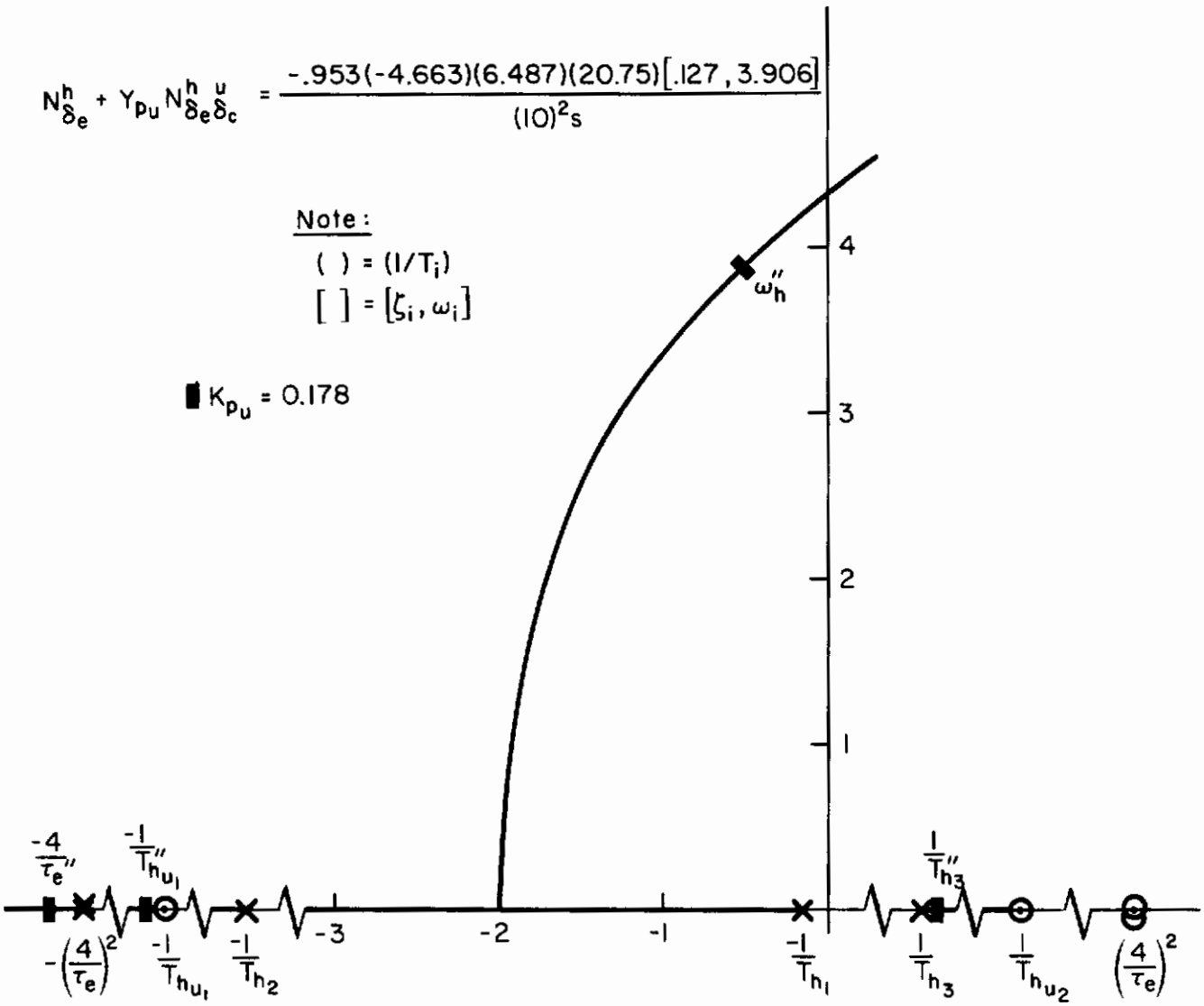

Figure E-4. Factorization of $N^h_{\delta_e} + Y_{pu} N^{h\ u}_{\delta_e \delta_c}$

$$\left(\frac{h}{h_\epsilon}\right)_{\substack{\theta \to \delta_e \\ u \to \delta_c \\ h \to \delta_e}} = \frac{Y_{p_h} Y_{p_\theta}\left(N^h_{\delta_e} + Y_{p_u} N^{h\ u}_{\delta_e \delta_c}\right)}{\Delta} = \frac{-7.52\, K_{p_h}(.943)(-10)^2(-4.66)(6.49)(20.75)[.127, 3.91]}{s\,(.478)(1.8)(19.47)(21.0)[.167, 2.816][.308, 3.974]}$$

Note:

$(\ ) = (1/T_i)$

$[\ ] = [\zeta_i, \omega_i]$

$$Y_{p_\theta} = \frac{7.9\,(s + 9.43)(s - 10)^2}{(s + 10)^2}$$

$Y_{p_h} = K_{p_h}$

$K_{p_h} = 0.0066$

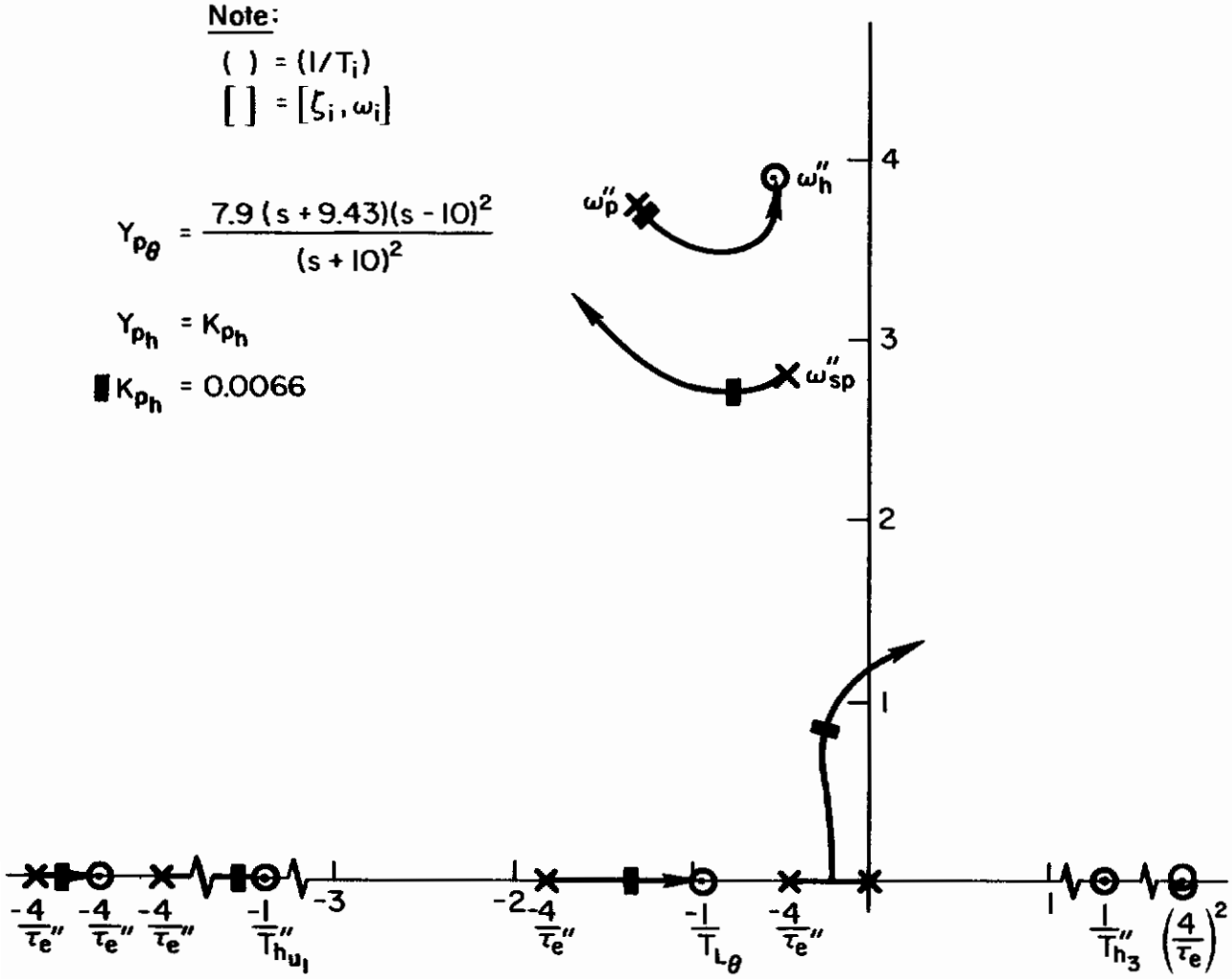

Figure E-5. $h \to \delta_e$ Closure with $\theta \to \delta_e$ and $u \to \delta_c$ Loops Closed

UNCLASSIFIED
Security Classification

DOCUMENT CONTROL DATA - R&D

(Security classification of title, body of abstract and indexing annotation must be entered when the overall report is classified)

1. ORIGINATING ACTIVITY (Corporate author)	2a. REPORT SECURITY CLASSIFICATION
Systems Technology, Inc. 13766 S. Hawthorne Blvd Hawthorne, California 90250	Unclassified
	2b. GROUP N/A

3. REPORT TITLE ANALYSIS OF VTOL HANDLING QUALITIES REQUIREMENTS
Part I. Longitudinal Hover and Transition

4. DESCRIPTIVE NOTES (Type of report and inclusive dates)
Final Report - Jun 1966 to July 1968

5. AUTHOR(S) (Last name, first name, initial)
Craig, Samuel J.
Campbell, Anthony

6. REPORT DATE	7a. TOTAL NO. OF PAGES	7b. NO. OF REFS
October 1968	195	31

8a. CONTRACT OR GRANT NO.	9a. ORIGINATOR'S REPORT NUMBER(S)
AF33(615)-3736 b. PROJECT NO. 698DC c. Task No. 698DC 00 001 d.	STI TR 171-1
	9b. OTHER REPORT NO(S) (Any other numbers that may be assigned this report) AFFDL-TR-67-179, Part I

10. AVAILABILITY/LIMITATION NOTICES This document is subject to special export controls and each transmittal to foreign governments or foreign nationals may be made only with prior approval of the Handling Qualities Group, Control Criteria Branch, Air Force Flight Dynamics Laboratory, Wright-Patterson Air Force Base, Ohio, 45433.

11. SUPPLEMENTARY NOTES	12. SPONSORING MILITARY ACTIVITY
N/A	AFFDL (FDCC) Wright-Patterson AFB, Ohio 45433

13. ABSTRACT Analyses of results from available handling qualities experiments were performed to determine dynamic and control requirements for VTOL aircraft. The basis for this treatment was an examination of the pilot/vehicle as a closed-loop servo system. The quasi-linear pilot describing function has been applied. The results of the studies suggest that the primary factors identifying satisfactory and unacceptable hover mode dynamic features are primarily related to the closed-loop pilot/vehicle system. Preliminary consideration is given to the longitudinal techniques and multiloop control structures suitable for manual control in transition.

DD FORM 1 JAN 64 1473

UNCLASSIFIED
Security Classification

14. KEY WORDS	LINK A		LINK B		LINK C	
	ROLE	WT	ROLE	WT	ROLE	WT
VTOL Handling Qualities Pilot Vehicle Analysis Longitudinal Hover Longitudinal Transition						

INSTRUCTIONS

1. ORIGINATING ACTIVITY: Enter the name and address of the contractor, subcontractor, grantee, Department of Defense activity or other organization *(corporate author)* issuing the report.

2*a*. REPORT SECURITY CLASSIFICATION: Enter the overall security classification of the report. Indicate whether "Restricted Data" is included. Marking is to be in accordance with appropriate security regulations.

2*b*. GROUP: Automatic downgrading is specified in DoD Directive 5200.10 and Armed Forces Industrial Manual. Enter the group number. Also, when applicable, show that optional markings have been used for Group 3 and Group 4 as authorized.

3. REPORT TITLE: Enter the complete report title in all capital letters. Titles in all cases should be unclassified. If a meaningful title cannot be selected without classification, show title classification in all capitals in parenthesis immediately following the title.

4. DESCRIPTIVE NOTES: If appropriate, enter the type of report, e.g., interim, progress, summary, annual, or final. Give the inclusive dates when a specific reporting period is covered.

5. AUTHOR(S): Enter the name(s) of author(s) as shown on or in the report. Enter last name, first name, middle initial. If military, show rank and branch of service. The name of the principal author is an absolute minimum requirement.

6. REPORT DATE: Enter the date of the report as day, month, year; or month, year. If more than one date appears on the report, use date of publication.

7*a*. TOTAL NUMBER OF PAGES: The total page count should follow normal pagination procedures, i.e., enter the number of pages containing information.

7*b*. NUMBER OF REFERENCES: Enter the total number of references cited in the report.

8*a*. CONTRACT OR GRANT NUMBER: If appropriate, enter the applicable number of the contract or grant under which the report was written.

8*b*, &c, & 8*d*. PROJECT NUMBER: Enter the appropriate military department identification, such as project number, subproject number, system numbers, task number, etc.

9*a*. ORIGINATOR'S REPORT NUMBER(S): Enter the official report number by which the document will be identified and controlled by the originating activity. This number must be unique to this report.

9*b*. OTHER REPORT NUMBER(S): If the report has been assigned any other report numbers *(either by the originator or by the sponsor)*, also enter this number(s).

10. AVAILABILITY/LIMITATION NOTICES: Enter any limitations on further dissemination of the report, other than those imposed by security classification, using standard statements such as:

(1) "Qualified requesters may obtain copies of this report from DDC."

(2) "Foreign announcement and dissemination of this report by DDC is not authorized."

(3) "U. S. Government agencies may obtain copies of this report directly from DDC. Other qualified DDC users shall request through _____."

(4) "U. S. military agencies may obtain copies of this report directly from DDC. Other qualified users shall request through _____."

(5) "All distribution of this report is controlled. Qualified DDC users shall request through _____."

If the report has been furnished to the Office of Technical Services, Department of Commerce, for sale to the public, indicate this fact and enter the price, if known.

11. SUPPLEMENTARY NOTES: Use for additional explanatory notes.

12. SPONSORING MILITARY ACTIVITY: Enter the name of the departmental project office or laboratory sponsoring *(paying for)* the research and development. Include address.

13. ABSTRACT: Enter an abstract giving a brief and factual summary of the document indicative of the report, even though it may also appear elsewhere in the body of the technical report. If additional space is required, a continuation sheet shall be attached.

It is highly desirable that the abstract of classified reports be unclassified. Each paragraph of the abstract shall end with an indication of the military security classification of the information in the paragraph, represented as *(TS)*, *(S)*, *(C)*, or *(U)*.

There is no limitation on the length of the abstract. However, the suggested length is from 150 to 225 words.

14. KEY WORDS: Key words are technically meaningful terms or short phrases that characterize a report and may be used as index entries for cataloging the report. Key words must be selected so that no security classification is required. Identifiers, such as equipment model designation, trade name, military project code name, geographic location, may be used as key words but will be followed by an indication of technical context. The assignment of links, rules, and weights is optional.